RILEM State-of-the-Art Reports

Mario de Rooij
Kim Van Tittelboom
Nele De Belie
Erik Schlangen *Editors*

# Self-Healing Phenomena in Cement-Based Materials

## State-of-the-Art Report of RILEM Technical Committee 221-SHC: Self-Healing Phenomena in Cement-Based Materials


Springer

# RILEM State-of-the-Art Reports

Volume 11

RILEM, The International Union of Laboratories and Experts in Construction Materials, Systems and Structures, founded in 1947, is a non-governmental scientific association whose goal is to contribute to progress in the construction sciences, techniques and industries, essentially by means of the communication it fosters between research and practice. RILEM's focus is on construction materials and their use in building and civil engineering structures, covering all phases of the building process from manufacture to use and recycling of materials. More information on RILEM and its previous publications can be found on www.RILEM.net.

The RILEM State-of-the-Art Reports (STAR) are produced by the Technical Committees. They represent one of the most important outputs that RILEM generates - high level scientific and engineering reports that provide cutting edge knowledge in a given field. The work of the TCs is one of RILEM's key functions.

Members of a TC are experts in their field and give their time freely to share their expertise. As a result, the broader scientific community benefits greatly from RILEM's activities.

RILEM's stated objective is to disseminate this information as widely as possible to the scientific community. RILEM therefore considers the STAR reports of its TCs as of highest importance, and encourages their publication whenever possible.

The information in this and similar reports is mostly pre-normative in the sense that it provides the underlying scientific fundamentals on which standards and codes of practice are based. Without such a solid scientific basis, construction practice will be less than efficient or economical.

It is RILEM's hope that this information will be of wide use to the scientific community.

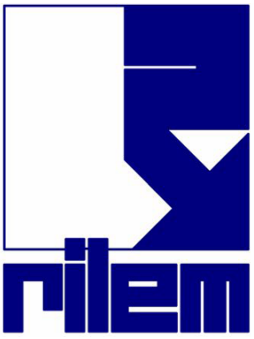


For further volumes:
http://www.springer.com/series/8780

Mario de Rooij · Kim Van Tittelboom
Nele De Belie · Erik Schlangen
Editors

# Self-Healing Phenomena in Cement-Based Materials

## State-of-the-Art Report of RILEM Technical Committee 221-SHC: Self-Healing Phenomena in Cement-Based Materials

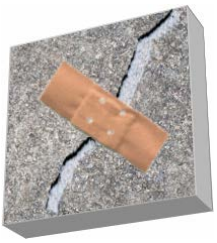

Springer

*Editors*
Mario de Rooij
TNO
Delft
The Netherlands

Nele De Belie
Department of Structural Engineering
Ghent University
Ghent
Belgium

Kim Van Tittelboom
Department of Structural Engineering
Ghent University
Ghent
Belgium

Erik Schlangen
Faculty of Civil Eng. and Geosciences
Delft University of Technology
Delft
The Netherlands

ISSN 2213-204X
ISBN 978-94-007-6623-5
DOI 10.1007/978-94-007-6624-2
Springer Dordrecht Heidelberg New York London

ISSN 2213-2031 (electronic)
ISBN 978-94-007-6624-2 (ebook)

Library of Congress Control Number: 2013933102

# RILEM Publications

RILEM Publications are presented in 6 collections, corresponding to the 5 clusters of active RILEM Technical Committees, sorted by fields of expertise, and a 6th multithematic collection dedicated to journals and compendiums:

A. Mechanical Performance and Fracture
B. Materials Characterization, Properties Evaluation and Processing
C. Design and Service Life
D. Performance and Deterioration Mechanisms
E Special Construction Materials and Components
F Journals and Compendiums

Each publication is assigned to one of the following series: reports (REP), proceedings (PRO), compendiums (COMP) and journals. The former CD-ROM series is now included in one of these series.

Each publication is available in at least one of the three following editions: print (PR), CD or DVD-ROM (CD), or online (OL).

Online editions are available through our web site, at http://www.rilem.net
The following list is presenting our global offer, sorted by series.

**RILEM PROCEEDINGS**

**PRO 1:** Durability of High Performance Concrete (ISBN: 2-912143-03-9); *Ed. H. Sommer*
**PRO 2:** Chloride Penetration into Concrete (ISBN: 2-912143-00-04); *Eds. L.-O. Nilsson and J.-P. Ollivier*
**PRO 3:** Evaluation and Strengthening of Existing Masonry Structures (ISBN: 2-912143-02-0); *Eds. L. Binda and C. Modena*
**PRO 4:** Concrete: From Material to Structure (ISBN: 2-912143-04-7); *Eds. J.-P. Bournazel and Y. Malier*
**PRO 5:** The Role of Admixtures in High Performance Concrete (ISBN: 2-912143-05-5); *Eds. J. G. Cabrera and R. Rivera-Villarreal*
**PRO 6:** High Performance Fiber Reinforced Cement Composites - HPFRCC 3 (ISBN: 2-912143-06-3); *Eds. H. W. Reinhardt and A. E. Naaman*
**PRO 7:** 1st International RILEM Symposium on Self-Compacting Concrete (ISBN: 2-912143-09-8); *Eds. Å. Skarendahl and Ö. Petersson*

**PRO 8:** International RILEM Symposium on Timber Engineering (ISBN: 2-912143-10-1); *Ed. L. Boström*
**PRO 9:** 2nd International RILEM Symposium on Adhesion between Polymers and Concrete ISAP '99 (ISBN: 2-912143-11-X); *Eds. Y. Ohama and M. Puterman*
**PRO 10:** 3rd International RILEM Symposium on Durability of Building and Construction Sealants (ISBN: 2-912143-13-6); *Eds. A. T. Wolf*
**PRO 11:** 4th International RILEM Conference on Reflective Cracking in Pavements (ISBN: 2-912143-14-4); *Eds. A. O. Abd El Halim, D. A. Taylor and El H. H. Mohamed*
**PRO 12:** International RILEM Workshop on Historic Mortars: Characteristics and Tests (ISBN: 2-912143-15-2); *Eds. P. Bartos, C. Groot and J. J. Hughes*
**PRO 13:** 2nd International RILEM Symposium on Hydration and Setting (ISBN: 2-912143-16-0); *Ed. A. Nonat*
**PRO 14:** Integrated Life-Cycle Design of Materials and Structures - ILCDES 2000 (ISBN: 951-758-408-3); (ISSN: 0356-9403); *Ed. S. Sarja*
**PRO 15:** Fifth RILEM Symposium on Fibre-Reinforced Concretes (FRC) - BEFIB'2000 (ISBN: 2-912143-18-7); *Eds. P. Rossi and G. Chanvillard*
**PRO 16:** Life Prediction and Management of Concrete Structures (ISBN: 2-912143-19-5); *Ed. D. Naus*
**PRO 17:** Shrinkage of Concrete – Shrinkage 2000 (ISBN: 2-912143-20-9); *Eds. V. Baroghel-Bouny and P.-C. Aïtcin*
**PRO 18:** Measurement and Interpretation of the On-Site Corrosion Rate (ISBN: 2-912143-21-7); *Eds. C. Andrade, C. Alonso, J. Fullea, J. Polimon and J. Rodriguez*
**PRO 19:** Testing and Modelling the Chloride Ingress into Concrete (ISBN: 2-912143-22-5); *Eds. C. Andrade and J. Kropp*
**PRO 20:** 1st International RILEM Workshop on Microbial Impacts on Building Materials (CD 02) (e-ISBN 978-2-35158-013-4); *Ed. M. Ribas Silva*
**PRO 21:** International RILEM Symposium on Connections between Steel and Concrete (ISBN: 2-912143-25-X); *Ed. R. Eligehausen*
**PRO 22:** International RILEM Symposium on Joints in Timber Structures (ISBN: 2-912143-28-4); *Eds. S. Aicher and H.-W. Reinhardt*
**PRO 23:** International RILEM Conference on Early Age Cracking in Cementitious Systems (ISBN: 2-912143-29-2); *Eds. K. Kovler and A. Bentur*
**PRO 24:** 2nd International RILEM Workshop on Frost Resistance of Concrete (ISBN: 2-912143-30-6); *Eds. M. J. Setzer, R. Auberg and H.-J. Keck*
**PRO 25:** International RILEM Workshop on Frost Damage in Concrete (ISBN: 2-912143-31-4); *Eds. D. J. Janssen, M. J. Setzer and M. B. Snyder*
**PRO 26:** International RILEM Workshop on On-Site Control and Evaluation of Masonry Structures (ISBN: 2-912143-34-9); *Eds. L. Binda and R. C. de Vekey*
**PRO 27:** International RILEM Symposium on Building Joint Sealants (CD03); *Ed. A. T. Wolf*
**PRO 28:** 6th International RILEM Symposium on Performance Testing and Evaluation of Bituminous Materials - PTEBM'03 (ISBN: 2-912143-35-7; e-ISBN: 978-2-912143-77-8); *Ed. M. N. Partl*

**PRO 29:** 2nd International RILEM Workshop on Life Prediction and Ageing Management of Concrete Structures (ISBN: 2-912143-36-5); *Ed. D. J. Naus*
**PRO 30:** 4th International RILEM Workshop on High Performance Fiber Reinforced Cement Composites - HPFRCC 4 (ISBN: 2-912143-37-3); *Eds. A. E. Naaman and H. W. Reinhardt*
**PRO 31:** International RILEM Workshop on Test and Design Methods for Steel Fibre Reinforced Concrete: Background and Experiences (ISBN: 2-912143-38-1); *Eds. B. Schnütgen and L. Vandewalle*
**PRO 32:** International Conference on Advances in Concrete and Structures 2 vol. (ISBN (set): 2-912143-41-1); *Eds. Ying-shu Yuan, Surendra P. Shah and Heng-lin Lü*
**PRO 33:** 3rd International Symposium on Self-Compacting Concrete (ISBN: 2-912143-42-X); *Eds. Ó. Wallevik and I. Níelsson*
**PRO 34:** International RILEM Conference on Microbial Impact on Building Materials (ISBN: 2-912143-43-8); *Ed. M. Ribas Silva*
**PRO 35:** International RILEM TC 186-ISA on Internal Sulfate Attack and Delayed Ettringite Formation (ISBN: 2-912143-44-6); *Eds. K. Scrivener and J. Skalny*
**PRO 36:** International RILEM Symposium on Concrete Science and Engineering – A Tribute to Arnon Bentur (ISBN: 2-912143-46-2); *Eds. K. Kovler, J. Marchand, S. Mindess and J. Weiss*
**PRO 37:** 5th International RILEM Conference on Cracking in Pavements – Mitigation, Risk Assessment and Prevention (ISBN: 2-912143-47-0); *Eds. C. Petit, I. Al-Qadi and A. Millien*
**PRO 38:** 3rd International RILEM Workshop on Testing and Modelling the Chloride Ingress into Concrete (ISBN: 2-912143-48-9); *Eds. C. Andrade and J. Kropp*
**PRO 39:** 6th International RILEM Symposium on Fibre-Reinforced Concretes - BEFIB 2004 (ISBN: 2-912143-51-9); *Eds. M. Di Prisco, R. Felicetti and G. A. Plizzari*
**PRO 40:** International RILEM Conference on the Use of Recycled Materials in Buildings and Structures (ISBN: 2-912143-52-7); *Eds. E. Vázquez, Ch. F. Hendriks and G. M. T. Janssen*
**PRO 41:** RILEM International Symposium on Environment-Conscious Materials and Systems for Sustainable Development (ISBN: 2-912143-55-1); *Eds. N. Kashino and Y. Ohama*
**PRO 42:** SCC'2005 - China: 1st International Symposium on Design, Performance and Use of Self-Consolidating Concrete (ISBN: 2-912143-61-6); *Eds. Zhiwu Yu, Caijun Shi, Kamal Henri Khayat and Youjun Xie*
**PRO 43:** International RILEM Workshop on Bonded Concrete Overlays (e-ISBN: 2-912143-83-7); *Eds. J. L. Granju and J. Silfwerbrand*
**PRO 44:** 2nd International RILEM Workshop on Microbial Impacts on Building Materials (CD11) (e-ISBN: 2-912143-84-5); *Ed. M. Ribas Silva*
**PRO 45:** 2nd International Symposium on Nanotechnology in Construction, Bilbao (ISBN: 2-912143-87-X); *Eds. Peter J. M. Bartos, Yolanda de Miguel and Antonio Porro*

**PRO 46:** ConcreteLife'06 - International RILEM-JCI Seminar on Concrete Durability and Service Life Planning: Curing, Crack Control, Performance in Harsh Environments (ISBN: 2-912143-89-6); *Ed. K. Kovler*

**PRO 47:** International RILEM Workshop on Performance Based Evaluation and Indicators for Concrete Durability (ISBN: 978-2-912143-95-2); *Eds. V. Baroghel-Bouny, C. Andrade, R. Torrent and K. Scrivener*

**PRO 48:** 1st International RILEM Symposium on Advances in Concrete through Science and Engineering (e-ISBN: 2-912143-92-6); *Eds. J. Weiss, K. Kovler, J. Marchand, and S. Mindess*

**PRO 49:** International RILEM Workshop on High Performance Fiber Reinforced Cementitious Composites in Structural Applications (ISBN: 2-912143-93-4); *Eds. G. Fischer and V.C. Li*

**PRO 50:** 1st International RILEM Symposium on Textile Reinforced Concrete (ISBN: 2-912143-97-7); *Eds. Josef Hegger, Wolfgang Brameshuber and Norbert Will*

**PRO 51:** 2nd International Symposium on Advances in Concrete through Science and Engineering (ISBN: 2-35158-003-6; e-ISBN: 2-35158-002-8); *Eds. J. Marchand, B. Bissonnette, R. Gagné, M. Jolin and F. Paradis*

**PRO 52:** Volume Changes of Hardening Concrete: Testing and Mitigation (ISBN: 2-35158-004-4; e-ISBN: 2-35158-005-2); *Eds. O. M. Jensen, P. Lura and K. Kovler*

**PRO 53:** High Performance Fiber Reinforced Cement Composites - HPFRCC5 (ISBN: 978-2-35158-046-2); *Eds. H. W. Reinhardt and A. E. Naaman*

**PRO 54:** 5th International RILEM Symposium on Self-Compacting Concrete (ISBN: 978-2-35158-047-9); *Eds. G. De Schutter and V. Boel*

**PRO 55:** International RILEM Symposium Photocatalysis, Environment and Construction Materials (ISBN: 978-2-35158-056-1); *Eds. P. Baglioni and L. Cassar*

**PRO 56:** International RILEM Workshop on Integral Service Life Modelling of Concrete Structures (ISBN 978-2-35158-058-5); *Eds. R. M. Ferreira, J. Gulikers and C. Andrade*

**PRO 57:** RILEM Workshop on Performance of cement-based materials in aggressive aqueous environments (e-ISBN: 978-2-35158-059-2); *Ed. N. De Belie*

**PRO 58:** International RILEM Symposium on Concrete Modelling - CONMOD'08 (ISBN: 978-2-35158-060-8); *Eds. E. Schlangen and G. De Schutter*

**PRO 59:** International RILEM Conference on On Site Assessment of Concrete, Masonry and Timber Structures - SACoMaTiS 2008 (ISBN set: 978-2-35158-061-5); *Eds. L. Binda, M. di Prisco and R. Felicetti*

**PRO 60**: Seventh RILEM International Symposium on Fibre Reinforced Concrete: Design and Applications - BEFIB 2008 (ISBN: 978-2-35158-064-6); *Ed. R. Gettu*

**PRO 61:** 1st International Conference on Microstructure Related Durability of Cementitious Composites 2 vol., (ISBN: 978-2-35158-065-3); *Eds. W. Sun, K. van Breugel, C. Miao, G. Ye and H. Chen*

**PRO 62:** NSF/ RILEM Workshop: In-situ Evaluation of Historic Wood and Masonry Structures (e-ISBN: 978-2-35158-068-4); *Eds. B. Kasal, R. Anthony and M. Drdácký*

**PRO 63:** Concrete in Aggressive Aqueous Environments: Performance, Testing and Modelling, 2 vol., (ISBN: 978-2-35158-071-4); *Eds. M. G. Alexander and A. Bertron*

**PRO 64:** Long Term Performance of Cementitious Barriers and Reinforced Concrete in Nuclear Power Plants and Waste Management - NUCPERF 2009 (ISBN: 978-2-35158-072-1); *Eds. V. L'Hostis, R. Gens, C. Gallé*

**PRO 65:** Design Performance and Use of Self-consolidating Concrete - SCC'2009 (ISBN: 978-2-35158-073-8); *Eds. C. Shi, Z. Yu, K. H. Khayat and P. Yan*

**PRO 66:** 2nd International RILEM Workshop on Concrete Durability and Service Life Planning - ConcreteLife'09 (ISBN: 978-2-35158-074-5); *Ed. K. Kovler*

**PRO 67**: Repairs Mortars for Historic Masonry (e-ISBN: 978-2-35158-083-7); *Ed. C. Groot*

**PRO 68:** Proceedings of the 3rd International RILEM Symposium on 'Rheology of Cement Suspensions such as Fresh Concrete (ISBN 978-2-35158-091-2); *Eds. O. H. Wallevik, S. Kubens and S. Oesterheld*

**PRO 69:** 3rd International PhD Student Workshop on 'Modelling the Durability of Reinforced Concrete (ISBN: 978-2-35158-095-0); *Eds. R. M. Ferreira, J. Gulikers and C. Andrade*

**PRO 70:** 2nd International Conference on 'Service Life Design for Infrastructure' (ISBN set: 978-2-35158-096-7, e-ISBN: 978-2-35158-097-4); *Ed. K. van Breugel, G. Ye and Y. Yuan*

**PRO 71:** Advances in Civil Engineering Materials - The 50-year Teaching Anniversary of Prof. Sun Wei' (ISBN: 978-2-35158-098-1; e-ISBN: 978-2-35158-099-8); *Eds. C. Miao, G. Ye, and H. Chen*

**PRO 72:** First International Conference on 'Advances in Chemically-Activated Materials – CAM'2010' (2010), 264 pp, ISBN: 978-2-35158-101-8; e-ISBN: 978-2-35158-115-5, *Eds. Caijun Shi and Xiaodong Shen*

**PRO 73:** 2nd International Conference on 'Waste Engineering and Management - ICWEM 2010' (2010), 894 pp, ISBN: 978-2-35158-102-5; e-ISBN: 978-2-35158-103-2, *Eds. J. Zh. Xiao, Y. Zhang, M. S. Cheung and R. Chu*

**PRO 74:** International RILEM Conference on 'Use of Superabsorsorbent Polymers and Other New Addditives in Concrete' (2010) 374 pp., ISBN: 978-2-35158-104-9; e-ISBN: 978-2-35158-105-6; *Eds. O.M. Jensen, M.T. Hasholt, and S. Laustsen*

**PRO 75:** International Conference on 'Material Science - 2nd ICTRC - Textile Reinforced Concrete - Theme 1' (2010) 436 pp., ISBN: 978-2-35158-106-3; e-ISBN: 978-2-35158-107-0; Ed. W. Brameshuber

**PRO 76**: International Conference on 'Material Science - HetMat - Modelling of Heterogeneous Materials - Theme 2' (2010) 255 pp., ISBN: 978-2-35158-108-7; e-ISBN: 978-2-35158-109-4; Ed. W. Brameshuber

**PRO 77:** International Conference on 'Material Science - AdIPoC - Additions Improving Properties of Concrete - Theme 3' (2010) 459 pp., ISBN: 978-2-35158-110-0; e-ISBN: 978-2-35158-111-7; *Ed. W. Brameshuber*
**PRO 78:** 2nd Historic Mortars Conference and RILEM TC 203-RHM Final Workshop – HMC2010 (2010) 1416 pp., e-ISBN: 978-2-35158-112-4; *Eds J. Válek, C. Groot, and J. J. Hughes*
**PRO 79:** International RILEM Conference on Advances in Construction Materials Through Science and Engineering (2011) 213 pp., e-ISBN: 978-2-35158-117-9; *Eds Christopher Leung and K.T. Wan*
**PRO 80:** 2nd International RILEM Conference on Concrete Spalling due to Fire Exposure (2011) 453 pp., ISBN: 978-2-35158-118-6, e-ISBN: 978-2-35158-119-3; *Eds E.A.B. Koenders and F. Dehn*
**PRO 81:** 2nd International RILEM Conference on Strain Hardening Cementitious Composites (SHCC2-Rio) (2011) 451 pp., ISBN: 978-2-35158-120-9, e-ISBN: 978-2-35158-121-6; *Eds R.D. Toledo Filho, F.A. Silva, E.A.B. Koenders and E.M.R. Fairbairn*
**PRO 82:** 2nd International RILEM Conference on Progress of Recycling in the Built Environment (2011) 507 pp., e-ISBN: 978-2-35158-122-3; *Eds V.M. John, E. Vazquez, S.C. Angulo and C. Ulsen*
**PRO 83:** 2nd International Conference on Microstructural-related Durability of Cementitious Composites (2012) 250 pp., ISBN: 978-2-35158-129-2; e-ISBN: 978-2-35158-123-0; *Eds G. Ye, K. van Breugel, W. Sun and C. Miao*
**PRO 85:** RILEM-JCI International Workshop on Crack Control of Mass Concrete and Related issues concerning Early-Age of Concrete Structures – ConCrack 3 – Control of Cracking in Concrete Structures 3 (2012) 237 pp., ISBN: 978-2-35158-125-4; e-ISBN: 978-2-35158-126-1; *Eds F. Toutlemonde and J.-M. Torrenti*
**PRO 86:** International Symposium on Life Cycle Assessment and Construction (2012) 414 pp., ISBN: 978-2-35158-127-8, e-ISBN: 978-2-35158-128-5; *Eds A. Ventura and C. de la Roche*

**RILEM REPORTS**

**Report 19:** Considerations for Use in Managing the Aging of Nuclear Power Plant Concrete Structures (ISBN: 2-912143-07-1); *Edited* by D. J. Naus
**Report 19:** Considerations for Use in Managing the Aging of Nuclear Power Plant Concrete Structures (ISBN: 2-912143-07-1); *Ed. D. J. Naus*
**Report 20:** Engineering and Transport Properties of the Interfacial Transition Zone in Cementitious Composites (ISBN: 2-912143-08-X); *Eds. M. G. Alexander, G. Arliguie, G. Ballivy, A. Bentur and J. Marchand*
**Report 21:** Durability of Building Sealants (ISBN: 2-912143-12-8); *Ed. A. T. Wolf*
**Report 22:** Sustainable Raw Materials - Construction and Demolition Waste (ISBN: 2-912143-17-9); *Eds. C. F. Hendriks and H. S. Pietersen*
**Report 23:** Self-Compacting Concrete state-of-the-art report (ISBN: 2-912143-23-3); *Eds. Å. Skarendahl and Ö. Petersson*

**Report 24:** Workability and Rheology of Fresh Concrete: Compendium of Tests (ISBN: 2-912143-32-2); *Eds. P. J. M. Bartos, M. Sonebi and A. K. Tamimi*
**Report 25:** Early Age Cracking in Cementitious Systems (ISBN: 2-912143-33-0); *Ed. A. Bentur*
**Report 26:** Towards Sustainable Roofing (Joint Committee CIB/RILEM) (CD 07) (e-ISBN 978-2-912143-65-5); *Eds. Thomas W. Hutchinson and Keith Roberts*
**Report 27:** Condition Assessment of Roofs (Joint Committee CIB/RILEM) (CD 08) (e-ISBN 978-2-912143-66-2); *Ed. CIB W 83/RILEM TC166-RMS*
**Report 28:** Final report of RILEM TC 167-COM 'Characterisation of Old Mortars with Respect to Their Repair (ISBN: 978-2-912143-56-3); *Eds. C. Groot, G. Ashall and J. Hughes*
**Report 29:** Pavement Performance Prediction and Evaluation (PPPE): Interlaboratory Tests (e-ISBN: 2-912143-68-3); *Eds. M. Partl and H. Piber*
**Report 30:** Final Report of RILEM TC 198-URM 'Use of Recycled Materials' (ISBN: 2-912143-82-9; e-ISBN: 2-912143-69-1); *Eds. Ch. F. Hendriks, G. M. T. Janssen and E. Vázquez*
**Report 31:** Final Report of RILEM TC 185-ATC 'Advanced testing of cement-based materials during setting and hardening' (ISBN: 2-912143-81-0; e-ISBN: 2-912143-70-5); *Eds. H. W. Reinhardt and C. U. Grosse*
**Report 32:** Probabilistic Assessment of Existing Structures. A JCSS publication (ISBN 2-912143-24-1); *Ed. D. Diamantidis*
**Report 33:** State-of-the-Art Report of RILEM Technical Committee TC 184-IFE 'Industrial Floors' (ISBN 2-35158-006-0); *Ed. P. Seidler*
**Report 34:** Report of RILEM Technical Committee TC 147-FMB 'Fracture mechanics applications to anchorage and bond' Tension of Reinforced Concrete Prisms – Round Robin Analysis and Tests on Bond (e-ISBN 2-912143-91-8); *Eds. L. Elfgren and K. Noghabai*
**Report 35:** Final Report of RILEM Technical Committee TC 188-CSC 'Casting of Self Compacting Concrete' (ISBN 2-35158-001-X; e-ISBN: 2-912143-98-5); *Eds. Å. Skarendahl and P. Billberg*
**Report 36:** State-of-the-Art Report of RILEM Technical Committee TC 201-TRC 'Textile Reinforced Concrete' (ISBN 2-912143-99-3); *Ed. W. Brameshuber*
**Report 37:** State-of-the-Art Report of RILEM Technical Committee TC 192-ECM 'Environment-conscious construction materials and systems' (ISBN: 978-2-35158-053-0); *Eds. N. Kashino, D. Van Gemert and K. Imamoto*
**Report 38:** State-of-the-Art Report of RILEM Technical Committee TC 205-DSC 'Durability of Self-Compacting Concrete' (ISBN: 978-2-35158-048-6); *Eds. G. De Schutter and K. Audenaert*
**Report 39:** Final Report of RILEM Technical Committee TC 187-SOC 'Experimental determination of the stress-crack opening curve for concrete in tension' (ISBN 978-2-35158-049-3); *Ed. J. Planas*
**Report 40:** State-of-the-Art Report of RILEM Technical Committee TC 189-NEC 'Non-Destructive Evaluation of the Penetrability and Thickness of the Concrete Cover' (ISBN 978-2-35158-054-7); *Eds. R. Torrent and L. Fernández Luco*

**Report 41:** State-of-the-Art Report of RILEM Technical Committee TC 196-ICC 'Internal Curing of Concrete' (ISBN 978-2-35158-009-7); *Eds. K. Kovler and O. M. Jensen*
**Report 42:** 'Acoustic Emission and Related Non-destructive Evaluation Techniques for Crack Detection and Damage Evaluation in Concrete' - Final Report of RILEM Technical Committee 212-ACD (e-ISBN: 978-2-35158-100-1); *Ed. M. Ohtsu*

**COMPENDIUMS**

**COMP 01:** Trilingual Dictionary for Materials and Structures (English-French-German) (CD01) (1970)
**COMP 02:** 1947-1997: 50 years of evolution of Building Materials and Structures - e-ISBN: 2-912143-86-1; *Edited by F. Wittmann*
**COMP 03:** General Conference of RILEM TCs' Chairmen and RILEM Seminar 'Advancing the Knowledge in Materials and Structures' (CD10) (2000) e-ISBN: 2-912143-85-3
**COMP 06:** Concrete Science and Engineering Journal - Vol. 1, 2, 3, 4 (1999-2002) (CD05)

**Contributors – RILEM Technical Committee 221-SHC**

**TC Membership:**

**Chairman:**
Dr. Erik SCHLANGEN, The Netherlands
**Secretary:**
Dr. Mario DE ROOIJ, The Netherlands
**Members:**
Dr. Oguzhan COPUROGLU, The Netherlands
Prof. Nele DE BELIE, Belgium
Dr. Carola EDVARDSEN, Denmark
Prof. Mette GEIKER, Denmark
Prof. Dr. N. HAN, China
Mr. Chengwei HAO, China
Prof. R. Doug HOOTON, Canada
Dr. Shin-ichi IGARASHI, Japan
Prof. Konstantin KOVLER, Israel
Dr. Jianzhong LAI, China
Prof. Robert LARK, United Kingdom
Prof. Victor C. LI, United States of America
Dr. Ahmed LOUKILI, France
Prof. Dr. Viktor MECHTCHERINE, Germany
Prof. Hirozo MIHASHI, Japan
Mr. Tomoya NISHIWAKI, Japan
Dr. Shunzhi QIAN, China
Prof. Dr. Hans W. REINHARDT, Germany
Mr. Yeqing SHEN, China
Mr. Luguang SONG, China
Dr. Pavel TRTIK, Switzerland
Prof. Dr. Klaas van BREUGEL, The Netherlands
Mrs. Kim VAN TITTELBOOM, Belgium
Prof. Jason WEISS, United States of America
Dr. Guang YE, The Netherlands
Mrs. Xiongzhou YUAN, China

# Foreword

Self-healing materials are man-made materials, which have the built-in capability to repair structural damage autogenously or with the minimal help of an external stimulus. Self-healing materials is a new dynamically developing area of materials research. Since healing presupposes the presence of a defect and a defect generally emerges at a very small scale, probably at the nanoscale, it is not surprising that self-healing is one of the promising application fields of nanotechnology.

Self-healing of cement-based materials is not a completely new issue. As early as 1836 the French Academy of Science has reported about self-healing in water retaining structures, culverts and pipes. Those and later studies in the first half of the twentieth century often concentrated on leakage problems in liquid retaining structures, but also studies on healing of cracks in bridges were mentioned. Some twenty years ago work on self-healing of cementitious materials has been published in which it was shown that the so called Kaiser effect (absence of acoustic emission, which is usually observed at repeated loading of structural element, until the load exceeds the previously achieved level) disappears for concrete kept under water for a long time before a new loading. Recently self-healing of microcracks has been suggested the reason why the diffusion coefficient of concrete in marine structures reduces with time. Thus self-healing would become a relevant factor in view of the service life of concrete structures and hence contributes to the sustainability of the built environment.

The present State-of-the-Art Report has been prepared jointly by the members of the RILEM Technical Committee TC 221-SHC "Self-Healing Phenomena in Cement-Based Materials" during the years 2005–2012, under the leadership of its chair Prof. Erik Schlangen and secretary Dr. Mario De Rooij. The report summarizes the knowledge gained by the international research community working in this field for the last 20–25 years. Developing concepts for self-healing by design, or active self-healing, was considered the main topic and challenge of this RILEM committee. In view of this, this State-of-the-Art is unique. I have no doubt that the experts dealing with advanced materials (not only concrete) will enjoy reading this book, find much new information and fresh ideas for the implementation of the materials and methods promoting self-healing in concrete, sealers, coatings and other engineering materials.

Prof. Konstantin Kovler, Technion – Israel Institute of Technology
Prof. Klaas van Breugel, Delft University of Technology

# Contents

# 1 Introduction

M.R. de Rooij[1], E. Schlangen[2], and C. Joseph[3]

[1] TNO, The Netherlands
mario.derooij@tno.nl
[2] Microlab, Delft University of Technology, The Netherlands
H.E.J.G.Schlangen@tudelft.nl
[3] Cardiff School of Engineering, Cardiff University, United Kingdom

## 1.1 Self-Healing Phenomena

A small cut in one's finger is 'treated' by applying an adhesive bandage. The adhesive bandage, however, merely protects the cut allowing the body to self-heal with fewer disturbances. Such processes, while common for living plants and animals are generally not found in man-made materials and one could wonder why. In this state-of-the-art report the leap is taken beyond the assumed boundary condition of the necessity of living matter. All it really takes is a different perspective.

Take the previously mentioned cut. This is obviously the consequence of the skin not being able to withstand a (cutting) force. The skin has shown not to be strong enough. Strength, in more general terms, deals with the ability of a material to sustain a high load without disintegrating and forming new surfaces. Often in engineering science, material improvement is focused on increasing strength or stiffness in order to withstand bigger loads. However, also application of a load just below the fracture load may or may not cause permanent or plastic deformation of a material due to displacements of atoms. Such displacements will ultimately lead to internal defects which can grow into larger cracks and finally cause the degradation of the product. In that case, again the material has failed.

In his book *The new science of strong materials, or why you do not fall through the floor*, the late professor J.E. Gordon [1.1] provided a clear picture of the principal guidelines to solve material failure through the development of stronger engineering materials. To make strong and stiff materials one needs to assemble as many atoms with a high bond strength to neighbouring atoms in as small a volume as possible. As such, not surprisingly, diamond comprised of densely packed small carbon atoms each having a high-covalent bond strength, is the stiffest and possibly the strongest material of all.

Hence, based on the preceding simplified picture of material design, one can argue that the common design philosophy to create a stronger material is based on creating microstructures, which oppose the formation or extension of micro-cracks. Thus, our materials become so strong that the load level necessary to create damage will never be reached. In the book *Self-healing materials* [1.2] this philosophy is termed the paradigm of Damage Prevention. The design concept of Damage Prevention has proven to be a very useful productive concept. However,

M. de Rooij et al. (Eds.): *Self-Healing Phenomena in Cement-Based Materials*, RILEM 11, pp. 1–17.
DOI: 10.1007/978-94-007-6624-2_1 

as the formation of damage during use can never be completely excluded, it also means that structures made out of current materials invariably need periodic inspection to monitor possible damage development. Furthermore, any damage observed calls for action and costs, sooner or later.

Therefore, in the book *Self-healing materials* [1.2] the alternative concept of Damage Management is introduced, which forms the basis of the field of self-healing materials. This paradigm is based on the notion that the formation of damage is not problematic as long as it is counteracted by a subsequent process of 'recovery' or 'healing' the damage. This means that damage in a material can still occur and develop, but that the amount of damage after a certain time is less than what the amount of damage used to be. In other words, self-healing materials have a *negative* rate of damage formation at one or more stages in their lifetime. The final material performance of a self-healing material depends on two time depending processes: the rate of damage formation versus the rate of damage recovery or healing.

In order to transform the concept of self-healing materials from idea to practice it is worthwhile to discuss here first some essential steps in more details.

A first step is the acceptance of damage, or actually a range of damage possibilities. Failure of a material is not regarded as a yes/no failure state (broken or not broken), but much more as the gradual process it so often is in reality (the amount of cracks is increasing). This change of perception provides the possibility for (partial) recovery of the process, i.e. healing.

A next step is the necessity of a trigger mechanism. While damage is being introduced by an action (load), a recovery reaction against this action should be triggered at some point to start the healing process. This trigger mechanism needs dimensions in both location (where is the damage) and time (amount of damage).

Once the trigger mechanism has initiated a healing process, some sort of transport is required. In this transport step a healing agent is moved towards the location of the damage in order to perform its healing function. It could be that the healing agent is e.g. filling, replacing and/or reacting in order to counteract the damage in the material.

These general self-healing phenomena are present in all self-healing materials. In this state-of-the-art report the focus is on self-healing phenomena in cement-based materials.

## 1.2 Why Self-Healing in Cement-Based Materials

Concrete is the most widely used man-made building material on the planet, and cement is used to make approximately 2.5 metric tonnes (over one cubic metre) of concrete per person alive per year [1.3]. It is a quasi-brittle material, strong in compression but relatively weak in tension. The concept of concrete dates back to at least the Roman era, see Fig. 1.1. An assembly of stones or gravel can convey compressive loads provided that that assembly is held together. This can be done by mechanical means, but already the Romans knew that some glue would be helpful. In building a wall they used for the visible sides cut stones to form a

network, but all kinds of smaller stones and rubble were used for the foundation and middle parts of the wall. To withstand larger compressive loads the available space within a formwork should be filled as efficiently as possible. Therefore, the smaller pores were filled with sand, dirt and initially some binding lime that would dry out and harden under the influence of air. Over time, it was discovered that the lime binding component would also provoke some hardening under water, when the dirt included volcanic ashes.

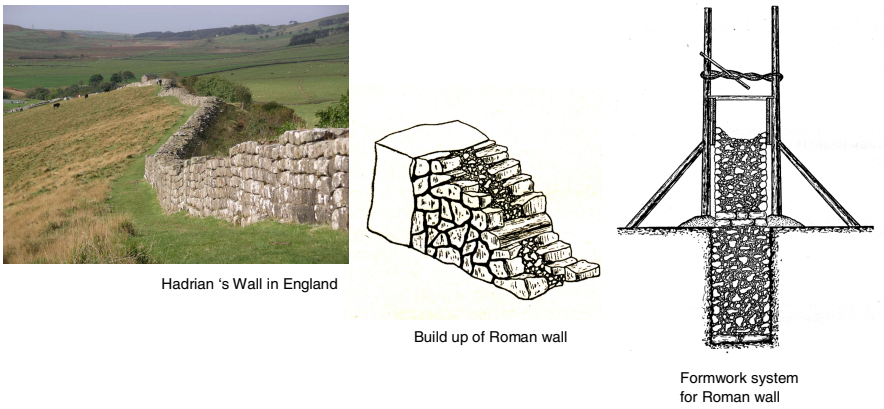


**Fig. 1.1** Hadrian's Wall in England and a scheme of Roman wall building

Surprisingly, modern concrete initiated with the patenting of Portland cement in the nineteenth century is quite a look-alike of its Roman predecessor. The same principle of filling space within formworks as economically as possible using only the smallest amount of a binding constituent to keep everything together is still being pursued today. Today Portland cement forms the overwhelming majority of our binding constituent. The reaction of Portland cement with water results in hydration products, which glue the constituents together.

The production of 1 tonne of Portland cement, for example, produces approximately 1 tonne of $CO_2$ when the emissions due to calcination and fuel combustion required to power the kiln are combined [1.3]. Considering that about $2.35 \times 10^9$ tonnes of cement are used annually worldwide (2007), the $CO_2$ emissions associated with the production of cement are very significant, and are estimated to be in the order of 5 - 7% of the total $CO_2$ production in the world. Given the rapid growth of China's and India's economies, which are the two largest consumers of cement currently, this figure is expected to increase if the technology to produce cement remains unchanged.

An enhanced service life of concrete structures will reduce the demand for new structures. This, in turn, results in the use of less raw materials and an associated reduction in pollution, energy consumption and $CO_2$ production. Statistics convincingly show the enormous amounts of money spent by society due to the

lack of quality and durability of concrete structures. The cost for reconstruction of bridges in the USA has been estimated between $20 billion and $200 billion [1.4]. The average annual maintenance cost for bridges in that country is estimated at $5.2 billion. Comprehensive life cycle analyses indicate that the indirect costs due to traffic jams and associated lost productivity are more than 10 times the direct cost of maintenance and repair [1.5]. In The Netherlands one third of the annual budget for large civil engineering works is spent on inspection, monitoring, maintenance, upgrading and repair. In the United Kingdom repair and maintenance costs account for over 45% of the UK's annual expenditure on construction [1.6]. With such large impacts on society it seems reasonable to take a closer look at cementitious materials.

The compressive strength of traditional concrete varies between 20 and 60 MPa. By using a low water/cement ratio, improved particle packing and special additives, high strength concrete can be produced with strength values up to 150 to 200 MPa. Cement-based composites have even been produced with compressive strengths up to 800 MPa. As an optimised stacking of particles, concrete can bear far less tensile loading than compressive loading. Therefore, concrete elements loaded in bending or in tension easily crack. To counteract that effect reinforcement is installed. Passive reinforcement is activated as soon as the concrete cracks. The formation of cracks is considered an inherent feature of reinforced concrete. It must be emphasized that in reinforced concrete structures cracks as such are not considered as damage or failure and cracking as such does not indicate a safety problem. The crack width, however, should not exceed a prescribed crack width limit. Cracks which are too wide may reduce the capacity of the concrete to protect the reinforcing steel against corrosion. Corrosion of reinforcing steel is the major reason for premature failure of concrete structures. Apart from these macro-cracks very fine cracks, i.e. microcracks, may occur within the matrix due to restraint of shrinkage deformations of the cement paste. Microcracks are an almost unavoidable feature of ordinary concrete. If microcracks form a continuous network of cracks they may substantially contribute to the permeability of the concrete, thus reducing the concrete's resistance against ingress of aggressive substances.

Even though cracks can be judged as an inherent feature of reinforced concrete and the existence of cracks does not necessarily indicate a safety problem, cracks are generally considered undesirable for several reasons. It can be caused by (among other things) shrinkage, loading, thermal expansion, phase expansion during freezing and thawing, or creep. The presence of cracks may reduce the durability of concrete structures. In cases where structures have to fulfil a retaining function, cracks may jeopardize the tightness of the structure. Completely tight concrete may be required in case the structure has to protect the environment against radiation from radioactive materials or radioactive waste. Cracks may also be undesirable for aesthetic reasons.

The performance of structures with elapse of time is often presented with graphs like that shown in Fig. 1.2 [1.2]. Curve A describes how after some time gradual degradation occurs until the moment that first repair is urgently needed.

The durability of concrete repairs is often a point of concern. Very often a second repair is necessary only ten to fifteen years later. Spending more money initially in order to ensure a higher quality often pays off. The maintenance-free period will be longer and the first major repair work can often be postponed for many years (Fig. 1.2 curve B and Fig. 1.2b). Apart from saving direct costs for maintenance and repair the savings due to reduction of the indirect costs are generally most welcomed by the owner.

The experience is that a higher initial quality of the material results in postponement of repair and, in the end, a reduction of the costs for maintenance and repair. This raises a logical question concerning the optimum balance between increasing the initial costs and the cost savings for maintenance and repair. The extreme case would be that no costs for maintenance and repair have to be considered at all because the material is able to repair itself.

Fig. 1.2c schematically shows the performance of a structure made with self-healing material. On the occurrence of a small crack or the start of any physical or chemical degradation process, the material gradually starts to self-heal and the structure will regain its original level of performance or a level close to that. Fig. 1.2d illustrates the anticipated costs for such a material. In this figure inflation and interest are not considered. The initial costs will be substantially higher than that of a structure made with traditional concrete mixtures. The absence of maintenance and repair costs, however, could finally result in a financially positive situation for the owner.

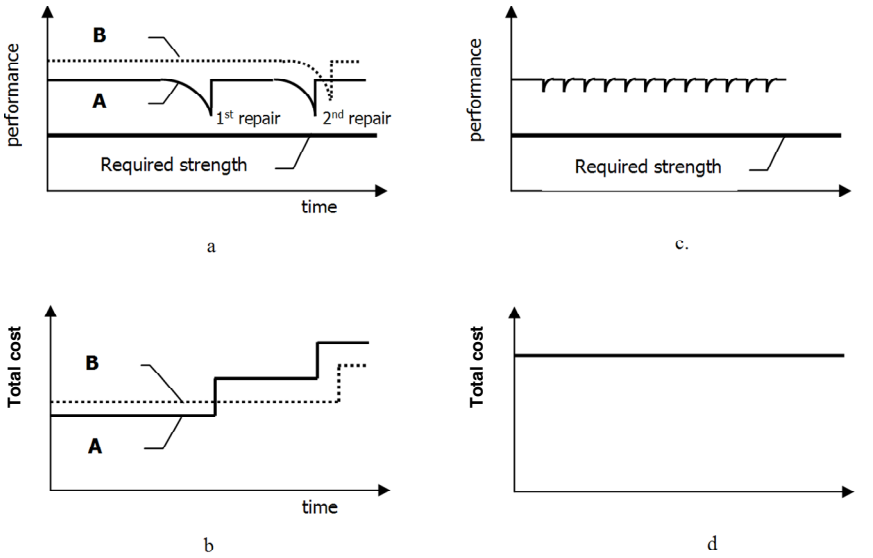


**Fig. 1.2** Performance (a) and costs (b) with elapse of time for normal (A) and high quality (B) structures. Direct costs of repair included. Interest and inflation not considered. Performance (c) and cost (d) of a structure made with self-healing material (concrete) with elapse of time. Interest and inflation not considered.

Historically, concrete in structures has been designed to meet predefined specifications at the start of its life. Longevity of the structure is then monitored through maintenance programs. More recently, however, material scientists have begun to adopt a change in philosophy whereby adaptability or 'self-healing' of the material over time is explicitly considered.

## 1.3 Definitions in an Emerging Field

### *1.3.1 General Framework*

The first association with the word 'damage' is often 'broken' especially in a field of science with a very brittle material like cement-based materials. This has resulted in a wave of research on cracks and fractures. How can cracks be sealed and strength regained? It is easy to get carried away in this direction. Also this state-of-the-art report starts with a crack (cut) in a skin layer.

However, there are many more types of damage that could benefit from healing, e.g. headache or carbonation. A general framework to discuss self-healing should be set-up in such a way that it allows including future inventions such as for instance self-healing of concrete damaged by fire.

In order to do so, the current RILEM committee TC-221 has adapted the reasoning set out in the new *fib* Model Code [1.7]. The Model Code starts from a performance point of view. Such a performance has to be fulfilled according to a maximum design action (e.g. maximum load). In order to do so, the designed structure /material is capable of resisting the maximum design action. At this point the Model Code framework ends.

Taking over in the self-healing concept, damage can occur when either the action (load) is larger than the design load, or the resistance against the action has degenerated due to e.g. environmental actions. The consequence is in both cases that the resistance against future actions is reduced due to the damage. In order to regain more resistance some sort of recovery or self-healing is necessary. When the recovery is provided through the material design concept itself, it is defined as self-healing. When the recovery involves replacement of material by human intervention the action is called repair.

Working from this framework provides a basis for a consistent set of definitions. Not the consequence (a fracture) is taken as the center point of self-healing, but the recovery of performance function is set as the focal point. In the next sections it is shown how this has led to sets of definitions in the emerging field of self-healing.

### *1.3.2 Japan Concrete Institute*

From April 2007 to March 2009 the technical committee TC-075B 'Autogeneous healing in cementitious materials' from the Japan Concrete Institute (JCI) has studied the topic of self-healing intensively. There state-of-the-art report was published in 2009 and a summary of their findings was published in [1.8].

Representatives of JCI TC-075B are also members of RILEM TC-221 and hence the RILEM committee has benefited greatly from the definitions discussions in JCI. It is therefore that first the JCI definitions are introduced here.

Autogenous healing is a common phenomenon seen in a human body. Damage or injuries are automatically healed without any serious operation for themselves. Such a healing function is also provided in concrete. Although concrete is a common material with a long history, with regard to autogenous healing in terms of engineering evolution, we have just begun quantitative approaches with the aim of designing concrete materials and structures that have appropriate healing functions. The phenomenon is well known, but neither its beneficial effects nor their limitations have been well understood yet.

There are many approaches for the autogenous healing in concrete. They can be divided into several groups based on their essential mechanisms of healing. Some of them are often covered by one technical term whereas they are different from each other in the mechanisms. Therefore, in order to clearly understand the concepts concerning the healing in concrete, the committee has proposed the Venn diagram to explain the terminology, as shown in Fig. 1.3.

Let **U** be the universal set that is the collection of all the mechanisms to improve a performance of damaged concretes. It should be noted that this improvement does not necessarily mean the complete recovery of the damaged concretes. As long as a certain property after healing is better than before, the healing function is included as an element of **U**. Therefore, it is likely that a certain property such as permeability is improved after a healing mechanism, but others are not (Fig. 1.4).

There are two subsets **X** and **Y** that represent two major self-healing mechanisms within **U**. Using the sets and the Venn diagram, each technical term is defined as follows;

- **X** Autogenous Healing; a natural process of filling and sealing cracks without any external operations and works.
- **Y** Engineered Healing/Repairing; artificial and intentional methods for filling and sealing cracks. The healing materials or devices are introduced as a designed function into concrete in advance.
- $\mathbf{X \cup Y}$ Self-healing/Repairing; processes of filling and sealing cracks that automatically take place in situ without any practical works by workers.
- $\mathbf{[A] = X \cap Y^c}$ Natural Healing; natural phenomena of filling and sealing cracks that result from some chemical reactions (i.e. late hydration and carbonation) or mechanical blocking at crack faces. Those reactions for the healing are inherent function of concrete.
- $\mathbf{[B] = X \cap Y}$ Autonomic Healing; involuntary healing of cracks that are provided by admixtures. The admixtures such as fly ash and a specific expansive agent are intentionally incorporated into concrete in advance.
- $\mathbf{[C] = X^c \cap Y}$ Activated Repairing; Automatic repairing using some artificial devices which usually consist of sensors and actuators. Repairing function is given by different substances from original constitutions of concrete. This may be considered as “intelligent materials” or “smart systems” for concrete structure.

- $(X \cup Y)^c$ Repairing; general repairing which needs practical works and treatments in situ by workers. Decision to repair cracks or defects is made by responsible engineers after the inspection of deteriorated concrete structure.

It should be noted in Fig. 1.3 that the areas of each subset, their union and intersection do not have any strict meanings in a set space of the healing technology. However, if the number of elements is considered as a measure of each set, the areas may approximately correspond to the numbers of possible

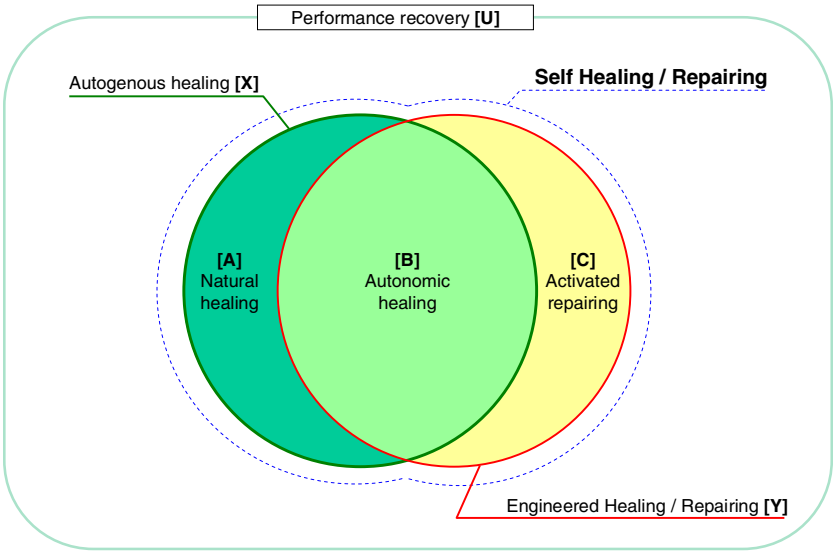


**Fig. 1.3** Venn diagram to explain terminology of self-healing according to JCI TC-075B

**Table 1.1** Examples of elements belonging to each set in Fig. 1.3 according to JCI TC-075B

| Sets | Terms on healing | Examples | Evolution of mechanisms |
|---|---|---|---|
| [A] | Natural healing | Hydration of residual cement<br>Carbonation / precipitation of reaction products | Potential |
| [B] | Autonomic healing | Pozzolanic reaction of fly ash<br>ECC with fly ash<br>Special expansive agents<br>Geo-materials | |
| [C] | Activated repairing | Micro capsules<br>Healing material containing brittle pipes that are embedded in concrete<br>Heat evolution from devices<br>Usage of shape memory alloy<br>Combination with monitoring techniques | Engineered |

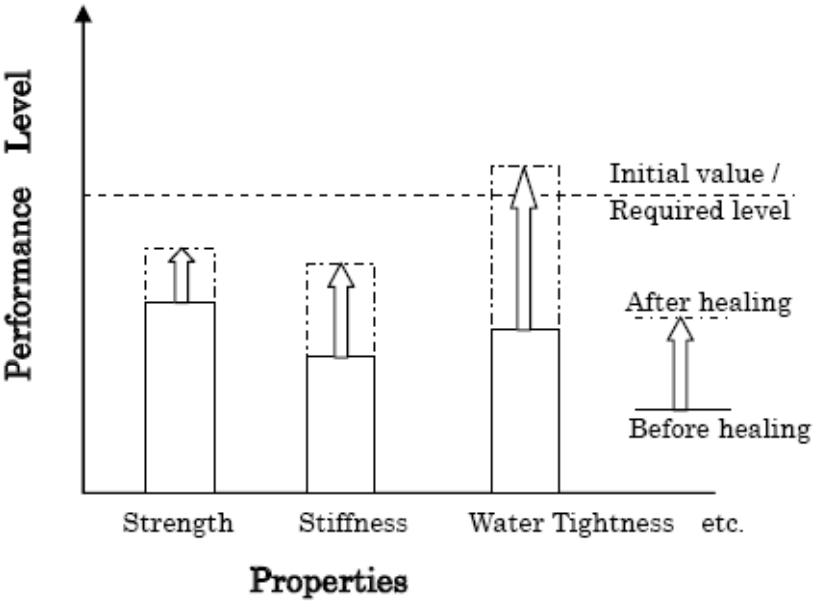


**Fig. 1.4** Concept of performance recovery by a healing function

approaches in each healing mechanism. Examples of approaches or methods used hitherto for each healing function are given in Table 1.1. There are relatively many approaches in $\mathbf{[C] = X^c \cap Y}$ whereas $\mathbf{[A] = X \cap Y^c}$ has a few.

### *1.3.3 Evolved Definitions Proposed by RILEM*

The definition discussion within RILEM evolved to proposing clear definitions for general processes (beyond cracking) that honoured the strong brand name of self-healing. Also the definitions should not be too detailed, thereby making the necessary definitions too complex. This resulted in the following set of definitions by RILEM;

- Self-healing: any process by the material itself involving the recovery and hence improvement of a performance after an earlier action that had reduced the performance of the material.
  - Autogenic: the self-healing process is autogenic when the recovery process uses materials components that could otherwise also be present when not specifically designed for self-healing (own generic materials).
  - Autonomic: the self-healing process is autonomic when the recovery process uses materials components that would otherwise not be found in the material (engineered additions).

Cementitious materials have the innate autogenic ability to self-heal, since re-hydration of a concrete specimen in water can serve to kick-start the hydration process, when the water reacts with pockets of unhydrated cement in the matrix. Also the formation of calcite can be placed here. Autonomic systems, in which foreign materials disperse chemicals in response to cracking, have received the bulk of the attention in research. Inspired by the development of self-healing plastics and composites [1.9, 1.10], these methods include glues and resins contained in brittle fibers [1.11, 1.12], self-healing mechanisms activated by heating devices [1.13], 'expansive agents' coupled with various carbonate additives [1.14], and minerals excreted by immobilized microorganisms [1.15, 1.16].

Using this set of definitions the entire field of self-healing can be described. The committee stresses, that many discussions can be solved by giving attention to the actual self-healing mechanism and particularly the trigger mechanism of the self-healing process. For instance, a sensor showing a result to a human, who in turn needs to press a button or to provide heat input to the material in order to start the self-healing process, is still all considered part of a self-healing process. According to the committee these differences rather point to the level of intelligence of the material (see next section). Only when material needs to be replaced or added from outside, the process is not considered self-healing anymore, but should be termed repair.

Compared to the JCI definitions there is a large interpretation difference for the terms autogenic and autonomic self-healing. According to the RILEM set the terms define two different types of self-healing processes. According to JCI however, the autonomic self-healing is part of the autogenic self-healing processes. Furthermore, according to the RILEM definitions, adding some more cement to increase the amount of unhydrated cement grains is considered to be a autogenic self-healing solution; unhydrated cement is also present in common concrete. However, according to the JCI definitions the intentional addition of extra cement moves the type of self-healing from natural healing to autonomic healing. The RILEM committee thought this would over complicate the definition issues.

Terming all solutions based on components that would otherwise not be present in a material autonomic self-healing, groups together all engineered additions based on non-generic materials: a glass vial with glue as healing agent for instance. The glass nor the glue would normally be present in the material if it hadn't been designed to provide self-healing solutions. In the terminology of JCI the glass vial with glue would categorize as an activated repairing.

In an emerging field like self-healing it is unavoidable that these different definitions for the same processes are used. Hopefully with this state-of-the-art report some agreements on the use of terms will surface.

### *1.3.4 Different Levels of Intelligent Materials*

As was already mentioned in the previous section, sometimes the definitions are taken even one step further to include the passive or active nature of the

self-healing abilities. A passive mode smart structure has the ability to react to an external stimulus without the need for human intervention, whereas an active mode smart structure requires intervention in order to complete the healing process. Both systems have been tested, in respect to concrete by Dry [1.11], and are illustrated in Fig. 1.5 and Fig. 1.6. A fully passive release system draws its main benefits from the omission of the need for human inspection, repair and maintenance. The requirement for human intervention in an active mode system, nonetheless, allows for a larger degree of control to be exercised, and is thus likely to inspire greater confidence within the end user.

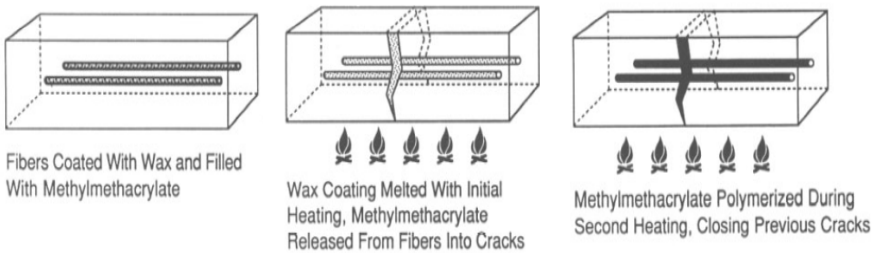


**Fig. 1.5** Active release mode illustrated through the melting of a wax coating on porous fibres containing methylmethacrylate healing agent (Dry [1.11])

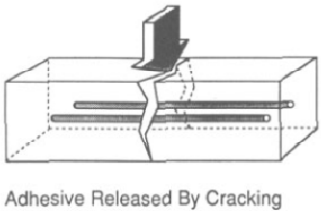


**Fig. 1.6** Passive release mode illustrated through the physical cracking of the brittle fibre under loading (Dry [1.11])

According to the RILEM committee these type of classifications do not refer so much to the self-healing mechanism as it does to the trigger that starts the self-healing process. Hence, it is much more logical to describe the different levels of triggers. Such a description relates to a number of terms which have been used in the literature, such as: intelligent materials, smart materials, smart structures, and sensory structures. There is some ambiguity regarding the definition of these terms within the literature. Based on work of Mihashi *et al.* [1.17] and Sharp and Clemeña [1.18] the following classification is introduced, see Fig. 1.7.

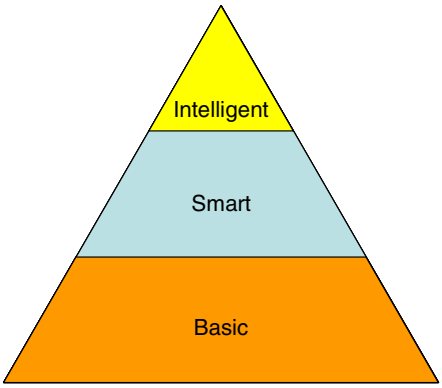


**Fig. 1.7** Hierarchy of materials based on different levels of intelligence

The vast majority of materials belong to the group of *basic materials*. These are the materials that just are. They have no response features.

The next level of materials is the *smart materials*. Smart materials are engineered materials which are able to provide a unique beneficial response when a particular change occurs in its surrounding environment [1.18]. Examples of smart materials include piezoelectric materials, magnetostrictive materials, shape memory materials, temperature-responsive polymers which are able to change colour with temperature, and smart gels which are able to shrink or swell by factors of up to 1000 in response to chemical or physical stimuli. It should be noted that also the term smart structures can be found. However, smart structures are different from smart materials, as smart structures are engineered composites of basic materials which exhibit sensing and actuation properties, due to the properties of their individual components.

The highest level is the *intelligent materials*. These are materials which 'incorporate the notion of information as well as physical index such as strength and durability' as defined by Mihashi *et al.* [1.17]. This higher level function or 'intelligence' is achieved through the systematic incorporation of various individual functions. As a result, intelligent materials exhibit a self-control capability whereby they are not only able to sense and respond to various external stimuli, but conduct this response in a regulated manner. The difference between a smart material and an intelligent material is therefore defined by the degree to which the material can gather information, combine and process this information, followed by reacting accordingly.

This is analogous to the behaviour exhibited by many natural materials such as skin, bone, tendons etc. Schmets [1.19] identifies this inherent 'intelligent' adaptability of natural materials, and states that their outstanding mechanical properties are a consequence of their highly organised hierarchical structure, which is omnipresent at all levels (length scales) of the material. Given their complexity, it is not surprising that such materials are currently not used in practice. The development of man made intelligent materials are still largely at the conceptual and

early design stages, and are confined mainly to the fields of medicine, bionics, and aeronautics/astronautics [1.17].

When the intelligence hierarchy is used for self-healing materials, then the following set of examples can be used to illustrate the different levels. Ordinary concrete materials where cracks are closed by a process of carbonation and mechanical blocking (dirt) rather than anything else (a form of autogenic self-healing) fall in the category of basic materials. Moving from basic to smart materials would be the introduction of encapsulated healing agents like encapsulated bacteria spores that 'wake up' once water reaches their position through a crack. The bacteria then start to produce calcite to close the crack. An example of the intelligent materials level would need to include some sort of sensor and feedback mechanism. This could be e.g. a corrosion sensor on reinforcement only triggering a self-healing mechanism when the reinforcement actually has started to corrode. The majority of the current self-healing processes are in the level of basic to some smart intelligence.

## 1.4 Outline of the Report

The outline of this state-of-the-art report is one of discovery development: with each chapter more and more is revealed on the possibilities of self-healing processes.

After the introduction and definitions as presented in chapter one, chapter two provides information on the different experimental techniques that have been used to study self-healing. It is one thing to damage a sample; it requires more skill to apply the same level of damage and the same type of damage in order to study the effect of self-healing processes.

In chapter three and four a shift is made towards the actual self-healing mechanisms. In chapter three the focus is on recovery against environmental actions. Regaining durability performance is the goal here. In chapter four the bar is raised to regain (also) mechanical strength. Sometimes arbitrary choices have been made as many processes occur to recover both durability and strength. Leading has been in such cases the primary reason for introducing self-healing mechanisms.

In chapter five some of the processes that have been dealt with in chapters three and four are approached by using computer modeling. Such an approach provides insight in boundary conditions, maximum levels of recovery and future potential.

Chapter six starts with a brief but inspiring overview of self-healing in materials other than cement-based systems. Next, some first examples of self-healing cement-based materials in practice are shown. These examples introduce the era of application: it is really possible to make and rely on self-healing materials. The second part of this chapter builds on these examples and paints a panorama of possibilities for the (near) future and what still needs to be done to achieve this.

## 1.5 Link to Other RILEM TC's

Self-healing phenomena as defined and described in this state-of-the-art report has many links to topics in the RILEM community. In this section a cross-section with RILEM TC's has been made on four specific matters: repair, design of materials, durability and testing. A brief overview follows from RILEM Technical Committees active in these areas.

### *1.5.1 Field of Repair*

The origin of self-healing starts obviously with the notion of repair. Self-healing is not necessary if materials do not need to be repaired because they never failed to fulfill their functions. As TC-193 'Bonded cement-based material overlays for the repair, the lining or the strengthening of slabs or pavements' has noted, millions of square meters of concrete overlays are performed each year throughout the world, still without much guarantee of success from a durability standpoint. Hence, repair is a necessity. The committee objective is to set up design rules and practical recommendations specific to cement-based bonded overlays, specifically in the field of repairs in order to eliminate or reduce drastically hazard in the design and in the process. With the work described in the current state-of-the-art report an additional route of dealing with such problems may be provided.

### *1.5.2 Design of Materials*

Once self-healing is considered as a possible solution for prevention of future repairs, the necessary preventive or repair action needs to be designed into the material concept. As one alternative may be ongoing hydration, the key question becomes the availability of water. C-196 'Internal curing of concrete' has this topic as their main field of activity. Although initiated from the phenomena of autogeneous shrinkage, their report [1.20] contains many aspects also influencing self-healing.

One step further would be designing sensoring and actuating mechanisms into the material itself to induce self-healing processes. At this nano-level of designing, the work of TC-197 'Nanotechnology in constructing materials' is worth mentioning. The aim of the committee is to identify where in the area of construction materials nanotechnology already has, or shows potential, to have a significant effect.

### *1.5.3 Durability*

When asked where to apply self-healing materials, common replies include places where it is difficult to get to for other forms of repairs; or places where you rather would not get close to for repairs. Examples of the latter are nuclear waste facilities. Reinforced concrete is a major construction material for the facilities

and structures involved in the processing, the long-term storage, and the disposal of radioactive waste materials generated by the nuclear fuel cycle. TC-226 'Reinforced concrete in the context of nuclear waste management' is active in this area, and repair techniques to extend the performance period are one of their attention areas.

Long exposure in a completely different field is found in aqueous environments. While it is often crucial to have some sort of transport medium available in self-healing processes, too long of an exposure could be harmful in itself. When concrete is subjected to a process of degradation whereby ion exchange reactions occur, the microstructure can be broken down and the material is weakened. TC-211 'Performance of cement-based materials in aggressive aqueous environments' focus on processes where the main form of degradation relates to leaking or hydrate alteration by ion exchange.

Even more severe than gradual breakdown is concrete cracking. TC-214 'Concrete cracking and its relation to durability: Integrating material properties with structural performance' considers the influence of cracking in the life-cycle performance of concrete facilities. The current state-of-the-art report includes self-healing of cracks and does provide interesting material for TC-214.

Reducing cracks through self-closing requires that crack width is not too large. One option to reduce this is by using Strain-Hardening Cement Composites (SHCC). These are classes of fibre-reinforced cement-based composites in which crack formation in the cement-based matrix is controlled by fibres bridging cracks to the extent that multiple, closely spaced fine cracks form at increasing tensile deformation and force. This unique class of concrete material exhibits strain-hardening behaviour under uniaxial tension in contrast to tension-softening behaviour in most other cementitious materials and is under investigation by TC-208 'High performance fibre reinforced cementitious composites'. TC-FDS 'A framework of durability design of fibre-reinforced strain-hardening cement-based composites' has just started looking into the durability framework of these materials.

Another committee having a framework approach is TC-230 'Performance-based specifications and control of concrete durability'. The aim of the work of the committee is to develop guidelines on how to apply methods in practice for performance-based specifications of durability and for checking the compliance of the final product (the finished structure) with the specification. They especially look to the penetrability and thickness of the concrete cover, as a function of the exposure conditions and service life design, and for its compliance control through suitable site and/or core testing. It is thought that many of these techniques would also be very valuable for checking the level of self-healing or self-closing that is achieved.

### *1.5.4 Testing*

At the end of the day, when self-healing has occurred, some reliable results on the effectiveness of the self-healing is very useful. Two committees are currently

working in testing areas that could provide very useful information to be used in verifying self-healing effectiveness as well.

TC-212 'Acoustic emission and related NDE techniques for crack detection and damage evaluation in concrete' acknowledges the need for development of advanced and effective inspection techniques. They focus on inspection techniques by means of detecting elastic waves.

TC-218 'Sonic methods for quality control of fresh cementitious materials' takes similar methods one step further, from solid materials to the flowable mortar stage [1.21]. This could mean that also liquid like healing agents can be followed non-destructively. Again this could open up more possibilities to study the actual healing process itself.

## References

1.1. Gordon, J.E.: The new science of strong materials, or why you don't fall through the floor. Princeton University Press, Princeton (1968)
1.2. van der Zwaag, S. (ed.): Self-healing materials, an alternative approach to 20 ceturies of materials science. Springer Series in Materials Science, vol. 100. Springer, Dordrecht (2007)
1.3. van Oss, H.G.: Background facts and issues concerning cement and cement data. Open-file report 2005-1152, US Dept. of the Interior & US Geological Survey (2005)
1.4. Yunovich, M., Thompson, N.G.: Corrosion of highway bridges: Economic impact and control methodologies. Concrete Int. 25(1), 52–57 (2003)
1.5. Freyermuth, C.L.: Life-cycle cost analysis for large segmental bridges. Concrete Int. 23(2), 89–95 (2001)
1.6. DTI. Construction statistics annual report 2006, London TSO (2006)
1.7. fib Bulletin No. 55, Model Code 2010 – First complete draft, vol. 1, p. 318 (2010)
1.8. Igarashi, S., Kunieda, M., Nishiwaki, T.: Research activity of JCI technical committee TC-075B: Autogenous healing in cementitious materials. In: Proceedings of 4th International Conference on Construction Materials: Performance, Innovations and Structural Implications, ConMat 2009, Nagoya, Japan. Keynote Lecture, pp. 89–96 (2009)
1.9. Lee, J.Y., Buxton, G.A., Balazs, A.C.: Using nanoparticles to create selfhealing composites. The Journal of Chemical Physics 121(11), 5531–5540 (2004)
1.10. White, S.R., et al.: Autonomic healing of polymer composites. Nature 409(6822), 794–797 (2001)
1.11. Dry, C.: Matrix cracking repair and filling using active and passive modes for smart timed release of chemicals from fibers into cement matrices. Smart Materials and Structures 3(2), 118–123 (1994)
1.12. Li, V.C., Lim, Y.M., Chan, Y.-W.: Feasibility study of a passive smart selfhealing cementitious composite. Composites Part B: Engineering 29(6), 819–827 (1998)

1.13. Nishiwaki, T., et al.: Development of Self-Healing System for Concrete with Selective Heating around Crack. Journal of Advanced Concrete Technology 4(2), 267–275 (2006)
1.14. Kishi, T., et al.: Self-healing behaviour by cementitious recrystallization of cracked concrete incorporating expansive agent. In: First International Conference on Self-healing Materials, pp. 1–10. Springer, Noordwijk aan Zee (2007)
1.15. Bang, S.S., Galinat, J.K., Ramakrishnan, V.: Calcite precipitation induced by polyurethane-immobilized Bacillus pasteurii. Enzyme and Microbial Technology 28, 404–409 (2001)
1.16. Ghosh, P., et al.: Use of microorganism to improve the strength of cement mortar. Cement and Concrete Research 35(10), 1980–1983 (2005)
1.17. Mihashi, H., Kaneko, Y., Nishiwaki, T., Otsuka, K.: Fundamental study on development of intelligent concrete characterized by self-healing capability for strength. Transactions of the Japan Concrete Institute 22, 441–450 (2000)
1.18. Sharp, S.R., Clemena, G.G.: State of the art survey of advanced materials and their potential application in highway infrastructure, pp. 1–41. Virginia Transportation Research Council, Charlottesville (2004)
1.19. Schmets, A.J.M.: Self-healing: an emerging property for new materials. Leonardo Times (2003), http://www.tudelft.nl/live/binaries/ca7822ae-5305-4162-8477-28a88507da1f/doc/Article%20Self%20Healing%20Materials.pdf (accessed: April 23, 2008)
1.20. Kovler, K., Jenssen, O.M. (eds.): Internal curing of concrete – State-of-the-art report of RILEM Technical Committee 196-ICC. RILEM Publications SARL (2007)
1.21. Reinhardt, H.W., et al.: Recommendation of RILEM TC 218-SFC: Sonic methods for quality control of fresh cementitious materials. Materials and Structures 44(6), 1047–1062 (2011)

# 2 Experimental Techniques Used to Verify Healing

O. Çopuroğlu[1], E. Schlangen[1], T. Nishiwaki[2], K. Van Tittelboom[3], D. Snoeck[3], N. De Belie[3], and M.R. de Rooij[4]

[1] Microlab, Delft University of Technology, The Netherlands
{o.copuroglu,H.E.J.G.Schlangen}@tudelft.nl
[2] Tohoku University, Japan
ty@archi.tohoku.ac.jp
[3] Magnel Laboratory for Concrete Research, Ghent University, Belgium
{Kim.VanTittelboom,Didier.Snoeck,Nele.DeBelie}@UGent.be
[4] TNO, The Netherlands
mario.derooij@tno.nl

## 2.1 Introduction

There are many techniques to study materials. In this chapter the focus of experimental techniques to verify crack sealing (recovery against environmental actions) or crack healing (recovery against mechanical actions) has been limited to techniques that have been used and reported in self-sealing and self-healing research.

To get a look and feel of the topic the chapter starts with a section on techniques which can be used to examine crack healing such as microscopy, X-ray diffraction and Raman spectroscopy. Next, the attention shifts from observing that something has been repaired to how well the repair has been. Following the definitions set out in chapter one, a differentiation has been made between techniques to verify recovery against environmental or mechanical actions. For recovery against environmental actions it turns out that permeability tests are often applied, while for recovery against mechanical actions the regain in strength by mechanical testing is the preferred choice.

## 2.2 Techniques Used to Examine Crack Healing

### *2.2.1 Microscopy*

#### 2.2.1.1 What Can Be Studied with Microscopy?

Traditionally, concrete quality has been evaluated by non-destructive and destructive mechanical tests. In the last two decades, microscopic methods for characterizing the concrete microstructure and assessing its quality have become relatively popular, probably due to the increased availability of related equipment. However, concrete microscopy techniques are certainly not new and have been serving the community since the late 1800s after the initial works of Le Chatelier

M. de Rooij et al. (Eds.): *Self-Healing Phenomena in Cement-Based Materials*, RILEM 11, pp. 19–63.
DOI: 10.1007/978-94-007-6624-2_2 

and Tornebohm on cement clinker minerals. Later, the works of Katharine and Bryant Mather on standardization, Gunnar Idorn on popularizing the use of thin sections, Chatterji and Jeffery on the use of electron microscopy and Walker and Marshall on the use of fluorescent microscopy, set the milestones in the concrete microscopy history [2.1].

Today, concrete microscopy techniques are being used extensively in concrete quality control and mechanical and durability related damage characterization (forensic investigations). Naturally, these techniques are fully applicable to the studies on self-healing of concrete, where characterization of self-healing capable cement-based materials and healing agents, examination of possible damage formations/mechanisms and most importantly assessing the degree of healing is of interest.

In concrete technology, traditionally *fluorescence microscopy* has been applied for studying the nature, frequency and type of cracks. Fluorescence microscopy is a very effective tool for increasing the contrast between space and solid phases which helps to distinguish capillary porosity, air voids and cracks from the hydration products and other solids in the cement-based material microstructures (see Fig. 2.1). This technique is one of the primary tools in (molecular and cell) biology science already for decades while its advantages are proven to be essential in concrete technology since 1980's.

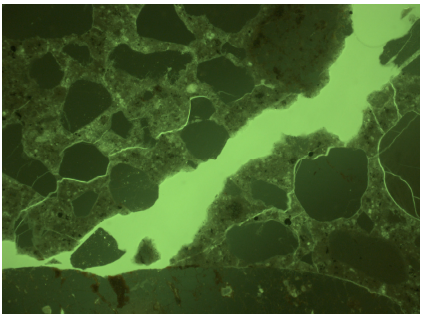

**Fig. 2.1** Photomicrograph of a cracked concrete under the fluorescence light microscope equipped with an excitation filter D470/40x and an emission filter E515LP. Image width [2.87mm].

Fluorescence microscopy is based on exciting fluorescent particles with a typically shorter wavelength light that causes light emission. With the use of special filter sets, it is possible to selectively isolate the area of interest in the material microstructure. In case of concrete, Hudson yellow is by far the most popular fluorophore that is mixed with low viscosity epoxy for impregnating porous concrete. A suitable set for Hudson Yellow comprises excitation and emission filters of SWP450-490nm and LP515nm, respectively. However, the pigment properties used for fluorescence microscopy may vary, therefore for an appropriate selection of filter sets it is recommended to refer to the absorption and emission spectrums provided by the manufacturers.

*Polarized light microscopy* (POL) is a widely used technique in earth sciences and biology due to its remarkable advantages in identification of crystalline solids over other microscopy techniques. Identification can be accomplished relatively quickly based on studying a number of optical properties such as color, relief, birefringence, cleavage etc. Details of this techniques can be found in many text books e.g. [2.2]. Due to the fact that cement-based materials are rich in crystalline materials, POL microscopy plays an important role in characterizing the nature and quantity of primary (hydration related) and secondary reaction products. This technique is also valuable in the contemporary self-healing research because of the fact that important number of healing agents and the healing products are mainly based on crystalline solids like calcite ($CaCO_3$) although amorphous or poorly crystalline phases can also be found.

*Optical microscopy* and *electron microscopy* are two essential techniques in today's cement and concrete research. Both techniques have their strong and weak points.

Arguably the most striking difference between these two techniques is the type of electromagnetic radiation used for rendering an image; light vs. electrons. Being inversely related to the resolution, extreme low wavelength of electrons are able to produce significantly high resolution images compared to its counterpart. Another unique advantage of electron microscopy is that it can detect X-rays emitted after the electron-specimen interaction with the help of an add-on equipment such as energy-dispersive wave-length spectrometer. An additional advantage of electron microscopes is the ability to obtain large depth of field so that also a rough specimen surface can be simultaneously in focus. Optical microscopes, on the other hand, give shallower depth of field as the resolving power is increased.

However, there are a number of points where optical microscopes take the lead. First of all, optical microscopes provide the color of a specimen where it is projected in shades of grey for the electron microscopes. Large field of view is another important aspect which can be achieved by stereo or compound optical microscopes. This point is important especially for quantitative distribution analysis. Need for being able to observe large areas at a glance is very useful and rather representative for the actual concrete quality. The important parameters that can be identified better by increased field of view are among others; crack distribution and length, porosity, air void distribution, aggregate form and distribution, cement paste homogeneity, chemical and mineral admixtures distribution, as well as self-healing agents. It is a possibility that with electron microscopy, one needs to observe numerous views instead of a single view under an optical microscope.

As discussed above, both techniques do have different approaches, however, when available, using both in tandem with each other can produce one of the strongest analytical tools in the material characterization research (Fig. 2.2).

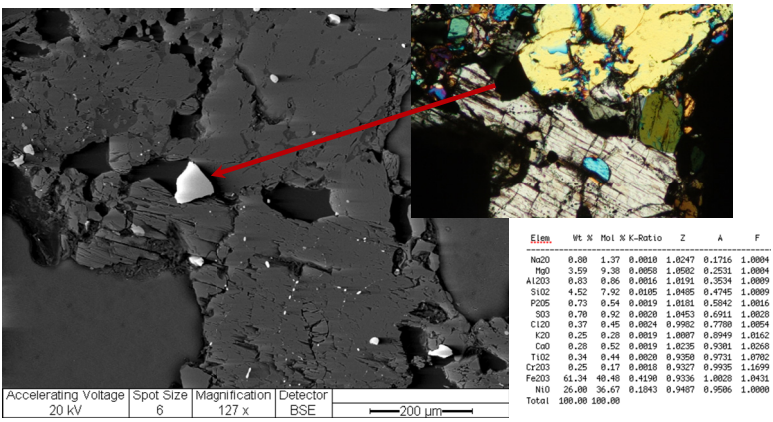


**Fig. 2.2** Backscattered electron and crossed-polarized light photomicrographs of an identical spot on a concrete aggregate. Using both techniques in combination with EDS/WDS increases the degree of accuracy of phase identification.

One of the most overlooked subjects in microscopy analysis studies is the quality of photomicrography. It is not uncommon to see overblown, out-of focus or incorrectly composed photomicrographs of concrete specimens in literature. Good photomicrography is important because of a number of reasons. First of all for archival purposes, photomicrographs must contain as much information as possible. It is often not practical to re-do the work therefore lossless data acquisition is of great importance. Another reason is to disseminate the findings through publications with a high quality. In Fig. 2.3, a good and a bad example of concrete photomicrography can be seen.

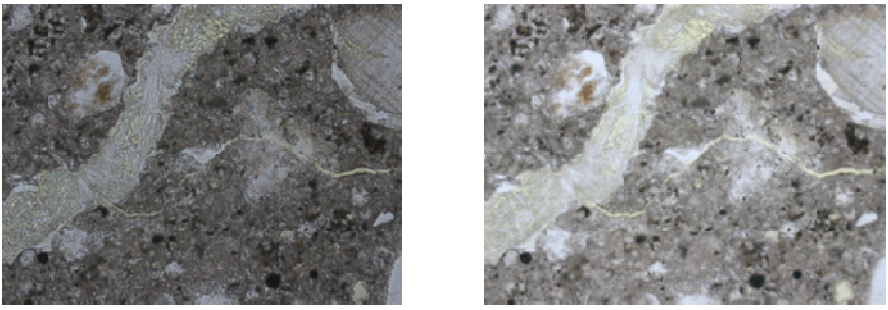

**Fig. 2.3** Optical photomicrographs of crack filling ettringite in concrete. Left; too much contrast, poor resolution and low brightness. Right; optimal resolution and contrast through adjusting the optical elements of the POL microscope according to the Koehler illumination technique. Plane-polarized light. Image width 0.71mm.

As stated by Rost and Oldfield [2.3], good photomicrography is nine-tenth good microscopy and one-tenth good photography. Therefore it is essential to use good quality equipment with correct settings and adjustments. In electron microscopy, image is affected by parameters such as; chamber pressure, electron beam spot size, accelerating voltage and scan rate, so one should adjust these parameters to an optimum degree in order to achieve the best image quality. In optical microscopy, image quality is mainly affected by the placement of the optical elements and illumination source, field and condenser diaphragm settings, and to a lesser degree by the filters. Different from electron microscopy, (digital) cameras are separate equipment and are generally attached to a trinocular tube on a stereo or compound optical microscope. Today, almost all dedicated microscope cameras in the market can deliver acceptable performance as long as color correction is taken care of and camera adapter conversion factor is chosen correctly according to the camera sensor size and microscope's optical system. Alternatively modern digital single lens reflex (DSLR) cameras can be attached to an optical microscope with a proper optical adapter. However, for a demanding scientific work, dedicated microscope cameras with high dynamic range, high color fidelity and low noise features are recommended.

Polymineralic nature of concrete requires high dynamic range cameras, especially in crossed-polarized light microscopy and fluorescence microscopy modes where extreme darkness and brightness coexist. Therefore, one should pay attention to the image histogram and adjust the exposure time accordingly when needed. There is only so much that image adjustment software like Adobe Photoshop or Paint Shop Pro can do after the image is taken.

Once a proper photomicrograph is acquired, it is often necessary to quantify the features of interest unless a qualitative assessment is sufficient. In self-healing materials research these features can be the amount of crack filling healing products or quantification of a change in the porosity of concrete. For such purposes, image analysis (or image processing) software is used. There are many high quality commercial software packages for general use, however for specific applications, the software features should be reviewed before the purchase. A good quality freeware alternative is ImageJ, developed originally for molecular biology research but since its inception, its usefulness is proven in other research disciplines, including concrete research [2.4].

In a typical image analysis software; particle/object size and shape analysis, distribution analysis, filtering, image enhancement, thresholding, area analysis, and point counting are some of the useful features that can be utilized in the self-healing research.

Microscopic investigation in self-healing studies can be grouped as follows:

1. Efficiency and quality control of an employed self-healing material design.
2. Characterization of damage
3. Assessing degree of self-healing

These topics will be discussed in the next sections.

### 2.2.1.2 Efficiency and Quality Control

Ordinary cement-based materials are mainly composite materials which are formed by mechanically mixing various ingredients i.e. cement, water, aggregates and admixtures. Therefore, it is often required to verify if the intended configuration has been realized in the final product. In special cement-based materials like self-healing concrete, the need for controlling the distribution of essential components is additionally critical. A good example for this is the distribution of encapsulated healing agents, where microscopy can be successfully utilized to see whether the distribution is homogeneous and optimal. A number of examples showing the initial conditions of various self-healing materials can be found in the compilation work of v.d. Zwaag [2.5].

Microscopic comparison of pristine, damaged and self-healed specimens has been used by a number of researchers. Li and Yang [2.6] presented self-healing ECC concrete microstructures before and after the self-healing process by use of environmental electron microscopy (ESEM). Jonkers [2.7-2.8] also used ESEM to characterize and compare control concrete specimens and concrete with immobilized bacteria (see Fig. 2.4).

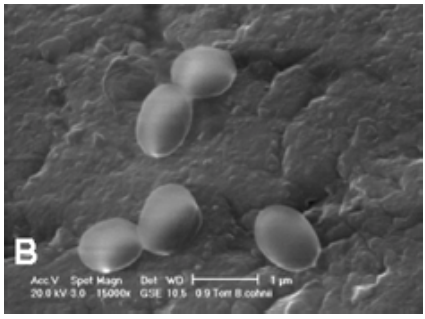


**Fig. 2.4** ESEM photomicrograph of isolated *B. cohnii* spores showing that spore diameter sizes are up to 1 µm [2.8]

### 2.2.1.3 Characterization of Damage

Damage in cement-based materials can be mainly considered in the forms of crack formation and degradation/alteration of other qualities. In order to study the degree of damage, microscopy techniques such as fluorescence microscopy and polarized light microscopy are noteworthy.

In self-healing studies on cement-based materials, fluorescent microscopy plays an important role in quantitative microscopy. This technique helps to correctly measure the dimensional features and frequency of the cracks in a field of interest. Ter Heide *et al.* [2.9] successfully used fluorescence microscopy for in order to observe crack healing. Any change in the porosity of self-healing material can also be easily and accurately monitored by fluorescent microscopy photomicrography. Copuroglu and Sisomphon [2.10] used fluoresence microscopy to document the efficiency of sodium monofluorophosphate healing agent against carbonation in blast furnace slag cement systems (Fig. 2.5).

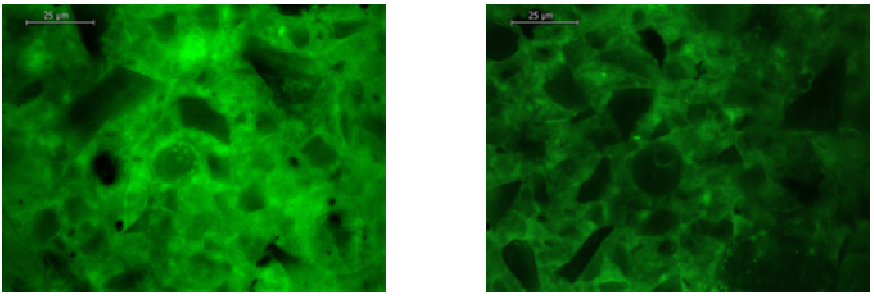

**Fig. 2.5** Photomicrographs of the highly porous carbonated blast furnace slag cement paste (left) and the denser microstructure of an identical paste incorporating sodium monofluorophosphate as a healing agent, upon carbonation (right)

#### 2.2.1.4 Assessing Degree of Self-Healing

An important advantage of using microscopy is to be able to assess the degree of self-healing by combining photomicrography with the quantitative image analysis. One obvious way is to detect the width of a crack before and after the self-healing has been accomplished. Kishi *et al.* [2.11] used stereo optical and electron microscopy to assess the degree of self-healing in concrete containing $C_4A_3\underline{S}$ as the self-healing agent. Wiktor and Jonkers [2.12] also applied stereo optical microscopy on the bacterial concrete surface to observe the self-healing of cracks up to 160 μm with "white crystalline precipitates" (Fig. 2.6). Komatsu *et al.* [2.13], in their conceptual study, used stereo optical microscopy and image analysis to quantitatively measure the (areal) percentage of produced ettringite-based healing material in an artificially generated crack.

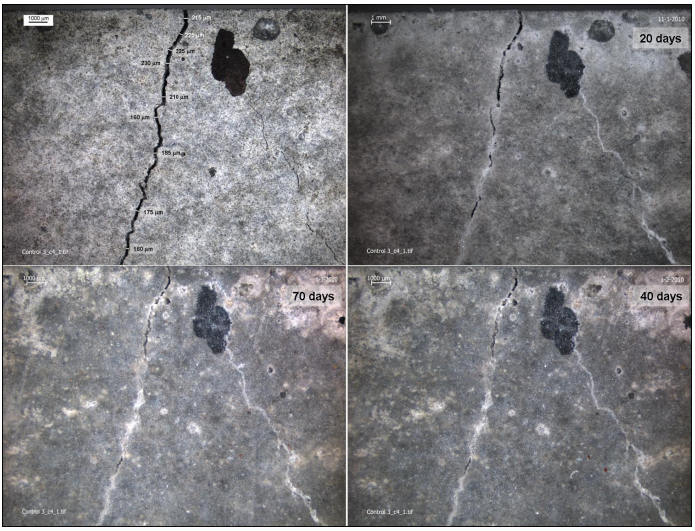


**Fig. 2.6** Stereo optical microscope observation of crack healing on a bacterial concrete surface [2.12]

As calcite is one of the important minerals as a self-healing product POL microscopy is a valuable tool for studying crystalline self-healing products. Calcite is a polymorph of calcium carbonate, which is a crystalline solid, exhibiting a number of unique distinguishing features i.e. extreme birefringence and pleochroism. A variety of complementary staining techniques have also been developed to distinguish carbonate phases. Ettringite, another mineral related to cement hydration is used as a self-healing product to essentially fill in the cracks. Again, POL microscopy is very suitable to distinguish and study this mineral's optical properties such as its needle-like form, low birefringence, and parallel extinction.

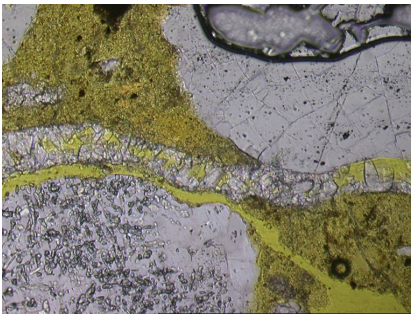

**Fig. 2.7** POL microscope photomicrograph showing re-precipitated $CaCO_3$ effectively closing a crack without completely filling it; 200x magnification (0.7 x 0.45 mm), plane polarized light (Defence wall, Den Bosch); note the relatively well developed crystal faces [2.14].

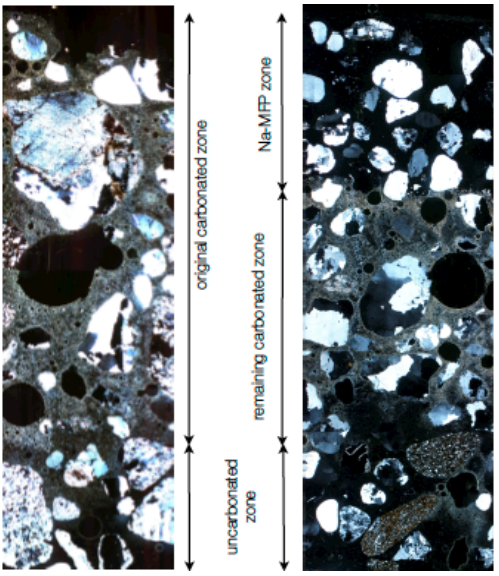


**Fig. 2.8** Condition of carbonated GGBFS cement mortar before (left) and after (right) Na-MFP treatment. Amorphization of the carbonated cement paste is indicated as Na-MFP zone. Image dimensions are ~1.8×5.1mm, Cross polarized light image.

Application of POL microscopy in self-healing cement-based materials is so-far quite limited. Lubelli *et al.* [2.14] used this technique to show self-healing phenomenon in some historical Dutch lime-based mortars. There, the authors indicated the self-healing mechanism by precipitated calcite and portlandite crystals in the cracks (see Fig. 2.7). Copuroglu and Sisomphon [2.10] used POL microscopy for studying carbonated slag-rich mortar and its transformation into amorphous apatite-like solids through a self-healing mechanism triggered by carbonation and sodium-monofluorophosphate. In Fig. 2.8, effect of the healing agent is presented in stitched crossed-polarized light photomicrographs which gives significantly large field of view to see the dispersion of the material condition.

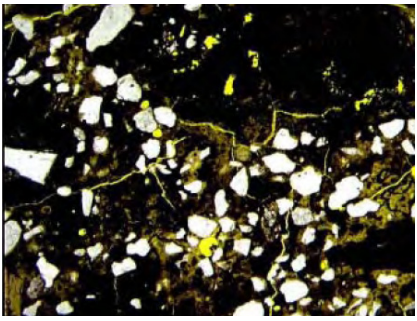

**Fig. 2.9** Microphotograph illustrating cracking in 19th century lime mortar (View 5.4 x 3.5 mm, cross polarized light) [2.15]

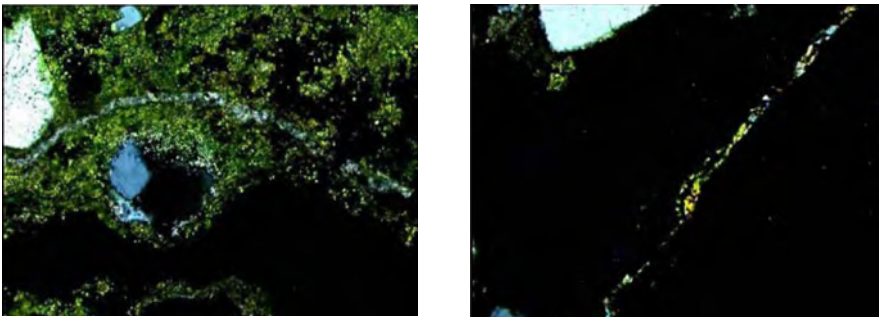

a b

**Fig. 2.10** Microphotograph showing a crack in 19th century lime mortar, filled completely by calcite (View 0.7 x 0.45 mm, cross polarized light) (a) Microphotograph showing a crack in 19th century lime mortar, filled completely by fine grained portlandite (View 0.7 x 0.45 mm, cross polarized light) (b) [2.15]

Nijland *et al.* [2.15] used microscopy to study self-healing of cracks in historic mortars. In Fig. 2.9 a 19$^{th}$ century masonry mortar from a quay wall is shown. The mortar shows severe cracking due to frost action. Several cracks in the mortar show self-healing. In one case, the cracks are filled with Ca-carbonate, almost certainly calcite (Fig. 2.10a). This type of self-healing is common in lime mortars.

Interestingly, there are also cracks filled by fine grained portlandite (Fig. 2.10b). Probably, these represent non-carbonated precursors of the calcite-filled cracks, illustrating that the mechanism of self-healing may be active repeatedly.

## 2.2.2 X-ray Diffraction

The atomic planes of a crystal cause an incident beam of X-rays to interfere with one another as they leave the crystalline material. This phenomenon is called X-ray diffraction. When the diffracted X-rays are recorded, the spacings between layers or rows of atoms can be determined and in this way the crystal structure of an unknown material can be found. XRD was used by Ahn and Kishi [2.16, 2.17] and Haddad and Bsoul [2.18] to study the healing agent. Ahn and Kishi used this technique to examine the crack during healing as shown in Fig. 2.11.

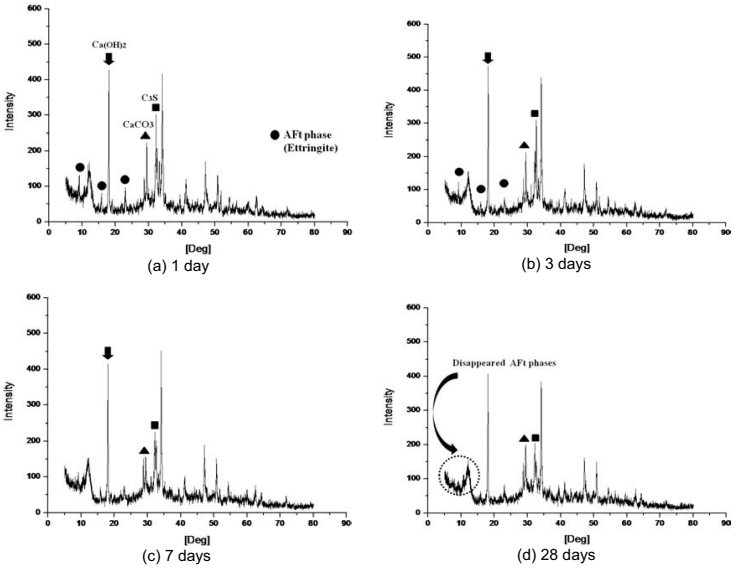


**Fig. 2.11** Main hydration products determined at the age of 1 day, 3 days, 7 days, and 28 days [2.17]

## 2.2.3 Raman Spectroscopy

Raman spectroscopy is a spectroscopic technique based on inelastic scattering of monochromatic light, usually from a laser source. Inelastic scattering means that the frequency of photons in monochromatic light changes upon interaction with a sample. Photons of the laser light are absorbed by the sample and then reemitted. Frequency of the reemitted photons is shifted up or down in comparison with original monochromatic frequency, which is called the Raman effect. This shift provides information about vibrational, rotational and other low frequency

transitions in molecules. Raman spectroscopy can be used to study solid, liquid and gaseous samples.

In order to examine the chemical composition of the self-healing products, Homma *et al.* [2.19] used Raman spectroscopy (see Fig. 2.12). Samples were taken from the uncracked area, the cracked area, and pure calcium carbonate crystals. It can be seen from Fig. 2.12 that the peaks of the cracked area coincided with those of pure calcium carbonate crystals. On the other hand, in the case of uncracked area, such a peak couldn't be observed. Therefore, the authors concluded that the formation of self-healing products was attributed to calcium carbonate crystals.

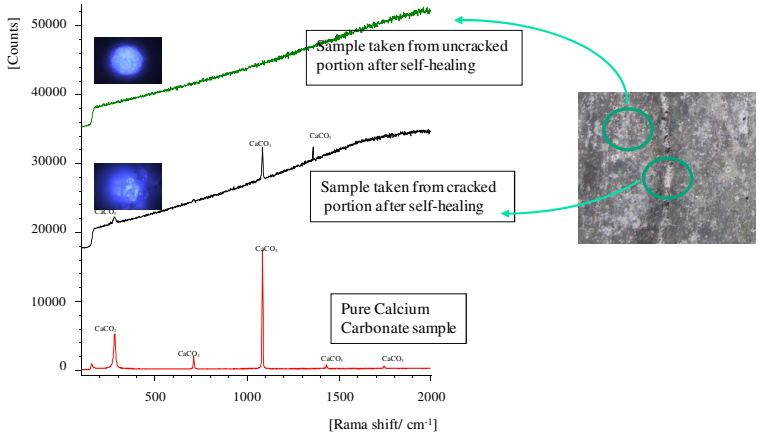


**Fig. 2.12** Raman spectroscopy used to study the products deposited in the healed crack [2.19]

## 2.3 Techniques Used to Verify Recovery against Environmental Actions

### *2.3.1 Permeability*

#### 2.3.1.1 Producing Controlled Cracks

Many of the water permeability devices used currently are inspired by the setup described by Wang *et al.* [2.20-2.21] and Aldea *et al.* [2.22]. Such a setup requires a disc shaped specimen in which a controlled crack needs to be introduced. This can be accomplished by fracturing the concrete disc in a deformation controlled tensile splitting test as shown in Fig. 2.13. The crack opening is measured with LVDT's on the front and back of the specimen and the signal is used as a feedback. At a predefined crack opening the test is stopped and the specimen is unloaded, as shown in Fig. 2.14. This procedure results in cracks with reproducible crack widths.

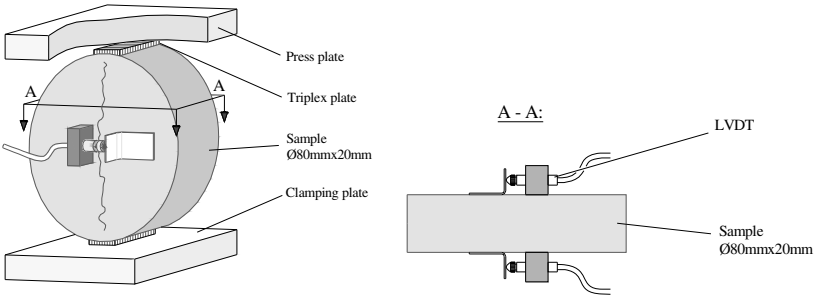


**Fig. 2.13** Side view and top view of the splitting test setup [2.23]

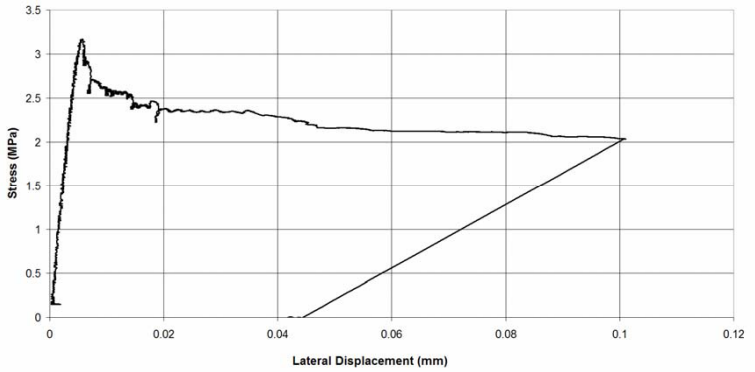


**Fig. 2.14** Typical stress - crack opening displacement in tensile splitting test

Nishiwaki *et al.* [2.24] performed a wedge spitting test in order to create a controlled crack into prismatic specimens. The test setup is shown in Fig. 2.15.

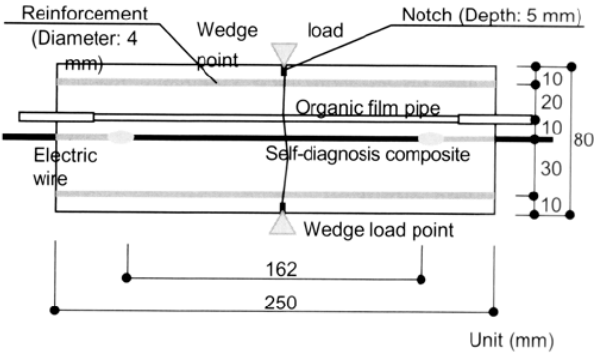


**Fig. 2.15** Wedge splitting test performed by Nishiwaki *et al.* [2.24]

When fibers are mixed in, in order to control the crack width, it is not possible to create one single crack as multiple cracks will appear upon loading. In order to have a comparable amount of cracks, strain-hardening cement-based composite (SHCC) specimens are loaded in a uni-axial tensile test until a predefined strain level is reached. In Fig. 2.16, the uni-axial test setup used by Morimoto *et al.* [2.25] is shown.

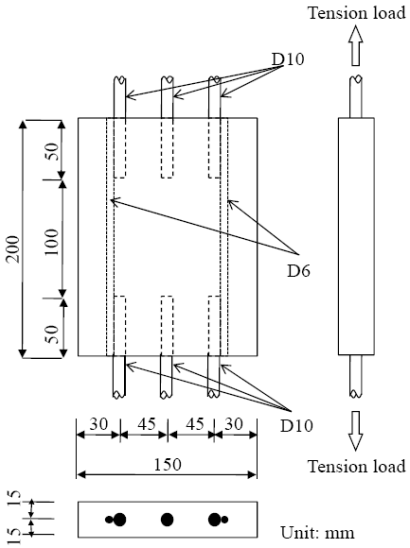


**Fig. 2.16** Uni-axial test setup used by Morimoto *et al.* [2.25]

### 2.3.1.2 Water Permeability

*2.3.1.2.1 Test Devices*

A simple way to confirm effect of self-closing is a permeability test as shown in Fig. 2.17 [2.24]. Nishiwaki *et al.* [2.24] adapted and employed a testing method for water permeability through coating materials. The interface gap between the pipette funnel and the testing plate was sealed with a silicon gel material. The test was carried out until a water volume of 5 cc penetrated through the surface. A comparable test setup has been used by Morimoto *et al.* [2.25].

Fig. 2.18 shows the relationship between the generated crack width and the quantity of water leakage through the crack for relative large cracks. When the test was repeated with a self-closing system, the leakage was very much reduced.

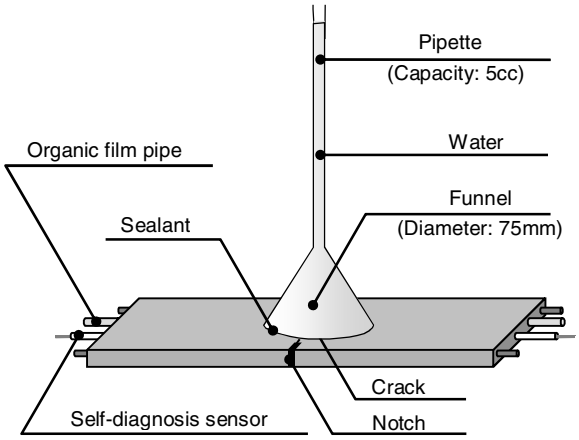


**Fig. 2.17** Water leakage test setup [2.24]

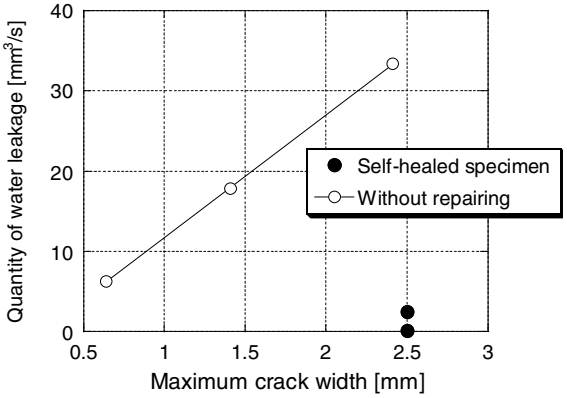


**Fig. 2.18** Relationship between generated maximum crack width versus quantity of water leakage

A slightly modified version was described by Wang *et al.* [2.20-2.21] and Aldea *et al.* [2.22], see Fig. 2.19. In this test, water pressure is generated at the top of the samples by means of a water column. This test can be considered as a low pressure water permeability test. The description that follows is from the procedure as used at the Magnel Laboratory for Concrete Research (Ghent University).

First, cracked samples are vacuum saturated, as described by NBN B 24-213 [2.26], to minimize the amount of air bubbles inside the samples. Afterwards, the test specimens, glued into PVC rings, are mounted between two cylindrical compartments made of Plexiglas as shown in Fig. 2.19. Rubber seals between the

Plexiglas and PVC ring are used to ensure a water-tight setup. At the outer end of the Plexiglas rings, square cover plates, with 2 holes each, are applied and the cell is clamped together with four threaded bars. In one opening in the upper plate a glass pipette with an inner diameter of 10 mm is positioned and it is covered to avoid evaporation. A piece of millimetre paper is adhered to the pipette for measuring the descent of the water column. In the lower plate hole a rubber drain tube is attached and the free end of this tube is positioned level with the lower end of the concrete sample. The two other holes in the top and bottom plate are sealed with a plug and serve to fill both upper and lower cell, including pipette and drain tube, with water. The drop in water level in the pipette, due to water flow through the cracked specimen, is measured at regular time intervals, normally once a day, depending on the water flow rate of the specimen, and water is restored each time to the original level.

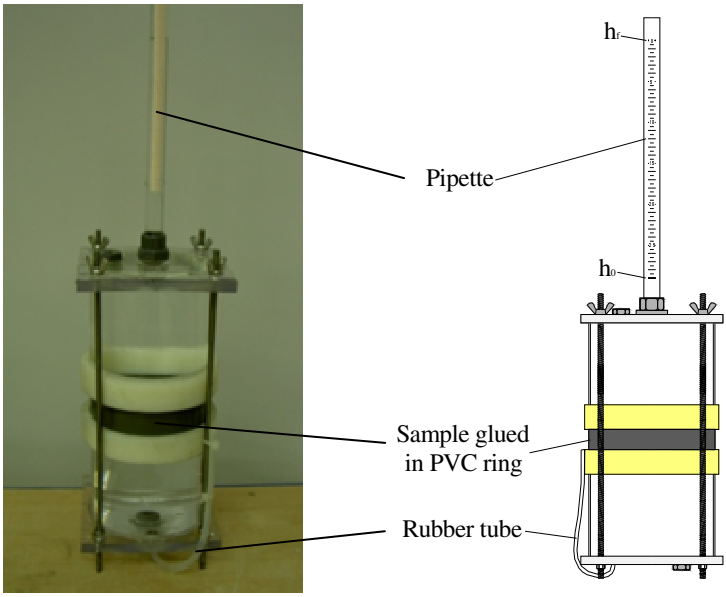


**Fig. 2.19** Schematic of water permeability test equipment at Ghent University

The measured water permeability is not immediately constant but decreases during several days. The decrease is supposedly due to incomplete saturation of the specimens and unavoidable existence of air bubbles in the specimens, even though special care is taken. Consequently, measurements are repeated during several days until a steady state flow is reached and all air bubbles are supposed to have disappeared. A steady state flow is considered to be reached when similar results, for the drop in water level, are obtained during 5 subsequent days. The calculated coefficient of water permeability is based on the average of the latest 5 measurements.

**Fig. 2.20** Set-up for high pressure permeability measurements

At Delft University of Technology a similar setup has been transformed to a high pressure permeability test setup (between 1 and 6 bar, depending on the permeability of the sample). Now the disc is placed in a steel ring and an epoxy is used to ensure that there is no leakage at the edges between disc and steel ring. The steel ring is placed in the device (see Fig. 2.20) and a water pressure is applied at the top of the specimen. The water percolating through the specimen is measured over time via an accurate balance coupled to a computer.

Water permeability has recently also be visualized by means of neutron radiography [2.28]. Small cylindrical specimens, 10 mm in diameter and 20 mm high, were wrapped with self-adhesive aluminum foil along the height. The top and bottom circular planes remained open. The foil reached over the ends of the specimen to obtain two reservoirs that could be used as inlet or outlet. Then, the specimens were manually cracked by means of a screw jack at an age of 7 days. The setup is analogous to the one used in the Brazilian splitting test. The force was manually and slowly increased until a 150 µm crack was formed through the long axis of the cylinder. The aluminum foil provided sufficient stability to maintain a constant crack opening.

At an age of 28 days, the specimens were subjected to water permeability tests and the water movement was visualized by means of neutron radiography [2.28]. The cylindrical specimens, used for the water permeability tests, were positioned as shown in Fig. 2.21, and the upper reservoir was filled with water during the test. The water head applied was 20 mm, the total height of a specimen. With an exposure time of 3 s, every 5 s an image was taken to investigate the time needed for emptying the reservoir through the crack (Fig. 2.22).

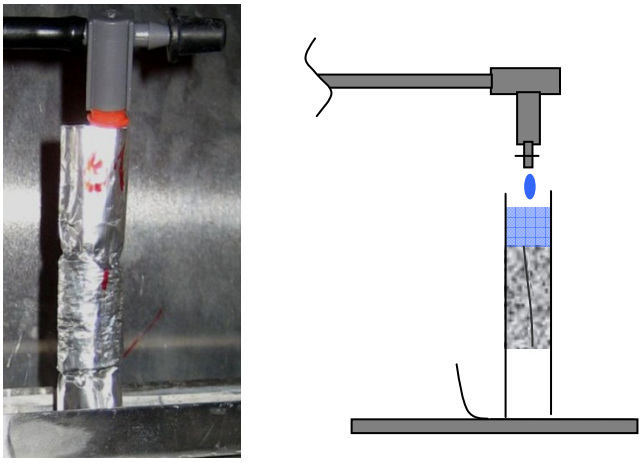

**Fig. 2.21** Schematization of the test setup used for water permeability tests with neutron radiography [2.28]

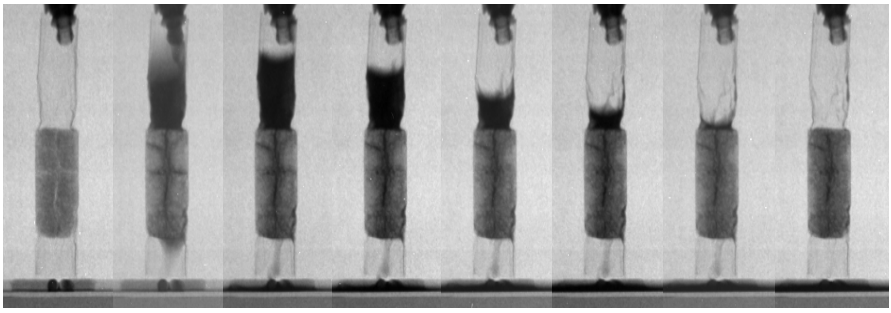

**Fig. 2.22** Visualization of a water permeability test by means of neutron radiography [2.28]

In the research group of Kishi *et al.* [2.27], a field test was conducted to evaluate the water tightness of their self-healing concrete containing expanding additives. Therefore, box-shaped water retaining containers were made from self-healing concrete (Fig. 2.23). After several months curing, cracks were induced at the center of two target side walls by means of a hydraulic jack. Just after inducing the cracks, water was poured into the containers and the amount of water leakage with time was measured at several time steps to estimate the sealing effect by cementitious recrystallization. It was confirmed that sealing of the water leakage through penetrating cracks was improved when using cementitious composite materials with self-healing capability.

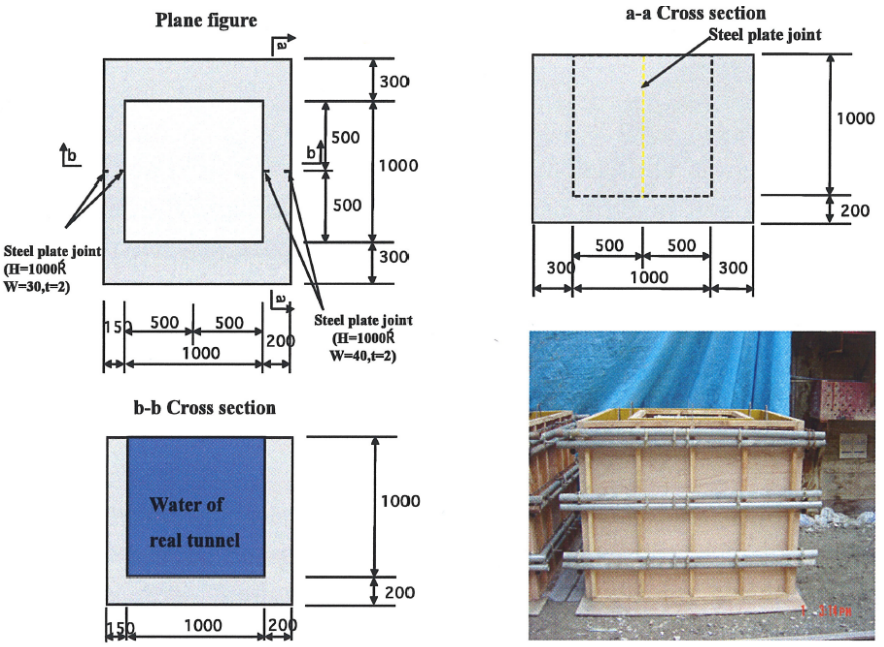


**Fig. 2.23** Outline of the box-shaped water retaining container [2.27]

*2.3.1.2.2 Calculating Water Permeability*

The water permeability coefficient can be calculated using Darcy's law, assuming a (slow) laminar flow. Darcy's law states:

$$Q = k A \frac{\Delta h}{L} \tag{2.1}$$

where $Q$ = the flow rate through the specimen (dV/dt), $k$ = the water permeability coefficient, $A$ = the surface area of the disc specimen, $L$ = the thickness of the specimen and $\Delta h$ = the pressure drop over the sample thickness. Assuming a continuous flow, the amount of water flowing out of the pipe is given by Equation (2.2).

$$\frac{dV}{dt} = -A' \left( \frac{dh}{dt} \right) \tag{2.2}$$

where $V$ = the total volume of water that travels through the sample, $dh$ = the differential of pressure between the initial pressure head $h_0$ and the remaining pressure head $h_1$ at the measured time $t$ and $A'$ = the cross-sectional aea of the pipe. By combining Equations (2.1) and (2.2), Equation (2.3) is obtained.

$$k\frac{\Delta h}{L}A = -\frac{A'\,dh}{dt} \tag{2.3}$$

By integrating Equation (**2.3**),

$$k\int_0^t dt = -L\frac{A'}{A}\int_{h_0}^{h_1}\frac{dh}{\Delta h} \tag{2.4}$$

The water permeability coefficient is finally given by

$$k = L\frac{A'}{At}\ln\frac{h_0}{h_1} \tag{2.5}$$

Another possibility to calculate the flow through a crack is by using the Poiseuille's law

$$q_p = \frac{\Delta p\, w^3 L}{12\, d\, \eta} \tag{2.6}$$

with $q_p$ = the fluid flow [$m^3$/s], $\Delta p$ = pressure difference [Pa], $w$ = crack width [m], $L$ = crack length [m], $d$ = member thickness (depth) [m] and $\eta$ = dynamic viscosity of the fluid [Pa s]. The most important of this law is the third power of the crack width. This means that a small reduction of crack width has a great effect on the flow. Poiseulle's law leads to an overestimation of the flow because it is valid for a parallel opening with smooth surfaces. There are several proposals for the modification of Poiseulle's law, the most simple of which is a constant coefficient of 0.125, i.e. the flow is then $q = 0.125\, q_p$ [2.29].

### 2.3.1.3 Air Permeability

*2.3.1.3.1 Test Devices*

Among many techniques which could be used to measure the permeability of cementitious materials, gas permeability using liquid methanol as the gas source is one of the easiest and fastest. Yang *et al.* [2.30] determined the permeability coefficient of mortar specimens after being subjected to compression loading. Therefore, cylinders, with and without self-healing properties, with a diameter of 50 mm and 100 mm height were loaded under 80% of their respective ultimate compressive strength and set aside for 24 hours. After that, 10 mm thick cylindrical disk specimens were cut from the middle of the cylinders. After vacuum drying for 24 hours, samples were placed on top of the test setup and the edges were sealed with epoxy sealer to avoid leakage of methanol vapour (Fig. 2.24). The initial weight of the setup, including the cell, the methanol liquid, the disk specimens and epoxy sealer was measured at the beginning of the test. The

values of mass variation versus time due to vaporization of methanol liquid at a constant 40°C water bath were continuously recorded until a steady state mass loss was reached.

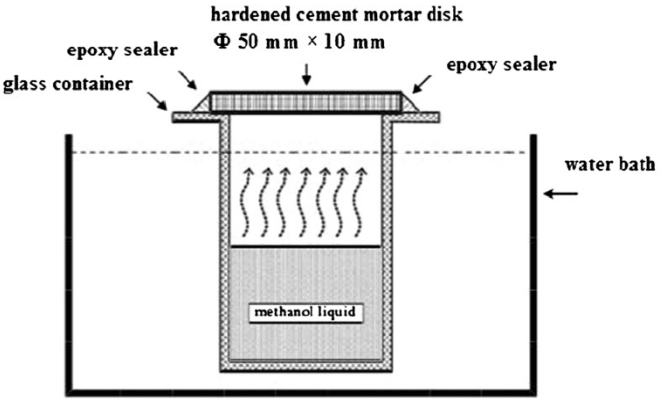


**Fig. 2.24** Schematic illustration of experimental setup for the gas permeability test [2.30]

Morimoto *et al.* [2.25] performed air permeability tests on cementitious specimens, before cracking, immediately after cracking and after crack healing. Air permeability tests were conducted using the Torrent Permeability Tester (TPT), proposed by Torrent [2.31]. It is an absolutely non-destructive test method to check the denseness of the cover concrete and to evaluate durability of concrete structures. The Torrent Permeability Tester device is shown in Fig. 2.25a. The device consists of a chamber, a vacuum pump, a pressure sensor, and a logger. Fig. 2.25b shows a diagram of the chamber. During the measurement, the chamber is put to the concrete surface. The chamber has two cells, inner chamber and outer chamber. Equalizing the pressure of the both chambers, it is possible to make unidirectional air flow.

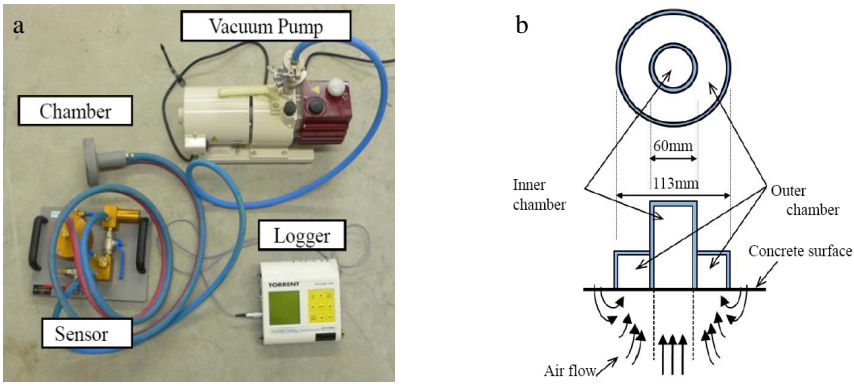


**Fig. 2.25** Torrent permeability tester (a); Conceptual diagram of the chamber (b)

*2.3.1.3.2 Calculating Air Permeability*

Yang *et al.* [2.30], calculated the gas permeability coefficient using the following equations.

$$p_v = 10^{\left(8.0809 - \frac{1582.2}{239.76+T}\right)} \tag{2.7}$$

$$\eta = 10^{-7}\left(4.7169T^{0.618} - 99e^{-8.7593\,x\,10^{-4}\,T} + 94e^{-7.916\,x\,10^{-3}\,T} + 5\right) \tag{2.8}$$

$$Q = \frac{266x10^{-3}\,m'}{10^{\left(8.0809 - \frac{1582.2}{239.76+T}\right)}}T \tag{2.9}$$

$$k = \frac{2L\eta P_2 Q}{A(P_1^2 - P_2^2)} \tag{2.10}$$

Where $p_v$ = the absolute pressure of vapor (N/m²), T = the absolute temperature (K), η = the dynamic viscosity (Ns/m²), Q = the volumetric flow rate (m³/s), m' is het rate of mass loss (g/s), k = the intrinsic permeability coefficient (m²), $P_1$ = the inlet pressure (N/m²), $P_2$ = the outlet pressure (N/m²), L = the length of the sample (m) and A = cross sectional area perpendicular to the flow direction (m²).

Morimoto *et al* [2.25] calculated the air permeability coefficient from Equation (2.11) according to the model of Torrent [2.31].

$$k = 4\left(\frac{V_c(dP_I/dt)}{A(P_a^2 - P_I^2)}\right)^2 \frac{\mu P_a}{\varepsilon}\int_{t_0}^{t}\left[1 - \left(\frac{P_I}{P_a}\right)^2\right]dt \tag{2.11}$$

Where $k$ = air permeability coefficient (m²), $V_c$ = volume of the inner chamber (m³), $A$ = cross-sectional area of the inner chamber (m²), $P_I$ = pressure in inner chamber (N/m²), $P_a$ = atmospheric pressure (N/m²), μ = dynamic viscosity of air (Ns/m²) and ε = empty porosity of the concrete.

### 2.3.1.4 Osmosis

Water, gas and ions permeate through continuous gaps inside cementitious materials. It is known that hardened cement paste has a selective permeability depending on the type and properties of the permeating material, the physical state of the hardened cement pores and the correlation with the chemical properties of the pore surface. Because of the selective permeability, hardened cement, installed between two solutions of different concentrations will allow water to permeate but the solutes and ions will hardly be able to permeate in contrast to water. Due to this, osmotic pressure is generated across the hardened cement [2.32].

On the other hand, hardened cement paste with cracks will contain more gaps or pathways through which water, solutes and ions can pass. In other words there will be a difference in osmotic pressure between hardened cement paste with and

without cracks. Moreover, if cracks are healed as the result of incorporated self-healing properties in the cement paste, the osmotic pressure will also be different [2.32].

Consequently, Song *et al.* [2.32] decided to interpret the crack self-healing efficiency based on the osmotic pressure difference. Therefore, they prepared cylindrical mortar samples (Ø 100 mm, height 8 mm). These samples were polished and adjusted to 4 mm $\pm$ 0.2 mm, after curing for two days at 20 $\pm$ 3°C . Then samples were cured a second time in water for 28 days at 20 $\pm$ 3°C. Afterwards, the osmotic pressure of the reference sample (P1) was measured. In another sample (P2), also consisting of plain concrete, cracks were introduced before the osmotic pressure was measured. For the third sample, with self-healing properties (T1), the osmotic pressure was measured after crack formation and 60 days of water curing at 20 $\pm$ 3°C. The outcome of this experiment is shown in Fig. 2.26.

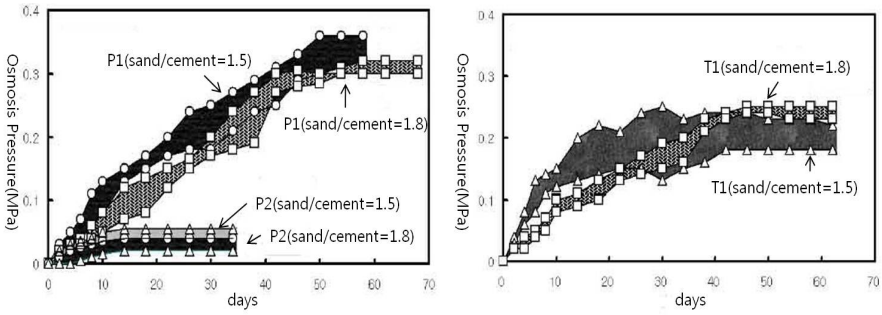


**Fig. 2.26** Osmotic pressure of plain and cracked traditional mortar (A) and osmotic pressure of cracked and healed mortar with self-healing properties (B) [2.32]

## *2.3.2 Capillary Water Absorption*

As the water permeability tests performed by Van Tittelboom *et al.* [2.23] are quite time consuming, they also investigated the possibility to evaluate the crack healing efficiency by measuring capillary water absorption. When cracked mortar samples with and without self-healing properties were 1 month old, they were placed in an oven at a temperature of 50°C. After one week, specimens were removed and the area of the cracked surfaces was determined. Then, the adjacent surfaces were covered with self-adhesive aluminum foil in order to impose unidirectional moisture movement during the test. One day later, specimens were weighed and afterwards the cracked surface was placed on two line supports in a container which was filled with water in such a way that the lower 0.5 cm of the specimens were immersed in water. At regular time intervals, specimens were taken out of the container and placed onto a non-absorptive support for one minute before they were weighed. In Fig. 2.27 results are shown for a cracked mortar sample with and without self-healing properties.

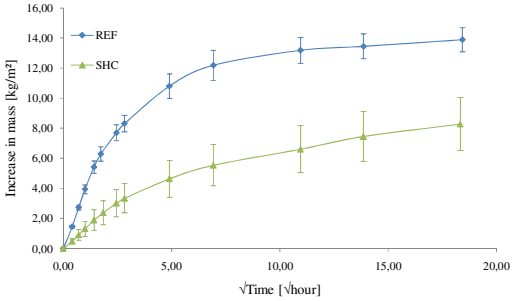


**Fig. 2.27** Capillary water absorption in function of time

A clear distinction can be noticed between the specimens with and without healed cracks. From this, the authors concluded that capillary water absorption tests can also be used to determine crack healing.

The capillary water absorption of the samples mentioned above was also visualized by means of neutron radiography and X-ray radiography [2.33, 2.34]. While the cracked test samples were placed in a water basin, migration of the water front inside the samples was visualized as the difference in intensity of the neutron / X-ray beam passing through the samples. In Fig. 2.28 the test setup of the neutron radiography and X-ray radiography measurements is shown.

From both the X-ray and neutron radiographs water uptake over time could clearly be visualized. In Fig. 2.29 differential X-ray radiographs are shown for a sample with an untreated crack after several contact times with water. The crack and the location of the upper and lower reinforcement bar can clearly be noticed in the X-ray radiographs. In addition, it can be seen that already after 1 minute of contact with water, the crack becomes completely filled with water. Next to the crack, also the zone around the crack at the height of the lower reinforcement bar becomes filled with water. During crack formation, damage will have occurred in the zone around the reinforcement bar and thus these micro-cracks also fill with water. As time goes on, the water front migrates horizontally from the crack into the sample and a bigger part of the sample becomes saturated with water. It becomes more obvious that next to the macro crack, small cracks are present around the lower reinforcement bar as the zone around this bar becomes further filled with water. After two hours of continuous contact width water, almost half of the sample is saturated [2.34].

In Fig. 2.30 for one representative sample of the reference series (untreated crack, REF) and the series with self-healing properties (autonomously healed crack, SHC_PUR), a differential X-ray radiographic image, obtained after 2 h of contact with water, is shown. In the radiographic image of the sample from the test series ‘SHC_PUR’ the positions of the capsules can be noticed.

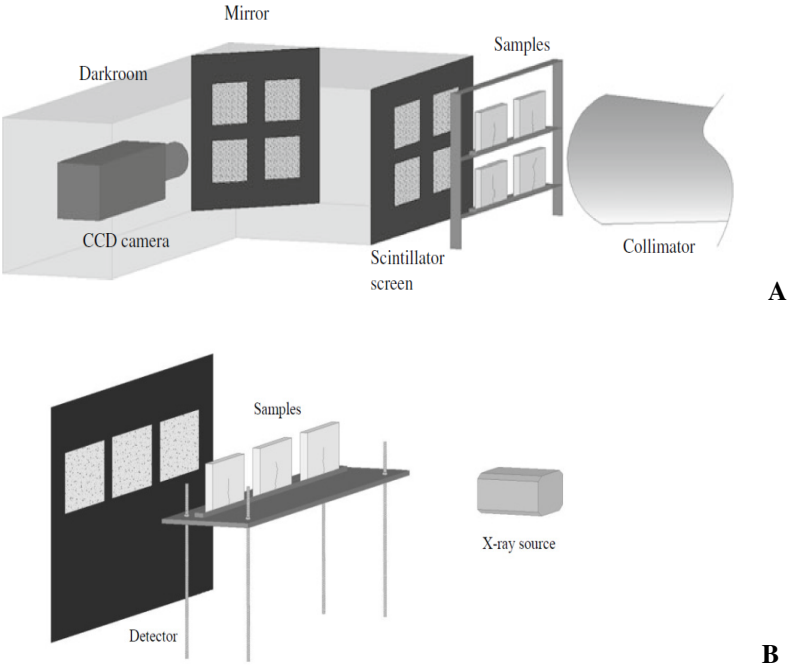


**Fig. 2.28** Test setup used during the neutron radiography experiments. The neutron beam leaving the collimator was attenuated by the samples and detected by the scintillator. When passing the scintillator screen, the beam was turned in the direction of the CCD camera by means of a mirror. (A) [2.33] Test setup used during the X-ray radiographic measurements. The X-ray beams leaves the source, is attenuated by the samples and recorded by the detector. (B) [2.34].

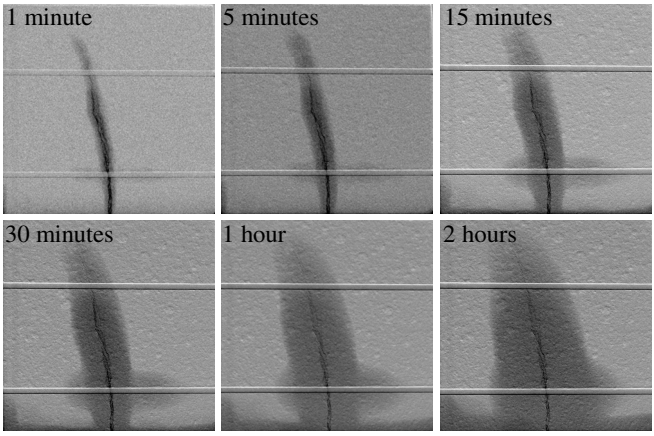


**Fig. 2.29** Differential X-ray radiographs showing the water front at different time intervals inside a sample with an untreated crack [2.34]

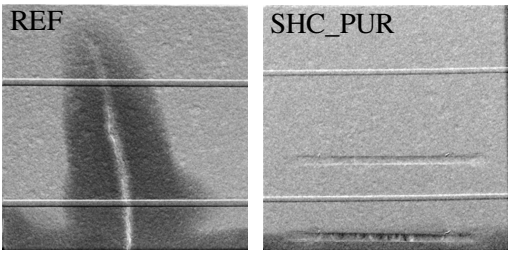


**Fig. 2.30** Differential X-ray radiographs showing the water front after 2 hours of contact with water for one representative sample of each test series [2.34]

After 2 h of contact with water, both samples contain a certain amount of water due to capillary water absorption along the pores of the cementitious matrix. However, the amount of water taken up is dependent on the crack treatment. When the crack has been left untreated, the water front almost reaches the upper side of the sample. When encapsulated polyurethane is embedded inside the matrix, water will not enter the crack even after 2 h of contact with water. In order to prevent reinforcement corrosion, it is important that the water front does not reach the reinforcement location. For a cracked sample which is left untreated the water front reached the reinforcement already after a few seconds of contact with water and thus at that time corrosion may initiate. When cracks are autonomously healed with polyurethane, the reinforcement remains in the dry zone even after 2 h of contact with water.

As neutrons offer a higher hydrogen detection sensitivity compared to X-rays, neutron radiography was additionally used to evaluate the self-healing efficiency. While X-ray radiography can be used to visualize the water uptake by cementitious materials, the advantage of neutron radiography is that next to visualization of the water uptake, this method serves to calculate the amount of water taken up and to plot water absorption profiles.

In Fig. 2.31 (middle), for one representative sample of each test series, a differential neutron radiographic image, obtained after 30 seconds and 24 hours of contact with water, is shown. On the left a picture of the samples themselves is shown on which the crack location and the zone used in the quantitative analysis are indicated. In the graphs on the right, the moisture profile is shown when the sample was in contact with water for 30 s, 1 min, 5 min, 15 min, 30 min, 1 h, 2 h, 4 h and 24 h. The moisture profile was determined as the average water content over a band width of 160 pixels symmetric around the crack and perpendicular to the moisture front (see indicated rectangles in Fig. 2.31 left). In the radiographic image of the sample with self-healing properties the positions of the capsules can be noticed. Also in the graphs the capsule locations are noticed as positions with reduced water content.

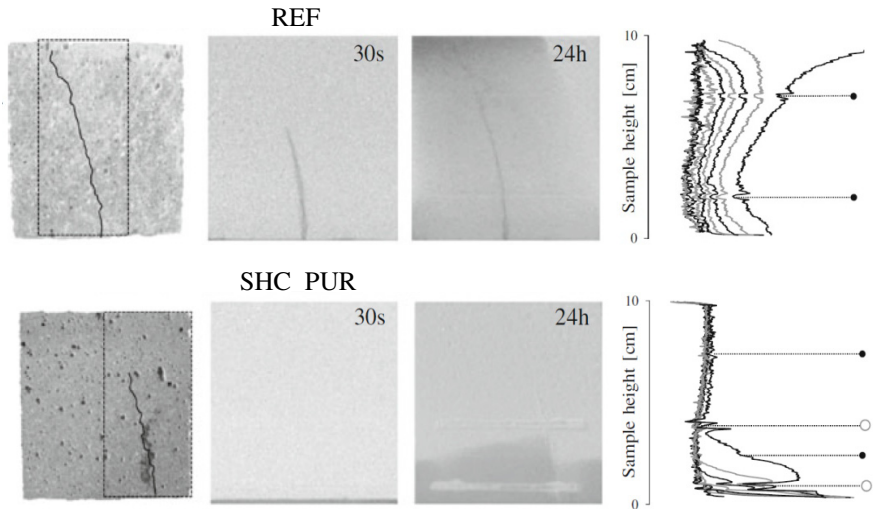


**Fig. 2.31** Neutron radiographs obtained after 30 s and 24 h of contact with water for one representative sample of each test series. The moisture profiles determined at different time intervals are shown on the right. Closed dots represent the position of the reinforcement, open dots render the position of the capsules. On the left a picture of the sample under investigation is shown together with the location of the crack and the zone in which the average water content was calculated. [2.33]

Based on the neutron radiographs, the same conclusions can be drawn as from the X-ray radiographs. The water absorption profiles showed that, in comparison with an uncracked sample (result not shown), a higher amount of water penetrated in the matrix just beside the crack. This is possibly because the mortar matrix was less dense in the zone under the capsules as the capsules prevented the air bubbles, arising during vibration, to escape. As the neutron radiographs also allow a quantitative analysis of the water uptake, the water taken up by each sample of both test series was calculated after 4 hours of contact with water. A significant difference is seen between the efficiency of untreated cracks and autonomously healed cracks. While the mean amount of water absorbed by untreated cracks amounted to 7.3 g, samples with encapsulated polyurethane only took up 2.4 g of water.

### *2.3.3 Resonant Frequency Analysis*

In self-healing of ordinary concrete, Aldea *et al.* [2.35] observed substantial drops in water permeability accompanied by only slight increases in resonant frequency, implying that cracks were filled during the healing process, but that they were unable to totally close. For this reason, water permeability tests are often complimented by resonant frequency analysis.

The presence of cracks causes a drop in the ease with which elastic waves can propagate through cementitious materials. Resonant frequency measurements, based on ASTM C215 (Standard Test Method for Fundamental Transverse, Longitudinal and Torsional Resonant Frequency of Concrete Specimens) can be used to determine the extent of damage (and therefore of healing). This technique is simple, rapid, and non-destructive, but requires standardization using specimens that have been strained to known values before testing is carried out. Control samples must be placed in identical conditions so as to compensate for further bulk hydration caused by exposure conditions (e.g. multiple wet/dry cycles), which can cause changes in resonant frequency values, but is not directly related to the healing process.

### *2.3.4 Ultrasonic Measurements*

Since ultrasonic waves travel much easier in hardened concrete (4000-5000 m/s) than in water (1480 m/s) or in air (350 m/s), they will travel around an open fissure leading to an increase in transmission time. However, when the crack is sealed, the waves will be able to travel through the sealant and the travel time will be reduced. In their research, Abdel-Jawad *et al.* [2.36], Abd-Elmoaty [2.37] and Haddad and Bsoul [2.18] used this technique to determine the self-healing efficiency of concrete specimens. Van Tittelboom *et al.* [2.38] used this technique to determine the crack healing efficiency of bacteria. The used test setup is shown in Fig. 2.32.

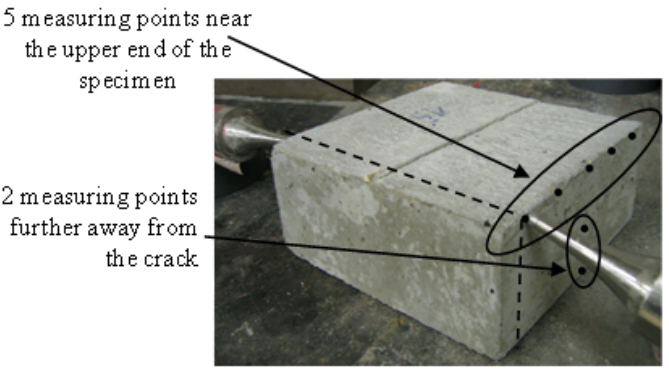


**Fig. 2.32** Ultrasonic transmission measurements with indication of the measuring points (●) and the part of the sample that was sawn off for visual examination (---) [2.38]

### *2.3.5 Electrochemical Impedance Measurements*

Yang *et al.* [2.39], evaluated the efficiency of their self-healing approach using a Gamry Reference 600 Potentiostat/Galvanostat/ZRA instrument to measure

electrochemical impedance spectra (EIS). Electrochemical impedance measurements were performed at 28 days, just after being loaded under 80% of compressive strength, 24 hours and 7 days after being loaded under 80% of compressive strength. Before the EIS measurements were performed, the ends of the specimens were carefully polished and coated with a layer of silver paint. Subsequently, a carbon conductive sheet was adhered to eliminate possible errors resulting from poor contact between the specimens and the electrodes (Fig. 2.33). The EIS measurements were taken by polarizing the working electrode at $\pm$ 10 mV around its open circuit potential, using sinusoidal perturbations with a frequency between 1 MHz and 0.01 Hz.

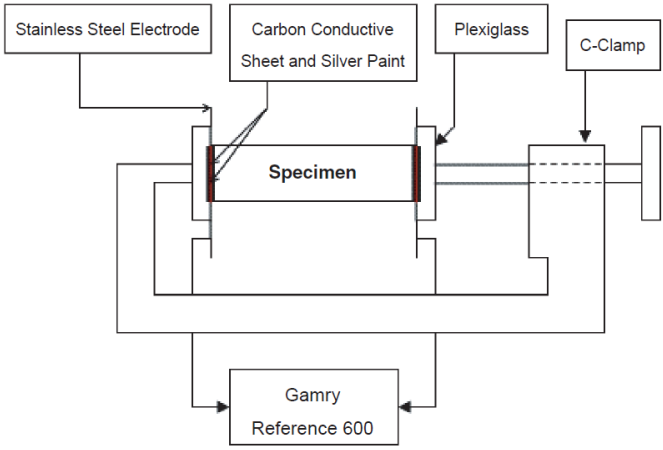


**Fig. 2.33** Schematic illustration of experimental setup for electrochemical impedance measurements of mortar samples [2.39]

As EIS measurements have been effective in revealing the microstructure of cementitious composites, Yang *et al.* [2.39] decided to use these measurements to evaluate the microstructural properties and self-healing effect of their fiber-reinforced mortar samples. The complex impedance of composite materials depends on the frequency of an externally exposed alternating current polarization signal, allowing for the representation of a system with an equivalent circuit typically consisting of resistors and capacitors. Yang *et al.* [2.39], used the equivalent circuit and the microstructure of a mortar specimen to interpret the EIS data (Fig. 2.34).

As seen in Fig. 2.34 there are three types of paths in a carbon microfiber reinforced mortar structure: continuous conductive paths (CCPs), discontinuous conductive paths (DCPs) and matrix condustive paths. The CCPs are the continuously connected pores or cracks in the mortar microstructure, whereas the DCPs are the discontinuous pores or cracks whose continuity is blocked by the cement paste layer denoted as discontinuous points. Apart from the DCPs and CCPs, the mortar matrix consisting of cement paste particles and carbon microfibers can act as another kind of conductive path.

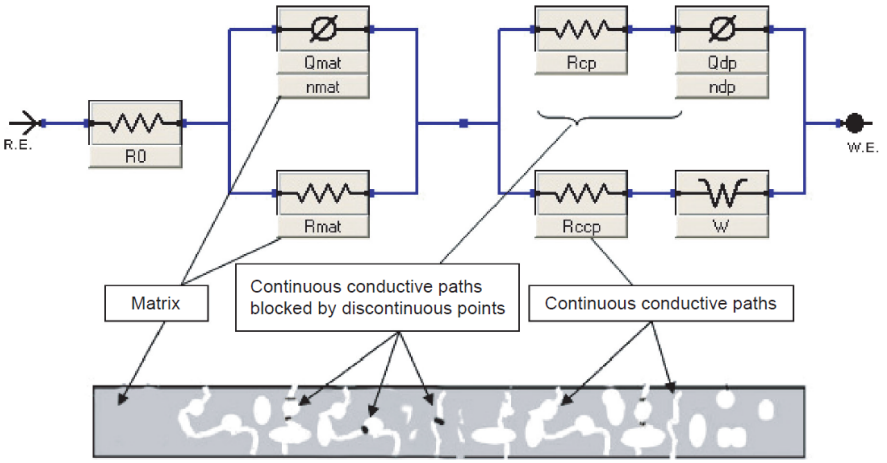


**Fig. 2.34** Equivalent circuit and microstructure of mortar specimen used for fitting the impedance spectra (R.E. = reference electrode, W.E. = working electrode) [2.39]

Based on the above consideration, Yang *et al.* [2.39], decided to use the following parameter to represent the microstructure of fiber-reinforced mortars: $R_{mat}$ (resistance of mortar matrix), $R_{CCP}$ (resistance of continuously connected pores or cracks) and $R_{CP}$ (resistance of discontinuously connected pores or cracks), $Q_{mat}$ (constant phase element across the mortar matrix) and $Q_{dp}$ (constant phase element of the cement paste layers blocking the discontinuously connected pores or cracks in the mortar). In addition, the Warburg impedance (W) was assigned to one electrode and mortar interface, characterizing the diffusion of species through the interface and $R_0$ was assigned to represent the total resistance of metal electrodes, carbon conductive sheet and electrical wires in the circuit.

### *2.3.6 Computed Tomography*

Radiography is the recording of a shadow image of an optically opaque object using penetrating X-rays and a recording medium. Tomography is an extension of radiography. In general terms it is a non-destructive technique to investigate the inner structure of an object in 3D. Basically the 3D object under study is reconstructed based on a set of 2D projections (or radiographies) taken from different angles by rotating the sample around a defined axis. First, this technique was used in medicine to study the internal of the body. More recently, X-ray tomography has become an important technique for non-destructive testing (NDT) in other fields too. It is used in biology, geology, archaeology, industry.

Mihashi *et al.* [2.40] made use of computed tomography to investigate the possibility of their proposed self-healing method. They used contrast medium instead of repairing agent to fill the glass tubes.

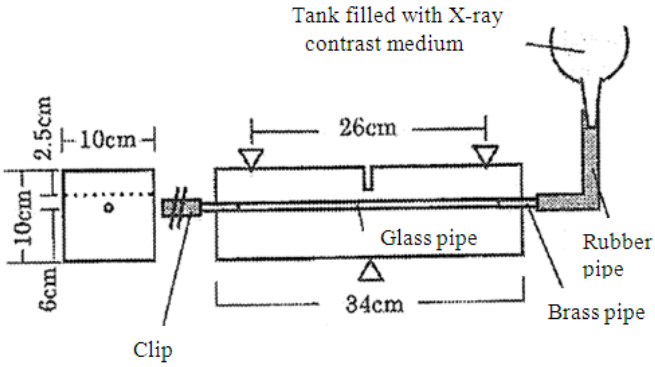


**Fig. 2.35** Test setup and specimen [2.40]

Tests were carried out onto specimens in which a glass pipe was embedded (Fig. 2.35). The contrast medium was applied from the outside. During the bending test, X-ray permeation photographs were continuously taken while the load was gradually increased. The images, processed in real time, were observed on a TV monitor.

The results from the bending test and the CT scans near the notch tip are shown in Fig. 2.36. The numbers specified in the load CMOD curve are associated with the numbers of the X-ray pictures. From the pictures it could be observed that as the glass pipe is broken responding to the concrete fracture, the installed contrast medium is discharged into the crack. The authors concluded that a similar behaviour may be observed by embedding the glass pipe with repairing agent instead of the X-ray contrast medium.

Van Tittelboom *et al.* [2.41] proposed the use of high resolution X-ray computed tomography (HRXCT) to visualize the crack healing efficiency of delivery tubes with a different internal diameter. In their research the authors, encapsulated the healing agent into tubular capsules with a diameter of 2 mm and 3 mm, respectively. As healing agent, a commercially available two-component polyurethane was used. The capsules were prepared in sets of two, one tube being filled with the prepolymer and the other tube with a mixture of accelerator and water. At the age of 7 days, the mortar prisms were put through a crack width controlled three-point-bending test, in order to create a crack and trigger the healing mechanism.

After healing occurred, the samples were scanned using the in house developed HRXCT system of the Centre for X-ray Tomography of Ghent University (UGCT) [2.42]. The system was composed of a Feinfocus X-ray tube with tungsten target, a Varian Paxscan 2520 A-Si flat panel detector and a Micos air-bearing rotation stage. For each of the samples a region of 1880x1496 pixels of the detector was used in non-binned mode of 127 µm pixel size and 1200 projections were taken at 0.3° of rotation interval over 360°. The mortar samples were scanned at 150 kV tube voltage and with a 2 mm Cu filter. The projection data were reconstructed into HRXCT slices using Octopus [2.43] with 50 µm voxel pitch.

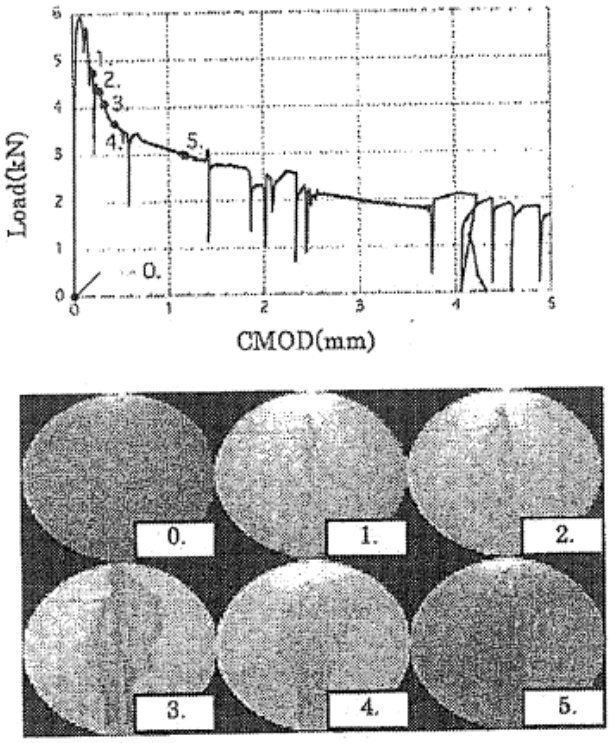


**Fig. 2.36** Load versus CMOD relation and X-ray photograph near the notch [2.40]

The scans resulted in more than a thousand slices in the Z-orientation, these were resliced in the Y direction (Fig. 2.37) in order to get a cross-section in the same plane as the four glass tubes. This way it is possible to compare how efficiently the tubes have been emptied during the formation of the crack and how the polyurethane has infiltrated.

Although the polyurethane foam had very low X-ray absorption compared to mortar, the remaining polyurethane inside the tubes and filling of the crack with polyurethane were clearly visible. Neither of the tubes had completely been emptied during crack formation. The dark parts which are seen inside the tubes correspond to air bubbles which were formed when part of the healing agent was released from the tubes. Furthermore, it was observed that the released healing agent effectively filled the crack gap. Regions where there was no polyurethane could be clearly distinguished.

It became obvious that neither the 2 mm or 3mm tubes have completely been emptied during formation of the crack. The efficiency of emptying is dependent on several parameters such as the capillary forces but an alteration in the diameter of the glass tubes from 2 mm to 3 mm did not seem to give significant differences in outcome.

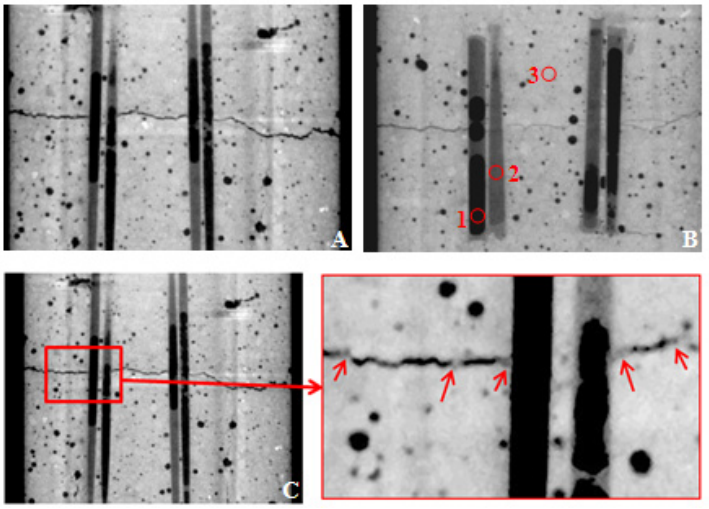


**Fig. 2.37** Y-direction μ-CT cross-section through the glass tubes: (A) sample with 2 mm diameter tubes, (B) sample with 3 mm diameter tubes and (C) magnified region of interest of the 2 mm sample μ-CT data. Filling of the crack with polyurethane is indicated with arrows. Air voids are coloured black as indicated by region (1), polyurethane is coloured light grey as indicated by (2) and mortar is coloured darker grey as indicated by region (3).

Polyurethane can be visualized in the tubes as well as in the cracks with μ-CT. Fig. 2.37.C illustrates a magnified sub-region of a cross section of the sample with 2 mm tubes. Although the difference in contrast is small, it is still clearly visible where the polyurethane has filled up the crack compared to regions where there is no polyurethane.

Based on these results it may be concluded that HRXCT can be used to evaluate the efficiency of autonomous crack healing actions. It should be pointed out that the authors [2.41] scanned real size mortar samples (60 mm x 60 mm x 220 mm) instead of the meticulous samples of some millimeters which have been used in previous studies. Based on the promising first results obtained here, further development of the system could make it possible to perform also a quantitative evaluation of the healing efficiency for concrete or even visualize breakage of the tubes and the release kinetics of the healing agent like done in the study of Mookhoek *et al.* [2.44] for small composite specimens.

### *2.3.7 Resistance against Corrosion*

Pelletier *et al.* [2.45] and Dry and Corsaw [2.46] used corrosion monitoring to evaluate the self-healing efficiency of their approach. Both used a sodium chloride solution in order to induce corrosion. This solution was placed at the top of the samples to allow the ingress of chloride ions via the concrete matrix or via cracks in the direction of the steel reinforcement. During the measurement, a voltmeter

was connected to the reinforcement bars and the open circuit potential of the rebars was monitored over time until the steel bars were corroded.

### 2.3.8 *Fourier-Transform Infrared Spectroscopy – FTIR*

Infrared spectroscopy is a technique based on the vibrations of the atoms of a molecule. It is used for the determination of molecular structure or the identification of chemical species. A vibration will be infrared active if a change in the dipole moment of the molecule occurs during the vibration. An infrared spectrum consists of a series of bands or peaks which result from the absorption by a part of the molecule of the incident radiation at a particular energy.

FTIR spectroscopy was used by Wiktor and Jonkers [2.47] to identify the chemical composition of the precipitate formed at the crack surface of bacteria-based mortar specimen during self-healing operation. The FTIR spectra obtained from 3 different samples showed that this mineral precipitate was composed of a mixture of calcite and aragonite, two polymorphs of $CaCO_3$ (Fig. 2.38). The presence of aragonite and the absence of such precipitate on the control specimen suggested that the $CaCO_3$ precipitation was mediated by bacteria.

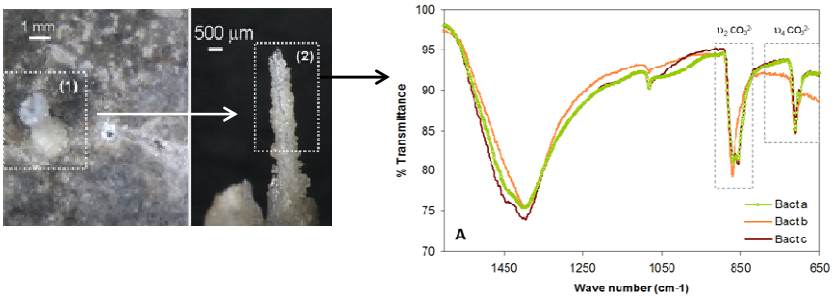


**Fig. 2.38** FTIR spectroscopy used to identify precipitate chemical composition [2.47]

## 2.4 Techniques Used to Verify Recovery against Mechanical Actions

### 2.4.1 *Regain in Strength and Stiffness*

#### 2.4.1.1 Producing Controlled Cracks

In order to study the effect of crack healing, first cracks have to be made in the concrete in a controlled way. For this purpose a three-point-bending test is chosen on prismatic concrete specimens. The deformation is measured with two linear variable differential transformers: LVDT's (at front and back) fixed at the bottom of the specimen (in the centre), as shown in Fig. 2.39. The deformation measured

with these LVDT's gives a bending strain at the bottom of the specimen. This value is a measure (although not exact) of the crack opening. The tests are performed in deformation control using the average signal of the two LVDT's as the feed back signal. In the test the loading is stopped when the predefined crack width is reached. Then, the specimen is unloaded and taken out of the machine Fig. 2.40. The crack opening decreases after unloading but the crack will not completely close.

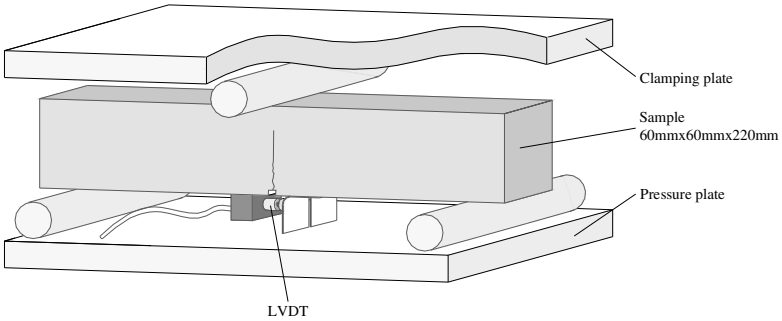


**Fig. 2.39** Setup of the three-point-bending test [2.23]

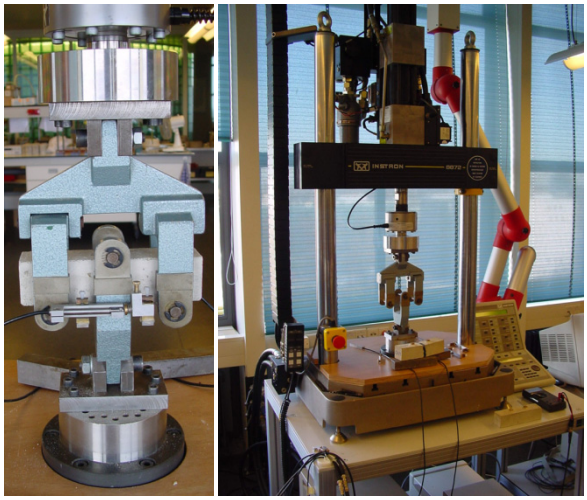

**Fig. 2.40** Producing cracks via 3-point bending test

To develop multiple cracking in Engineered Cementitious Composites, a displacement-controlled uni-axial tensile test (Fig. 2.41) or a four-point-bending test (Fig. 2.42) is applied. The loading is stopped when the pre-defined tensile strain is reached. The deformation is hereby measured with linear variable differential transformers. Afterwards, the residual crack widths are determined.

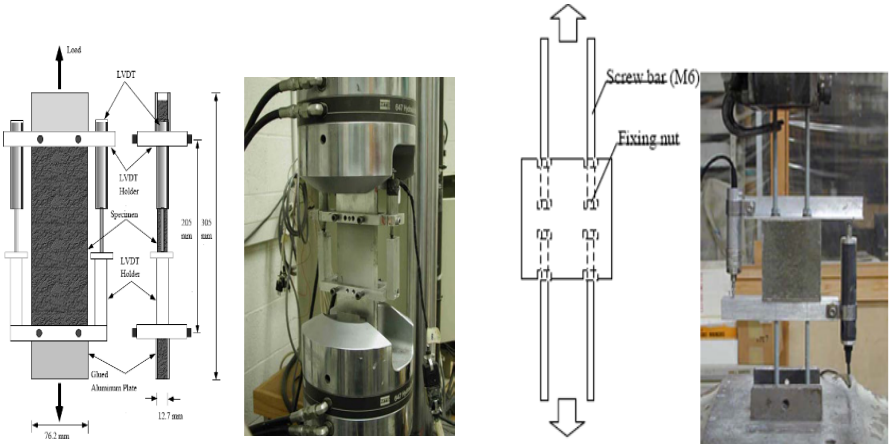


**Fig. 2.41** Setup of a uni-axial tensile test [2.49-2.51]

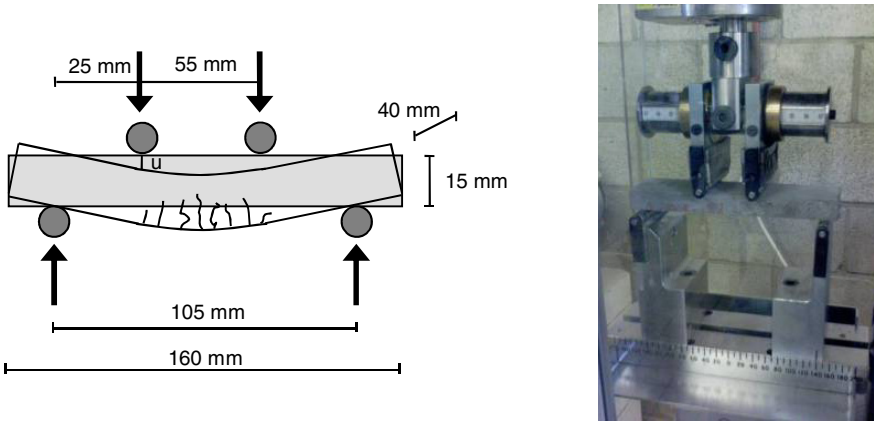


**Fig. 2.42** Setup of a four-point-bending test [2.52]

### 2.4.1.2 Determination of Regain in Mechanical Properties

In order to examine the mechanical properties of the healed crack, the specimens are, after a certain period of healing, again tested in three-point-bending. To be able to judge the recovery of the mechanical properties of the crack, the results have to be compared with cracks that are not healed and with cracks that are made after the healing process. Therefore, virgin specimens stored in the same environment and with the same age as the healed specimens were also tested. These specimens are first loaded in deformation control up to a predefined displacement. Then the specimen is unloaded and tested again. The maximum load reached in the second stage of the test is taken to be the maximum flexural stress for a specimen with an unhealed crack.

The regain in mechanical properties in four-point-bending after a healing period, serves as a quantification of the healing. The mechanical properties that can be compared are the first-cracking strength, the modulus of elasticity, the ultimate strength and the multiple-cracking behavior [2.52-2.54].

### 2.4.2 *Fatigue Resistance*

In order to evaluate the self-healing efficiency of their approach, Yang *et al.* [2.30] and Pang *et al.* [2.48] performed fatigue tests onto samples/structures with self-healing properties. Fatigue is defined as the formation of progressive and permanent internal damage in a material subjected to repeated loading. This is attributed to the propagation of internal micro cracks which result in a significant increase of irrecoverable strain [29].

In their experiments, Yang *et al.* [2.30] made use of cylindrical mortar specimens (Ø 50 mm x 100 mm) which were first loaded to 80% of their static ultimate compressive strength. After being set aside for 24 hours, samples were subjected to cyclically loading between 25% and 95% of their static ultimate compressive strength until failure. The frequency of loading was 1 Hz.

Test results were depicted as the relationship between the fatigue strain and the number of loading cycles until failure (Fig. 2.43). The fatigue strain development featured three distinct stages: the first stage characteristic of quick strain increase up to approximately 10% of the total life, the second stage characteristic of gradual strain increase from approximately 10-80% of the total life (attributed to the development of a large amount of small cracks in the mortar matrix) and the last stage characteristic of another quick strain increase until failure. Relative to the control, the SPSM (samples with sulfonated polystyrene particles admixed) and SHM (samples with microcapsules filled with MMA and TEB admixed) showed a significant prolonged second stage and their strain increment curves were less steep, demonstrating the beneficial role of the micro particles in inhibiting the initiation and propagation of cracks.

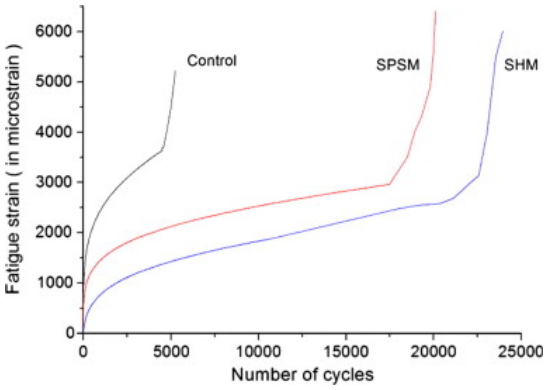


**Fig. 2.43** Relationship between the fatigue strain and the number of cycles under uniaxial compression cyclic loading for SHM, SPSM and control mortar specimens respectively [2.30]

### 2.4.3 Acoustic Emission Analysis

Acoustic emission (AE) is a microseismic (elastic) wave generated from dislocations, microcracks and other irreversible changes in a stressed material. The transmitted waves are detected by transducers on the surface of a specimen. Aside from applications in geophysics and in geotechnical engineering [2.55], AE technique has been mainly developed to monitor and inspect structures because an increase of acoustic activity is generally a very sensitive precursor to failure of structural components (see e.g. Ref. [2.56]). For concrete structures, this property has been highlighted initially by Rusch in 1960 [2.57]. In more recent works on concrete fracture such as those by Landis [2.58], or Chen and Liu [2.59] among others, the correlation between cracking and the cumulated number of acoustic event is clearly exhibited.

Granger *et al.* [2.60] used AE to qualify autogenous crack healing in ultra high performance concrete. In the present study, all specimens were instrumented with an AE system, during the pre-cracking and reloading phase. The transducers were placed on one side of the specimen, and coupled to the material with silicon glue. Mechanical tests had shown the contribution of the selfhealing phenomenon on the properties of initially cracked specimens. The main aim of the AE analyses performed during the mechanical tests was thus to highlight that this contribution was related to the precipitation of new crystals in the crack. For this, determination of the location of the AE after ageing during the second mechanical tests was the major information to be obtained from which a comparison wuld be made between healed (cured in water) and non-healed (cured in air) specimens. Fig. 2.44 presents the typical microcracking map of a specimen, just after the pre-cracking phase. The transducers which form the rectangular array are represented in the corners, and the other points are the microcracks detected. It shows a very dense area of acoustic events, due to the development of the fracture process zone.

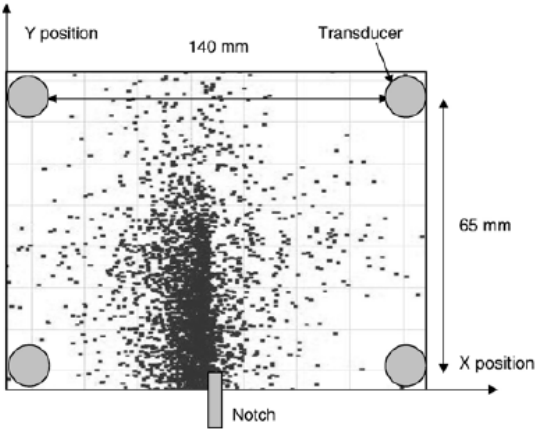


**Fig. 2.44** Micro cracking map of a specimen after the pre-cracking phase –result without all events

In order to have a more accurate location of the macrocrack, which is of interest if we want to locate the microcracking of new crystals in this crack during the reloading phase, selection of the detected signals was necessary. The authors chose to eliminate the events with an energy less than 2% of the maximal energy. Fig. 2.46 presents the result of this data processing. Compared to Fig. 2.45, it can be seen that most of the events are located in a narrower band which follows more closely the macrocrack surface.

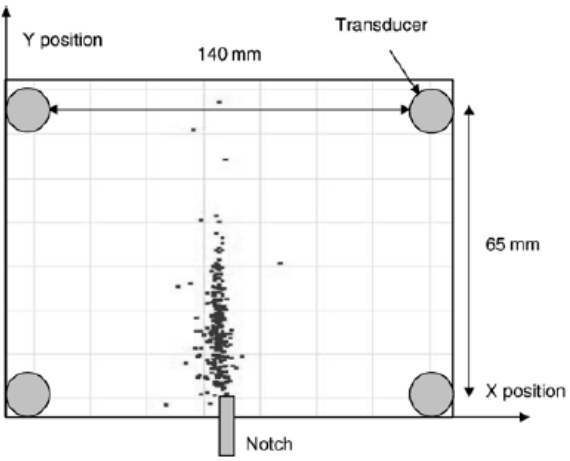


**Fig. 2.45** Micro cracking map of a specimen after the pre-cracking phase – result with selection in energy: events with an energy higher than 1000 aJ

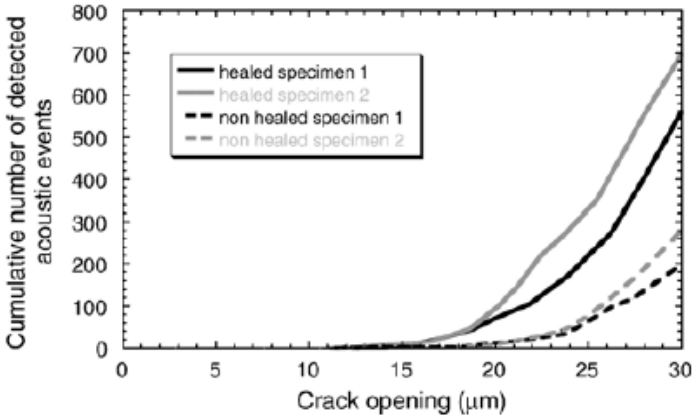


**Fig. 2.46** Cumulative number of acoustic events during the reloading phase for healed and non-healed specimens

Fig. 2.46 shows the evolution of the cumulative number of detected events with crack opening for four specimens cured during 10 weeks. There is a significant difference between healed and non-healed specimens responses. For crack openings larger than 20 μm, the crack length is greater than the initial one, prior to healing. The number of events recorded on healed specimens (cured into water) is at least twice the number observed for unhealed specimens.

Fig. 2.47 presents the maps for a specimen aged in water and for a specimen aged in air, both during 10 weeks. It is noticeable that acoustic activity appears for the healed specimen in the region of the initial crack, while nearly nothing is detected for a nonhealed specimen. In view of the mechanical results which exhibit stiffness and strength recovery, one can say that in the first case, there is a damage of the newly formed crystals in the crack, and in the second case, there is only the re-opening of the existing crack, with very little acoustic activity (some due to friction probably). Note that for non-healed specimens, performing the same AE localisation analysis without removing the less energetic events would still provide little acoustic activity, less than that observed for healed specimens.

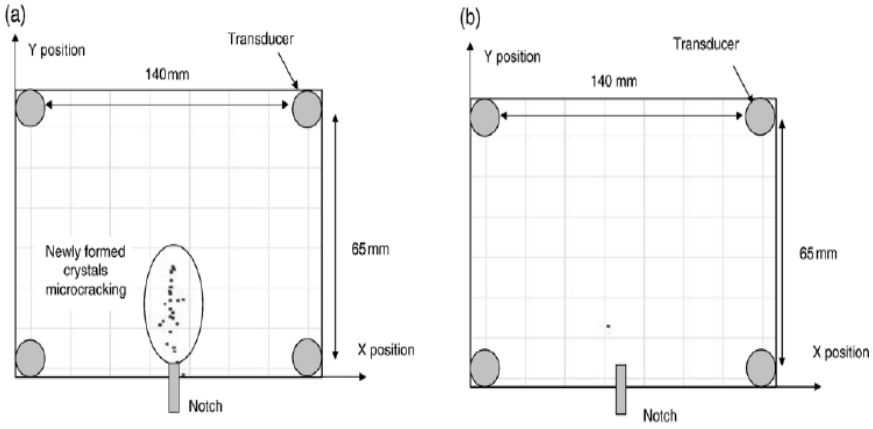


**Fig. 2.47** Microcracking maps, during the reloading phase (until 18 μm –pre-peak regime) of specimens aged for 10 weeks, (a) ageing in water, (b) ageing in air

Van Tittelboom *et al.* [2.61] proposed to use AE analysis in order to evaluate the autonomic healing efficiency of concrete with embedded encapsulated healing agents. Cracks were created by means of a crack width controlled three-point-bending test. When the predefined crack width was reached, the beams were unloaded. During crack formation all beams were instrumented with an AE system. The instrumentation consisted of eight piezoelectric transducers (see Fig. 2.48).

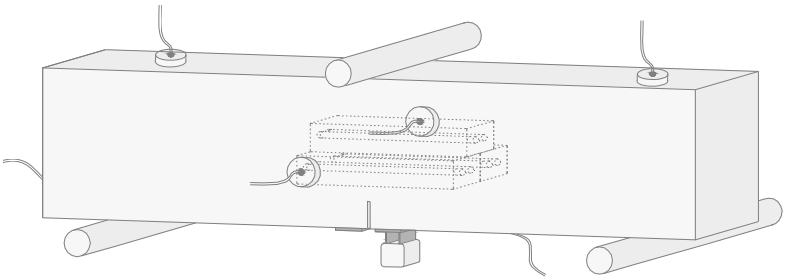

**Fig. 2.48** Setup of the experiment showing the position of the protected ceramic tubes inside the concrete beam together with the position of some of the sensors

For beams with self-healing properties, the healing mechanism was activated upon crack appearance. Cracks of the samples belonging to the test series 'PUR' and 'EPO' were treated immediately after crack formation with, respectively, polyurethane and epoxy. 24 hours after crack repair, the specimens were reloaded in three-point bending in order to test the crack healing efficiency. During this reloading cycle sensors were coupled again in the same position as during crack creation.

For each event the according energy was determined and events were subdivided into seven classes based on their energy. In Fig. 2.49 the loading curves during crack creation (light grey) and reloading (dark grey) are displayed together with the emitted events (also light and dark grey). Each event is represented by means of a dot and based on their energy class they are represented in different levels.

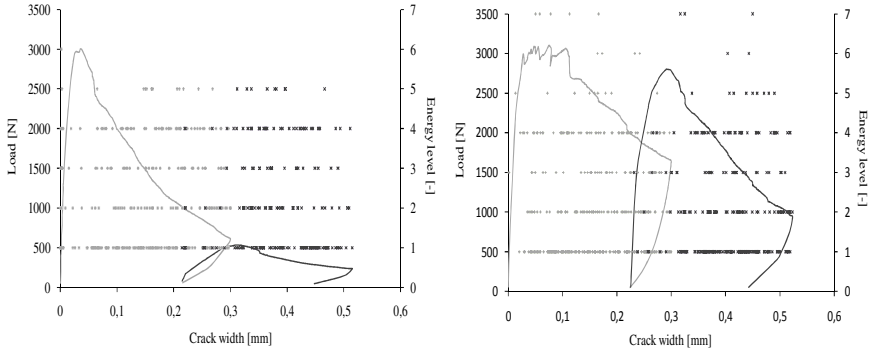


**Fig. 2.49** Loading curve obtained during crack creation and reloading for an untreated (left) and autonomously healed (right) crack. The captured events are represented by means of dots depending on their energy level.

Only for beams with encapsulated healing agent events from the highest energy level were noticed. It was thought that these events were caused by breakage of the embedded tubes as they were accompanied by drops in load and audible 'pop' sounds. Also during reloading, the energy released for autonomously healed cracks is higher than for the other test series. This could be explained by the fact that some additional tubes broke upon reloading. This was also heard during the test and seen from the reloading curves. Due to the second release of healing agent, a second healing action may occur, as already noticed in previous experiments.

Upon reloading of the beams different phases could be distinguished. In the first phase the crack just reopens for the reference beams or the cracks appear in the healing agent in case of beams with healed cracks. When the crack opening, which was reached during crack creation, is reached again, new cracks start to form in the concrete matrix. This is the start of the second phase. The third phase corresponds to the moment when the adjusted crack width is reached, loading is stopped and the crack width decreases. As the second and the third phase are equal for all test series, and quite some events are produced during the second phase, these events may mask the differences between the first phases of the different test series.

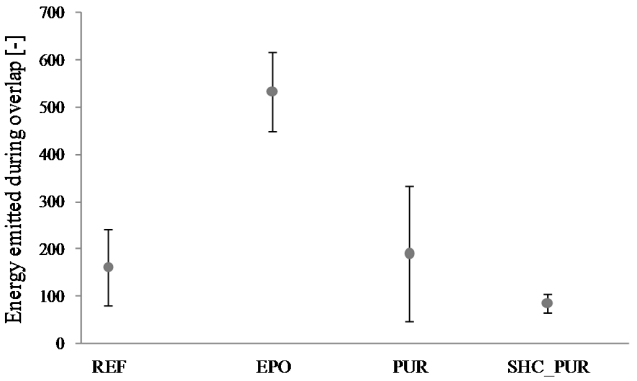


**Fig. 2.50** Energy emitted during the first phase of reloading (this means during the overlap of pre-cracking and reloading); dots represent the mean value, error bars represent the standard error (n=5)

Therefore, the energy of all events which occurred during the first phase was cumulated. A significant difference was noted between the energy released for cracks manually healed with epoxy and the other test series (Fig. 2.50). For the specimens where the cracks were healed with polyurethane (manually or automatically) no significant difference was noted; however, from the regain in mechanical properties [2.61] it was seen that these cracks were healed. That no significant difference is seen by means of AE can be explained by the fact that crack formation into the polyurethane foam does not cause events with high energy.

From this study the authors concluded that breakage of the tubes of self-healing concrete can be proven by means of AE measurements. Although self-healing of cracks using PU as healing agent is not yet proven, crack healing is proven in the case epoxy resin is used as healing agent. The possibility to use AE as indicator for self-healing of cracks, will therefore depend on the mechanical properties of the healing agent used.

## References


2.1. Jana, D.: Concrete petrography - past, present and future. In: 10th Euroseminar on Microscopy Applied to Building Materials, Scotland (2005)
2.2. Nesse, W.D.: Introduction to Optical Mineralogy. Oxford University Press, USA (2012)
2.3. Rost, F., Oldfield, R.: Photography with a microscope. C.U. Press, UK (2000)
2.4. Abramoff, M.D., Magelhaes, P.J., Ram, S.J.: Image Processing with Image. J. Biophotonics International 11(7), 36–42 (2004)
2.5. van der Zwaag, S. (ed.): Self-Healing Materials: An Alternative Approach to 20 Centuries of Materials Science. Springer Series in Materials Science, vol. 100, 388 p. (2007)
2.6. Li, V., Yang, E.H.: Self-healing in concrete materials. In: Van der Zwaag, S. (ed.) Self-healing Materials: An Alternative Approach to 20 Centuries of Materials Science, pp. 161–194. Springer Science, Dordrecht (2007)
2.7. Jonkers, H.M.: Self-healing concrete: A biological approach. In: van der Zwaag, S. (ed.) Self-healing Materials: An Alternative Approach to 20 Centuries of Materials, pp. 195–204. Springer Science, Dordrecht (2007)
2.8. Jonkers, H.M., et al.: Application of bacteria as self-healing agent for the development of sustainable concrete. Ecological Engineering 36(2), 230–235 (2010)
2.9. ter Heide, N.: Crack healing in hydrating concrete. Faculty of Civil Engineering and Geosciences, p. 128. Delft University of Technology (2005)
2.10. Copuroglu, O., Sisomphon, K.: Stabilization of vaterite and aragonite in carbonated GGBFS cement paste by Na-MFP. In: 32nd ICMA Meeting, New Orleans, USA (2010)
2.11. Kishi, T., Ahn, T.-H., Hosoda, A., Suzuki, S., Takaoka, H.: Self-healing behaviour by cementitious recrystallization of cracked concrete incorporating expansive agent. In: Proceedings of the First International Conference on Self-healing Materials, Noordwijk aan Zee, The Netherlands (2007)
2.12. Wiktor, V., Jonkers, H.M.: Bio-chemical self-healing agent to prevent reiforcement corrosion in concrete. In: White, S., Bond, I. (eds.) 2nd International Conference on Self-healing Materials, Chicago, USA, p. 118 (2010)
2.13. Komatsu, et al.: Fundamental study on self-healing of cement paste by calcium aluminate based agents. In: Proceedings of Japanese Concrete Institute, pp. 131–136 (2010)
2.14. Lubelli, B., Nijland, T.G., van Hees, R.P.J.: Self-healing of lime based mortars: microscopy observations of case studies. Heron 56(1/2), 75–91 (2011)

2.15. Nijland, T.G., Larbi, J.A., van Hees, R.P.J., Lubelli, B., de Rooij, M.: Self-healing phenomena in concretes and masonry mortars: a microscopic study. In: Proceedings of the First International Conference on Self-healing Materials, Noordwijk aan Zee, The Netherlands, p. 31 (2007)
2.16. Ahn, T.H., Kishi, T.: The effect of geo-materials on the autogneous healing behaviour of cracked concrete. In: Alexander, M.G., Beushausen, H.-D., Dehn, F., Moyo, P. (eds.) Concrete Repair, Rehabilitation and Retrofitting II, London, pp. 235–240 (2009)
2.17. Ahn, T.H., Kishi, T.: Crack self-healing behaviour of cementitious composites incorporating various mineral admixtures. Journal of Advanced Concrete Technology 8(2), 171–186 (2010)
2.18. Haddad, R.H., Bsoul, M.A.: Self-healing of polypropylene fiber reinforced concrete; pozzolan effect, pp. 1412–1421
2.19. Homma, D., Mihashi, H., Nishiwaki, T., Mizukami, T.: Experimental study on the self-healing capability of fiber reinforced cementitious composites. In: 7th RILEM International Symposium on Fibre Reinforced Concrete: Design and Applications, Chennai, India, RILEM, pp. 769–774 (2008)
2.20. Wang, K., Jansen, D.C., Shah, S.P., Karr, A.F.: Permeability study of cracked concrete. Technical report 46, National Institute of Statistical Sciences (1996)
2.21. Wang, K., et al.: Permeability study of cracked concrete. Cement and Concrete Research 27(3), 381–393 (1997)
2.22. Aldea, C.-M., Ghandehari, M., Shah, S.P., Karr, A.: Combined effect of cracking and water permeability of concrete. In: 14th Engineering Mechanics Conference, Austin, Texas (2000)
2.23. Van Tittelboom, K., De Belie, N.: Self-healing concrete: suitability of different healing agents. International Journal of 3R's 1(1), 12–21 (2010)
2.24. Nishiwaki, T., Mihashi, H., Jang, B.-K., Miura, K.: Development of self-healing system for concrete with selective heating around crack. Journal of Advanced Concrete Technology 4(2), 267–275 (2006)
2.25. Morimoto, T., Kunienda, M., Ueda, N., Nakamura, H.: Self-healing properties of Ultra High Performance Strain Hardening Cementitious Composites (UHP-SHCC). In: Proc. of 4th International Conference on Construction Materials, Nagoya, Japan, pp. 319–326 (2009)
2.26. NBN B 24-213, in Belgische norm: Proeven op metselstenen - Wateropslorping onder vacuum (1976)
2.27. Kishi, T., et al.: Field test of self-healing concrete on the recovery of water tightness to leakage through cracks. In: Bond, I., Varley, R. (eds.) 3rd International Conference on Self-healing Materials, Bath, UK, pp. 297–298 (2011)
2.28. Snoeck, D., et al.: Visualization of water penetration in cementitious materials with superabsorbent polymers by means of neutron radiography. Cement and Concrete Research 42, 1113–1121 (2012)
2.29. Clear, C.A.: Leakage of cracks in concrete - summary of work to date. Cement and Concrete Association (1982) (Internal Publication)
2.30. Yang, Z., et al.: A self-healing cementitious composite using oil core/silica gel shell microcapsules. Cement and Concrete Composites 33(4), 506–512 (2011)

2.31. Torrent, R.: A two-chamber vacuum cell for measuring the coefficient of permeability to air of the concrete cover on site. Materials and Structures 25(6), 358–365 (1992)
2.32. Song, M., Jeon, S., Song, Y.: The change of osomis pressure by crack self-healing of cementitious materials. In: Bond, I., Varley, R. (eds.) 3rd International Conference on Self-healing Materials, Bath, UK, pp. 295–296 (2011)
2.33. Van Tittelboom, K., et al.: Use of neutron radiography and tomography to visualize the autonomous crack sealing efficiency in cementitious materials. Materials and Structures (2012) (Published online: July 3, 2012)
2.34. Van Tittelboom, K., Dierick, M., De Belie, N.: Durable concrete structures with cracks which heal themselves. In: Brandt, A.M., et al. (eds.) Brittle Matrix Composites, Warsaw, Poland, pp. 285–294 (2012)
2.35. Aldea, C.-M., Song, W.-J., Popovics, J.S., Shah, S.P.: Extent of healing of cracked normal strength concrete. Journal of Materials in Civil Engineering 12(1), 92–96 (2000)
2.36. Abdel-Jawad, Y., Dehn, F.: Self-healing of self-compacting concrete. In: Proceedings of SCC 2005, Orlando, Florida, USA, pp. 1023–1029 (2005)
2.37. Abd-Elmoaty, A.-E.: Self-healing of polymer modified concrete. Alexandria Engineering Journal 50(2), 171–178 (2011)
2.38. Van Tittelboom, K., et al.: Use of bacteria to repair cracks in concrete. Cement and Concrete Research 40(1), 157–166 (2010)
2.39. Yang, Z., et al.: Laboratory assessment of a self-healing cementitious composite. Journal of the Transportation Research Board 2010 (2142), 9–17 (2010)
2.40. Mihasi, H., Kaneko, Y., Nishiwaki, T., Otsuka, K.: Fundamental study on development of intelligent concrete characterized by self-healing capability for strength. Transactions of the Japan Concrete Institute 22, 441–450 (2000)
2.41. Van Tittelboom, K., Van Loo, D., De Belie, N., Jacobs, P.: Evaluation of the efficiency of self-healing in concrete by means of micro-CT. In: Proceedings of the 3rd International Workshop on X-ray CT for Geomaterials, New Orleans, pp. 132–139 (2010)
2.42. Masschaele, B.C., Cnudde, V., Dierick, M., Jacobs, P., Van Hoorebeke, L., Vlassenbroeck, J.: UGCT: New X-ray radiography and tomography facility. Nuclear Instruments and Methods in Physics Research - Section A 580(1), 266–269 (2007)
2.43. Vlassenbroeck, J., Dierick, M., Masschaele, B., Cnudde, V., Van Hoorebeke, L., Jacobs, P.: Software tools for quantification of X-ray microtomography at the UGCT. Nuclear Instruments and Methods in Physics Research - Section A 580(1), 442–445 (2007)
2.44. Mookhoek, S.D., Mayo, S.C., Hughes, A.E., Furman, S.A., Fischer, H.R., van der Zwaag, S., Ludwig, W.: Using synchrotron X-ray micro tomography to quantitatively analyze fracture and healing processes in self-healing thermoplastics. In: Proceedings of the Second International Conference on Self-healing Materials, Chicago, p. 72 (2009)
2.45. Pelletier, M., et al.: Self-healing concrete with a microencapsulated healing agent (2010)

2.46. Dry, C.M., Corsaw, M.J.T.: A time-release technique for corrosion prevention. Cement and Concrete Research 28(8), 1133–1140 (1998)
2.47. Wiktor, V., Jonkers, H.M.: Quantification of crack-healing in novel bacteria-based selfhealing concrete. Cement and Concrete Composites 33(7), 763–770 (2011)
2.48. Pang, S.D., Tran Diep, P.T., Quek, S.T.: Self-healing concrete structural elements. In: Bond, I., Varley, R. (eds.) 3rd International Conference on Self-healing Materials, Bath, UK, pp. 322–323 (2011)
2.49. Yang, Y., et al.: Autogenous Healing of Engineered Cementitious Composites under Wet-dry Cycles. Cement and Concrete Research 39, 382–390 (2009)
2.50. Homma, D., et al.: Self-Healing Capability of Fibre Reinforced Cementitious Composites. Advanced Concrete Technology 7, 217–228 (2009)
2.51. Li, V.C., et al.: Tensile strain-hardening behavior of polyvinyl alcohol engineered cementitious composites (PVA-ECC). ACI Materials Journal 94, 555–564 (1997)
2.52. Snoeck, D., et al.: Self-healing cementitious materials by the combination of microfibres and superabsorbent polymers. Journal of Intelligent Material Systems and Structures (2012)
2.53. Snoeck, D., et al.: The use of superabsorbent polymers as a crack sealing and crack healing mechanism in cementitious materials. In: 3rd International Conference on Concrete Repair, Rehabilitation and Retrofitting, Cape Town, pp. 152–157 (2012)
2.54. Snoeck, D., De Belie, N.: Mechanical and self-healing properties of cementitious composites reinforced with flax and cottonised flax, and compared with polyvinyl alcohol fibres. Biosystems Engineering 111, 325–335 (2012)
2.55. Hardy, H.R.: Acoustic emission / Microseismic activity - Volume 1: Principles, Techniques and geotechnical applications, ed. A.A. Balkema (2003)
2.56. Proust, A., Marlot, D., Lenain, J.C.: Application of acoustic emission to detect damage in concrete structures, illustrated with full scale examples. In: 1st International Conference on Concrete Repair, Saint Malo, France (2003)
2.57. Rüsch, H.: Research towards a general flexural theory for structural concrete. ACI Journal 57, 1–28 (1960)
2.58. Landis, E.N.: Micro-macro fracture relationships and acoustic emissions in concrete. Construction and Building Materials 13(1-2), 65–72 (1999)
2.59. Chen, B., Liu, J.: Experimental study on AE characteristics of three-point-bending concrete beams. Cement and Concrete Research 34(3), 391–397 (2004)
2.60. Granger, S., et al.: Experimental characterization of the self-healing of cracks in an ultra high performance cementitious material: Mechanical tests and acoustic emission analysis. Cement and Concrete Research 37(4), 519–527 (2007)
2.61. Van Tittelboom, K., De Belie, N., Lehmann, F., Grosse, C.: Use of acoustic emission analysis to evaluate the self-healing capability of concrete. In: International Symposium on Nondestructive Testing of Materials and Structures - NDTMS 2011, Istanbul, Turkey (2011) (submitted)

# 3 Recovery against Environmental Action

H.W. Reinhardt[1], H. Jonkers[2], K. Van Tittelboom[3], D. Snoeck[3], N. De Belie[3], W. De Muynck[3,4], W. Verstraete[3], J. Wang[3,4], and V. Mechtcherine[5]

[1] University of Stuttgart, Germany
reinhardt@iwb.uni-stuttgart.de
[2] Microlab, Delft University of Technology, The Netherlands
H.M.Jonkers@tudelft.nl
[3] Magnel Laboratory for Concrete Research, Ghent University, Belgium
{Kim.VanTittelboom,Didier.Snoeck,Nele.DeBelie,
Willem.DeMuynck,Willy.Verstraete,Jianyun.Wang}@UGent.be
[4] Laboratory for Microbial Ecology and Technology, Ghent University, Belgium
[5] Technische Universität Dresden, Germany
Mechtcherine@tu-dresden.de

## 3.1 Autogenic Self-Healing

Autogenic self-healing has been defined in chapter 1 as a self-healing process where the recovery process uses materials components that could also be present when not specifically designed for self-healing (own generic materials).

### *3.1.1 Causes of Autogenic Self-Healing*

An example of recovery against environmental action through self-healing is the width of a through-crack that diminishes with time. The cause for this is manifold. One can distinguish between physical, chemical, and mechanical causes [3.1], see also Fig. 3.1.

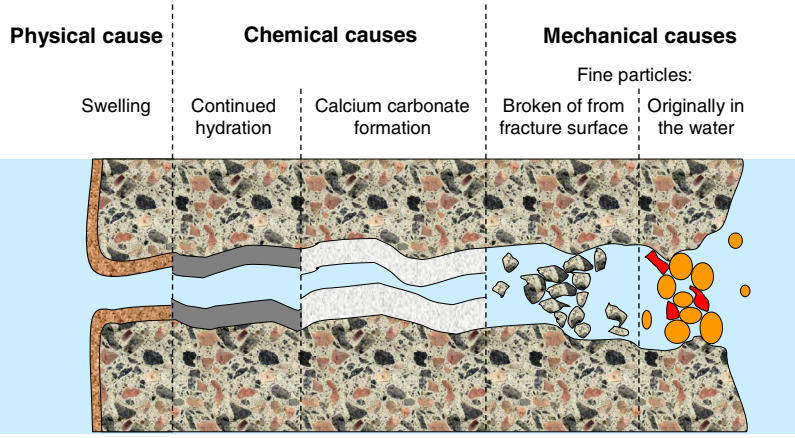


**Fig. 3.1** Different causes that can lead to autogenic self-healing

M. de Rooij et al. (Eds.): *Self-Healing Phenomena in Cement-Based Materials*, RILEM 11, pp. 65–117.
DOI: 10.1007/978-94-007-6624-2_3 

The physical cause is due to swelling of hydrated cement paste (HCP) near the crack faces. This phenomenon occurs when water is absorbed by HCP and reaches the space between the constituents of HCP. When the effect of swelling is estimated it turns out that this is marginal and does cause a reduction of the fluid flow by less than 10%.

There are two chemical processes. The first is the continued hydration of cement which has not reacted hitherto due to lack of water. When new reaction products are formed they grow into the free space of the crack. The hydration products occupy about double the space of the original cement grain. The continued hydration cannot be responsible for a complete self-closing of a crack, but, assuming a small crack width of 0.1 mm and assuming a simultaneous action of swelling and hydration, one can get self-healing. With larger crack width the influence becomes minor.

The second chemical process is the formation of calcium carbonate and the growth of crystals on the crack faces. Calcium ions from the pore water of concrete ($Ca^{2+}$) react with the carbonate ions of the water in the crack ($CO_3^{2-}$) and combine to $CaCO_3$ which precipitates in the crack. The reaction depends on temperature, pH, and concentration of the reactants. The mechanism has been investigated by Edvardsen in great detail [3.1]. It has been shown that this mechanism gives by far the most important contribution to self-healing.

There are two mechanical causes which are contributing to self-healing, i.e. the presence of fine particles in the water which leaks through the crack, and the fracturing of small concrete particles from the crack faces. However, these effects are of minor importance.

The above mentioned causes of self-healing are influenced by the concrete, by the water in the crack, and by the crack geometry. Table 3.1 shows the influencing factors schematically.

**Table 3.1** Influencing factors on self-healing [3.1]

| Concrete | Water | Crack |
|---|---|---|
| Type of cement | Pressure | Width |
| Type of additions | Pressure gradient | Length |
| Type of aggregate | Hardness | Through-crack vs. bending crack |
| Age | pH | Branched crack |
| | Temperature | Accumulated crack |

Concrete is a compound of matrix and aggregates. The matrix is composed of HCP, additions, and the very fine material of the aggregates. When cement hydrates calcium silicate hydrates (CSH), aluminates, and calcium hydroxide are formed. Calcium hydroxide is soluble in water and supplies the calcium ions which are necessary for the formation of calcium carbonate in the crack. (CSH is almost insoluble and will only supply calcium ions when the ions from calcium hydroxide are exhausted.) The supply of calcium ions from the HCP is the larger the more clinker is in the cement, i.e. Portland cement is the richest.

In composite cements, a part of calcium hydroxide is used for the formation of hydration products from a second main constituent like fly ash or pozzolanas. The

same is true for blast furnace slag cement which uses calcium hydroxide as an activator. The effects of such increasing demands of calcium hydroxide over time are shown in Fig. 3.2. One can see that the amount is larger for Portland cement than for blast furnace cement and that fly ash reduces the amount of calcium hydroxide with ongoing hydration.

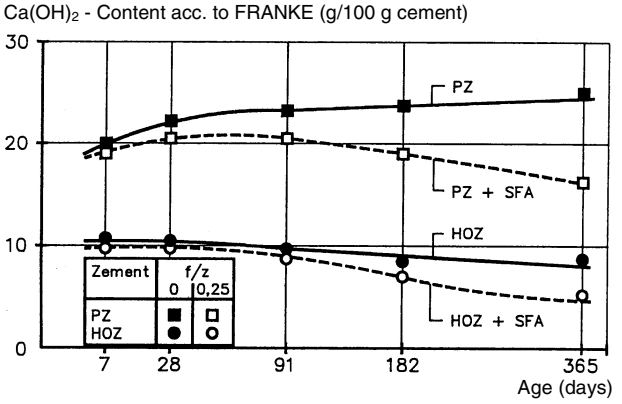


**Fig. 3.2** Amount of calcium hydroxide as function of age and type of cement [3.2]. PZ = Portland cement, HOZ = blast furnace cement, SFA = fly ash.

As the type of aggregate is concerned limestone aggregates may support self-healing. Furthermore, the shape of the aggregate grains and the grading curve can influence the crack geometry. The influence of the aggregate size is exemplified in Fig. 3.3. For a given crack width $w_m$ which is measured on the surface, the responsible opening for the flow of water is larger in case of small aggregates than with large aggregates. In concrete with a continuous grading of aggregates the situation is more complex but the same principle still holds.

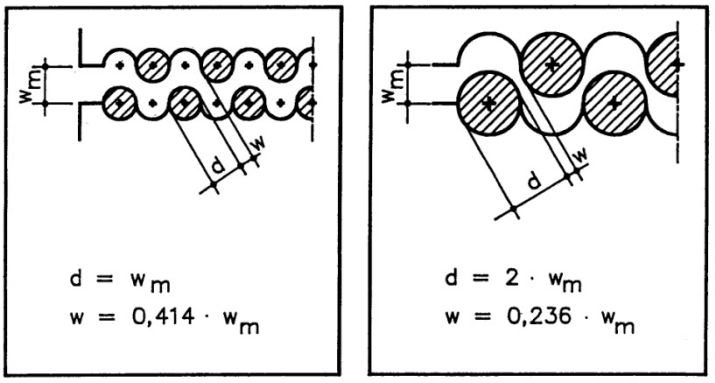


**Fig. 3.3** Idealised cracks in concrete with different aggregate size [3.4]

Water in the crack is the most important factor for autogenic self-healing. Without water there is no self-healing because water is needed for the chemical reaction and for the transport of fine particles. If carbon dioxide is present in water there is always a certain equilibrium between bound $CO_2$, half-bound $CO_2$, and free $CO_2$ which can be divided into complementary $CO_2$ and surplus $CO_2$. The surplus $CO_2$ is responsible for concrete attack where calcium carbonate dissolves to soluble calcium bicarbonate, whereas the complementary $CO_2$ leads to the formation of calcium carbonate from calcium hydroxide. There are several classifications of the aggressiveness of $CO_2$ on concrete (see for instance [3.3]).

The calcium carbonate grows on the crack surface as shown in Fig. 3.4. The calcite crystals ($CaCO_3$) form a dense layer which blocks the flow of water. The complete theory on crystal growth can be found in [3.5].

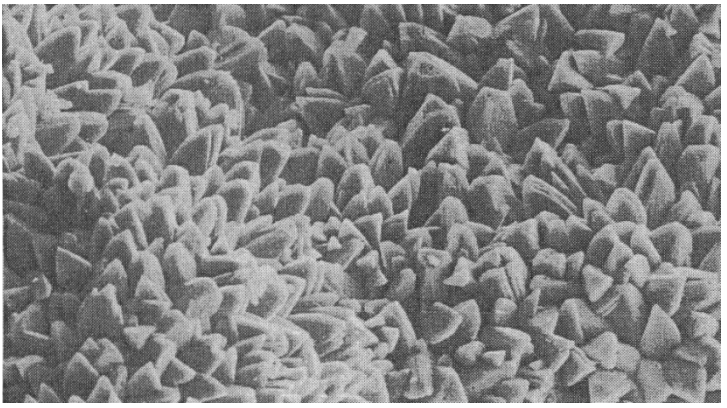

**Fig. 3.4** Calcite crystals on a crack face after opening the crack [3.1]

### *3.1.2 Experimental Evidence on Autogenic Self-Healing*

The self-healing phenomenon has been experienced since long time. Edvardsen performed a literature survey which will be used in the following paragraphs in short [3.1]. The first observation has been made by the French Academy of Science in 1836. Early publications mention the effect of self-healing [3.6-3.13]. Loving reported on self-healing of cracked concrete tubes mentioning the deposition of calcium carbonate in the crack [3.14]. Wagner [3.15] carried out experiments on the cement lining in steel pipes and found that cracks of 0.05 mm healed completely after 60 h. Cracks of 0.1 mm healed only after 1 year. Lauer and Slate [3.16] and Hannant and Keer [3.17] investigated the tensile strength of cracked hydrated cement paste (HCP) stored in water. They could show that 1 d old HCP regained about 25 % of its original strength whereas 28 d old HCP got only 7 % back. After 2 years moist storage [3.17] found even 50 % recovery. The authors concluded that continued hydration was the cause for the recovery. The influence of concrete age, ambient conditions, type of cement and aggregates, and

concrete composition have been studied by [3.18]. They concluded from the tests that the moisture supply is the most important factor for self-healing. They confirmed the conclusion by Lauer and Slate that the age at first cracking is also essential. The investigations by Clear [3.19] on cracked concrete cubes showed no influence of type of cement. He found that the smaller the initial flow was, the better the self-healing effect was. He found also that a slow increase of the pressure gradient during water exposure has a positive effect. As cause of self-healing, blocking of the crack by fine particles and the precipitation of calcium carbonate are assumed. Ripphausen [3.20] performed tests on reinforced concrete blocks. A main result was that the initial flow could be reduced to 1 to 10 % after 3 days. The most important parameters were found to be crack width and water pressure gradient. Meichsner [3.21] postulated two sources of self-healing. The first is the quick blocking of the crack by fine particles and the subsequent cause is the forming of calcium carbonate on the crack faces. Coarse aggregates in concrete yield a rougher crack surface and therefore a better self-healing effect. With increasing pressure gradient, the time until complete sealing becomes longer.

Edvardsen [3.1] performed systematic water permeability tests on small specimens with a single tensile through-crack. A typical result is shown in Fig. 3.5. The striking result is that the flow of water comes to standstill after 300 to 700 h.

The type of cement had a marginal influence. Several test series have been carried out with variation of water source (hardness), type of addition in the concrete, type of aggregate, pressure gradient, and crack width. It turned out that the first three parameters had hardly an effect on the results. The influence of the crack width is illustrated by Fig. 3.6. A 0.1 mm crack shows a flow reduction by

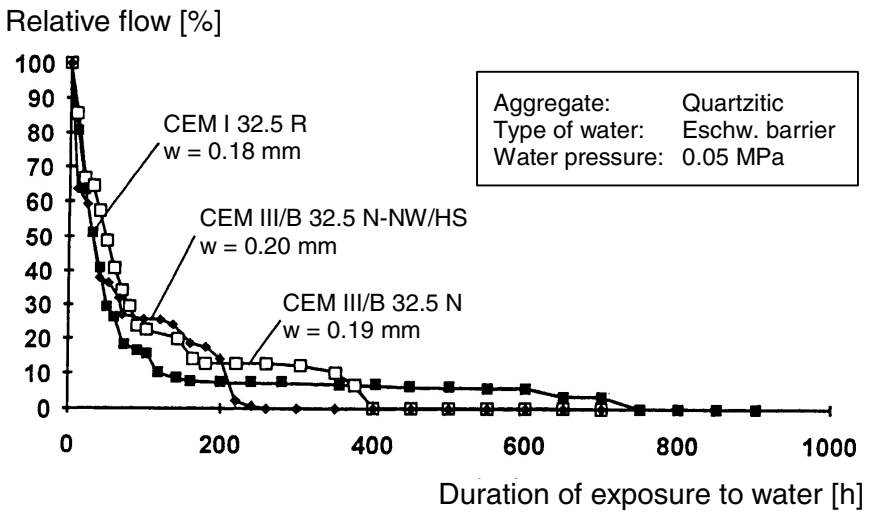


**Fig. 3.5** Flow relative to initial flow vs. duration of exposure to water [3.1]. CEM I = OPC, CEM III = BFSC.

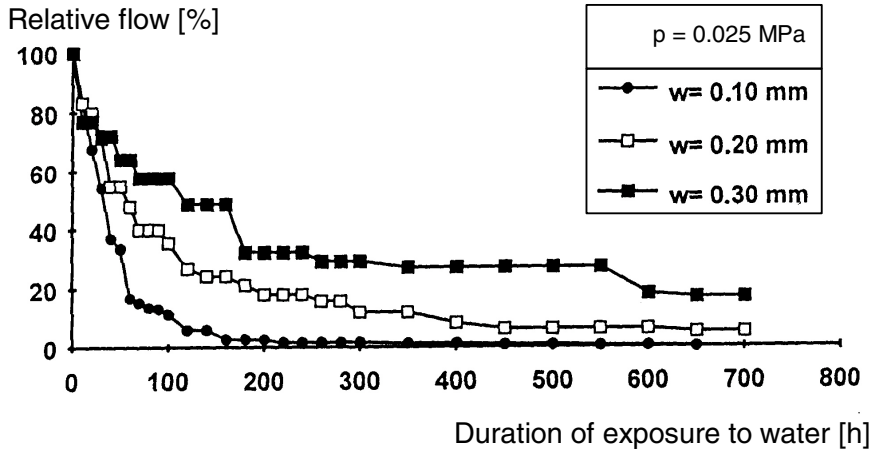


**Fig. 3.6** Influence of crack width on flow relative to initial flow [3.1]

about 90 % after 100 h, the 0.2 mm crack a reduction by 60 % and the 0.3 mm crack a reduction by 40 %. After 300 h, the 0.1 mm crack is blocked whereas the 0.2 mm crack has a leakage rate of 10 % and the 0.3 mm crack of a little less than 40 %. After 700 h, the leakage rate of the 0.2 mm crack is almost zero whereas the 0.3 mm crack has still a leakage rate of about 20 %. However, one should also look to the initial flow which is given in Fig. 3.7. The initial flow can be approximated by Poiseuille's third power law and it depends on the pressure gradient. Evaluating Fig. 3.6 and Fig. 3.7 together one can postulate that the reduction of flow in absolute sense is strongest for the larger crack width.

Edvardsen explains the self-healing effect by crystallisation of $CaCO_3$ in the cracks. X-ray diffraction experiments from crack faces show $CaCO_3$ as the main element. The author presents also a model governing the nucleation of calcium carbonate based on two different crystal growth processes. In the initial phase of water exposure, the kinetics of crystal growth is surface controlled (reactions with crystals on the crack surfaces) and later it is diffusion controlled (reactions with ion diffusing through the calcium carbonate layer already crystallized). The author shows that blocking of flow path by broken concrete particles is of less importance [3.22].

The influence of temperature between 20 and 80 °C and crack width between 0.05 and 0.15 mm on self-healing has been investigated by Reinhardt and Jooss [3.23]. Fig. 3.8 shows the results for high-strength concrete ($f_C$ = 93 MPa) with a constant crack width of 0.05 mm. The pressure gradient was 1 MPa/m over a specimen which was 50 mm thick. It is clearly visible that those specimens which were installed at 80 °C show the most efficient self-healing behaviour. After 75 h, the 20 °C specimen had a flow rate of 30 % of the initial flow rate, the 50 °C specimen about 10 % and the 80 °C specimen merely 3 %. After 330 h, the flow rate in all specimens went asymptotically to zero, i.e. complete sealing. Similar

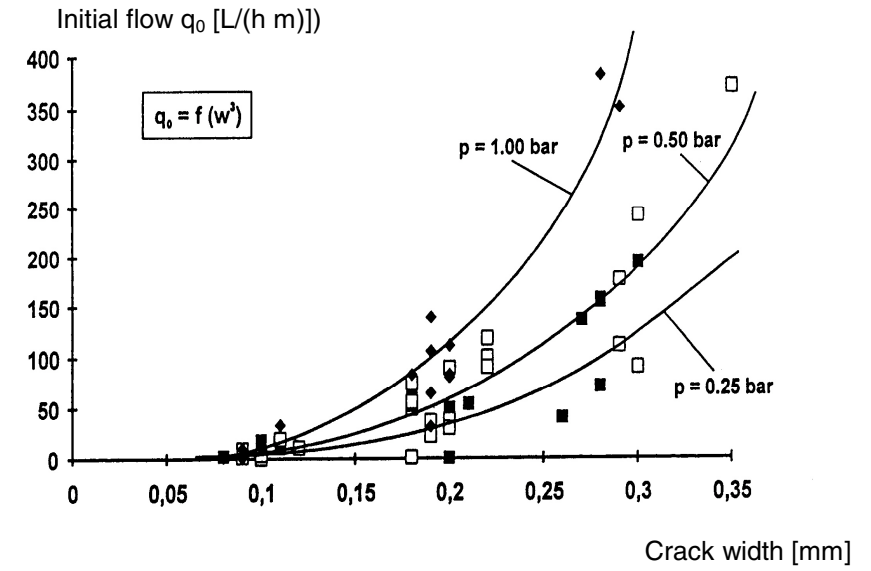


**Fig. 3.7** Initial flow through cracks of various widths for 1 m length [3.1]

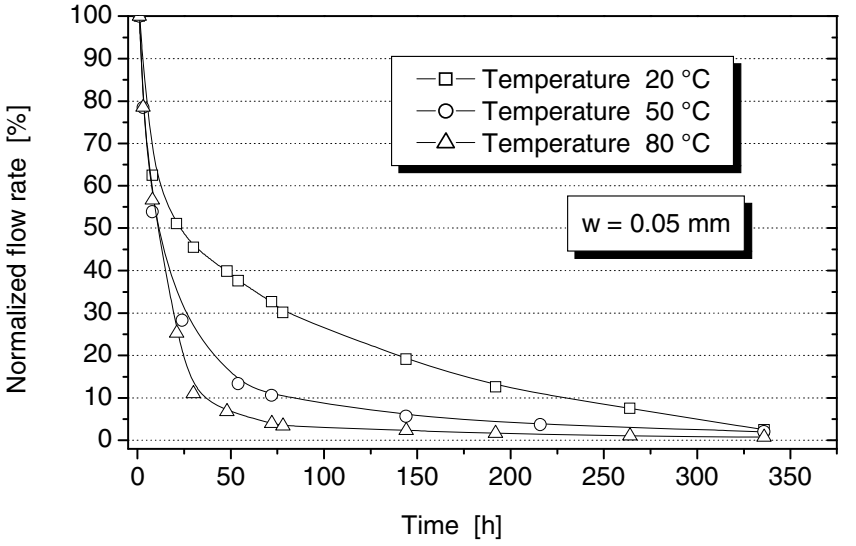


**Fig. 3.8** Decrease of normalized flow rate of high-strength concrete at various temperatures [3.23]

graphs could also be drawn for 0.10 and 0.15 mm crack width. However, it should be kept in mind that the absolute flow is about 3 times higher for the 80 °C water than for the 20 °C water since the viscosity of water drops from 1.00 mPa s to 0.35 mPa s at the same time.

The following two paragraphs are partly literally taken from [3.22]. Hearn [3.24, 3.25] carried out water permeability tests on mortar with 78 % hydrated clinker and 26 years old water-cured concrete with insignificant amount of unhydrated clinker. The author shows that without drying, especially on virgin never dried old concrete, there is no self-healing of cracks whereas drying results in an increasing initial permeability followed by self-healing. The author carried out chemical analyses and could find a phenomenon of dissolution-deposition, especially of $CaCO_3$. Moreover, self-healing was completely absent where water was replaced by propan-2-ol as a permeant. That is the most convincing evidence that physical clogging is not responsible for the phenomenon since its viscosity is close to that of water. Flow reversal tests show that self-healing is permanent. Concerning continued hydration, it is important for early-age concrete but not for mature one.

Another type of experiments was carried out by Jacobsen *et al.* [3.26, 3.27]. It consisted of damaging concrete cubes by rapid freeze-thaw cycles, and then storing them in 20 °C warm water for 3 months. Two types of concrete at water-cement ratio of 0.4, one with silica fume and the other without silica fume, were tested. Deterioration and healing was measured by resonance frequency (converted to dynamic modulus of elasticity) and compressive strength. Freeze-thaw cycles led to loss in both properties. Self-healing gave a substantial recovery of the frequency, but only a small recovery in compressive strength. It was explained by SEM observations that the cracks were only partly filled with new products. Most of the crystals seen in the cracks were newly formed CSH. Portlandite ($Ca(OH)_2$) was also observed locally. The study demonstrates that self-healing is less apparent in concrete containing silica fume than in concrete without silica fume.

Tests on Portland limestone composite cement (PLC) in comparison to OPC have been performed in order to study the self-healing properties of cracks which were 0.07 to 0.14 mm wide [3.28]. The authors did not find a difference between OPC and PLC. The results showed that the sealing time varied between 20 h for crack width of 0.10 mm and 70 h for crack width of 0.13 mm. However, this is only a rough indication since the scatter was rather large.

Some researchers [3.29-3.41] try to stimulate the self-closing potential of cementitious materials by replacing part of the cement by fly ash or blast furnace slag. In their study, Van Tittelboom *et al.* [3.41] prepared mortar specimens, with 8 different mix compositions. Three different cement types were used: CEM I or Portland cement, containing 100% Portland clinker; CEM II/B-M or also called Portland composite cement, containing 65-80% Portland clinker and 20-35% of a mixture of blast furnace slag, fly ash and limestone; and CEM III/B or blast furnace cement, containing 20-35% Portland clinker and 65-80% blast furnace slag. For some of the mixtures made with ordinary Portland cement (CEM I), respectively 30 and 50% of cement weight was replaced by fly ash and in two other mixes 50 and 70% of cement weight was substituted by blast furnace slag. All mortar mixtures were made with a water-to-binder ratio of 0.4, except for one mixture where a water-to-binder ratio of 0.5 was used. In Table 3.2, the composition of each mix is shown.

**Table 3.2** Composition of the mortar mixes giving weight of each constituent in gram [3.40]

| | Composition | | | | | | |
|---|---|---|---|---|---|---|---|
| | Sand | Cement | | | Fly ash | Blast furnace slag | Water |
| | DIN 196-1 | CEM I 52.5 N | CEM II/ B-M 32.5 N | CEM III/ B 32.5 HSR/LA | | | |
| CEMI-0.4 | 1350 | 450 | | | | | 180 |
| CEMI-0.4-30FA | 1350 | 315 | | | 135 | | 180 |
| CEMI-0.4-50FA | 1350 | 225 | | | 225 | | 180 |
| CEMI-0.4-50BFS | 1350 | 225 | | | | 225 | 180 |
| CEMI-0.4-70BFS | 1350 | 135 | | | | 315 | 180 |
| CEMII-0.4 | 1350 | | 450 | | | | 180 |
| CEMIII-0.4 | 1350 | | | 450 | | | 180 |
| CEMI-0.5 | 1350 | 450 | | | | | 225 |

When specimens were cured for 1 month and a half, they were fractured in a crack opening controlled splitting test. Subsequently, the crack width of each sample was measured at different locations, equally divided along the crack length. The average value was used to characterize the crack width of each specimen. The effect of the mortar composition on the self-healing potential was investigated by measuring the evolution in water permeability of the cracked specimens. A low pressure water permeability test setup was used. The drop in water level, due to water flow through the cracked specimen, was measured once a day and water was restored each time to the original level. Darcy's law was used to calculate the water permeability coefficient $k$.

During the test it was seen that the water flow through the specimens decreased. Van Tittelboom and De Belie [3.40] attributed the decrease during the first days of the test to disappearance of air bubbles present in the specimens. The ongoing decrease in water flow after 5 days from the beginning of the test was ascribed to crack-closing. For each specimen, the difference in the water permeability coefficient calculated at day 5 of the test and at the end of the test, being 14 days later, was calculated. In Fig. 3.9, the result is displayed.

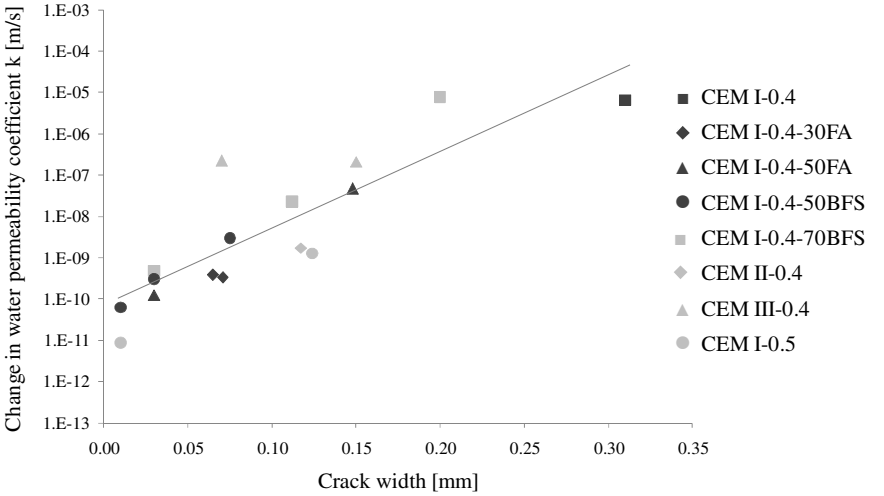


**Fig. 3.9** Decrease in water permeability coefficient k [m/s] due to autogenous closing of the crack in specimens with different crack widths [mm] and with different mix compositions; the grey line indicates the mean change in water permeability [3.40]

Van Tittelboom and De Belie [3.40] determined that for increasing crack widths, the difference in water permeability coefficient and consequently also the self-healing potential increased. It was supposed that mixes with a higher amount of cement particles or a lower water-to-binder ratio would contain more unhydrated particles and thus result in a higher degree of self-healing. However, this was not clear in the results. No big difference in self-healing potential was found between samples with a water-to-binder ratio of 0.4 and 0.5. By contrast a clear difference in self-healing potential was noticed depending on the mix composition. The degree of self-healing was higher when a higher amount of slag was used. It was supposed that part of the slag had not yet been hydrated during curing of the mortar and that unhydrated particles reacted during the water permeability test. As blast furnace slag is a latent hydraulic component, it may have been activated upon contact with water and quicker in the presence of free lime. In the case Portland clinker was replaced by fly ash, no big decrease in water permeability was detected. It seemed that the alkalinity in the crack environment was high enough to cause a fast hydration of blast furnace slag in the presence of water. However, this was not the case for fly ash. Van Tittelboom and De Belie stated that this difference could also be caused by the fact that the reaction of fly ash is slower than the reaction of blast furnace slag. From these experiments Van Tittelboom and De Belie concluded that the self-healing potential of cementitious materials may be altered by changing the mix composition.

### *3.1.3 Limiting Crack Width for Autogenic Self-Healing*

There are several hypotheses as the maximum crack width is concerned which can heal. Self-healing of bending cracks is more likely than of through-cracks. Ter Heide [3.38] postulated that a through-crack can never heal completely because of lack-of-fit of the crack faces. However, several other investigators have performed experiments on tensile cracks which were made by uniaxial pre-cracking or splitting. In these cases, a through-crack develops. They have found that such cracks can heal completely. However, one should consider the age and the composition of the concrete, the ambient environment, and the water supply. It turned out that young concrete heals faster, and that concrete with silica fume shows minor self-healing. There must always be water available and carbon dioxide because the main cause of self-healing seems to be the formation and precipitation of calcium carbonate.

Jacobsen *et al.* [3.42] made a survey and came to the conclusion that a through-crack, which is the most dangerous in water-retaining structures, of 0.2 mm can heal completely. The same value is supported by Meichsner [3.43]. Edvardsen [3.1] found that a crack of 0.3 mm can still heal. In her design proposal, she differentiates between water head (hydraulic gradient), crack width, and occurring movement of the crack [3.5, 3.44]. The proposal is shown in Table 3.3.

**Table 3.3** Permissible crack width for self-healing [3.5, 3.44]

| Hydraulic gradient, m/m | Design crack width, mm | |
|---|---|---|
| | With 10 % movement | With 10 to 20 % movement |
| 40 | 0.10 to 0.15 | 0.10 |
| 25 | 0.15 to 0.20 | 0.10 to 0.15 |
| 15 | 0.20 to 0.25 | 0.15 to 0.20 |

A crack movement of 10 % means that the crack may change its width by 10 % due to alternate loading, temperature, creep, or shrinkage/swelling of the structural element. Design crack width is a terminus technicus from DIN 1045-1 [3.45] and means the crack width which is calculated in the structural analysis. It is a probabilistic value with a certain distribution function. This value can be smaller or greater in real structures.

## 3.2 Autonomic Self-Healing

Autonomic self-healing has been defined in chapter 1 as a self-healing process where the the recovery process uses materials components that would otherwise not be found in the material (engineered additions).

### 3.2.1 Superabsorbent Polymers

Crack sealing can also be enhanced by using superabsorbent polymers (SAPs). These cross-linked polymers have the ability to absorb a significant amount of liquid from the surrounding environment (up to 500 times their own weight) and to retain the liquid within their structure without dissolving (Fig. 3.10).

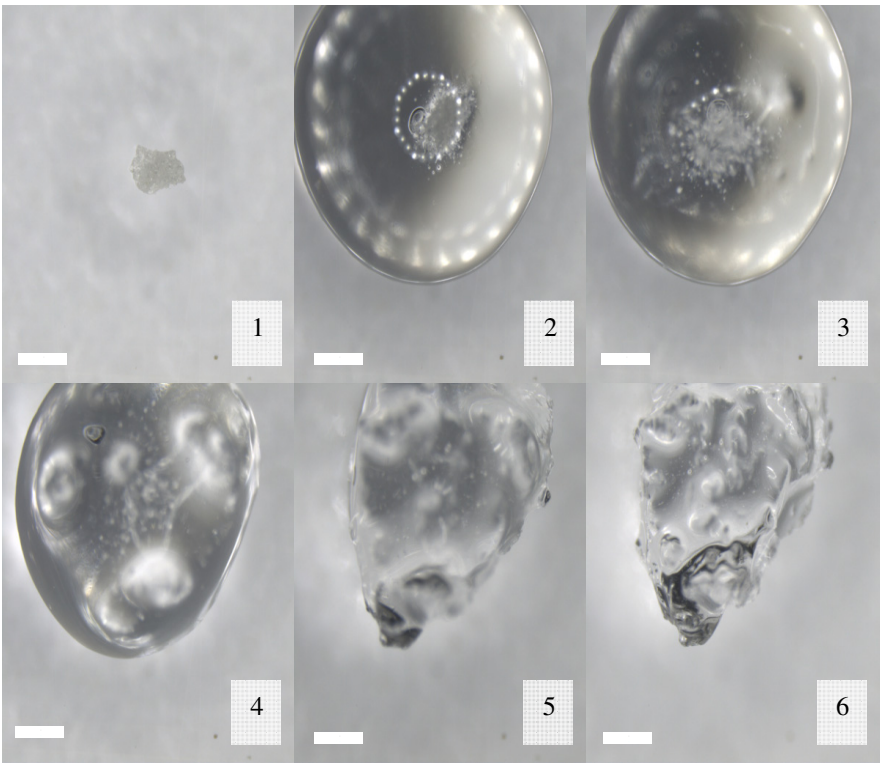


**Fig. 3.10** Absorption of water by a SAP particle. The scale bars on the bottom right have a lenght of 500 µm. [3.46]

Lee *et al.* [3.47] used superabsorbent polymers to obtain self-sealing properties. In his research, Lee used SAPs based on partially neutralized acrylates and acrylate/acrylamide copolymers and proved the sealing potential in different solutions between glass plates [3.47]. Cement pastes were also studied and the flow rate of a dilute sodium chloride solution through cracked specimens was measured (Fig. 3.11) [3.48]. The cumulative flow through specimens containing SAPs (xSy: x m% of cement weight of SAP y) was lower than for control specimens and specimens with 4-5 m% of SAPs by weight of cement (specimens 5S2 and 4S3) showed even a reduction up to 80% of the cumulative flow. When

cracking thus occurs, superabsorbent polymers are exposed to the humid environment and swell. In this way, the crack is blocked and the permeability is reduced.

Tsuji *et al.* [3.49] also investigated the effect of SAPs on the leakage of water through cracks. They found a decrease of the amount of water leaked through a crack in a mortar specimen containing 0.5 m% of cement weight of SAPs.

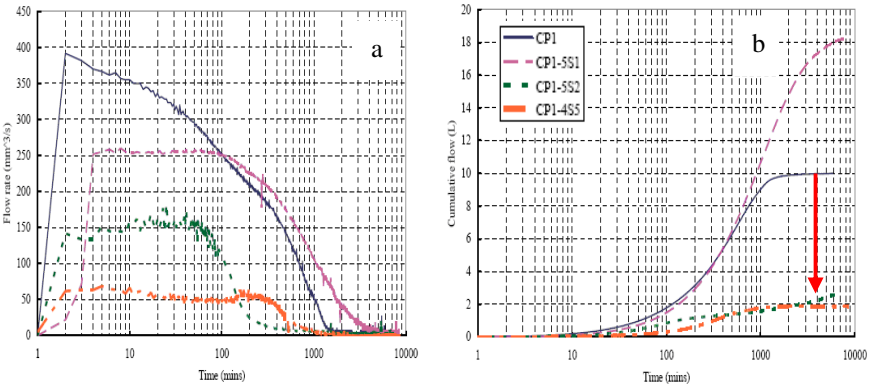


**Fig. 3.11** Flow rate (a) and cumulative flow (b) for specimens with a crack width of 200 µm [3.48]

Snoeck *et al.* [3.50] visualized water permeation by means of neutron radiography. Small specimens, 10 mm in diameter and 20 mm high with a crack width of 150 µm, were subjected to permeability tests and the change in water head was monitored in time. Fig. 3.12 shows the water permeability in time of the cracked samples without SAPs (0-CRA) and the cracked samples containing 1 m% of SAP B (1B-CRA) and 1 m% of SAP C (1C-CRA). It is clearly visible that all fluid has permeated through the samples containing no SAPs after 40 s. Samples containing SAPs are able to block the crack due to swelling of the SAP particles at the crack faces.

The water head on specimens without SAPs decreases rapidly. The water head on specimens with SAPs, however, did barely change in time. This proves the self-sealing effect of SAPs in cementitious materials.

The ability of three types of superabsorbent polymers (Table 3.4) to promote self-sealing and self-healing was investigated in water permeability tests by Snoeck *et al.* [3.46] (Fig. 3.13). Cracked specimens without SAP have a final k value of $1 \cdot 10^{-5}$ m/s. Specimens containing SAPs, however, show a decrease in permeability. This is mainly due to the swelling effect of SAPs and the blockage of the crack by SAPs. The SAP B particles are able to seal the crack more effectively in comparison to SAP A and SAP C. The difference noticed between

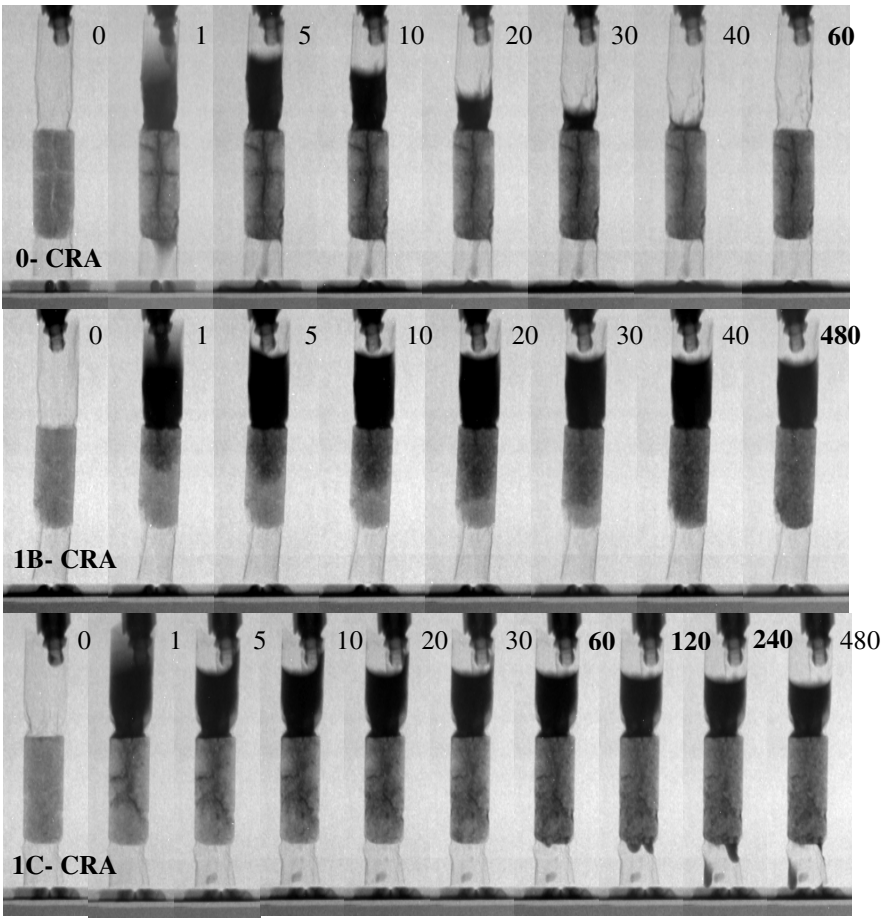


**Fig. 3.12** Water permeability of the samples without SAP and samples containing 1 m% SAP B and SAP C. In the upper right corner, the time is mentioned in seconds. [3.50]

SAP A and SAP B is due to the smaller particle size of SAP A. The small size is inappropriate for sealing as the small particles cannot bridge the crack as their expanding diameter does not reach over the total crack and water may flow in between the swollen particles. The difference noticed between SAP B and SAP C is due to a lower absorption capacity of SAP C (Table 3.4). As the particles swell less, they result in less crack sealing. SAP B in an amount of 1 m% relative to the cement weight provided the highest decrease in permeability over time. A higher amount of SAP B caused a coarser matrix (due to the formation of macro pores) and lower strength and thus more pathways for water to migrate.

**Table 3.4** Mean diameter of SAP A, SAP B and SAP C particles [µm] (n=50), absorption capacity of SAP [g fluid/g SAP] (n=3) in de-ionised water; tap water and cement slurry with standard deviations. [3.46, 3.50]

| Method | SAP A | SAP B | SAP C |
|---|---|---|---|
| Diameter | 100±22 | 477 ± 53 | 420 ± 148 |
| de-ionised water (pH=6.5) | 305.0 ± 3.7 | 283.2 ± 2.4 | 10.86 ± 0.16 |
| tap water (pH= 6.8) | 163.9 ± 1.2 | 148.9 ± 0.9 | 9.27 ± 0.22 |
| cement slurry (pH=12.8) | 61.0 ± 1.0 | 58.4 ± 1.7 | 7.42 ± 0.15 |

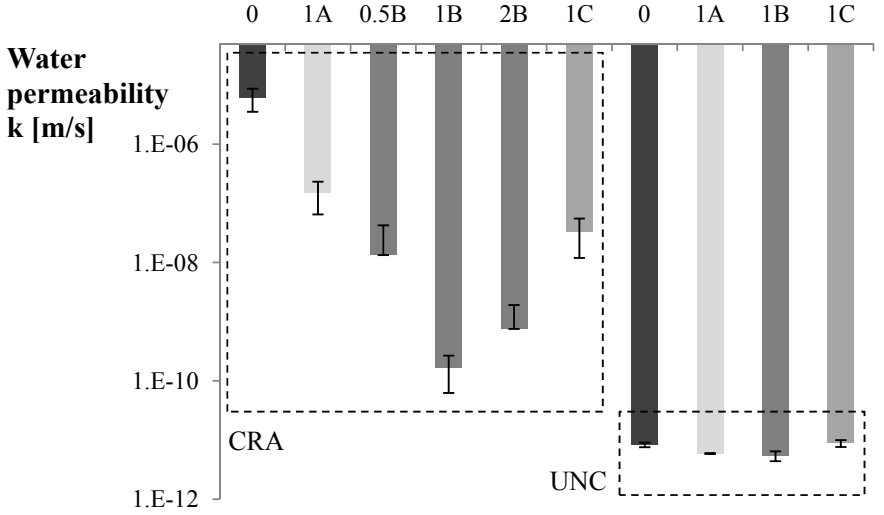


**Fig. 3.13** Water permeability k [m/s] at 30 days of the cracked (CRA) and un-cracked (UNC) specimens in the low-pressure water permeability test set-up (age of 37 days). The used code is xy (x m% of SAP y). The error bars show the standard deviation. (redrawn after [3.46, 3.51])

The swelling reaction not only seals the crack from intruding substances at first, but can also stimulate and enhance autogenic self-healing due to the release of their absorbed water into the cementitious matrix. Kim and Schlangen [3.52] and Snoeck *et al.* [3.46, 3.51] showed that superabsorbent polymers can contribute to the internal healing of a crack. The latter researchers conducted a thermo gravimetric analysis (TGA) to determine the composition of the white crystallization found in a crack after conducting permeability tests [3.46]. TGA showed that the crystals consisted of $CaCO_3$ and washed out hydration products. SAP particles were not found in the TGA analysis, supporting the conclusion that SAPs effectively seal the crack without dissolving or degrading.

### 3.2.2 *Protection against Carbonation of Blast Furnace Slag Mortar*

Sisomphon *et al.* [3.53, 3.54] made use of expanded clay particles impregnated with a sodium monofluorophosphate ($Na_2FPO_3$, Na-MFP) solution and coated with a slag containing cement paste layer to protect blast furnace slag mortar against carbonation (Fig. 3.14 I and II). When gaseous $CO_2$ diffuses into the matrix, carbonation attack will damage the microstructure and increase the

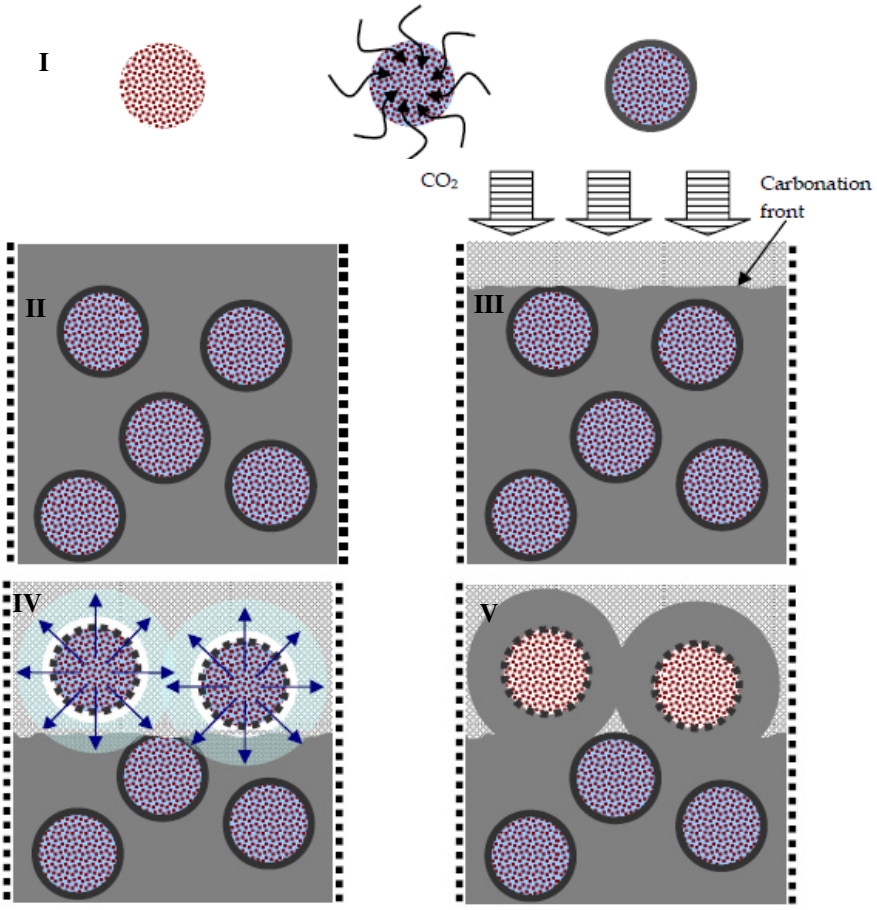


**Fig. 3.14** (I) LWAs impregnated with Na-MFP solution is prepared under vacuum. Then, the particles are encapsulated in a cement paste layer. (II) Encapsulated LWA embedded in the matrix. (III) Carbonation coarsens the matrix porosity. (IV) Carbonation damages the coating layer. Na-MFP is released to the matrix. (V) Healing takes place. The microstructure of the matrix is improved. [3.53]

porosity of both the matrix and the coating of the expanded clay particles (Fig. 3.14 III). With the presence of moisture, the $Na_2FPO_3$ solution diffuses into the degraded matrix to form phosphate and fluoride ions (Fig. 3.14 IV). These ions react with hydration and carbonation products to stable amorphous formations analogous to apatite resulting in a stronger and denser matrix and an improved frost scaling durability of the carbonated blast furnace slag matrix (Fig. 3.14 V).

### *3.2.3 Corrosion Prevention*

Dry and Corsaw [3.55] developed a technique to prevent corrosion of steel reinforcement. Corrosion of steel reinforcement is usually caused by chloride ions that penetrate in the concrete. Chloride sources include de-icing salts and marine waters. Methods to protect the concrete reinforcing steel against corrosion include the use of water repellent agents, such as silanes or siloxanes, additives such as microsilica and corrosion inhibitors such as calcium nitrite. Water repellent agents are sometimes unsuccessful because of their inability to protect the concrete if cracking occurs after treatment. In some structures containing microsilica, full-depth cracking has occurred due to high autogenous and drying shrinkage. Concretes containing calcium nitrite have generally performed well, however the set time of concrete may be affected [3.55].

The system proposed by Dry and Corsaw [3.55] involves the use of coated, hollow, porous (40%) polypropylene fibers (400 µm) filled with calcium nitrite. The fibers were filled by placing them in a solution of calcium nitrite into a vacuum flask and using vacuum saturation techniques to draw the calcium nitrite into the fibers. Because the used fibers were porous, they were treated with a coating to maintain the content. The coating controls the time-release of the calcium nitrite, ideally by responding to the environment of the pore solution. Polyol, one of the two types of coating used by Dry and Corsaw [3.55], breaks down in the presence of chloride ions. At the moment chloride ions penetrate, the steel reinforcement is endangered but at the same time the polyol coating will dissolve and the released calcium nitrite will protect the reinforcement. The second coating, paraffin wax, was applied to another set of fibers to simulate a mechanical release response. In this case the rebar should be heated to melt the wax and release the embedded calcium nitrite. After they were coated, the polypropylene fibers were wound around the reinforcement bars of the test samples. Both methods of response were investigated in this study. The efficiency was compared with specimens without any corrosion inhibitor and specimens with freely mixed calcium nitrite.

A plexiglass dam was built on each sample and sealed with silicone caulk to allow salt water to be ponded as shown in Fig. 3.15. The samples were ponded 1 week with a salt water solution that contained 1.321% sodium chloride and then allowed to dry 1 week. The voltage drop across a 100-ohm resistor, which was connected externally between the anode and the cathode, was measured weekly. Systems were compared by electrochemical measurements on the basis of the time to initiation of corrosion and the amount of corrosion occurring over time.

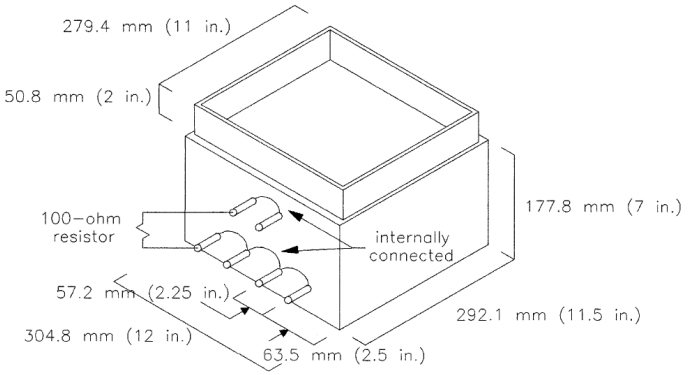


**Fig. 3.15** Setup to subject samples to salt solution and measure rebar corrosion [3.55]

The corrosion condition rating and expected time until the initiation of corrosion show that the time-release method delayed the onset and severity of corrosion, as shown in Fig. 3.16. Both the control group and the group with freely mixed calcium nitrite had much higher ratings than the other groups. In comparison both groups of fiber samples had almost less than half the rating of the control and freely mixed group.

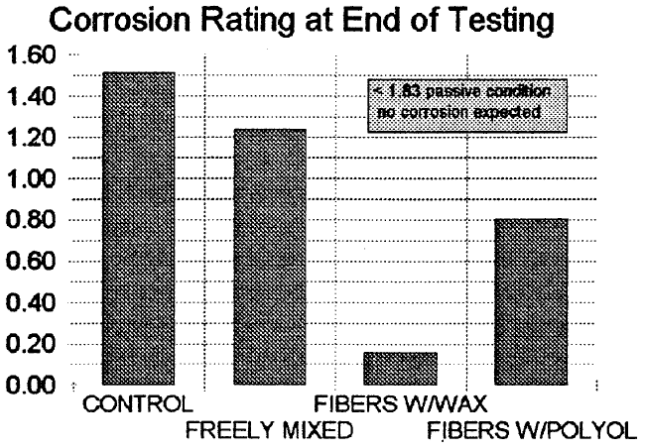


**Fig. 3.16** Corrosion rating measured for each of the different test series [3.55]

### *3.2.4 Textile-Reinforced Concrete*

Textile-reinforced concrete (TRC) is a high-performance, cement-based composite consisting of fine-grained concrete and textile reinforcement, the latter usually consisting of glass or carbon multi-filament yarns. When subjected to tensile

loading, TRC shows pronounced strain hardening behaviour accompanied by multiple cracking. Mechtcherine and Lieboldt [3.56] investigated transport of water and gases through cracked TRC at chosen strain levels under uniaxial tensile loading and the subsequent self-healing behaviour of the TRC specimens.

The matrix composition was developed with an eye to the requirements of workability, good bonding to the textile reinforcement, durability, and other considerations [3.57]. Table 3.5 shows the composition of the matrix used for the production of TRC specimens.

**Table 3.5** Mix proportions of the TRC matrix

| Material | Mass ratio [-] | Mix proportion [kg/m³] |
|---|---|---|
| CEM III B 32.5 N-NW/HS/NA | 2.0 | 550 |
| Fly ash | 0.9 | 248 |
| Micro silica suspension (solid:water = 1:1) | 0.2 | 55 |
| Fine sand 0/1 | 4.0 | 1101 |
| Water | 0.9 | 248 |
| Super plasticizer | 0.03 | 8 |

Four different types of biaxial textile reinforcements made of alkali-resistant glass (AR glass) and one made of carbon were used as reinforcement for the specimens in this investigation, see Table 3.6. Variable parameters were the fineness of the yarns and the presence or absence of a coating. A polymer coating composed of styrene-butadiene was used to improve the bond between the textile and the surrounding finely grained concrete matrix as well as the bond between the outer and inner filaments in the yarn.

**Table 3.6** Textile reinforcements

| Material | | Alkali-resistant glass (AR glass) | | | | Carbon |
|---|---|---|---|---|---|---|
| Yarn fineness | [tex][1] | 1280 | 2400 | 1280 | 2400 | 800 |
| Filament diameter | [µm] | 14 | 27 | 14 | 27 | 7 |
| Number of filaments per yarn | [-] | 3200 | 1600 | 3200 | 1600 | 12000 |
| Yarn spacing | [mm] | 7.2 | 7.2 | 7.2 | 7.2 | 7.2 |
| Mass/area | [g/m²] | 364 | 676 | 374 | 707 | 257 |
| Content of polymer coating | [% by mass] | - | - | 2.7 | 4.6 | 9.8 |

[1] tex = g/km

Rectangular plates 600 mm long, 100 mm wide, and 14 mm thick were produced with four textile layers. The plates were removed from the mould at a concrete age of two days and then stored in water up to an age of 7 days. Then the plates were stored in a climate-controlled room at 20 °C and 65% RH until testing or further preparation.

The in-situ permeation tests were performed at a specimen age of 56 days or slightly higher. At this age the hydration of binder components was to a large extent completed. A special permeation cell was developed which excluded any significant hindrance of the longitudinal deformation of the enclosed TRC specimens by the permeation cell, see Fig. 3.17.

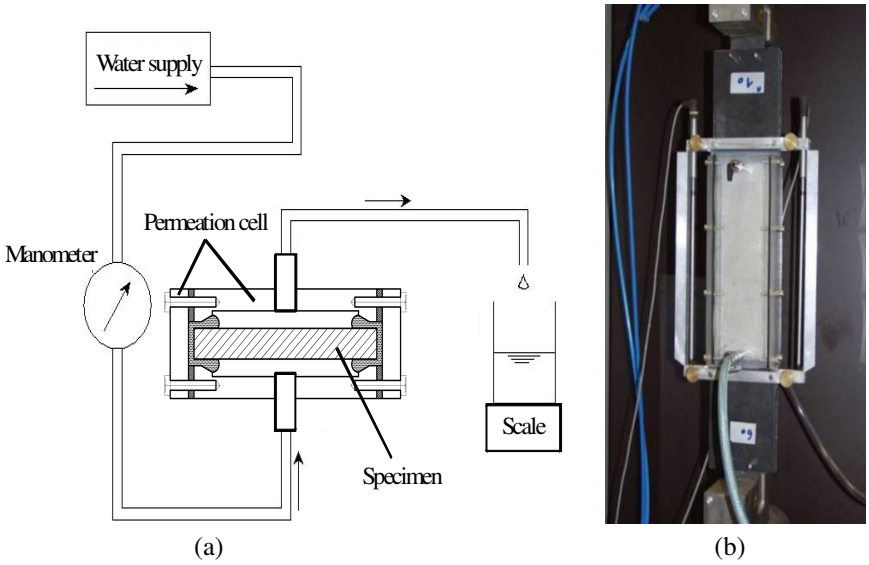


**Fig. 3.17** In-situ permeability measurements: a) schematic of the test set-up, b) testing under tensile load [3.56]

During the test, the specimen was exposed to constant water pressure on one surface, while the opposite surface was subjected to atmospheric pressure. The water amount passing through the specimen was measured and recorded automatically using a high precision balance. The effect of the strain on the volume flow rate in the quasi-stationary state is shown in Fig. 3.18 for TRC made of different textiles. The transport rates increased hyper-proportionally at strain levels above 0.2%. As expected, the tests on the specimens with finer crack patterns (large number of crack and accordingly smaller crack width for the same stain level) exhibited lower flow rates.

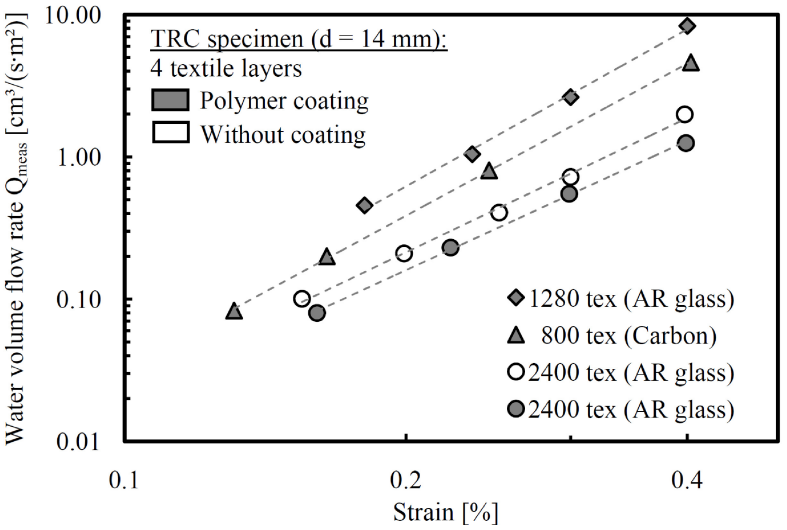


**Fig. 3.18** Effect of the imposed strain level on the specific water flow rate for TRC with different textile reinforcements, induced pressure 100 kPa [3.56]

Following the in-situ water permeation measurements, the samples were left in the permeation cell. In order to investigate the effect of self-healing on the transport properties of TRC, further water permeation measurements were carried out in the unloaded, saturated state of specimens at time intervals of 7 days. Fig. 3.19 shows the time-dependent reduction of the transport rates of samples with different reinforcement textiles. After storing the cracked specimens in water for 14 days, the flow rate was reduced to less than 50% of the value obtained on the same specimen before the water storing. No measurable volume flow occurred after continued water exposure of 21 to 35 days, the particular duration depending on the type of the textile reinforcement used. The samples containing uncoated AR glass yarns with low yarn fineness (1280 tex) needed a longer time until a negligible volume flow was reached, which can be traced back to the initially wider cracks in these specimens. The specimens containing coated carbon textile layers showed the fastest self-healing, which could be expected since they had the finest cracks.

The reduction in the flow rate resulted mainly from the formation of new crystal structures in the fine cracks and additional hydration of the previously non-reacted material as well as from the swelling of cement gel (primarily C-S-H) due to additional water intake. In order to eliminate the influence of swelling, a further oxygen permeability test was performed after water storage of up to 35 days. Since the specimens were dried before the oxygen permeation test, the effect of swelling of the cement matrix could be excluded. The verification should be apparent from the comparison of the oxygen permeability measured before the first loading cycle (crack-free samples) and after the second loading cycle

(cracked samples) with the results of the additional tests on the dried specimens after long-term water storage. Oxygen permeation was reduced to a minimum; the flow rates were similar to the reference measurement data of the crack-free samples before the first loading. Hence, the obvious explanations for the measured decrease in the gas volume flow rate are the self-healing of fine cracks and further hydration of the cement matrix.

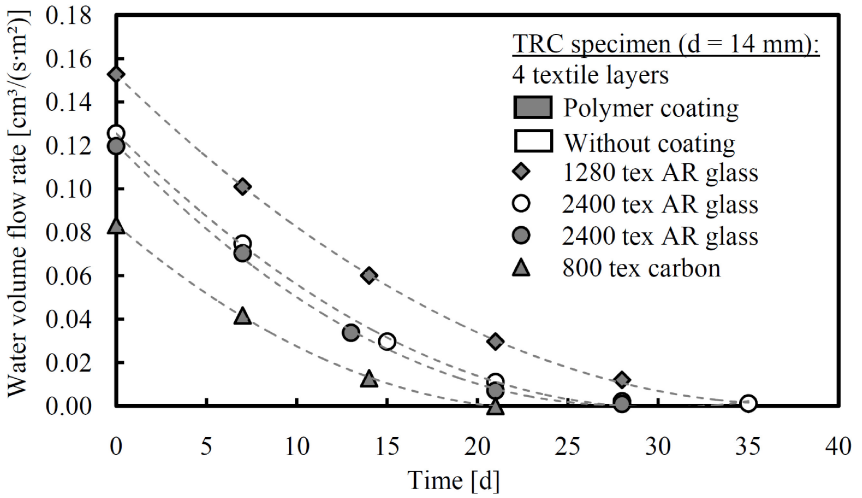


**Fig. 3.19** Time-dependent reduction of the water transport trough cracked TRC in unloaded state [3.56]

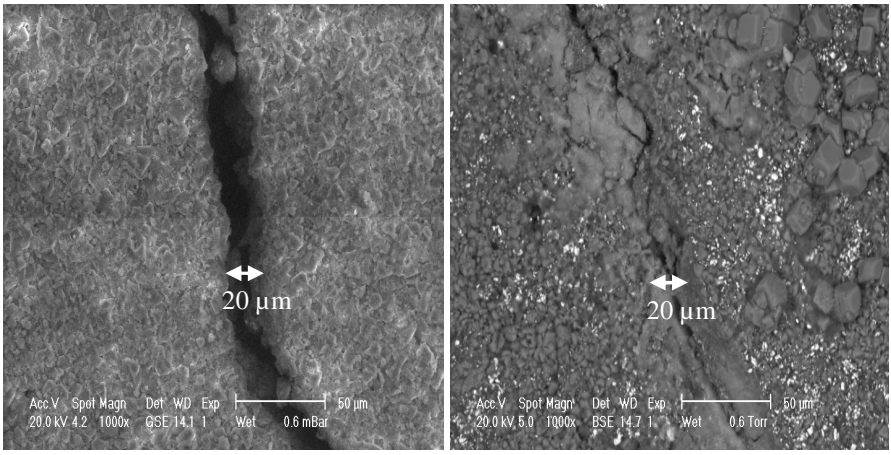


(a) (b)

**Fig. 3.20** Self-healing effect: a) crack before and b) after water exposure [3.56]

Using an ESEM (Environmental Scanning Electron Microscope), additional investigations of cracks before and after exposure to water revealed the formation of new crystal structures which closed the cracks to transport, cf. Fig. 3.20. Fig. 3.20a shows the original crack with a width of 20 µm before water contact. Fig. 3.20b illustrates the condition of a similar crack after the water permeability tests with duration of 21 to 35 days, indeed largely closed by deposits of calcium carbonate (calcite).

## *3.2.5 Microbially Induced Carbonate Precipitation*

In the last decades, microbially induced carbonate precipitation (MICP) has been investigated as an environment friendly method for surface consolidation and protection of decayed ornamental stone and concrete. The method has been first applied to form a compatible and highly coherent carbonate precipitate on limestone. Later, this technique has been explored for the improvement of the durability of cementitious materials. Furthermore, the same principle has also been used for the generation of a biological binder. An in-depth overview on the use of MICP has recently been published [3.56] and has been used as a basis for the first part of this chapter, to provide a deeper insight into the principles and important parameters of MICP. Recent advances indicate the potential use of this technique for the remediation of cracks in building materials, strength improvement and self-healing of cementitious materials.

### 3.2.5.1 The Principles of Microbially Induced Carbonate Precipitation (MICP)

Like other biomineralization processes, calcium carbonate ($CaCO_3$) precipitation can occur by two different mechanisms: biologically controlled, or induced [3.59]. In biologically controlled mineralization, the organism controls the process, i.e. nucleation and growth of the mineral particles, to a high degree. However, calcium carbonate production by bacteria is generally regarded as “induced”, as the type of mineral produced is largely dependent on the environmental conditions [3.60] and no specialized structures or specific molecular mechanism are thought to be involved [3.61]. Different types of bacteria, as well as abiotic factors (salinity and composition of the medium) seem to contribute in a variety of ways to calcium carbonate precipitation in a wide range of different environments [3.62, 3.63].

Calcium carbonate precipitation is a rather straightforward chemical process governed mainly by four key factors [3.64]:

1) the calcium concentration,
2) the concentration of dissolved inorganic carbon (DIC),
3) the pH and
4) the availability of nucleation sites.

$CaCO_3$ precipitation requires sufficient calcium and carbonate ions so that the ion activity product (IAP) exceeds the solubility constant ($K_{so}$) (Eq. (3.1) and (3.2)).

$$Ca^{2+} + CO_3^{2-} \leftrightarrow CaCO_3 \tag{3.1}$$

$$\Omega = \frac{(Ca^{2+}).(CO_3^{2-})}{K_{so}} \tag{3.2}$$

with $K_{so\ calcite,\ 25°C} = 4.8 \times 10^{-9}$.

The concentration of carbonate ions is related to the concentration of DIC and the pH of a given aquatic system. In addition, the concentration of DIC depends on several environmental parameters such as temperature, salinity and the partial pressure of carbon dioxide (for systems exposed to the atmosphere). The equilibrium reactions and constants governing the dissolution of $CO_2$ in aqueous media (25°C and 1 atm) are given in equations (3.3) to (3.6) [3.65].

$$CO_{2(g)} \leftrightarrow CO_{2(aq.)} \quad (pK_H = 1.468) \tag{3.3}$$

$$CO_{2(aq.)} + H_2O \leftrightarrow H_2CO_3* \quad (pK = 2.84) \tag{3.4}$$

$$H_2CO_3* \leftrightarrow H^+ + HCO_3^- \quad (pK_1 = 6.352) \tag{3.5}$$

$$HCO_3^- \leftrightarrow CO_3^{2-} + H^+ \quad (pK_2 = 10.329) \tag{3.6}$$

With $H_2CO_3^* = CO_{2(aq.)} + H_2CO_3$

Microorganisms can influence precipitation by altering almost any of the precipitation parameters described above, either separately or in various combinations with one another [3.64]. However, the primary role has been ascribed to their ability to create an alkaline environment through various physiological activities. Both autotrophic and heterotrophic pathways are involved in the creation of such an alkaline environment (for an extensive review, see Castanier *et al.* [3.66]. A first heterotrophic pathway involves the sulphur cycle, in particular the dissimilatory sulphate reduction, which is carried out by sulphate reducing bacteria under anoxic conditions. A second heterotrophic pathway involves the nitrogen cycle, and more specifically, (1) the oxidative deamination of amino acids in aerobiosis, (2) the dissimilatory reduction of nitrate in anaerobiosis or microaerophily and (3) the degradation of urea or uric acid in aerobiosis. Another microbial process that leads to an increase of both the pH and the concentration of dissolved inorganic carbon is the utilization of organic acids [3.67], a process which has been commonly used in microbial carbonate precipitation experiments. The precipitation pathways described above are general in nature, which accounts for the common occurrence of microbial carbonate precipitation and validates the statement by Boquet *et al.* [3.68]) that under suitable conditions, most bacteria are capable of inducing carbonate precipitation.

Besides changes induced in the macro-environment, bacteria have also been reported to influence calcium carbonate precipitation by acting as sites of nucleation or calcium enrichment [3.69]. Due to the presence of several negatively charged groups on the cell wall, at a neutral pH, positively charged metal ions can be bound on bacterial surfaces [3.70, 3.71]. Such bound metal ions (e.g. calcium) may subsequently react with anions (e.g. carbonate) to form an insoluble salt (e.g. calcium carbonate). The anion (e.g. carbonate) in this reaction may be a product of the bacterial metabolism, or it may have an abiotic origin [3.71].

The evidence of microbial involvement in carbonate precipitation has subsequently led to the exploration of this process in a variety of fields. A first series of applications is situated in the field of bioremediation. In addition to conventional bioremediation strategies which rely on the biodegradation of organic pollutants [3.72, 3.73], the use of MICP has been proposed for the removal of metal ions. Applications include the treatment of groundwater contaminated with heavy metals [3.74] and radionucleotides [3.75], the removal of calcium from wastewater [3.76, 3.77]. Another series of applications aims at modifying the properties of soil, i.e. for the enhancement of oil recovery from oil reservoirs [3.78], plugging [3.79] and strengthening of sand columns [3.80, 3.81]. Moreover, microbially induced precipitation has been investigated for its potential to improve the durability of construction materials such as limestone and cementitious materials. The latter can be divided into processes for the deposition of a protective surface layer with consolidating and/or waterproofing properties i.e. biodeposition, and processes for the generation of a biologically induced binder, i.e. biocementation.

#### 3.2.5.2 Biodeposition

Boquet *et al.* [3.68] were among the first to demonstrate the ability of soil bacteria to precipitate calcium carbonate under laboratory conditions. Among the organisms tested, several Bacillus strains (incl. *Bacillus cereus*) and *Pseudomonas aeruginosa* were observed to form crystals. Adolphe *et al.* [3.82] were among the first to consider the use of microbially induced carbonate precipitation (MICP) for the protection of ornamental stone. They applied for a patent regarding the use of calcinogenic bacteria on stone surfaces. Since the best performance was obtained with *B. cereus*, which could also be easily produced on an industrial scale, this organism was selected for *in situ* applications [3.83]. The nutritional medium was designed to stimulate the production of carbonate through the nitrogen cycle metabolic pathways. More specifically, the media contain a source of proteins for the oxidative deamination of amino acids in aerobiosis and a source of nitrate for the dissimilatory reduction of nitrate in anaerobiosis or microaerophily. In addition, a fungicide was added to prevent the unwanted growth of fungi present on the stone, or deposited from the air [3.84]. The proposed *in situ* treatment consists of first spraying the entire surface to be protected with a suitable bacterial suspension culture. Subsequently, the deposited culture is fed daily or every two

days (about five applications in total) with the suitable medium in order to create a surficial calcareous coating [3.85]. The first application *in situ* was carried out in 1993 in Thouars on the tower of the Saint Médard Church, consisting of Tuffeau limestone. The presence of the biocalcin decreased the water absorption rate to a significant extent (5 times) while retaining the permeability for gas. Furthermore, no influence on the aesthetic appearance could be observed [3.85].

The promising results of this so called Calcite Bioconcept technique encouraged different research groups to evaluate alternative approaches for the biomediated carbonate precipitation on limestone. These approaches can be mainly divided into those falling within and those falling outside the specifications of the patent by Adolphe *et al.* [3.82], i.e. the application of calcinogenic bacteria to a stone surface. The first series of approaches, those falling within the patent specifications, are characterized by the use of different microorganisms, metabolic pathways or delivery systems to overcome some of the potential limitations of the Calcite Bioconcept technique. In the second series of approaches, no microorganisms are applied to the surface. These approaches can be divided into studies where inducing macromolecules are supplied to the stone together with a supersaturated solution of calcium carbonate and studies which obtain carbonate precipitation by the microbiota inhabiting the stone. In the latter, only nutrients are added to the stone.

#### *3.2.5.2.1 Biodeposition through the Application of Calcinogenic Bacteria to a Stone Surface*

At the University of Granada, Rodriguez-Navarro *et al.* [3.86] proposed the use of *Myxococcus xanthus* for the creation of a consolidating carbonate matrix in the porous system of limestone. For the production of carbonate ions, the authors proposed a medium containing a pancreatic digest of casein as the nitrogen source. Also, the effect of a phosphate buffer on the carbonate production was investigated. The authors observed carbonate cementation to a depth of several hundred micrometers (> 500 µm) without the occurrence of any plugging or blocking of the pores.

At Ghent University, Dick *et al.* [3.87] proposed the microbial hydrolysis of urea as a strategy to obtain a restoring and protective calcite layer on degraded limestone. The hydrolysis of urea presents several advantages over the other carbonate generating pathways, as it can be easily controlled and it has the potential to produce high amounts of carbonate within a short period of time. The hydrolysis of urea is catalyzed by means of urease. As a consequence, urea is degraded to carbonate and ammonium, resulting in an increase of the pH and carbonate concentration in the bacterial environment [3.88]. As calcium ions are bound to the cell wall as a result of the negative charge of the latter, this can result in the formation of crystals on the bacterial cell. A schematic overview, of the ureolytic carbonate precipitation occurring at the microbial cell wall is given in Fig. 3.21.

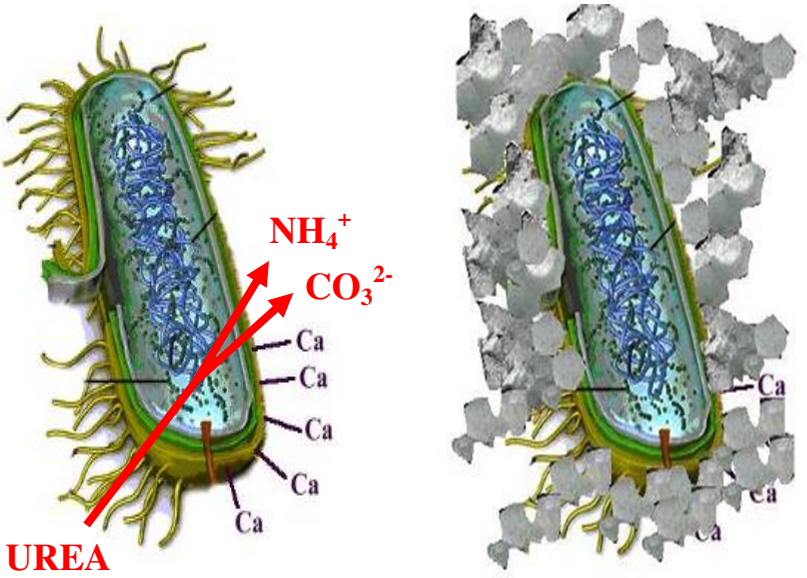


**Fig. 3.21** Principle of $CaCO_3$ precipitation by ureolytic bacteria (after 3.64)

First, Dick *et al.* [3.87] identified the microbial key factors which contribute to the performance of the biodeposition treatment. For the evaluation of the performance, the authors investigated the water absorption rate of treated and untreated Euville limestone. Of the parameters that were screened (calcite deposition on limestone cubes, pH increase, urea degrading capacity, EPS production, biofilm formation, ζ-potential and deposition of dense crystal layers), the ζ-potential proved to be the factor with the greatest predictive power for good limestone restoration, reflecting the effect on the initial water absorption rate. The ζ-potential is a measure of the potential of the electric layer at the surface of the cells, and is therefore an important parameter in the adhesion and surface colonization by bacteria. Due to the positive ζ-potential of the limestone, bacteria with a highly negative ζ-potential will be more easily retained. The second important key factor was the specific urea degradation rate. Bacteria with a high initial specific urea degradation rate show a high affinity for urea. This allows for a high substrate turnover for a limited amount of cells.

Although urease activity is widespread among different groups of microorganisms, it was mainly microorganisms closely related to the *Bacillus sphaericus* group which were shown to proliferate and express the urease gene under the given cultivation conditions [3.77]. From the screening procedure described above, 2 strains of *B. sphaericus* were selected for further experiments. These strains were shown to decrease the initial water absorption rate by approximately 50%.

As an extension to the above mentioned study, De Muynck *et al.* [3.89, 3.90] investigated the biodeposition with *B. sphaericus* as a surface treatment for cementitious materials (Portland cement mortar) with different porosities. All experiments were performed at 28°C under non-sterile conditions. The mortar specimens were immersed for 24 hours in a one day old culture of *B. sphaericus* containing *ca.* $10^7$ cells.mL$^{-1}$, after which they were transferred to fresh medium containing a calcium source. The specimens were removed from the solution after three days. The authors demonstrated that the biodeposition treatment resulted in an increased resistance of mortar specimens towards carbonation, chloride penetration and freezing and thawing, especially for more porous mortars with higher water to cement ratios (w/c). Moreover, the biodeposition treatment showed a similar protection towards degradation processes as some of the conventional surface treatments under investigation (silanes, siloxanes, silicates and acrylates). The biodeposition treatment on cementitious materials can be regarded as a coating system, since carbonate precipitation is mainly a surface phenomenon due to the limited penetration of the bacteria in the porous matrix. From thin section analyses, it was observed that the majority of the surface was covered with a layer of crystals with thicknesses within the range of 10-40 µm, in which often larger crystals (up to 110 µm) could be found. The morphology of the crystals was observed to be highly dependent on the medium composition. In the event calcium chloride was used as the calcium source, rhombohedral carbonate crystals were obtained (Fig. 3.22). In the presence of calcium acetate, spherulitic crystals were observed. However, no differences in the protective effect were observed between biodeposition treatments with a different calcium source.

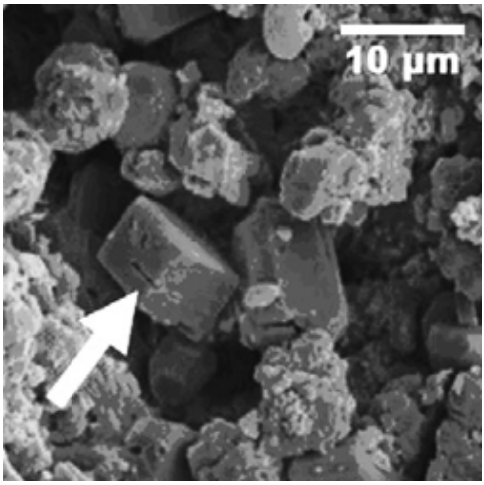


**Fig. 3.22** Scanning electron micrographs of rhombohedral $CaCO_3$ crystals on the surface of mortar specimens treated with *Bacillus sphaericus* and a nutrient medium consisting of urea and calcium chloride

The Biobrush (BIOremediation for Building Restoration of the Urban Stone Heritage) project consortium introduced the use of Carbogel into the field of biodeposition. According to the consortium, these delivery systems could be used to control the possible harmful side effects of bacteria to stone. Within the framework of the Biobrush project regarding biodeposition, bacteria isolated from a stream in Somerset (UK), and bacteria from culture collections that had been reported to have calcifying activity, were screened for their ability to deposit calcite. From the 10 isolates that were retained and assessed for their ability to deposit calcite on stone surfaces, *Pseudomonas putida* was chosen for further study in field trials. In these field trials, bacteria were applied to the stone by brushing. Subsequently, the bacteria were covered with moistened Japanese paper, above which a 1-1.5 cm thick layer of Carbogel prepared with modified B4 medium was applied. Tris-HCl buffer was added to the Carbogel to adjust the low pH of this carrier. Finally, the gel was covered with a polyethylene sheet. As a result of this treatment a decrease of the water absorption and open porosity by 1% and 5% respectively was obtained. In order for this treatment to be effective as a consolidant, a 2 week treatment was observed to be necessary.

*3.2.5.2.2 Biodeposition without the External Application of Micro-Organisms*

Tiano *et al.* [3.91] proposed the use of natural and synthetic polypeptides to control the growth of calcite crystals in the pores. The first suggestions in this direction already date from the time at which the Calcite Bioconcept treatment was developed. Tiano *et al.* [3.92, 3.93] proposed the use of organic matrix macromolecules (OMM) extracted from *Mytilus californianus* shells to induce the precipitation of calcium carbonate within the pores of the stone. The organic matrix was shown to produce a more relevant and durable carbonate precipitation compared to the single use of calcium chloride or hydroxide. This precipitation resulted in a slight decrease in porosity and water absorption by capillarity [3.93]. Tiano *et al.* [3.94] proposed the alternative use of acid functionalized proteins such as polyaspartic acid. Calcium and carbonate ions for crystal growth were supplied by means of an ammonium carbonate and calcium chloride solution or a saturated solution of bicarbonate, and were supplemented in some cases by calcite nanoparticles, in order to maintain a saturated carbonate solution in the pore over a prolonged period. Proteins, calcium ions and nanoparticles were introduced in the stone by means of spraying. According to the authors, the method is most suitable for the use on marble statues and objects of high aesthetic value where conservation is required with the minimum change in the chemistry of the object. Field test results, however, indicate that the effects of the treatment with bio-inducing macromolecules (BIM) were rather small [3.94].

The European Bioreinforce (BIOmediated calcite precipitation for monumental stones REINFORCEment) project consortium demonstrated the ability of autoclaved cells and cell fragments to induce calcite crystallization in liquid media. After application of dead cells and *Bacillus* cell fragments (BCF) to stone surfaces, a slight decrease in the water absorption was noticed; the effect was more pronounced on high porosity stones such as Tuffeau. Again, this method

only appeared to be useful for very delicate small calcareous stone objects, rather than for a monumental façade [3.95].

Jimenez-Lopez *et al.* [3.96] proposed the application of a culture medium, able to activate the calcinogenic bacteria from the microbial community of the stone, as a more user friendly method for the *in situ* consolidation of ornamental stone. In addition to their work on decayed limestone fragments [3.96, 3.97], this technique was recently proposed for the treatment of new stones used for replacement purposes [3.98]. Some of the identified bacteria in the stone, *Pseudomonas* and *Bacillus*, had already been reported to produce calcium carbonate both in laboratory conditions and in nature. From these findings, the authors proposed the use of bacto-casitone as a way to activate the calcinogenic bacteria from the stone microbial community. Bacto-casitone is a source of carbon and nitrogen, which favours alkalinisation due to the oxidative deamination of amino acids. Gonzalez Muñoz *et al.* [3.99] applied for a new patent for the protection and reinforcement of construction and ornamental materials by means of the application of an activator medium able to induce the formation of calcium carbonate. Due to the time required for the activation of the microbial community, Jimenez-Lopez *et al.* [3.96] proposed the additional use of *M. xanthus* for those restoration interventions in which time is an issue and fast formation of calcium carbonate is required. Very recently, the application of an activator medium has been successfully applied *in situ* on calcarenite stone (Monasterio de San Jeronimo and Hospital Real, Granada) [3.100]. Results showed surface strengthening of the stone without alteration of its appearance.

#### 3.2.5.3 Biocementation: Biological Mortar

Besides the deposition of a layer of carbonate on the surface of building materials, MICP has also been used for the generation of binder-based materials. Initial developments were mainly situated in the field of geotechnical engineering, i.e. plugging, strengthening and improvement of soils [3.78, 3.79, 3.81, 3.101]. Recent advances, however, indicate the potential use of this technique for the remediation of cracks in building materials, strength improvement and self-healing of cementitious materials.

A biological mortar refers to a mixture of bacteria, finely ground aggregates (limestone) and a nutritional medium containing a calcium salt. The term biological refers to the microbial origin of the binder, i.e. microbiologically produced calcium carbonate, which cements the aggregates together. The aim of the biological mortars is to avoid some of the problems related to chemical and physical incompatibilities of commonly used repair mortars with the underlying material, especially in the case of brittle materials [3.84, 3.85, 3.102]. The optimization of the mortar composition encompassed the dosage and composition of the three main components, i.e. limestone powder, nutrients and bacterial paste. The biological mortars necessitated the use of larger amounts of bacteria and as a result the composition of the nutrient medium had to be altered. Best results were obtained with one part of bacterial paste (containing $10^9$ cells.mL$^{-1}$), one part of nutritional medium and two parts of limestone powder. Limestone powder with a

granulometry between 40 and 160 µm was observed to be the most suited. The technique has already been successfully tested on a small scale on sculptures of the Amiens Cathedral and on a portal of the church of Argenton-Château (France). Visual observations two years after the treatment indicated a satisfactory appearance of the repaired zones [3.84, 3.85].

#### 3.2.5.4 Microbiological Remediation of Cracks in Concrete

In the recovery of heavy oil from oil fields, where water is more readily removed than the viscous oil, the ability to selectively plug porous rock to focus pumping energy in oil rich zones is highly desirable. For this purpose, the use of a microbial mineral plugging system based on the precipitation of carbonates was suggested and investigated by, amongst others, Ferris and Stehmeier [3.79], Zhong and Islam [3.101], Whiffin [3.103], Kucharski *et al.*, [3.104]. Zhong and Islam [3.101] used the consolidation of sand mixtures for the remediation of cracks in granite. Cracks in granite were packed with a mixture of bacteria, nutrients and a filler material. Among the different materials that were mixed with *S. pasteurii*, a silica fume (10%) and sand (90%) mixture lead to the highest compressive strength and lowest permeability. As a further extension to this research, Ramachandran *et al.* [3.105] investigated the microbiological remediation of cracks in concrete. The authors proposed MICP as an effective way to seal cracks. The appearance of cracks and fissures is an inevitable phenomenon during the ageing process of concrete structures upon exposure to weather changes. If left untreated, cracks tend to expand further and eventually lead to costly repair. Specimens with cracks filled with bacteria, nutrients and sand demonstrated a significant increase in compressive strength and stiffness values when compared with those without cells. Similar conclusions were obtained by Achal [3.106] for crack remediation with a mixture of sand and *Bacillus sp.* (strain CT-5 which they isolated from cement). The presence of calcite was, however, limited to the surface areas of the crack. The authors attributed this to the fact that *S. pasteurii* grows more actively in the presence of oxygen. Still, the highly alkaline pH (12-13) of concrete was a major hindering factor to the growth of the moderate alkaliphile *S. pasteurii*, whose growth optimum is around a pH of nine. In order to protect the cells from the high pH, Day *et al.* [3.107] investigated the effect of different filler materials on the effectiveness of the crack remediation. Beams treated with bacteria and polyurethane showed a higher improvement in stiffness compared to filler materials such as lime, silica, fly ash and sand. According to the authors, the porous nature of the polyurethane minimizes transfer limitations to substrates and supports the growth of bacteria more efficiently than other filling materials, enabling an accumulation of calcite in deeper areas of the crack. No differences could be observed between the overall performances of free or polyurethane immobilized cells in the precipitation of carbonate [3.108]. In addition to this research, Bachmeier *et al.* [3.109] investigated the precipitation of calcium carbonate with the urease enzyme immobilized on polyurethane. The

immobilization was shown to protect the enzyme from environmental changes, as the immobilized urease retained higher enzymatic activities at high temperatures and in the presence of high concentrations of pronase. While the rate of calcite precipitation of the immobilized enzyme was slower compared to that of the free enzyme, lower concentrations of the former where needed to obtain the theoretical maximum precipitation in a period of 24 hours. Although the authors mentioned ongoing research on the use of immobilized urease in the remediation of surface cracks in concrete, to our knowledge no published results are available at the moment.

As an extension to research of the Ghent University Group regarding biodeposition on cementitious materials, the use of microbially induced carbonate precipitation was further investigated for the repair of cracks in concrete [3.110, 3.111]. Both standardised cracks with a depth of 10 mm or 20 mm and a width of 0.3 mm, and realistic cracks were examined. For the biological crack healing, the *Bacillus sphaericus* strain LMG 222 57 was chosen because of its optimal $CaCO_3$ precipitation capabilities [3.87]. To protect the bacteria from the strong alkaline environment in concrete, the bacteria were, for some of the treatments, immobilised in silica gel (Levasil®200/30% sol, with a specific surface area of 200 $m^2/g$ and a solids content of 30%). The bacteria were suspended in a salt solution and then added to the silica sol. The obtained suspension was brought into the cracks by means of a syringe where the salt triggered the transformation of the silica sol into a silica gel. After treatment of the cracks, samples were placed in an equimolar urea-calcium solution, which enhanced the formation of carbonate crystals inside the pores of the silica gel and resulted in sealing of the crack. Samples were removed from the solution after 3 days. Treatments with *Bacillus sphaericus* in silica gel and provided with a calcium source appeared to be effective in healing realistic cracks of 0.01 to 0.9 mm wide (Fig. 3.23). As a result, a decrease of the water permeability, similar to that obtained with traditional epoxy injections, was observed. However, it was seen that the decrease in water flow was also obtained if autoclaved bacteria were used instead of active bacteria. This corroborates that the greater part of the decrease in water permeability is attributed to crack filling by the sol-gel matrix. TGA analysis on the crack repair material indicated that only in the case of active bacteria $CaCO_3$ crystals were present (Fig. 3.24). Precipitation of these crystals inside the gel-matrix may enhance the durability of this repair material. When only bacteria were used, without immobilization in silica gel, no $CaCO_3$ precipitation could be observed. Treatment with sol-gel, with or without successive immersion in BS + $CaCl_2$, resulted in cracking of the sol-gel matrix. Efficiency of the biological treatment was also evaluated by means of ultrasonic transmission measurements and visual examination [3.111]. Crack treatment with *Bacillus sphaericus*, immobilized in silica gel, resulted in an increase in ultrasonic pulse velocity, indicating that crack bridging was obtained.

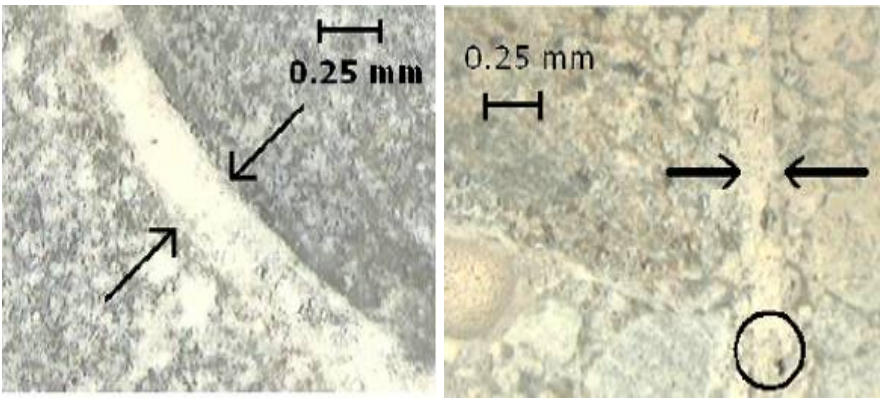


**Fig. 3.23** Visual evaluation of crack repair by *Bacillus sphaericus* in sol-gel; left: surface, right: cross section; the crack tip is encircled; arrows indicate the crack edges (Source: [3.110])

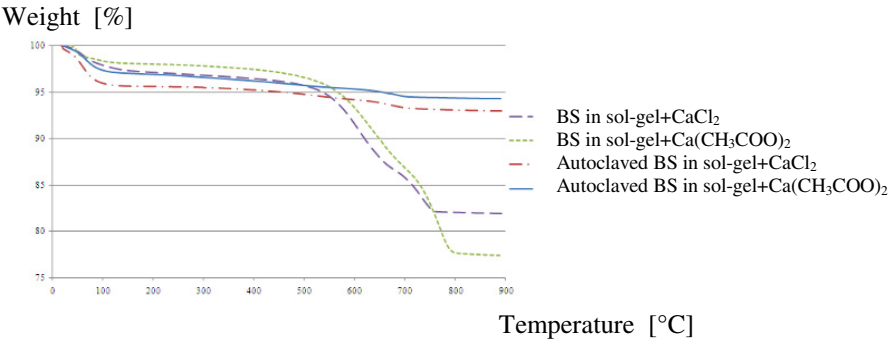


**Fig. 3.24** TGA results for different crack repair materials containing active or autoclaved Bacillus sphaericus (BS) bacteria, showing the reduction in weight versus temperature increase (Source: [3.111])

### 3.2.5.5 Bacterial Concrete

Besides external application of bacteria in the case of remediation of cracks, microorganisms have also been applied in the concrete mixture. Until now, research has mainly focused on the consequences of this addition on the material properties of concrete, i.e. strength and durability.

Ramachandran *et al.* [3.113] investigated the use of microbiologically induced mineral precipitation for the improvement of the compressive strength of Portland cement mortar cubes. This study identified the effect of the buffer solution and type and amount of microorganisms, i.e. *S. pasteurii* and *P. aeruginosa*, used. Furthermore, in order to study the effect of the biomass, the influence of both living and dead cells was investigated. Before addition to the mortar mixture,

bacteria were centrifuged and washed twice. The final pellets were then suspended in either saline or phosphate buffer, which was subsequently added to the mixture. After demolding, the mortar specimens were stored in a solution containing urea and calcium chloride for seven days. Subsequently, the specimens were cured in air until the measurement of the compressive strength.

At lower concentrations, the presence of *S. pasteurii* was shown to increase the compressive strength of mortar cubes. While the 28-day compressive strength of the control cubes amounted to about 55 ± 1 MPa, specimens treated with $10^3$ cells.cm$^{-3}$ had a compressive strength of about 65 ± 1 MPa. The contribution of *P. aeruginosa* to the strength was found to be insignificant. From the X-Ray diffraction (XRD) analysis, no significant increased amounts of calcite could be found in mortar specimens treated with bacteria. This could be attributed to the inhibition of the microorganisms by the high pH and the lack of oxygen inside the mortar mixture. The overall increase of strength, therefore, resulted from the presence of an adequate amount of organic substances in the matrix due to the microbial biomass. However, an increase of the biomass, as dead cells in particular, resulted in a decreased strength. According to the authors, this could be attributed to the disintegration of the organic matter with time, making the matrix more porous [3.113].

Ramakrishnan *et al.* [3.113] investigated the effect of this technique on the durability of concrete. The presence of bacteria was observed to increase the resistance of concrete towards alkali, sulfate, freeze thaw attack and drying shrinkage; the effect being more pronounced with increasing concentrations of bacterial cells. The authors attributed this to the presence of a calcite layer on the surface, as confirmed by XRD analysis, lowering the permeability of the specimens. The best results were obtained with the phosphate buffer.

Achal *et al.* [3.114] added a grown culture of *Sporosarcina pasteurii* (concentration corresponding to an optical density $OD_{600}$ of 1.0) to cement mortar, and cured in a medium containing lactose mother liquor, urea, $CaCl_2$ and NaCl. They found an increase in 28 days compressive strength of 17% compared to a control without bacteria or medium. When using *Bacillus sp.* (CT-5) and curing in a medium containing corn steep liquor, they even obtained a 44% increase in 28 days compressive strength. Curing in the media without adding bacteria into the mortar, did not result in strength enhancement [3.106].

Ghosh *et al.* [3.115] demonstrated the positive effect of the addition of *Shewanella* on the compressive strength of mortar specimens. Contrary to the aforementioned research, these authors did not intend mineral precipitation, as these specimens were cured in air and not in a nutrient containing medium. An increase of 25% of the 28 day compressive strength was obtained for a cell concentration of about $10^5$ cells.mL$^{-1}$ and a water-to-cement ratio of 0.4. For these samples, the presence of a fibrous material inside the pores could be noticed. As a result, a modification of the pore size distribution was observed. The positive effect of the addition of *Shewanella* improved with increasing curing times. For a concentration of $10^5$ cells.mL$^{-1}$, an increase of the compressive strength of 17% and 25% was observed after 7 and 28 days, respectively. However, no increase of

the compressive strength was observed with additions of *Escherichia coli* to the mortar mixture. This led the authors to suggest that the choice of the microorganism plays an important role in the improvement of the compressive strength. More specifically, the production of EPS by the bacteria seemed to be of importance. In a subsequent study Ghosh *et al.* [3.116] attributed strength improvement of bacteria-amended mortar specimens to the formation of new phases of silicates (Gehlenite) within the mortar matrix. This phenomenon was apparently triggered by a novel protein released by mortar embedded bacteria. Also the addition of only the protein to mortar mixtures was found to result in substantial improvement of mortar strength.

### 3.2.5.6 Self-Healing Concrete Using Bacteria

*3.2.5.6.1 Self-Healing Concrete with Bacteria in Porous Aggregates*

As part of a larger research program at TUDelft on the development of novel self-healing materials [3.117] the application of bacteria as self-healing agent in concrete was considered. In preliminary studies Jonkers [3.118] and Jonkers and Schlangen [3.119] added various species of alkali-resistant spore-forming bacteria (*Bacillus pseudofirmus* DSM 8715 and *B. cohnii* DSM 6307) to mortar mixtures and observed substantially higher production of mineral precipitates on crack surfaces of bacteria-based specimens compared to control ones (Fig. 3.25).

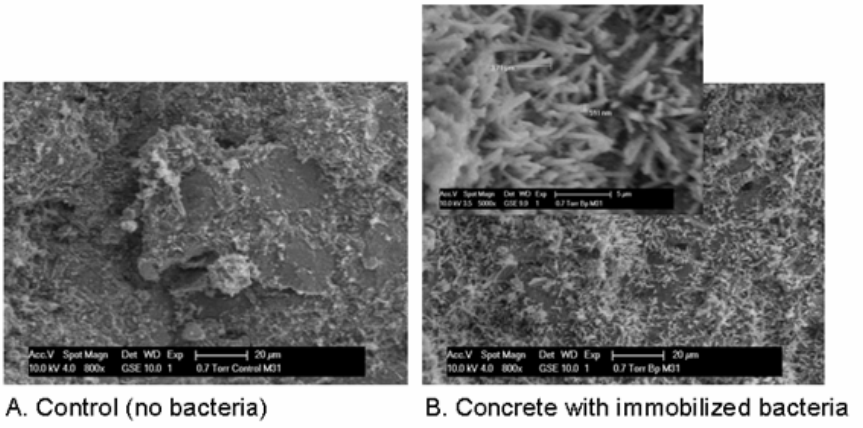


**Fig. 3.25** Cement stone samples, which were cured for 10 days and subsequently further incubated in yeast extract- and peptone-containing medium. (A) Control (cement stone without added bacteria) and (B) cement stone containing $10^9$ $cm^{-3}$ spores of *B. pseudofirmus*. The inset in Figure 2B (×5000 magnification) shows a close up of the massive calcite-like crystals formed on the specimen surface.

The formation of minerals was thought to be bacterially mediated due to metabolic conversion of dissolved organic compounds present in crack-ingress water to insoluble calcium carbonate-based minerals by embedded bacterial spores

after activation (germination). In order to obtain a truly self-healing material, in a follow-up study both bacterial spores and a suitable organic mineral precursor compound (calcium lactate) were added to the mortar mixture [3.120]. Although again profound mineral formation on crack surfaces was observed, the process appeared to be limited to very young (7 - 10 days) mortar specimens only (Fig. 3.26).

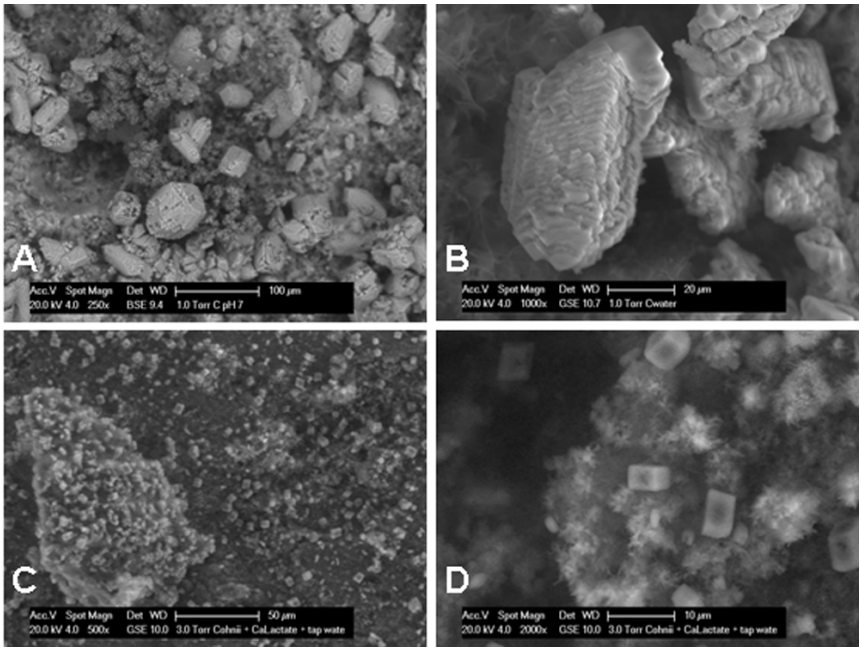


**Fig. 3.26** Cement stone specimens with incorporated healing agent (*B. cohnii* spores plus calcium lactate), cracked after 7 (panel A: 250x and B: 1000x magnification) or 28 days curing (panel C: 500x and D: 2000x magnification). The relatively large (20-80 µm sized) mineral precipitates visible on crack surfaces of young specimens (A and B) are presumably due to bacterial conversion of calcium lactate to calcium carbonate. The small (2-5 µm sized) precipitates on crack surfaces of older specimens (C and D) resemble those produced by abiotic specimens (see C and D), larger bacterial precipitates are not produced here likely due to loss of viability of cement stone embedded bacterial spores.

This phenomenon was attributed in that study to the limited viability of bacterial spores when directly (unprotected) added to the mortar mixture. In currently running studies therefore, both bacteria and nutrients are immobilized in porous expanded clay particles, acting as healing agent reservoir particles, prior to addition to the concrete mixture (Fig. 3.27).

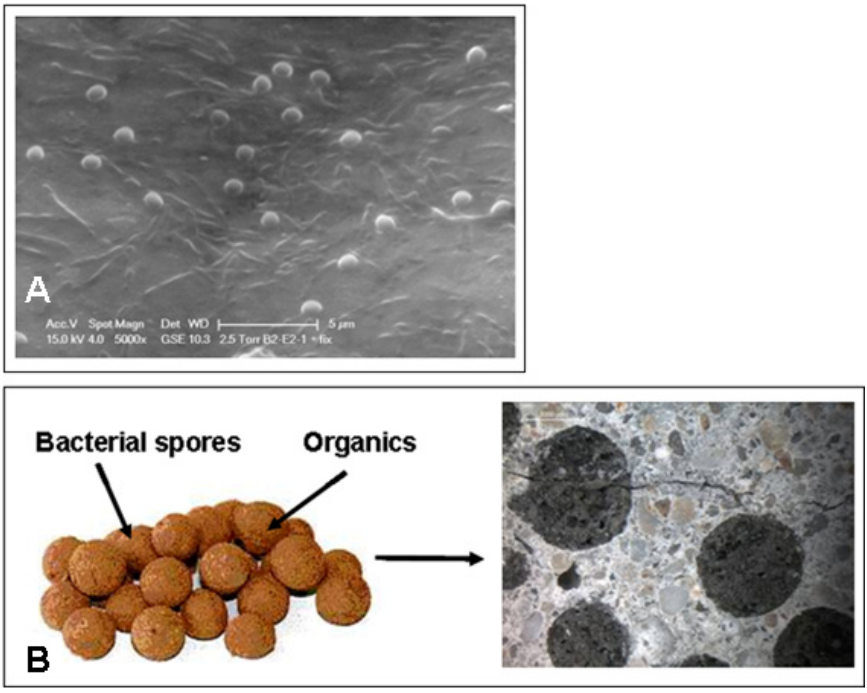


**Fig. 3.27** A: ESEM photomicrograph (5000x magnification) of alkali-resistant spore forming bacterium (Bacillus strain B2-E2-1). Visible are active vegetative bacteria (rods) and spores (spheres), showing that spore diameter sizes are in the order of one micrometer; B: Self-healing admixture composed of expanded clay particles (left) loaded with bacterial spores and organic bio-mineral precursor compound (calcium lactate). When embedded in the concrete matrix (right) the loaded expanded clay particles represent internal reservoirs containing the two-component healing agent consisting of bacterial spores and a suitable bio-mineral precursor compound.

Results of these studies appear promising as viability of concrete embedded bacterial spores increased due to this treatment from days to several months, while compared to control specimens also significantly improved healing (plugging) of cracks was observed [3.121, 3.122, 3.123] (Fig. 3.28).

A similar approach was also followed by Wang [3.124] and Standaert [3.125] at Ghent University. Two kinds of porous aggregates, i.e. expanded clay (argex) and lava, were used to immobilize *Bacillus cohnii* spores. The carriers used for immobilizing or encapsulating should have a suitable strength, particle size and surface pore size. The suitable surface pore size for encapsulating bacteria is 1.0 to 100 µm, preferably between 1.0 and 25 µm [3.126]. Pore analysis indicated that the fraction of the pores within this size range was larger for argex particles than for lava particles, which means that argex is more suitable to immobilize bacteria. However, lava was shown to have a positive effect on compressive strength and tensile strength, whereas argex has a negative effect (Fig. 3.29). Furthermore, the influence of a range of nutrients on the strength of the matrix was investigated (Fig. 3.30).

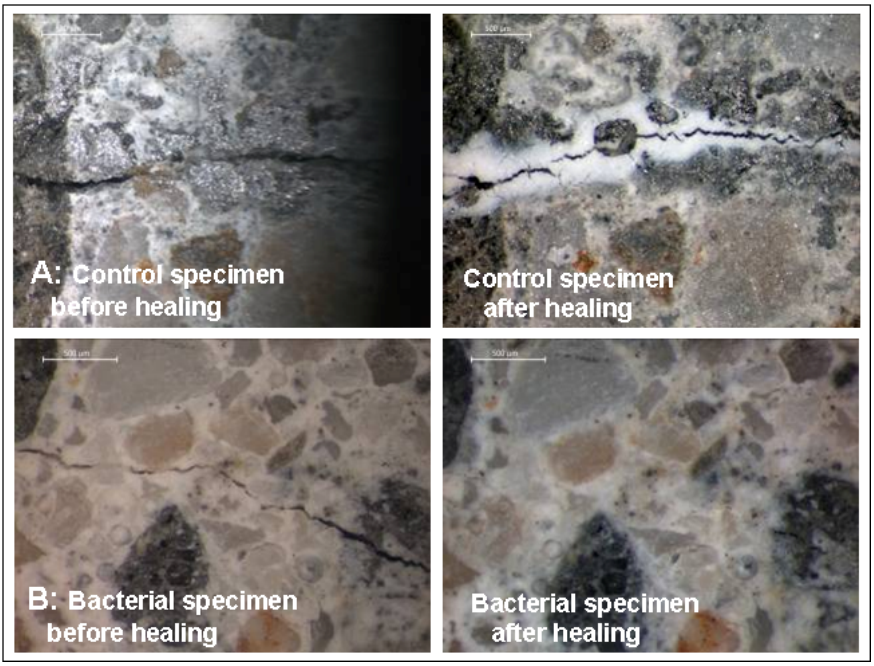


**Fig. 3.28** Light microscopic images (40 times magnification) of pre-cracked control (A) and bacterial (B) concrete specimen before (left) and after (right) healing (2 weeks submersion in water). Mineral precipitation occurred predominantly near the crack rim in control but inside the crack in bacterial specimens. Efficient crack healing occurred in all six bacterial and two out of six control specimens.

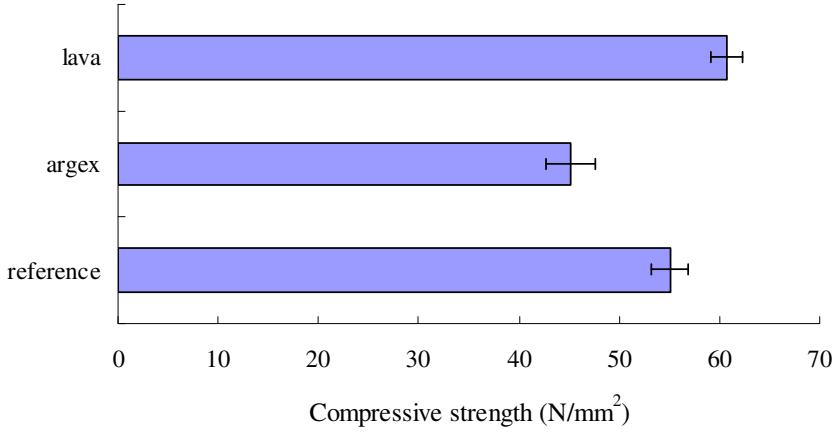


**Fig. 3.29** Compressive strength at 28 days of mortar prisms (160 x 40 x 40 $mm^3$) with different types of porous aggregates

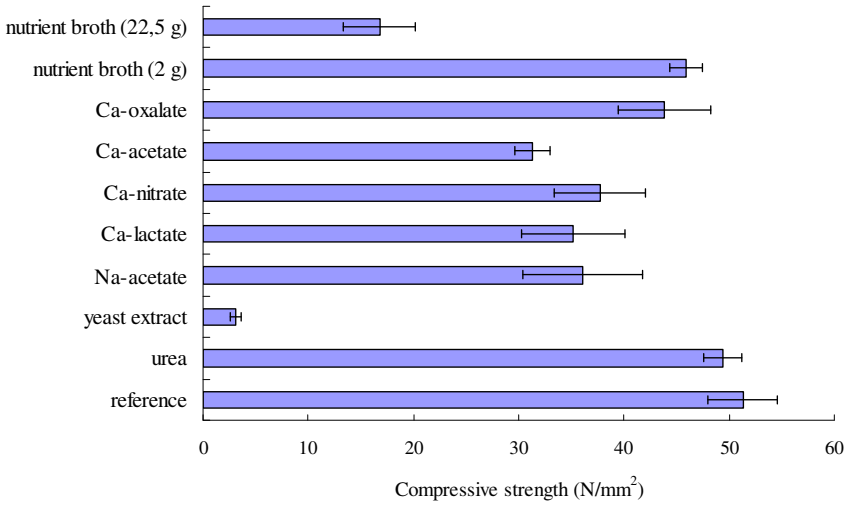


**Fig. 3.30** Compressive strength at 28 days of mortar prisms (160 x 40 x 40 $mm^3$) with different types of nutrients

To investigate the self-healing efficiency, the sand fraction 2/4 of mortar specimens was replaced by the same volume of porous aggregates. For each type of aggregate, 3 test series were prepared. The first one was the reference with aggregates that contained water, the second one was with aggregates that contained a solution of water and nutrients. The final series consisted of aggregates containing a spore suspension (*Bacillus cohnii*-spores) and nutrients. The expanded clay and lava aggregates were vacuum saturated with the solutions. For the third series, the spores and nutrients were added to separate aggregates. After saturation, the lava aggregates were provided with a cement coating to prevent leaching of the spores and nutrients. For each series, 4 cylinders (Ø: 76 mm, height: 20 mm) were made to investigate the evolution in water permeability. After 28 days, the prisms were subjected to a crack width controlled splitting test. The specimen was loaded until a crack-width of 0.4 mm was measured by an Linear Variable Displacement Transducer (resulting in a residual crack width after unloading of 0.1-0.2 mm). The cylinders were then positioned in a water permeability test facility as described by Aldea *et al.* [3.127]. The time of water flow through the cracked cylinders was measured daily and the water permeability coefficient was calculated according to Darcy's law.

A significant decline in the water permeability coefficient, in comparison with the reference and the specimens with only nutrients, was observed for specimens with spores and nutrients present in separate expanded clay particles. Precipitation was observed in the cracks of the specimens with nutrients and the specimens with nutrients and spores. This indicates that the precipitation might not be caused by the incorporated bacteria. Moreover, SEM analysis did not reveal differences in shape, size or degree of coverage of the precipitation noticed on the different

series. Also, the amount of $CaCO_3$ precipitation was not enough to completely heal the created cracks. SEM images of the specimens with lava saturated with nutrients and spores showed the presence of bacteria (Fig. 3.31). The bacteria appeared to be part of the crystals. This proves that the spores survived the immobilisation and germinated after crack formation.

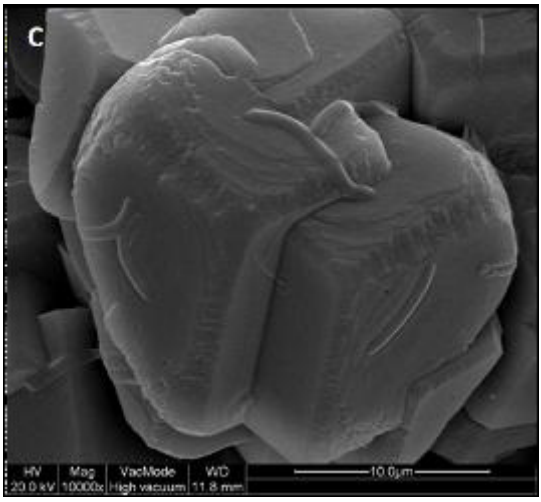


**Fig. 3.31** Bacteria within $CaCO_3$ crystals formed in cracked mortar specimens containing B. cohnii in coated lava particles

*3.2.5.6.2 Self-Healing Concrete with Bacteria in Diatomaceous Earth*

The Ghent University group suggested the use of diatomaceous earth (DE) as the carrier for the bacteria [3.128, 3.129]. Diatomaceous earth (DE) is a natural soft siliceous sedimentary rock that is very easily crumbled into fine powders. It has a particle size ranging from less than 1 µm to more than 1 mm, but typically 10 to 200 µm. The typical chemical composition of oven dried DE is 80% to 90% silica, with 2 to 4% alumina and 0.5% to 2% iron oxide. DE consists of fossilized remains of diatoms, which is a type of hard-shelled algae. Diatoms skeletons are highly porous, light in weight and chemically stable and inert. DE has been used in various fields. It is mainly used as filtration agent and functional fillers for paints and plastics. Furthermore, DE has been used before as a bacterial carrier, e.g. DE was used to incorporate non-pathogenic microbes inside a system for in-situ bioremediation of contaminated soil and ground water [3.130]. The aim of Wang *et al.* [3.128, 3.129] was to use DE as the protective carrier for the bacteria, which were added into the high pH cement environment of concrete as a self-healing agent.

First the activity of *Bacillus sphaericus* LMG 22557 (Belgian coordinated collection of microorganisms, Ghent) immobilized in DE, was tested in a cement slurry to mimic the high pH environment inside concrete. The pH of the suspension of Portland cement in water was about 12.5 after 1 day. Then a pre-mixture together with nutrients was added to the cement suspension. The pre-mixture was made of bacterial cells (concentration $10^8$ cells/mL), water and DE. The nutrients were composed of urea and yeast extract. The ureolytic activity of the bacteria after immobilization into DE was evaluated by the decomposition of urea in the cement slurry. The amount of urea decomposed was measured by the determination of total ammonium nitrogen (TAN). TAN concentrations were measured calorimetrically by the method of Nessler [3.131]. The results showed that *B. sphaericus* bacteria immobilized in DE can decompose a significant amount of urea (on average 25 g/L), whereas almost no urea was decomposed in control slurries with DE but no bacteria, or with bacteria that were not immobilized on DE.

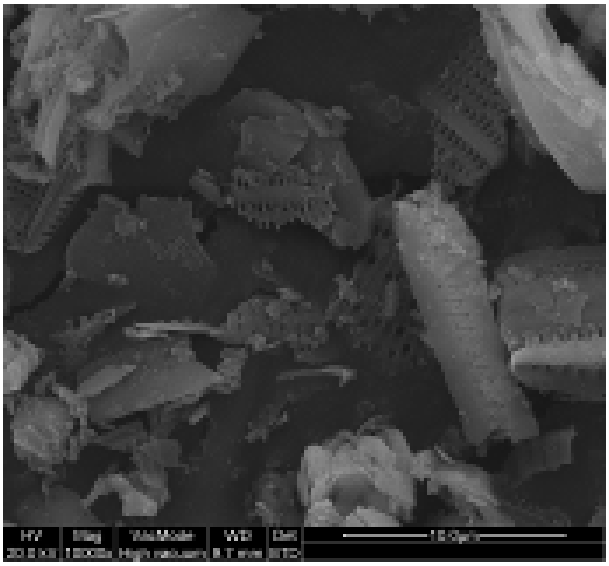

**Fig. 3.32** Porous DE

Subsequently, mortar specimens (60 mm x 60 mm x 220 mm) with DE immobilized bacteria were prepared: half of the DE contained nutrients and the other half contained bacterial cells. As shown in Fig. 3.33, the addition of diatomaceous earth clearly improved the compressive strength of the mortar. It is thought that DE may function as a filler, and probably also as an internal curing aid. However, if the addition of DE is more than 5% of the cement by mass, the mortar paste becomes very dry and the workability decreases a lot.

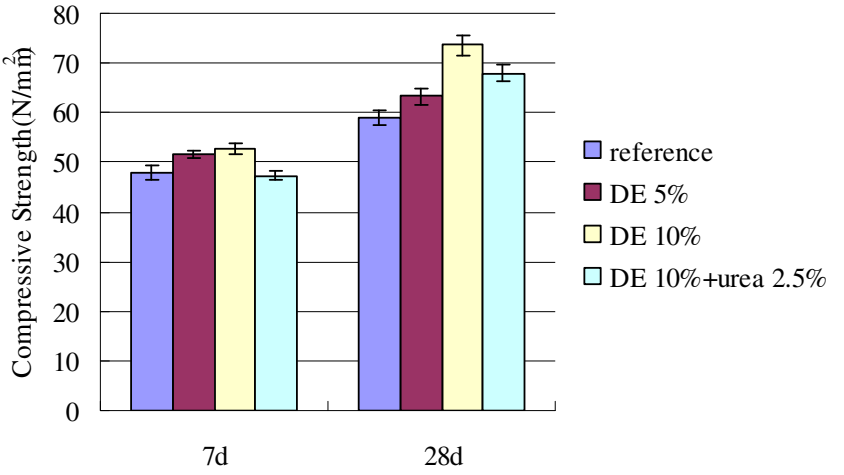


**Fig. 3.33** Compressive strength of mortar with or without diatomaceous earth (DE)

After 7 days, the mortar specimens were taken out of the curing room and cracks were created by means of a crack width controlled three-point bending test. After unloading, the remaining crack width ranged from 0.15 mm to 0.17 mm. Afterwards, three of the cracked specimens were immersed into water and three were immersed into the deposition medium (made of urea and $Ca(NO_3)_2$, 0.2M) for 40 days. It was found that the cracks were filled with white crystals. Samples were taken from the crack wall for SEM and EDAX analysis. As shown in Fig. 3.34 (a) and (b), the particles appear in different shapes, with size ranging from 5 μm to 40 μm. EDAX results indicated that the particles are $CaCO_3$.

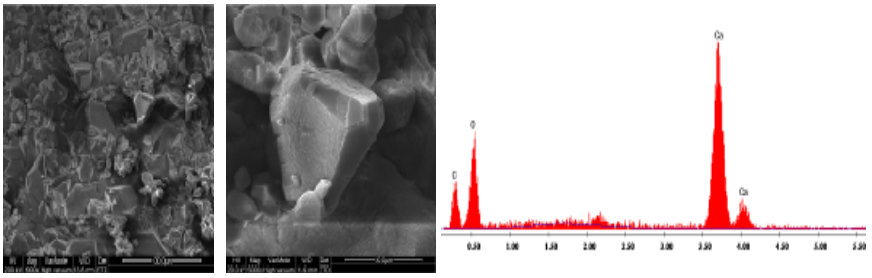

(a) 1000× (b) 5000× (c) EDAX

**Fig. 3.34** $CaCO_3$ precipitation by DE immobilized bacteria in the cracks

A capillary water absorption test was performed to measure the water penetration resistance of the cracked mortar specimens with or without bacteria. The specimens were dried at 40 ˚C in an oven until weight changes were lower than 0.1% in 24 h intervals. Before the test, the specimens were coated with a

waterproof paint at four sides adjacent to the bottom surface where the crack existed. Also part of the bottom surface was coated with the paint except for an area of 40 mm x 20 mm around the crack. The coated specimens were immersed to a depth of 5±1 mm in tap water and were weighed regularly. It appeared that the precipitation in the cracks profoundly decreased the water absorption of the cracked specimens. It can be seen from Fig. 3.35 that the speed of water absorption in the specimens without bacteria was much faster than in the ones with bacteria.

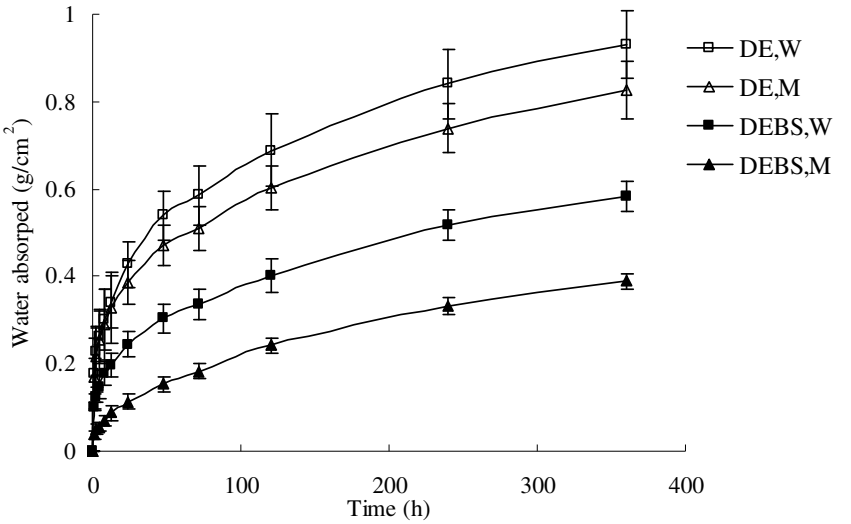


**Fig. 3.35** Capillary water absorption of cracked (and self-healed) specimens as a function of time; all specimens contained diatomaceous earth (DE); BS refers to the specimens with bacteria; W refers to the previous incubation in water and M to incubation in urea and $Ca(NO_3)_2$ medium for 40 days (Source: [3.129])

*3.2.5.6.3 Self-Healing Concrete with Bacteria in Tubular Capsules*

The Ghent university team is also focussing on protection of the bacteria in tubular carrier materials in order to introduce them in a concrete matrix to obtain autonomous self-healing. As described in Wang *et al.* [3.132, 3.133] bacteria and PU were encapsulated in glass tubes with three compartments which were embedded inside mortar specimens. One compartment of the tubes contained the first component of the PU (prepolymer of PU). The second compartment was filled with the nutrients for bacterial growth, and a calcium source (this deposition medium contained yeast extract 20 g/L, urea 20 g/L and $Ca(NO_3)_2.4H_2O$ 79 g/L) and the second component of the PU (accelerator). The last compartment was filled with the bacterial cells (*Bacillus sphaericus*, $10^8$ cells/mL). The glass tubes were then placed in the tensile zone of mortar specimens (60 mm x 60 mm x 220 mm) and cracks were created in two weeks old specimens by means of a crack width controlled three-point bending test. When a crack appears in the mortar

matrix, the glass tubes break and all components mentioned above can flow into the crack and mix together. For the tubes with PU carrier material, first, polymerization of the filling agent (polyurethane) is initiated and through this process strength regain is obtained. In a second step, the bacteria, which are dispersed through the filling material can precipitate $CaCO_3$ crystals in the pores of the PU and through this, an additional regain in strength may be obtained. Different from the method of Bang *et al.* [3.108] described higher, in which PU foam with immobilized bacteria was pre-formed and placed into the cracks manually, in this research, PU foam is formed in the crack automatically upon crack appearance.

After performance of the bending test, all specimens were placed again into a curing room at a temperature of 20°C and a relative humidity of more than 90%. One week later, strength regain was measured by reloading the specimens. The self-healing efficiency was evaluated by comparing the peak load obtained during the first loading cycle and the reloading cycle. Considerable strength regain, on average 60%, was obtained in the case of specimens with incorporated PU and bacteria. However, there was no obvious difference in strength regain between specimens with living bacteria and specimens with dead bacteria. Therefore, the healing effect was mostly caused by the PU foam and not by the bacterially precipitated $CaCO_3$. However, water permeability tests showed that the water permeability coefficient of the specimens with PU immobilized bacteria ($10^{-8}$ to $10^{-11}$ m/s) was a little bit lower than for those with PU only (about $10^{-7}$ to $10^{-11}$ m/s).

TGA measurements indicated that $CaCO_3$ crystals were present in the cracks but that the amount of precipitation was quite limited. The main reason might be that there is insufficient water for microbial activity inside PU foam. This will hinder the contact among bacteria, urea and $Ca^{2+}$. Current research focuses on increasing the amount of bio-$CaCO_3$ precipitation in PU foam and on selection of other suitable carrier materials. First results indicate that increasing the amount of bacteria inside PU, enhances the precipitation of more $CaCO_3$. Immobilization of the bacteria in PU did not lead to an obvious reduction in their ability to degrade urea. *B. sphaericus* immobilized into silica gel showed a somewhat higher activity than the same amount immobilized into PU.

Therefore as another alternative, the use of a two-component system was studied, existing of a tube with the bacteria suspended in silica sol, and a second tube with the deposition medium [3.124, 3.133]. The $Ca(NO_3)_2$ in the deposition medium also functions as activator for the silica gel formation. For the system with silica gel, this gel itself does not contribute to mechanical strength regain and only the precipitation of $CaCO_3$ crystals will allow regain in strength. For autonomously healed specimens with silica gel with or without bacteria, the water permeability coefficient of specimens was reduced much more in specimens with bacteria due to the bacterially induced $CaCO_3$ precipitation ($10^{-6}$ m/s for specimens with silica gel only, to $10^{-6}$ -$10^{-9}$ m/s for specimens with silica gel and bacteria).

## References


3.1. Edvardsen, C.K.: Water permeability and self-healing of through-cracks in concrete. DAfStb Bull 455 (1996) (in German)
3.2. Härtl, R.: Chemical binding of water during the hydration of portland cements and blast furnace slag cement bended with fly ash. In: 9th Intern. Congress on the Chemistry of Cement, New Dehli (1992)
3.3. Pisters, H.: Einwirkung von angreifenden Wässern auf Beton. Vom Wasser 30, 208–221 (1963)
3.4. Meichsner, H., Stelzner, S.: Über die Selbstdichtung von Rissen. Betontechnik 10(3), S.82–S.83 (1989)
3.5. Edvardsen, C.: Water permeability and autogenous healing of cracks in concrete. ACI Materials J. 96(4), 448–454 (1999)
3.6. Selbstheilung von Beton. Beton und Eisen 5/1935, S.96 (1935)
3.7. Von Emberger, F.: Neuere Bauwerke und Bauweisen aus Beton und Eisen. Bauwerke III. Wasserbau. Zeitschrift des österr. Ingenieur- und Architekten-Vereins Heft 24/1902, S.441–S.446 (1902)
3.8. Gilkey, H.J.: Die Selbstheilung von Beton und Mörtel. American Society for Testing Materials, Bd. 26, Teil ii, S. 470 und Bd. 29, Teil ii, S.593 (1926, 1929)
3.9. Maddocks, F.T.: Gebrochene Betonprüfkörper heilen und zeigen erhöhte Druckfestigkeit bei erneuter Prüfung, California Highways, p. S.11 (August 1925)
3.10. Merkle, G.: Wasserdurchlässigkeit von Beton. Springer, Berlin (1927)
3.11. Peckworth, H.F.: Selbstheilung von Beton. Concrete Pipe Handbook, Chicago, Kapitel XV (1965)
3.12. Soroker, V.M., Desov, A.J.: Selbstheilung von Beton, constructeur de cement armé, Bd. 18, Heft 197/1936, S.31. Zement, Bd. 25, Heft 30/1936, S.505 (1936)
3.13. Zschokke, B.: Über die Selbstdichtung von Betonblöcken bei den Wasserdurchlässigkeits-Proben. Schweizerische Wasserwirtschaft 2/1922, S.31–S.35 und 8/1923 (1923)
3.14. Loving, M.W.: Selbstheilung von Beton. American Concrete Pipe Association, Bulletin 13 (1936)
3.15. Wagner, E.F.: Autogenous healing of crack in cement-mortar linings for gray-iron and ductile-iron water pipe. Journal of the American Water Works Association 66(6), S.358–S.360 (1974)
3.16. Lauer, K.R., Slate, F.O.: Autogenious healing of cement paste. Journal of the American Concrete Institute 52(6), S.1083–S.1097 (1956)
3.17. Hannant, D.J., Keer, J.G.: Autogenous healing of thin cement based sheets. Cement and Concrete Research 13(3), S.357–S.365 (1983)
3.18. Dhir, R.K., Sangha, C.M., Munday, J.G.L.: Strength and deformation properties of autogeniously healed mortars. Journal of the ACI (3), S.231–S.236 (1973)
3.19. Clear, C.A.: Leakage of cracks in concrete - summary of work to date. Cement and concrete association (1982) (Internal Publication)
3.20. Ripphausen, B.: Untersuchungen zur Wasserdurchlässigkeit und Sanierung von Stahlbetonbauteilen mit Trennrissen. Dissertation RWTH Aachen (1989)

3.21. Meichsner, H., Wuenschig, R.: Institut für Ingenieur- und Tiefbau: Die Selbstdichtung von Rissen in Beton- und Stahlbetonbauteilen. IRB-Verlag, Stuttgart (1991)
3.22. Granger, S., Loukili, A., Pijaudier-Cabot, G., Chanvillard, G.: Mechanical characterization of the self-healing effect of cracks in ultra high performance concrete (UHPC). In: Banthia, N. (ed.) Construction Materials: Performance, Innovations and Structural Implications (3rd Int. Conference), p. 9. The University of British Columbia and CD-ROM, Vancouver (2005)
3.23. Reinhardt, H.-W., Jooss, M.: Permeability and self-healing of cracked concrete as a function of temperature and crack width. Cement and Concrete Research 33, 981–985 (2003)
3.24. Hearn, N.: Self-healing property of concrete - Experimental evidence. Materials and Structures 30, 404–411 (1997)
3.25. Hearn, N.: Self-sealing, autogenous healing and continued hydration: what is the difference? Materials and Structures 31, 563–567 (1999)
3.26. Jacobsen, S., Sellevold, E.J.: Self-healing of high strength concrete after deterioration by freeze/thaw. Cement and Concrete Research 26(1), 55–62 (1996)
3.27. Jacobsen, S., Marchand, J., Hornain, H.: Sem observations of the microstructure of frost deteriorated and self-healed concrete. Cement and Concrete Research 25(8), 1781–1790 (1995)
3.28. Nanayakkara, S.M.A., Elakneshwaran, T.: Self-healing of Cracks in Concrete with Portland Limestone Cement. In: Cement Combinations for Durable Concrete: Proceedings of the Int. Conference held at the University of Dundee, Scotland, UK, July 5-7, pp. S.675–S.684. Telford, London (2005)
3.29. Termkhajornkit, P., et al.: Self-healing ability of fly ash-cement systems. Cement and Concrete Composites 31(3), 195–203 (2009)
3.30. Taniguchi, M., et al.: Self-healing of frost-damaged concrete incorporating fly ash. In: Bond, I., Varley, R. (eds.) 3rd International Conference on Self-healing Materials, Bath, UK, pp. 48–49 (2011)
3.31. Na, S.H., et al.: Evaluation of self-healing effect of concrete using fly ash or ground granulated blast furnace slag. In: Bond, I., Varley, R. (eds.) 3rd International Conference on Self-healing Materials, Bath, UK, pp. 125–126 (2011)
3.32. Haddad, R.H., Bsoul, M.A.: Self-healing of polypropylene fiber reinforced concrete; pozzolan effect, pp. 1412–1421 (1999)
3.33. Morimoto, T., et al.: Self-healing properties of Ultra High Performance Strain Hardening Cementitious Composites (UHP-SHCC). In: 4th International Conference on Construction Materials, Nagoya, Japan, pp. 319–326 (2009)
3.34. Şahmaran, M., Li, V.C.: Durability properties of micro-cracked ECC containing high volumes fly ash. Cement and Concrete Research 39(11), 1033–1043 (2009)
3.35. Liu, X.-Y., et al.: Experimental study on self-healing performance of concrete. Journal of Building Materials (2) (2005)
3.36. Şahmaran, M., et al.: Self-healing of mechanically-loaded self consolidating concretes with high volumes of fly ash. Cement and Concrete Composites 30(10), 872–879 (2008)

3.37. Yang, E.-H., Yang, Y., Li, V.C.: Use of high volumes of fly ash to improve ECC mechanical properties and material greenness. ACI Materials Journal 104(6), 620–628 (2007)
3.38. ter Heide, N.: Crack healing in hydrating concrete. MSc thesis, Delft University of Technology, p. 128 (2005)
3.39. Liu, S., Zuo, M.: Influence of slag and fly ash on the self-healing ability of concrete. Advanced Materials Research 306-307, 1020–1023 (2011)
3.40. Van Tittelboom, K., De Belie, N.: Autogenous healing of cracks in cementitious materials with varying mix compositions. In: 2nd International Conference on Self-healing Materials, Chicago, USA, p. 160 (2009)
3.41. Van Tittelboom, K., et al.: Influence of mix composition on the extent of autogenous crack healing by continued hydration or calcium carbonate formation. Construction and Building Materials 37(0), 349–359 (2012)
3.42. Jacobsen, S., Marchand, J., Gerard, B.: Concrete Cracks I: Durability and Self-healing – a Review. In: Gjorv, O.E., Sakai, K., Banthia, N. (eds.) Concrete under Severe Conditions 2, CONSEC 1998: Environment and Loading; Proceedings of the 2nd International Conference, Tromso, Norway, June 21-24, pp. 217–231. E & FN Spon, London (1998)
3.43. Meichsner, H.: Über die Selbstdichtung von Trennrissen in Beton. Beton-und Stahlbetonbau 87(4), 95–99 (1992)
3.44. Edvardsen, C.: Self-healing of concrete cracks. Concrete 33 (April 1999)
3.45. DIN 1045-1, Concrete, reinforced and prestressed concrete structures – Part 1: Design, German Standardization Institute (July 2001)
3.46. Snoeck, D., et al.: Self-healing cementitious materials by the combination of microfibres and superabsorbent polymers. Journal of Intelligent Material Systems and Structures (2012)
3.47. Lee, H.X.D., et al.: Potential of superabsorbent polymer for self-sealing cracks in concrete. Advances in Applied Ceramics 109, 296–302 (2010)
3.48. Lee, H.X.D., et al.: Self-sealing cement-based materials using superabsorbent polymers. In: International RILEM Conference on Use of Superabsorbent Polymers and Other New Additives in Concrete, Lyngby, pp. 171–178 (2010)
3.49. Tsuji, M., et al.: Basic studies on simplified curing technique, and prevention of initial cracking ans leakage of water through cracks of concrete by appying superabsorbent polymers as new concrete admixture. Journal of the Society of Materials Science 48, 1308–1315 (1999)
3.50. Snoeck, D., et al.: Visualization of water penetration in cementitious materials with superabsorbent polymers by means of neutron radiography. Cement and Concrete Research 42, 1113–1121 (2012)
3.51. Snoeck, D., et al.: The use of superabsorbent polymers as a crack sealing and crack healing mechanism in cementitious materials. In: 3rd International Conference on Concrete Repair, Rehabilitation and Retrofitting, Cape Town, pp. 152–157 (2012)
3.52. Kim, J.S., Schlangen, E.: Super absorbent polymers to simulate self-healing in ECC. Presented at the 2nd International Symposium on Service Life Design for Infrastructures, Delft (2010)

3.53. Sisomphon, K., Copuroglu, O., Fraaij, A.: Application of encapsulated lightweight aggregate impregnated with sodium monofluorophosphate as a self-healing agent in blast furnace slag mortar. Heron 56(1/2), 13–32 (2011)
3.54. Sisomphon, K., Copuroglu, O., Fraaij, A.: Self-healing blast furnace slag mortar subjected to carbonation and frost salt scaling. In: White, S., Bond, I. (eds.) 2nd International Conference on Self-healing Materials, Chicago, USA, p. 159 (2009)
3.55. Dry, C.M., Corsaw, M.J.T.: A time-release technique for corrosion prevention. Cement and Concrete Research 28(8), 1133–1140 (1998)
3.56. Mechtcherine, V., Lieboldt, M.: Permeation of water and gases through cracked textile reinforced concrete. Cement Concrete Comp. 33, 725–734 (2011)
3.57. Butler, M., Mechtcherine, V., Hempel, S.: Experimental investigations on the durability of fibre-matrix interfaces in textile-reinforced concrete. Cement and Concrete Composites 31, 221–231 (2009)
3.58. De Muynck, W., Belie, N., Verstraete, W.: Microbial carbonate precipitation in construction materials: a review. Ecological Engineering 36(2), 118–136 (2010)
3.59. Lowenstan, H.A., Weiner, S.: On biomineralization. Oxford University Press, New York (1988)
3.60. Rivadeneyra, M.A., Delgado, R., del Moral, A., Ferrer, M.R., Ramos-Cormenzana, A.: Precipatation of calcium carbonate by Vibrio spp. from an inland saltern. FEMS Microbiol. Ecol. 13(3), 197–204 (1994)
3.61. Barabesi, C., Galizzi, A., Mastromei, G., Rossi, M., Tamburini, E., Perito, B.: Bacillus subtilis Gene Cluster Involved in Calcium Carbonate Biomineralization. J. Bacteriol. 189(1), 228–235 (2007)
3.62. Knorre, H., Krumbein, K.E.: Bacterial calcification. In: Riding, E.E., Awramik, S.M. (eds.) Microbial Sediments, pp. 25–31. Springer, Berlin (2000)
3.63. Rivadeneyra, M.A., Parraga, J., Delgado, R., Ramos-Cormenzana, A., Delgado, G.: Biomineralization of carbonates by Halobacillus trueperi in solid and liquid media with different salinities. FEMS Microbiol. Ecol. 48, 39–46 (2004)
3.64. Hammes, F., Verstraete, W.: Key roles of pH and calcium metabolism in microbial carbonate precipitation. Rev. Environ. Sci. Biotechnol. 1, 3–7 (2002)
3.65. Stumm, W., Morgan, J.J.: Aquatic chemistry, 2nd edn. John Wiley, New York (1981)
3.66. Castanier, S., Le Metayer-Levrel, G., Perthuisot, J.-P.: Ca-carbonates precipitation and limestone genesis – the microbiogeologist point of view. Sediment. Geol. 126(1-4), 9–23 (1999)
3.67. Braissant, O., Verrecchia, E., Aragno, M.: Is the contribution of bacteria to terrestrial carbon budget greatly underestimated? Naturwissenschaften 89(8), 366–370 (2002)
3.68. Boquet, E., Boronat, A., Ramos-Cormenzana, A.: Production of Calcite (Calcium Carbonate) Crystals by Soil Bacteria is a General Phenomenon. Nature 246(5434), 527–529 (1973)
3.69. Morita, R.: Calcite precipitation by marine bacteria. Geomicrobiol. J. 2, 63–82 (1980)
3.70. Douglas, S., Beveridge, T.J.: Mineral formation by bacteria in natural microbial communities. FEMS Microbiol. Ecol. 26(2), 79–88 (1998)

3.71. Ehrlich, H.L.: Geomicrobiology: its significance for geology. Earth-Sci. Rev. 45(1-2), 45–60 (1998)
3.72. Chaturvedi, S., Chandra, R., Rai, V.: Isolation and characterization of Phragmites australis (L.) rhizosphere bacteria from contaminated site for bioremediation of colored distillery effluent. Ecol. Eng. 27(3), 202–207 (2006)
3.73. Simon, M.A., Bonner, J.S., Page, C.A., Townsend, R.T., Mueller, D.C., Fuller, C.B., Autenrieth, R.L.: Evaluation of two commercial bioaugmentation products for enhanced removal of petroleum from a wetland. Ecol. Eng. 22(4-5), 263–277 (2004)
3.74. Warren, L.A., Maurice, P.A., Parmar, N., Ferris, F.G.: Microbially Mediated Calcium Carbonate Precipitation: Implications for Interpreting Calcite Precipitation and for Solid-Phase Capture of Inorganic Contaminants. Geomicrobiol. J. 18, 93–125 (2001)
3.75. Fujita, Y., Redden, G.D., Ingram, J.C., Cortez, M.M., Ferris, F.G., Smith, R.W.: Strontium incorporation into calcite generated by bacterial ureolysis. Geochim. Cosmochim. Acta 68(15), 3261–3270 (2004)
3.76. Hammes, F., Boon, N., de Villiers, J., Verstraete, W., Siciliano, S.D.: Strain-Specific Ureolytic Microbial Calcium Carbonate Precipitation. Appl. Environ. Microbiol. 69(8), 4901–4909 (2003)
3.77. Hammes, F., Seka, A., de Knijf, S., Verstraete, W.: A novel approach to calcium removal from calcium-rich industrial wastewater. Water Res. 37(3), 699–704 (2003)
3.78. Nemati, M., Voordouw, G.: Modification of porous media permeability, using calcium carbonate produced enzymatically in situ. Enzyme Microb. Technol. 33(5), 635–642 (2003)
3.79. Ferris, F.G., Stehmeier, L.G.: Bacteriogenic mineral plugging. USA Patent US5143155 (1992)
3.80. DeJong, J.T., Fritzges, M.B., Nusslein, K.: Microbially Induced Cementation to Control Sand Response to Undrained Shear. J Geotech. Geoenviron. 132(11), 1381–1392 (2006)
3.81. Whiffin, V.S., van Paassen, L., Harkes, M.P.: Microbial Carbonate Precipitation as a Soil Improvement Technique. Geomicrobiol. J. 24, 417–423 (2007)
3.82. Adolphe, J.P., Loubière, J.F., Paradas, J., Soleilhavoup, F.: Procédé de traitement biologique d'une surface artificielle. European patent 90400G97.0 (after French patent 8903517, 1990)
3.83. Orial, G.: La biomineralisation appliquée à la conservation du patrimoine: bilan de dix ans d'experimentation. Restaurar la memoria, Valladolid, Spain (2000)
3.84. Orial, G., Vieweger, T., Loubiere, J.F.: Les mortiers biologiques: une solution pour la conservation de la sculpture monumentale en pierre. Art Biology and Conservation, Metropolitan Museum New York (2002)
3.85. Le Metayer-Levrel, G., Castanier, S., Orial, G., Loubiere, J.F., Perthuisot, J.P.: Applications of bacterial carbonatogenesis to the protection and regeneration of limestones in buildings and historic patrimony. Sediment. Geol. 126(1-4), 25–34 (1999)

3.86. Rodriguez-Navarro, C., Rodriguez-Gallego, M., Ben Chekroun, K., Gonzalez-Munoz, M.T.: Conservation of Ornamental Stone by Myxococcus xanthus-Induced Carbonate Biomineralization. Appl. Environ. Microbiol. 69(4), 2182–2193 (2003)
3.87. Dick, J., De Windt, W., De Graef, B., Saveyn, H., Van der Meeren, P., De Belie, N., Verstraete, W.: Bio-deposition of a calcium carbonate layer on degraded limestone by Bacillus species. Biodegradation 17(4), 357–367 (2006)
3.88. Stocks-Fischer, S., Galinat, J.K., Bang, S.S.: Microbiological precipitation of $CaCO_3$. Soil Biol. Biochem. 31(11), 1563–1571 (1999)
3.89. De Muynck, W., Cox, K., De Belie, N., Verstraete, W.: Bacterial carbonate precipitation as an alternative surface treatment for concrete. Constr. Build. Mater. 22(5), 875–885 (2008)
3.90. De Muynck, W., Debrouwer, D., De Belie, N., Verstraete, W.: Bacterial carbonate precipitation improves the durability of cementitious materials. Cem. Concr. Res. 38(7), 1005–1014 (2008)
3.91. Tiano, P., Biagiotti, L., Mastromei, G.: Bacterial bio-mediated calcite precipitation for monumental stones conservation: methods of evaluation. J. Microbiol. Method 36, 139–145 (1999)
3.92. Tiano, P., Addadi, L., Weiner, S.: Stone reinforcement by induction of calcite crystals using organic matrix macromolecules: feasibility study. In: 7th International Congress on Deterioration and Conservation of Stone, Lisbon, pp. 1317–1326 (1992)
3.93. Tiano, P.: Stone Reinforcement by Calcite Crystal Precipitation Induced by Organic Matrix Macro-molecules. Stud. Conserv. 40(3), 171–176 (1995)
3.94. Tiano, P., Cantisani, E., Sutherland, I., Paget, J.M.: Biomediated reinforcement of weathered calcareous stones. J. Cult. Herit. 7(1), 49–55 (2006)
3.95. Mastromei, G., Marvasi, M., Perito, B.: Studies on bacterial carbonate precipitation for stone conservation. In: Proc. of. BioGeoCivil Engineering Conference, Delft, Netherlands, pp. 104–106 (2008)
3.96. Jimenez-Lopez, C., Rodriguez-Navarro, C., Piñar, G., Carrillo-Rosúa, F.J., Rodriguez-Gallego, M., Gonzalez-Muñoz, M.T.: Consolidation of degraded ornamental porous limestone by calcium carbonate precipitation induced by the microbiota inhabiting the stone. Chemosphere 68(10), 1929–1936 (2007)
3.97. Piñar, G., Jimenez-Lopez, C., Sterflinger, K., Ettenauer, J., Jroundi, F., Fernandez-Vivas, A., Gonzalez-Muñoz, M.T.: Bacterial community dynamics during the application of a Myxococcus xanthus-inoculated culture medium used for consolidation of ornamental limestone. Microb. Ecol. 66, 15–28 (2010)
3.98. Jimenez-Lopez, C., Jroundi, F., Pascolini, C., Rodriguez-Navarro, C., Piñar-Larrubia, G., Rodriguez-Gallego, M., González-Muñoz, M.T.: Consolidation of quarry calcarenite by calcium carbonate precipitation induced by bacteria activated among the microbiota inhabiting the stone. Int. Biodeterior. Biodegrad 62(4), 352–363 (2008)
3.99. Gonzalez Muñoz, M.T., Rodriguez-Navarro, C., Jimenez-Lopez, C., Rodriguez-Gallego, M.: Method and product for protecting and reinforcing construction and ornamental materials. WO 2008/009771 A1 (2008)

3.100. Jroundi, F., Fernández-Vivas, A., Rodriguez-Navarro, C., Bedmar, E.J., González-Muñoz, M.T.: Bioconservation of deteriorated monumental calcarenite stone and identification of bacteria with carbonatogenic activity. Microb. Ecol. 60, 39–54 (2010)

3.101. Zhong, L., Islam, M.R.: A new microbial plugging process and its impact on fracture remediation. In: Proc. of. Society of Petroleum Engineers. Annual Technical Conference, Dallas, Texas, pp. 703–715 (1995)

3.102. Castanier, S.: Nouvelles compositions pour mortier biologique, procédé de recourvrement d'un surface ou de comblement d'une cavité à l'aide des compositions. French patent. No 95 05861 (1995)

3.103. Whiffin, V.S.: Microbial CaCO3 precipitation for the production of Biocement. Ph.D thesis Murdoch University, Australia, p. 155 (2004), http://wwwlib.murdoch.edu.au/adt/browse/view/adt-MU20041101.142604

3.104. Kucharski, E.S., Cord-Ruwisch, R., Whiffin, V., Al-Thawadi, S.M.J.: Microbial biocementation. World intellectual property organization. WO 2006/066326 A1 (2006)

3.105. Ramachandran, S.K., Ramakrishnan, V., Bang, S.S.: Remediation of Concrete Using Micro-organisms. ACI Mater. J. 98, 3–9 (2001)

3.106. Achal, V.: Microbial remediation of defects in building materials and structures. PhD thesis, Thapar University, India (2010)

3.107. Day, J.L., Ramakrishnan, V., Bang, S.S.: Microbiologically induced sealant for concrete crack remediation. In: Proc. of. 16th Engineering Mechanics Conference, Seatlle (2003)

3.108. Bang, S.S., Galinat, J.K., Ramakrishnan, V.: Calcite precipitation induced by polyurethane-immobilized Sporosarcina pasteurii. Enzyme Microb. Technol. 28(4-5), 404–409 (2001)

3.109. Bachmeier, K.L., Williams, A.E., Warmington, J.R., Bang, S.S.: Urease activity in microbiologically-induced calcite precipitation. J. Biotechnol. 93(2), 171–181 (2002)

3.110. De Belie, N., De Muynck, W.: Crack repair in concrete using biodeposition. In: Alexander, M.G., Beushausen, H.-D., Dehn, F., Moyo, P. (eds.) Proceedings of the International Conference on Concrete Repair, Rehabilitation and Retrofitting (ICCRRR), Cape Town, South Africa, November 24-26, 2008, pp. 291–292 in abstract book; pp. 777–781 on CD-ROM. CRC Press, Boca Raton (2009) ISBN: 978-0-415-46850-3

3.111. Van Tittelboom, K., De Belie, N., De Muynck, W., Verstraete, W.: Use of bacteria to repair cracks in concrete. Cement and Concrete Research 40(1), 157–166 (2010)

3.112. De Belie, N.: Microorganisms versus stony materials: a love-hate relationship - Robert L'Hermite Medal lecture 2010. Materials and Structures 43(9), 1191–1202 (2010)

3.113. Ramakrishnan, S.K., Panchalan, R.K., Bang, S.S.: Improvement of concrete durability by bacterial mineral precipitation. In: 11th International Conference on Fracture, Turin, Italy (2001)

3.114. Achal, V., Mukherjee, A., Basu, P.C., Reddy, M.S.: Lactose mother liquor as an alternative nutrient source for microbial concrete production by Sporosarcina pasteurii. Journal of Industrial Microbiology and Biotechnology 36, 433–438 (2009)
3.115. Ghosh, P., Mandal, S., Chattopadhyay, B.D., Pal, S.: Use of microorganism to improve the strength of cement mortar. Cem. Concr. Res. 35(10), 1980–1983 (2005)
3.116. Ghosh, S., Biswas, M., Chattopadhyay, B.D., Mandal, S.: Microbial activity on the micro-structure of bacteria modified mortar. Cement & Concrete Composites 31, 93–98 (2009)
3.117. Van der Zwaag, S., van Dijk, N.H., Jonkers, H.M., Mookhoek, S.D., Sloof, W.G.: Self-healing behaviour in engineering materials: bio-inspired but respecting their intrinsic character. Philosophical Transactions of the Royal Society A-Mathematical Physical and Engineering Sciences 367, 1689–1704 (2009)
3.118. Jonkers, H.M.: Self-healing concrete: a biological approach. In: van der Zwaag, S. (ed.) Self-healing Materials: An Introduction, pp. 195–204. Springer, The Netherlands (2007)
3.119. Jonkers, H.M., Schlangen, E.: Crack repair by concrete-immobilized bacteria. In: Schmets, A.J.M., Van der Zwaag, S. (eds.) Proc. of. First International Conference on Self-healing Materials, Noordwijk, The Netherlands, p. 7 (2007)
3.120. Jonkers, H.M., Thijssen, A., Muyzer, G., Copuroglu, O., Schlangen, E.: Application of bacteria as self-healing agent for the development of sustainable concrete. Ecological Engineering 36(2), 230–235 (2010)
3.121. Wiktor, V., Jonkers, H.M.: Self-healing of cracks in bacterial concrete. In: Van Breugel, K., Guang, Y., Yong, Y. (eds.) Proc. 2nd Int. Symposium Service Life Design for Infrastructure, Delft, The Netherlands, October 4-6, pp. 825–831 (2010)
3.122. Wiktor, V., Jonkers, H.M.: Quantification of crack-healing in novel bacteria-based self-healing concrete. Cement and Concrete Composites 33(7), 763–770 (2011)
3.123. Jonkers, H.M.: Bacteria-based self-healing concrete. Heron 56, 1–12 (2011)
3.124. Wang, J.: Self-healing concrete using microorganisms. In: The 2nd CSC PhD Students Workshop. Ghent, September 3, pp. 11–22 (2010)
3.125. Standaert, L.: Zelfheling van beton met behulp van ingekapselde micro-organismen. Masterproef, Gent, Faculteit Ingenieurswetenschappen (2010)
3.126. Samonin, V.V., Elikova, E.E.: A study of the Adsoprtion of bacterial cells on porous materials. Microbiology 7(6), 696–701 (2004)
3.127. Aldea, C.M., Ghandehari, M., Shah, S.P., Karr, A.: Combined effect of cracking and water permeability of concrete. In: Fourteenth Engineering Mechanics Conference. American Society of Civil Engineers (2000)
3.128. Wang, J., De Belie, N., Verstraete, W.: Self-healing of mortar by bacteria encapsulated in diato-maceous earth. In: Godbout, S., Potvin, L. (eds.) Proceedings of the 7th International Symposium on Concrete for a Sustainable Agriculture (CSA), Quebec, September 18-21, pp. 17–24 (2011)
3.129. Wang, J.Y., De Belie, N., Verstraete, W.: Diatomaceous earth as a protective vehicle for bacteria applied for self-healing concrete. Journal of Industrial Microbiology and Biotechnology 39, 567–577 (2012)

3.130. Hunt, S.C.: Method and system for bioremediation of contaminated soil using inoculated diato-maceous earth. United States patent: US 005570973A (1996)
3.131. Ivanov, V.M., Figurovskaya, V.N., Barbalat Yu, A., Ershova, N.I.: Chromaticity characteristics of $NH_2$, $Hg_2$, $I_3$ and $I_2$: molecular Iodine as a test form alternative to Nessler's reagent. Journal of Analytical Chemistry 60(7), 707–710 (2005)
3.132. Wang, J., Van Tittelboom, K., De Belie, N., Verstraete, W.: Potential of applying immobilized Bacillus sphaericus to heal cracks in concrete autonomously. In: Zachar, J., Claisse, P., Naik, T.R., Ganjian, E. (eds.) Second International Conference on Sustainable Construction Materials and Technologies, Ancona, Italy, May 31-June 3, vol. 3, pp. 1807–1818 (2010) ISBN 978-1-4507-1490-7
3.133. Wang, J., Van Tittelboom, K., De Belie, N., Verstraete, W.: Use of silica gel or polyurethane immobilized bacteria for self-healing concrete. Construction and Building Materials 26, 532–540 (2012)

# 4 Recovery against Mechanical Actions

V.C. Li[1], A.R. Sakulich[1], H.W. Reinhardt[2], E. Schlangen[3], K. Van Tittelboom[4], D. Snoeck[4], N. De Belie[4], C. Joseph[5], D.R. Gardner[5], R.J. Lark[5], H. Mihashi[6], and T. Nishiwaki[7]

[1] University of Michigan, MI, USA
{vcli,a.sakulic}@umich.edu
[2] University of Stuttgart, Germany
reinhardt@iwb.uni-stuttgart.de
[3] Microlab, Delft University of Technology, The Netherlands
H.E.J.G.Schlangen@tudelft.nl
[4] Magnel Laboratory for Concrete Research, Ghent University, Belgium
{Kim.VanTittelboom,Didier.Snoeck,Nele.DeBelie}@UGent.be
[5] Cardiff School of Engineering, Cardiff University, United Kingdom
GardnerDR@cf.ac.uk, Lark@cardiff.ac.uk
[6] Tohoku Institute of Technology, Japan
mihashi@timos.str.archi.tohoku.ac.jp
[7] Yamagata University, Japan
ty@archi.tohoku.ac.jp

## 4.1 Autogenic Self-Healing

Autogenic self-healing has been defined in chapter 1 as a self-healing process where the recovery process uses materials components that could also be present when not specifically designed for self-healing (own generic materials).

### *4.1.1 Mechanisms of Autogenic Self-Healing*

The main mechanism of autogenic self-healing of a crack is the production of calcium silicate hydrate (C-S-H), a hydration product of cement which lends strength to hydrated cement paste (so mechanical properties may be regained) [4.1]. The production of C-S-H occurs when tricalcium silicate ($C_3S$/alite, Eq.(4.1)) and dicalcium silicate ($C_2S$/belite, Eq. (4.2)) react with water to form C-S-H and calcium hydroxide (CH/portlandite), the generalized equations for which are:

$$2Ca_3SiO_5 + 6H_2O \rightarrow 3CaO \cdot 2SiO_2 \cdot 3H_2O + 3Ca(OH)_2 \quad (4.1)$$

$$2Ca_2SiO_4 + 4H_2O \rightarrow 3CaO \cdot 2SiO_2 \cdot 3H_2O + Ca(OH)_2 \quad (4.2)$$

As alite contains more reactive calcium, it reacts more rapidly and is responsible for early strength, while belite reacts more slowly and provides strength increases at later ages. During cement hydration, some grains of cement containing alite and belite do not fully react, resulting in unhydrated cores surrounded by hydrated C-S-H and CH material – a natural encapsulation of reactive minerals more or less uniformly dispersed in the concrete. During cracking, these naturally encapsulated

M. de Rooij et al. (Eds.): *Self-Healing Phenomena in Cement-Based Materials*, RILEM 11, pp. 119–215.
DOI: 10.1007/978-94-007-6624-2_4 

particles are exposed to the atmosphere and begin to hydrate when exposed to water, which causes a volumetric expansion capable of completely closing microcracks.

The continued hydration of unreacted cement is present in all binders based on Portland cement. For cementitious systems containing significant additions of aluminosilicate materials such as fly ash, blast furnace slag, silica fume, or clay, the pozzolanic reaction may also provide a degree of self-healing capacity. In alkaline environments, silicate species can dissolve from the pozzolanic material to create silicic acid ($H_4SiO_4$/SH, Eq. (4.3)). Silicic acid can react with dissolved portlandite, the result of which is C-S-H (Eq.(4.4)) and water:

$$3Ca(OH)_2 + 2H_4SiO_4 \rightarrow 3Ca_2 + + 2H_2SiO_4^{2-} + 4H_2O + 2OH^- \quad (4.3)$$

$$3Ca^{2+} + 2H_2SiO_4^{2-} + 4H_2O + 2OH^- \rightarrow 3CaO \cdot 2SiO_2 \cdot 7H_2O \quad (4.4)$$

The C-S-H produced during the pozzolanic reaction can then heal fine cracks in the same manner as the C-S-H produced from the hydration of unreacted cement particles (e.g., volumetric change)

Because the rate of the pozzolanic reaction is coupled to the pH, it is substantially slower than the hydration of unreacted cement. In a cracked specimen, it is likely that the pozzolanic reaction will promote self-healing even on the longest timescales. Since the service life of infrastructure can be on the order of decades, the inclusion of pozzolans may ensure self-healing in structures undergoing repeated damaging even after available unreacted cement has been consumed.

Abd-Elmoaty [4.2] studied the autogenous healing behaviour inside polymer modified concrete (PMC). PMC is made by the dispersion of organic polymers inside the mixing water of concrete. Upon cement hydration, coalescence of the polymers occurs resulting in a co-matrix of hydrated cement and polymer film throughout the concrete. Abd-Emoaty stated that healing occurred in the same way as in traditional concrete. However, healing occurred to a larger extent and was extended over a longer period compared to traditional concrete as more unhydrated cement was available in the matrix because the polymers enclosed the cement particles as a kind of membrane.

### *4.1.2 Effect of Fibres on Autogenic Self-Healing*

Early investigations identified the presence of water and tight crack width as the two most important criteria for autogenic self-healing [4.3-4.5]. Without water, autogenic self-healing chemically cannot occur; without tight crack widths, self-healing products will build up on cracks faces, but fail to fill the crack.

To obtain a “robust” self-healing concrete, Li and Yang [4.6] proposed six requirements: *Pervasiveness* (the ability to heal as soon as, and wherever, a crack appears), *stability* (a healing mechanism that does not become less effective over time), *economic feasibility*, *reliability* (consistency of self-healing), *quality* (recovery of both closing characteristics and mechanical properties) and

*repeatability* (ability to repair damage from multiple events). Although standard concrete meets some of these requirements, the inability to control crack width hinders development of a fully robust system and largely limits possibilities to only autonomic healing, if at all. It is the brittle nature of normal concrete that makes controlling crack width difficult.

Li and coworkers were the first who proposed the use of a fiber reinforced strain hardening engineered cementitious composite (ECC) in order to restrict the crack width and thus promote autogenous healing. In their early research, polyethylene (PE) fibers were used [4.7], while later on, they started to use poly vinyl alcohol (PVA) fibers [4.6, 4.8-4.11]. A typical composition of ECC consists of 570 kg/m$^3$ OPC, 455 kg/m$^3$ silica sand with average grain size of 110 μm, 684 kg/m$^3$ fly ash, 5 kg/m$^3$ high range water reducer, poly-vinyl-alcohol fiber and 330 kg/m$^3$ water. The fiber content is 2 % by volume [4.12]. The tensile strength amounts to 4-5 MPa. The stress-strain diagram is similar to that of a rigid-plastic strain-hardening material.

ECC is micromechanically designed to suppress brittle fracture behavior in favor of distributed microcracking. This behavior is encouraged through the interactions between cement and short fibers, without use of large aggregates, and has found use in a number of applications worldwide [4.13]. Well distributed, tight microcracks are produced even at tensile deformations of up to 4% (Fig. 4.1). In ECC, crack width can be custom tailored to as low as 30 μm; it has been shown that a crack width below 150 μm, and preferably below 50 μm, is critical to the self-healing of any cementitious system [4.6].

The fibers in ECC themselves also encourage the production of healing products. First, bridging fibers lower the cross sectional area of a crack, effectively raising the pH by diminishing flow. Second, for reasons arising purely from fluid dynamics, when water flows around the fiber, a turbulent zone is created on the leeward side. In this zone water velocity can stagnate, encouraging precipitation of healing product and creating a composite fiber/healing product material that bridges the crack

The efficiency of steel cord (SC), polypropylene (PP), PE and PVA fibers was compared by Homma *et al.* [4.14] and Koda *et al.* [4.15]. While SC fibers showed minor crack closing efficiency as the steel started to corrode inside the crack, PVA fibers induced the highest healing efficiency. This was attributed to the fact that PVA fibers promoted the deposition of crystallization products, as hydroxyl groups, attached to the fiber structure, attracted calcium ions.

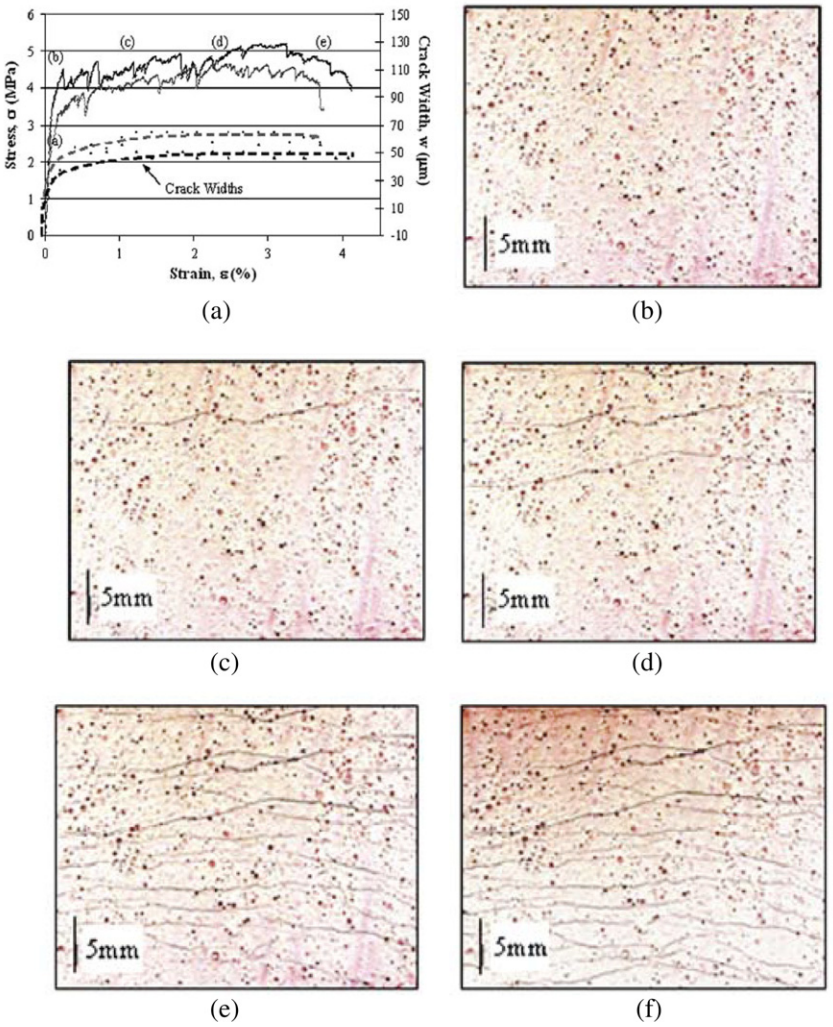


**Fig. 4.1** Uniaxial stress/strain curve and crack development in ECC [4.16]

Table 4.1 shows the mix proportions of materials used in a study by Homma *et al.* [4.17]. They studied three types of strain hardening cement-based composites (SHCC), named fibre reinforced cementitious composites (FRCC) by these authors: (1) containing micro polyethylene fibre (ø=12 μm, length=6 mm) (FRCC(PE)), (2) containing steel cord fibre (ø=0.4 mm, length=32 mm) (FRCC(SC)), and (3) containing hybrid composite fibres (i.e. both of PE and SC fibres) (HFRCC).

**Table 4.1** Mix proportion of FRCC specimens investigated by Homma *et al.* [4.17]

| Types of Mix | Water/Binder | Sand/Binder | Silica fume/Binder | SP/binder | PE fiber (Vol. %) | SC fiber (Vol. %) | Fiber content (no./m$^3$) |
|---|---|---|---|---|---|---|---|
| FRCC (SC) | 0.45 | 0.45 | 0.15 | - | - | 0.75 | 187 x $10^4$ |
| FRCC (PE) | | | | 0.09 | 1.5 | - | 221 x $10^8$ |
| HFRCC | | | | | 0.75 | 0.75 | 111 x $10^8$ |

Binder = Cement + Silica fume; SP = Superplasticizer (Polycarboxylate)

In all series, four specimens of 25 mm × 75 mm × 75 mm were prepared and cracks were introduced by means of a uni-axial tension test. Fig. 4.2 shows the outline of the tension test. During this test, each specimen was stretched to different strain levels in order to have different maximum crack widths. After the tension test, the crack surface was observed by means of a digital microscope and the crack width was measured (see Table 4.2). The microscopic observation was repeated at 3, 14 and 28 days in order to investigate the effect of the self-healing of cracks.

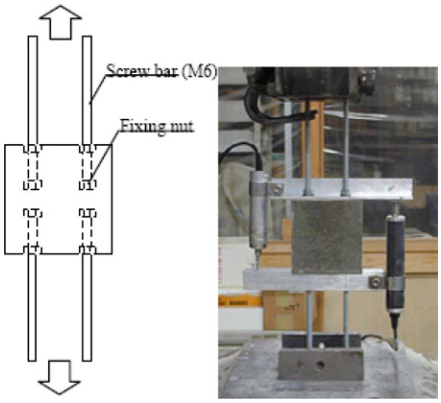


**Fig. 4.2** Uni-axial tensile test equipment

**Table 4.2** Maximum crack width (mm) evaluated by means of microscope observation

| | No. of specimens | | | |
|---|---|---|---|---|
| Type of mixes | No. 1 | No. 2 | No. 3 | No. 4 |
| FRCC (SC) | 0.035 | 0.076 | 0.088 | 0.757 |
| FRCC (PE) | 0.019 | 0.038 | 0.119 | 0.368 |
| HFRCC | 0.017 | 0.081 | 0.407 | 0.71 |

Table 4.3 shows photographs of the crack surface in FRCC(PE), FRCC(SC), and HFRCC. It can clearly be seen in these photographs that the crack surface of all specimens after the tension test is clear and there are no products on the surface. After 3 days the crack surfaces in FRCC(PE) and HFRCC were attached by self-healing products and the crack width decreased as the time advanced. The crack surface in FRCC(SC) was not decreased by the self-healing products. This could be because there were too few fibres that self-healing products could attach to. On the other hand in the place where of a lot of micro PE fibres bridged over the crack, especially in most of FRCC(PE) specimens, there were many attachments of self-healing products. Even in case of FRCC(PE), however, if there were rather a few fibres, the attachment of self-healing products depended on the volume content of PE fibres. Therefore it was concluded that amount of the PE fibre per volume has a great influence on self-healing. After 3 days, it was observed that the steel cords on the crack surface in FRCC(SC) and HFRCC were corroded and the volume expanded.

**Table 4.3** Microscopic observation of self-healing products at a crack surface

| | Elapsed time (day) | | | |
|---|---|---|---|---|
| | 0* | 3 | 14 | 28 |
| FRCC (SC) Steelcord fiber specimen No. 2 (crack width: 1.976mm) | 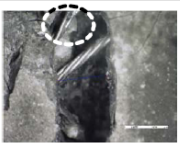 | 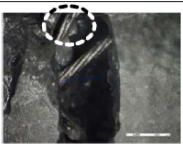 | 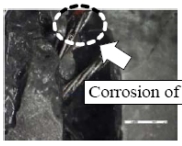  | 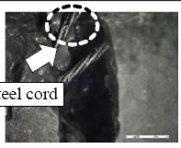 |
| FRCC (PE) Polyethylene fiber specimen No. 4 (crack width: 0.368mm) | 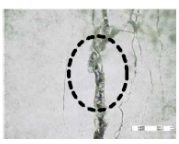 | 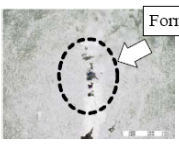  | 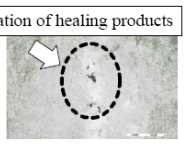 | 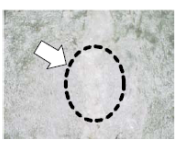 |
| HFRCC Steel-PE hybrid fiber specimen No. 1 (crack width: 1.532mm) | 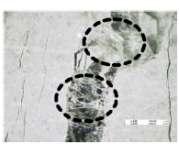 | 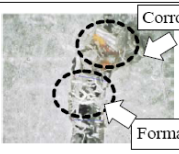  | 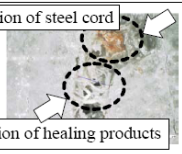 | 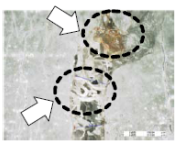 |

* Immediately after tension test before immersion in water.

Fig. 4.3 shows the time dependence of mean size of self-healing products attached to the crack surface. The increasing rate of the mean size during the first 3 days is higher than that after 3 days. This could be because $Ca^{2+}$ diffusion speed from the inside of FRCC was decreased as the time advanced because of the formation of a self-healing product layer. The order of the amount of the attached products in each FRCC material was FRCC(SC) < HFRCC < FRCC(PE). This order corresponded with that of the number of mixed in fibres per volume fraction

as shown in Table 4.1: FRCC(SC) < HFRCC < FRCC(PE). Therefore it was concluded that the number of mixed in fibres per volume has a dominant influence on the crack self-closing effects.

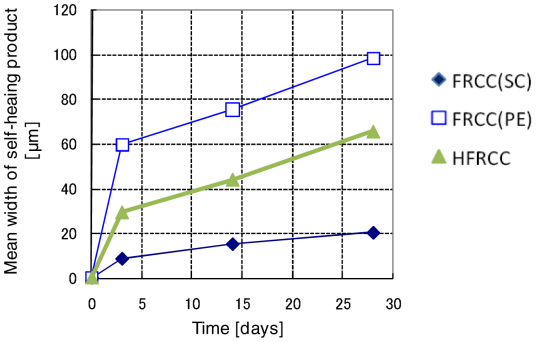


**Fig. 4.3** Time dependence of mean size of self-healing products attached at the crack surface

Fig. 4.4 shows the results of the low pressure water permeability test of the cracked and uncracked specimens. As can be seen in this figure, the coefficient of water permeability for all specimens decreased until 3 days except for the uncracked specimens. After 3 days the decreasing rate of the coefficient of water permeability slowed down significantly in all specimens. This corresponds with the microscopic observation results as shown in Fig. 4.3 in which the self-healing products attaching speed is faster until 3 days than after 3 days. It can also be noticed that, in the specimens with a wider crack, the coefficient of water permeability was almost constant after 3 days. This indicates that the formation of calcium carbonate crystals in the wider cracks do not contribute to the self-healing mechanism. On the other hand, in case of specimens with a smaller crack width, the coefficient of water permeability decreased as time advances even after 3 days and in some cases reached to the same values of those obtained in uncracked specimens. This indicates that, in such a small crack width, the formation of calcium carbonate crystals has a great effect on self-healing of cracks.

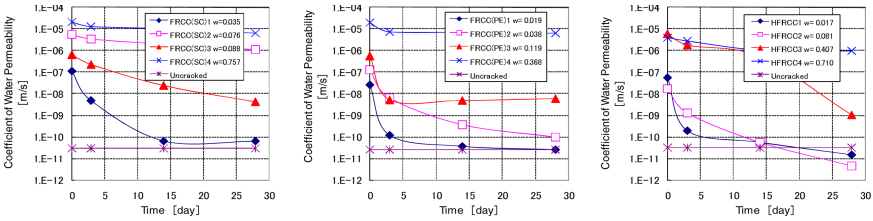


(a) FRCC(SC) (b) FRCC(PE) (c) HFRCC

**Fig. 4.4** Time dependence of water permeability coefficient in each FRCC

Fig. 4.5 shows the influence of time dependence of water permeability coefficient due to type of FRCC. The decrease of the water permeability coefficient in FRCC(PE) and HFRCC is more than that in FRCC(SC). This can be explained because the self-healing products could attach to the crack surface more in FRCC(PE) and HFRCC than in FRCC(SC).

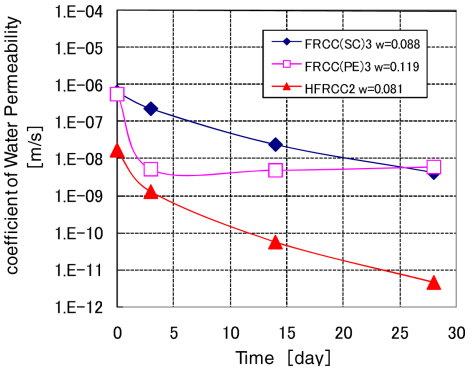


**Fig. 4.5** Influence of time dependence of water permeability coefficient due to type of FRCC

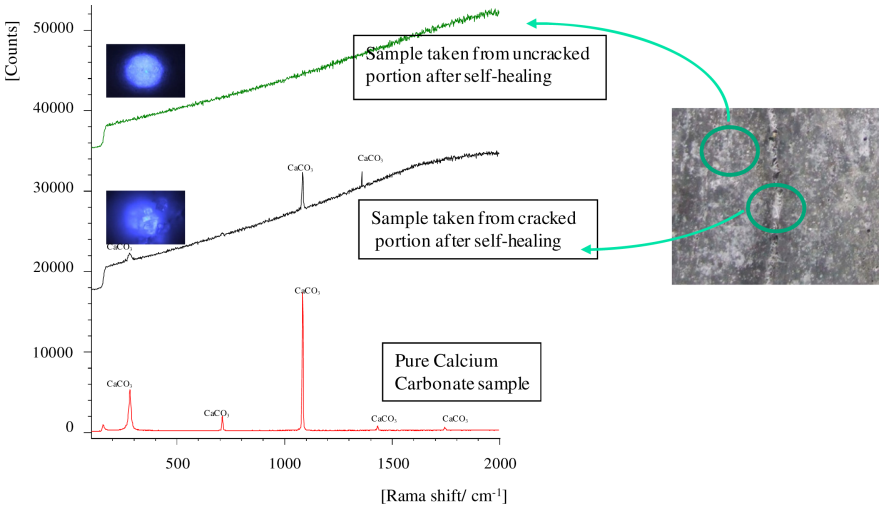


**Fig. 4.6** Raman spectroscopy of FRCC(PE) specimens

In order to examine the chemical composition of the self-healing products, FRCC(PE) specimens were analyzed by Raman spectroscopy. Fig. 4.6 shows the Raman spectroscopy of FRCC(PE) samples. In this figure, upper, middle, and lower profiles were taken from uncracked area, cracked area, and pure calcium carbonate crystals, respectively. It can be seen from this figure that the peaks of

the cracked area coincided with those of pure calcium carbonate crystals. On the other hand, in the case of uncracked area, such a peak couldn't be observed. Therefore the formation of self-healing products in FRCC was attributed to calcium carbonates crystals.

In order to evaluate the effect of self-healing on the tensile properties, the self-healed FRCC specimens were tested by uni-axial tension test again. Fig. 4.7 shows the tensile stress-elongation responses before and after the self-healing. Fig. 4.8 shows the schematic of general tensile stress-elongation response of FRCC. In order to compare each FRCC specimen, the strength recovery rate ($c$) was defined as follows:

$$c = \frac{\sigma_2 - \sigma_0}{\sigma_1 - \sigma_0} \times 100 \tag{4.5}$$

Where $\sigma_0$ = the stress at the unloading of the first tension test
$\sigma_1$ = the tensile strength at first tension test
$\sigma_2$ = the tensile strength after self-healing.

By use of this $c$, we can judge the curing capability of the strength in each FRCC as follows. If $c$ is over 100, this specimen can be considered to be recovered perfectly. If $c$ is over 0 and under 100, this one was recovered a little. If $c$ is equal to 0, this one was not recovered. If $c$ is under 0, this one was deteriorated. Fig. 4.9 shows the relationship between the strength recovery rate $c$ and residual elongation in each FRCC material.

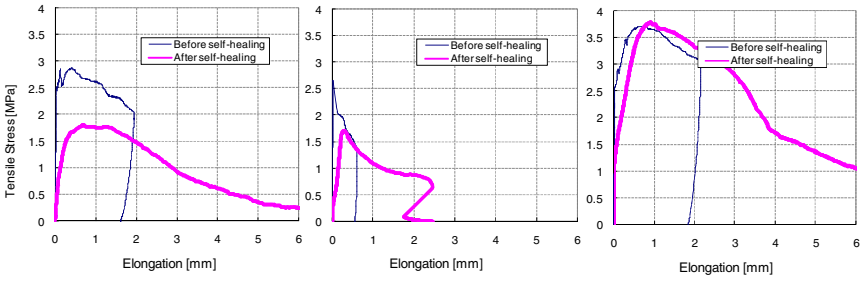


(a) FRCC(SC) (b) FRCC(PE) (c) HFRCC

**Fig. 4.7** Comparison of tensile properties of specimens before and after 28 days of self-healing

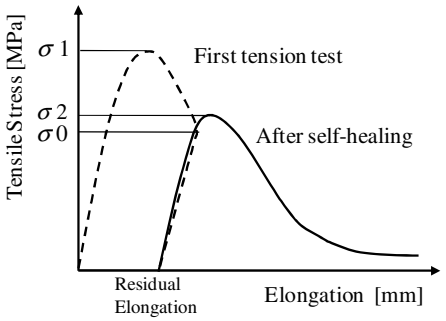


**Fig. 4.8** Schematic of the relationship between tensile stress and tensile elongation of FRCC

It can be seen in Fig. 4.9 that after 28 days the recovery rate of the FRCC(SC) was almost zero or even minus. This could be because the self-healing products were not attached to the crack surface and steel cords were corroded during 28 days.

In the case of the FRCC(PE), the recovery rate $c$ is located over 0 and under 100. The tensile strength after self-healing didn't reach the initial tensile strength, but could reach the first unloading stress. This could be because a lot of calcium carbonate crystals attached to many fibres. This indicated that, if the calcium carbonate crystals attaches to the crack surface, the tensile strength after self-healing can be recoverable. Moreover it can also be seen in Fig. 4.9 that the strength recovery rate becomes higher as residual elongation is smaller.

In the case of HFRCC, the recovery rate was higher than 100 when the residual elongation was less than 1.5 mm. It means that the tensile strength after self-healing could reach not only the first unloading stress, but also the first tensile strength. This could be because, similar to FRCC(PE), a lot of calcium carbonate crystals attached to the crack surface with very fine fibres. Moreover the bond property of the steel cord damaged by pull out stress might be recovered by the self-healing products.

By the crack surface observation after the tension test, corrosion of the steel cord in FRCC(SC) was confirmed not only outside, but also inside. However, corrosion of the steel cord in HFRCC was observed on the outside only. This could be because in HFRCC a lot of calcium carbonate crystals attached to the matrix around steel cord fibres. It corresponds with the increase of tensile strength after the self-healing.

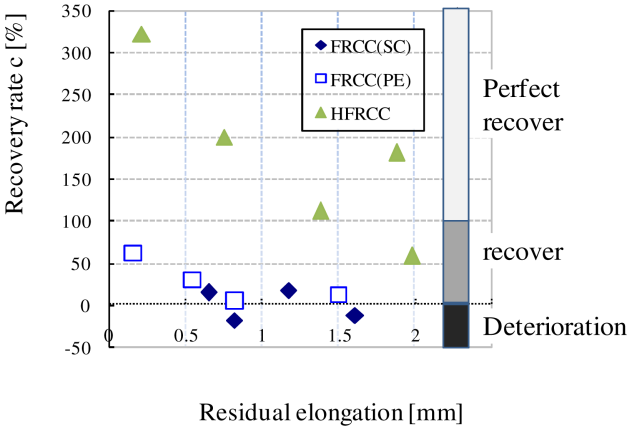


**Fig. 4.9** Relationship between recovery rate and residual elongation [4.17]

Due to the low water/binder ratio present in ECC (about 0.26), the presence of notable amounts of unreacted cement, and thus notable self-healing capacity, is almost certain. A specimen that has undergone healing will have a buildup of healing product on crack faces, thus decreasing the cross-sectional area and reducing the flow rate of water through the crack, resulting in a lower permeability coefficient.

In a standard ECC, Lepech and Li [4.16] observed a distribution of 60 μm-wide microcracks after pre-loading in tension up to 3.0%. Compared to a non-ECC reinforced mortar specimen pre-loaded to 1.5%, the permeability of the ECC specimen was six orders of magnitude lower. This was due mainly to the distributed microcracks (as opposed to fewer but larger cracks in the mortar) in the ECC specimen; additionally, substantial self-closing was observed that further reduced permeability.

Homma *et al.* [4.14] found that the water permeability of SHCC specimens with tight crack widths decreased continuously during healing until reaching values similar to those of uncracked specimens. For samples with wider cracks, the water permeability dropped during the first three days of healing, but improvement slowed thereafter. Coupled with microscopic observations, it was concluded that healing product was rapidly produced during the first three days after which healing slowed significantly. In large cracks, this meant a buildup of healing product on crack faces that was insufficient to fill the crack. For similar reasons, Li and Yang [4.6] found that the permeability of samples with crack widths below 150 μm improved after 10 wet/dry cycles; samples with crack widths of 150 μm or above did not improve.

Water permeability tests, however, are complicated by a number of factors. First, the act of carrying out the test itself can cause healing, swelling of C-S-H gel, or continued hydration of semi-hydrated cement to occur as water runs through the cracks. Second, cracks may become blocked by particulate matter that

reduce water flow but do not aid healing. Finally, water permeability accurately describes recovery against environmental action or *self-closing*, in which cracks are blocked to water flow, but does not necessarily describe self-healing in terms of recovery against mechanical action, which implies an improvement in mechanical properties.

Yang *et al.* [4.18] used transverse resonant frequencies to calculate 'Normalized Resonant Frequency,' the resonant frequency of a healed specimen divided by the resonant frequency of a virgin specimen undergoing the same curing regime. In this way, bulk hydration was accounted for, and recovery of properties was attributable solely to self-healing. Specimens with cracks less than 50 μm wide recovered 100% (Fig. 4.10 a). Between widths of 50 and 150 μm recovery diminished, while above 150 μm no recovery was observed. During uniaxial tensile testing after damage and re-healing, tensile strain capacity remained quite high (1.8% - 3.1%) even for samples that had undergone preloading of 2% or 3%. (Fig. 4.10 b) Yang concluded that at least 4-5 cycles were needed to attain the full benefits of self-healing, and noted a substantial recovery of stiffness during the healing cycle. Microscopic observation of failed samples identified both cracks propagating through the healing material as well as fresh cracks in the ECC matrix.

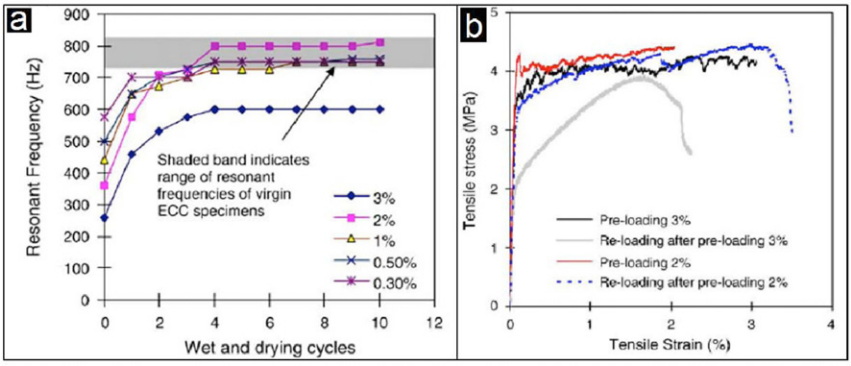


**Fig. 4.10** a) Resonant frequency recovery of ECC specimens pre-loaded between 0.30 and 3.0% after 10 wet/dry cycles; b) tensile stress/strain relationships of ECC specimens pre-loaded to 3.0 and 2.0% before and after 10 wet/dry cycles [4.18].

Homma *et al.* [4.14] investigated samples containing both short polyethylene fibers and steel cord which exhibited distributed microcracking behavior. These samples recovered at least 100% of their mechanical properties after 28 days of healing submerged in water after pre-loading. Continued hydration was discounted as a source of this improvement, which was attributed to self-healing products forming on fibers and crack faces. Composites containing only steel cord or short polyethylene fibers did not exhibit distributed microcracking, and thus healing of the ~ 60 μm size cracks was incomplete.

Yamamoto *et al.* [4.19] observed a dramatic increase in longitudinal resonant frequency after as little as one wet/dry cycle. Uniaxial tension tests again confirmed the link between resonant frequency and mechanical properties. Though the stiffness recovered to the same values as an un-healed specimen, at a tensile stress of approximately 2.5 MPa, the stress/strain curves "bent over." It was theorized that this is due either to the formation of mechanically inferior healing products (assumed to be calcite) or to poor adhesion at the healing product/matrix interface. Similarly, Kan *et al.* [4.20] observed significant improvement in RF ratio during the first 4-5 wet/dry cycles, after which improvement leveled off. For samples with 0.3 % and 0.5 % pre-load strain, the RF ratio returned to nearly 100% (indicating almost total healing); for 1.0 % and 2.0 % pre-load strain the RF ratio rose to 95 % and 90 %, respectively. Between 3- and 90-day old samples, the latter had many more cracks of smaller width, which led to slightly better resonant frequency recovery.

In an effort to increase the 'green' nature of ECC, Qian *et al.* [4.21] developed an ECC containing blast furnace slag (BFS) and limestone powder. As the presence of a limited amount of these two additives would lower the amount of unreacted cementitious material in the system after moderate curing times (28 days), it was theorized that the self-healing capacity of the final product would be somewhat reduced. Ultimate deflection capacity, related to flexural strength, was measured. Water-healed specimens had deflection capacities from 65 – 105 % of a virgin sample; air-healed specimens remained between only 40 – 62 %. In total, the mechanical properties seem to indicate that the inclusion of significant amounts of BFS and limestone powder does not negatively affect the self-healing capacity of ECC. Similarly, the incorporation of fly ash has been shown to have little, if any, effect on the healing capabilities of ECC.

In a study on the de-icing salt scaling resistance of both standard ECC and high fly ash ECC, Şahmaran and Li [4.22] observed a substantial recovery of mechanical stiffness in samples that were pre-loaded and then exposed to a de-icing salt solution. The self-healing contributed to the high durability that the ECC samples exhibited during testing, which resulted in their performing inside the limits prescribed by ASTM C672 (Standard Test Method for Scaling Resistance of Concrete Surfaces Exposed to Deicing Chemicals.) That ECC has been shown to undergo self-healing was mentioned by Şahmaran *et al.* [4.23] in a later study on the resistance of ECC to damage from freezing and thawing. Since the standard ASTM test requires relatively rapid cycling of the freezing and thawing cycles, not allowing test material to self-heal, the data obtained from such tests should therefore be considered absolute worst-case scenarios. ECC, incidentally, was shown to have excellent durability in such tests.

ECC specimens have been preloaded to a given strain, immersed in 3 % NaCl solution or cured in air for 30, 60, and 90 days. After the immersion time, the specimens were reloaded. Fig. 4.11 shows typical results. Fig. 4.11 a) is valid for the pre-cracked specimens to 0.5 % tensile strain, whereas Fig. 4.11 b) is valid for the specimens pre-cracked to a tensile strain of 1.5 %. The curves show an almost complete recovery of stiffness when re-loaded in direct tensile tests even after

periods of only one month exposed to NaCl solution. Preloaded ECC specimens with microcracks at 45 μm crack width induced by mechanical loading almost fully recovered their tensile strain. However, both pre-cracked and uncracked ECC specimens exposed to NaCl solution lost more than 10 % of their tensile strength probably due to leaching of calcium hydroxide. Microcracks of ECC specimens that were immersed in NaCl solution appeared completely sealed as a result of self-healing [4.12]. Similar results have been reported in [4.7, 4.8].

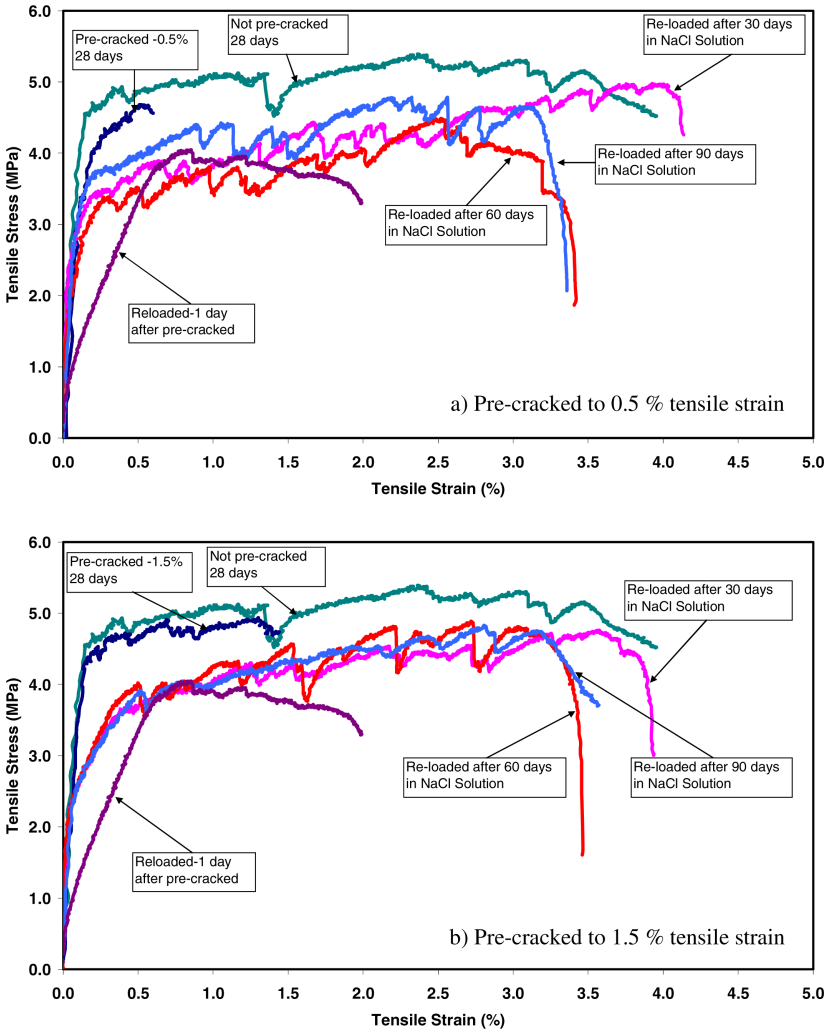


**Fig. 4.11** Tensile stress-strain curves of ECC before and after exposure to 3 % NaCl solution [4.12]

For ECC in the presence of water, healing products accumulate on the surface of cracks, and completely fill those with widths less than about 50 μm. The tight crack widths that are an inherent property of ECC require not only less healing product for total rehabilitation, but actively encourage production of healing material by maintenance of pH levels in the incident water. Bridging fibers provide further encouragement for the production of healing product, and are likely to provide sites for the precipitation of these products.

Mechanical testing shows that these products do not just seal the cracks and protect reinforcing steel but heal the cracks, leading to recovery of mechanical performance. Resonant frequency analysis has been shown to be a simple, inexpensive, and non-destructive method to observe the progress of self-healing; previous research has also shown that recovery of resonant frequency can be definitely linked to recovery of mechanical properties.

Little detailed chemical analysis has been performed on the healing products of cements and concretes in general, and ECC in particular. The healing product can be easily identified by optical microscopy (Fig. 4.12 a) or electron microscopy (Fig. 4.12 b), and can usually be observed by eye. Yamamoto [4.19] provided micrographs of the healing product, assuming it to be calcite based on the work by Edvardsen [4.3]; Yang [4.18] and Lepech [4.16] each concluded the healing product to be calcite based on EDS spectra; and Homma [4.14] identified healing product to be calcium carbonate (presumably calcite) based on Raman spectroscopy. It has been shown [4.24], however, that C-S-H can sometimes present a featureless spectrum in Raman analysis.

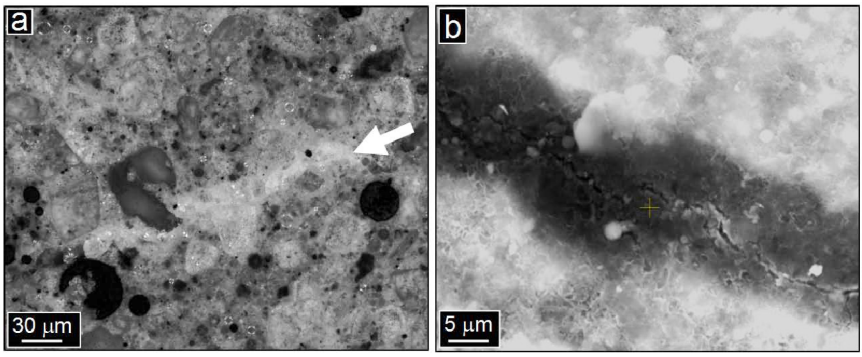


**Fig. 4.12** a) optical micrograph of healing product in ECC cement (arrow); b) SEM micrograph of a healed crack.

Kan *et al.* [4.20] observed two distinct healing products in ECC materials through use of scanning electron microscopy (SEM). In very tight cracks, 'fiber-like' C-S-H was identified; only in larger cracks were 'stone like' calcite grains formed. The compositions were confirmed by EDS, however, a large amount (~ 10 at.%) of Mg was also observed. It was speculated that this Mg could take the form of various magnesium carbonates (magnesite or dolomite), hydrates

(barringtonite, etc.) or hydroxides (brucite). The EDS results also indicated that the 'stone like' product, identified as calcite, could be a mixed system with additional C-S-H or portlandite due to an abundance of calcium; the fiber-like phase could also have included portlandite, since there was an abundance of calcium but no carbon. These findings were supplemented with limited TEM observations, which identified several grains of pure calcite. The minute sample sizes used for TEM work, however, mean that clear calcite exists in the healing product, but not how much.

Qian *et al.* [4.21] observed samples of their ECC containing BFS and limestone powder by SEM; EDS identified the healing product to be a calcite "and/or" C-S-H. As with the mechanical properties, it therefore appears that the inclusion of BFS and limestone powder had little, if any, effect on the capacity of the ECC for healing. Whether this C-S-H was produced by the hydration of unreacted cement particles or through the pozzolanic reaction is not discussed. Termkhajornkit *et al.* [4.25] investigated the self-healing properties of ordinary portland cement/fly ash blends at similar ages and found that the degree of healing increased with increasing fly ash content. Therefore, the pozzolanic reaction is likely to be the cause of at least some of the healing.

XRD experiments were used by Kan *et al.* [4.20] to identify calcite in the healing product (calcite produces XRD peaks at 30, 50, and 55 °2θ). XRD analysis only identifies crystalline materials, however; the presence of C-S-H in the healing product could be neither confirmed nor denied. FTIR analysis was also performed. Calcite was specifically identified (sharp peaks at 875 and 714 $cm^{-1}$) as well as a peak due to the presence of $CO_3^{2-}$ in general (a broad peak at 1460 $cm^{-1}$). The exact origin of this peak ($CaCO_3$ as opposed to $MgCO_3$, etc.) was indeterminate. Finally, peaks due to silicate bonding were present. Whether these peaks were produced from C-S-H in the healing product or C-S-H scraped from the edges of the healed cracks is uncertain. Slight differences in the peaks led the authors to speculate that $CO_2$ may be leaching Ca from C-S-H in the bulk, rather than consuming portlandite to form calcite. If true, the Si in the C-S-H in the bulk will become more highly polymerized, thus leading to a more complicated composite material.

### *4.1.3 Experimental Evidence in Ultra High-Performance Concrete*

Ultra High-Performance Concrete (UHPC) is a cementitious material with very low water-cement ratio. Granger *et al.* [4.26] used for their experiments a water-cement ratio of 0.2 and additionally silica fume. After 2 days water curing, the specimens were heat-cured at 90 °C and 100 % RH for 48 h. In a three-point bending test, the prismatic specimens with a center notch were loaded in a displacement controlled manner till reaching the peak load and further until a CMOD of about 30 μm. The unloading yielded a CMOD between 5 and 15 μm. Thereafter, the specimens were stored in water for a certain time.

Fig. 4.13 illustrates the deflection-softening behaviour of UHPC. The peak bending stress is about 7.3 MPa at a CMOD of 15 µm. Unloading took place at a load level of 2 kN which corresponds to a bending stress of 3.75 MPa. Reloading follows the original force-CMOD curve.

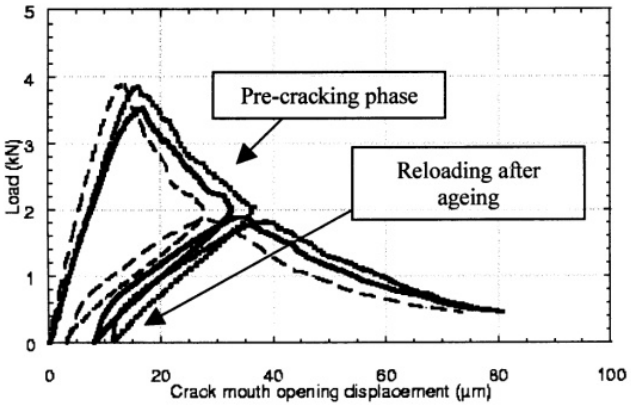


**Fig. 4.13** Load-CMOD behaviour of virgin specimen (Pre-cracking phase) and reloading after 3 weeks in air [4.26]

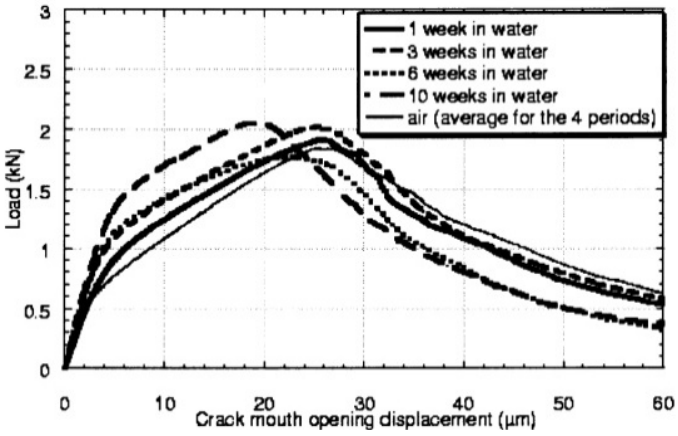


**Fig. 4.14** Load-CMOD behaviour of cured specimens and non-cured ones [4.26]

The storage in water led to slightly different behaviour as shown in Fig. 4.14. Prolonged water curing resulted in an increase of bending stress compared to non-cured specimens. The initial stiffness of cracked specimens (reloading stiffness) after 10 weeks storage in water is almost the same as the one of the virgin specimens. CMOD decreases with time of water storage. Resonance frequency and acoustic emission measurements let the authors conclude that a self-healing effect was present. The cause of self-healing is seen in the formation of new

products in the crack due to continued hydration of fractured unhydrated cement grains [4.27].

Morimoto *et al.* [4.28] developed a new type of strain hardening cementitious composite; ultra high performance strain hardening cementitious composites (UHP-SHCC). This material combines excellent protective performance, which is similar to that of ultra high performance fiber reinforced concrete (UHPFRC), with a significantly higher tensile strength and strain hardening at peak strength. Especially, the material has controlled fine cracks (less than 20 μm) and low water-to-binder ratio with unhydrated cement. In addition, silica fume, that causes pozzolanic reaction, was mixed in UHP-SHCC. These characteristic gave the advantages for self-healing after initial cracking.

Table 4.4 shows the mix proportions of UHP-SHCC used in this study. Two kinds of fiber volume ($V_f$), 1.25% and 1.5%, were used. To examine the effect of the expansion agent on recovery of resistance against permeation, 20 kg/m$^3$ expansion agent (ettringite/lime composite type) was mixed in the case of the mix proportions with 1.25%. fiber volume. 15% of the cement was replaced by silica fume. High strength polyethylene (PE) fibers were used with a diameter and length of 0.012 mm and 6 mm, respectively.

**Table 4.4** Mix proportions of UHP-SHCC

| Mix proportion | W/B | Water (kg/m$^3$) | Cement (kg/m$^3$) | Silica fume (kg/m$^3$) | Sand (kg/m$^3$) | Super-plasticizer (kg/m$^3$) | Air reducing agent (kg/m$^3$) | Expansion agent (kg/m$^3$) | Fiber (kg/m$^3$) |
|---|---|---|---|---|---|---|---|---|---|
| $V_f$=1.25% | 0.22 | 341 | 1316 | 232 | 155 | 15.5 | 0.062 | 0 | 12.1 |
| $V_f$=1.25%+EX | 0.22 | 340 | 1294 | 232 | 155 | 15.5 | 0.062 | 20 | 12.1 |
| $V_f$=1.50% | 0.22 | 340 | 1313 | 232 | 155 | 15.4 | 0.062 | 0 | 14.6 |

Plate-shaped specimens with a cross section of 150 mm×30 mm were prepared. There were two rebars of D6 in the specimen to improve the crack formation. Rebars of D10 were also embedded in both specimen ends to hold the specimen by a testing machine (see Fig. 4.15a). The specimens were demoulded one day after casting and cured in water in a constant temperature room (20°C). Then air permeability tests and water permeability tests were conducted at the age of 32~35 days after the specimens were dried in air for a couple of days. And at the age of 36~37 days, cracks were induced by uni-axial tensile test, as shown in Fig. 4.15b. Loading was controlled by LVDT fixed on both specimen surfaces (gauge length: 150 mm). Each specimen was loaded until the tensile strain of either 0.1% or 0.2%, and then unloaded. After the tensile tests, the air and water permeability test were conducted again. Afterwards, specimens were cured under air or in water at a constant temperature of 20°C for 20 days. Table 4.5 summarizes specimen series, unloading strain and re-curing conditions

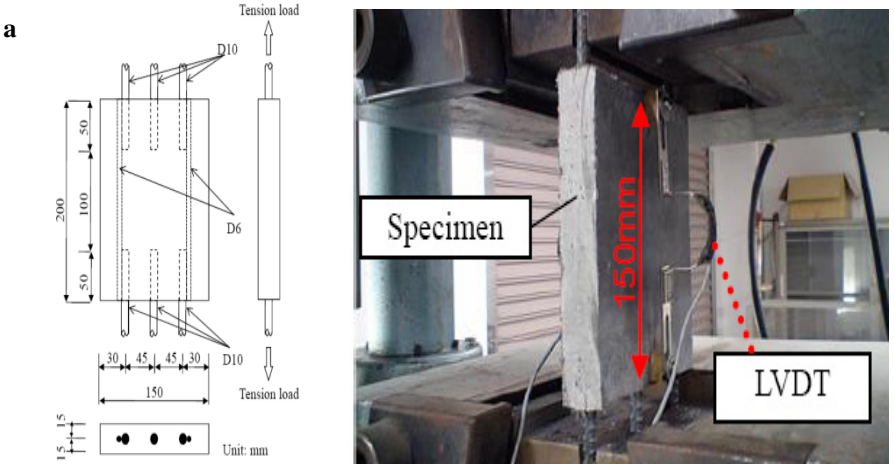


**Fig. 4.15** Shape of specimens used (a) and performance of uniaxial tensile test (b)

**Table 4.5** Types of specimens

| Series | Fiber volume | Unloading strain (%) | Re-curing condition |
|---|---|---|---|
| 1.25-0W | Vf=1.25% | 0 | Water |
| 1.25-0A | | | Air |
| 1.25-0.1W | | 0.1 | Water |
| 1.25-0.1A | | | Air |
| 1.25-0.2W | | 0.2 | Water |
| 1.25-0.2A | | | Air |
| 1.25EX-0W | Vf=1.25% +EX | 0 | Water |
| 1.25EX-0A | | | Air |
| 1.25EX-0.1W | | 0.1 | Water |
| 1.25EX-0.1A | | | Air |
| 1.25EX-0.2W | | 0.2 | Water |
| 1.25EX-0.2A | | | Air |
| 1.5-0W | Vf=1.5% | 0 | Water |
| 1.5-0A | | | Air |
| 1.5-0.1W | | 0.1 | Water |
| 1.5-0.1A | | | Air |
| 1.5-0.2W | | 0.2 | Water |
| 1.5-0.2A | | | Air |

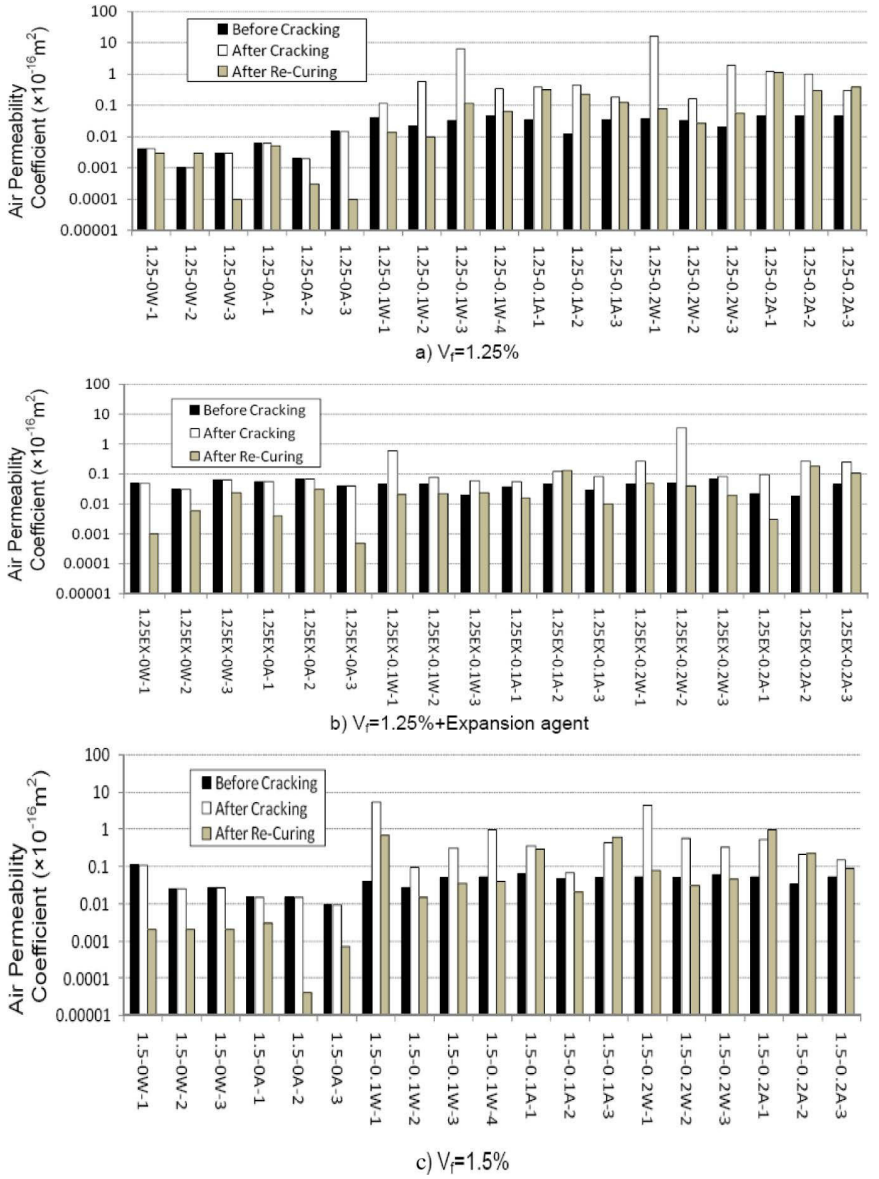


**Fig. 4.16** Recovery of air permeability coefficient for specimens containing 1.25% (without (a) and with (b) expansion agent) and 1.5% fibers (c)

In control specimens, air permeability coefficients became smaller with increase of time (Fig. 4.16). The authors [4.28] supposed that this decrease was due to densification of the matrix with increase of age. Air permeability coefficients of cracked specimens became dramatically larger just after loading. After re-curing, however, the air permeability coefficients of all cracked specimens, especially cured in water, became smaller. Regarding the different curing conditions, a difference in air permeability was observed. Curing in water was more effective for self-healing, compared to air-curing. When the results, obtained from the water permeability tests were examined (results not shown), the same conclusions were drawn. The authors stated that the main cause for recovery of the resistance against air and water permeability is both; densification of the matrix in UHP-SHCC and formation of re-hydration products along the induced cracks. Besides, the effect of the added expansion agent was not significant in this test.

### *4.1.4 Experimental Evidence in Early-Age Concrete*

Tests on early-age concrete have been performed at Delft University of Technology [4.29-4.31]. In the experiments several parameters are varied. The parameters that are discussed in this chapter are:

- the amount of compressive force applied during healing. The variation of this parameter is 0.0, 0.5, 1.0 and 2.0 MPa.
- the type of cement in the concrete mix, both a Blast Furnace Slag Cement (BFSC) and an Ordinary Portland Cement (OPC) is tested.
- the moment of creating the first crack in the specimen through a controlled 3-point bending test. The cracks are made at an age of 20, 27.5 (further named 1 day), 48 and 72 hours. The age at loading has some variation, since the specimens are cast at the same time, but for testing only one machine is available. Each test, including preparation, takes about 45 minutes.
- the crack (mouth) opening of the crack. Initial crack openings of 20, 50, 100 and 150 μm are discussed in this chapter.
- the influence of the Relative Humidity (RH) during healing. Specimens are stored under water and in a climate chamber with 95% and 60 % RH respectively.

In all cases only one parameter is varied at any one time. The default parameters in the tests are 1.0 MPa compressive stress, concrete made with BFSC, crack made at age of 1 day, crack opening of 50 μm and healing under water. All the tests are performed at least three times. In Table 4.6 the mix composition of the concrete is given. Where the concrete mix is changed the CEM III (BFSC) is replaced by the same amount of CEM I 52.5 R (OPC).

**Table 4.6** Mixture composition of self-healing concrete specimens

| Component | Type | Amount kg/m$^3$ |
|---|---|---|
| Cement | CEM III/b 42,5 LH HS | 375 |
| Water | | 187.5 |
| River gravel | 8 - 4 mm | 540 |
| | 2 - 4 mm | 363 |
| | 1 - 2 mm | 272 |
| | 0.5 - 1 mm | 272 |
| | 0.25 - 0.5 mm | 234 |
| | 0.125 - 0.25 mm | 127 |

The healing process took place either in a stress-free state or with an applied compressive stress. In the latter case the specimen is placed in a compression loading device which applies a compressive force to close the crack. This force is measured by means of the deformation of a calibrated steel spring. The amount of compressive force is varied in the tests. In Fig. 4.17 the compressive loading devices are shown with specimens subjected to 0.5, 1 and 2 MPa compressive stresses. The specimens are then stored for a specific period at a certain temperature and relative humidity (or under water) to undergo crack healing. In addition to healing of the crack the concrete will also undergo further hydration. This means that the mechanical properties of the material itself will also improve.

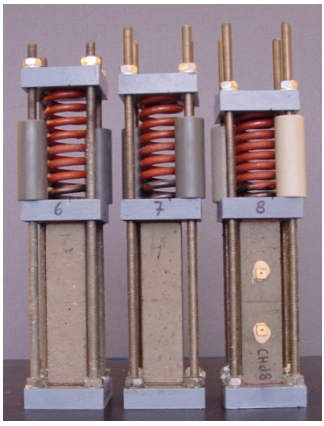


**Fig. 4.17** Compressive loading devices

A question which emanates from this work is whether the crack has the same length in a specimen tested at an age of 1 day as at 2 weeks, when in both cases the crack opening has reached a value of 50 µm. To be able to answer this, the

specimens have been vacuum impregnated with a fluorescence epoxy after the test. The cracks are then visualized under UV-light. The scatter in the crack length that is observed is rather large, but it turned out that in all the situations at a crack width of 50 µm, the crack tip had reached about half way up the height of the specimen.

The following figures show some results. The healing effect is expressed in terms of recovered bending strength and stiffness.

In Fig. 4.18 the flexural stress is plotted versus displacement for the reloading test after 2 weeks healing for a specimen with (1 MPa) and without (0 MPa) applied compressive stress. Furthermore, the graph is shown of the specimen without healing. The latter is obtained after reloading a specimen tested at an age of 2 weeks. The graph shows that when the crack is not closed (the compressive stress is 0 N/mm$^2$) the recovery of strength is minor. The same observations were done recently for similar tests on HPC [4.26]. However, with a compressive stress of 1 MPa both the stiffness and the strength of the specimen are recovered and show values close to the reference specimen.

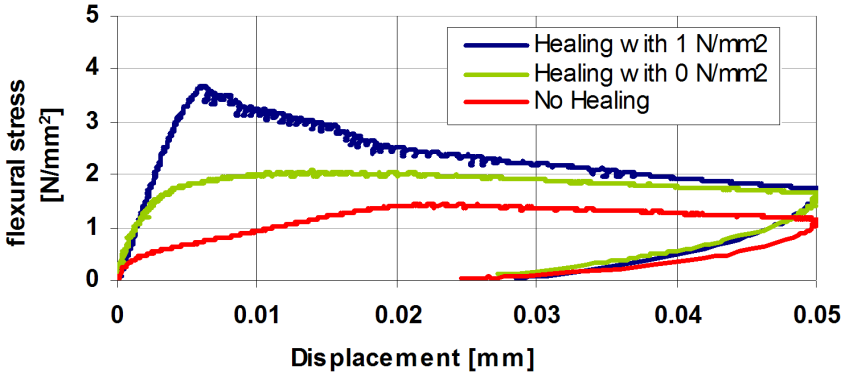


**Fig. 4.18** Bending stress vs. displacement diagram of specimens with and without healing [4.31]

Fig. 4.19 gives the relative strength of the specimen after healing for different amounts of compressive stress applied during healing. The relative strength is given as a percentage of the strength of the un-cracked virgin specimen tested at an age of 2 weeks (see Fig. 4.19, peak in first loading part). In the figure a line is also shown (with vertical bars showing the scatter) which represents the strength of the material of the unhealed specimen. The figure shows clearly that almost no increase in strength is obtained when the specimen is not loaded in compression (0 N/mm$^2$). Furthermore, it can be seen that when compressive loading is applied to close the crack, the amount of compressive stress does not significantly influence the strength gain.

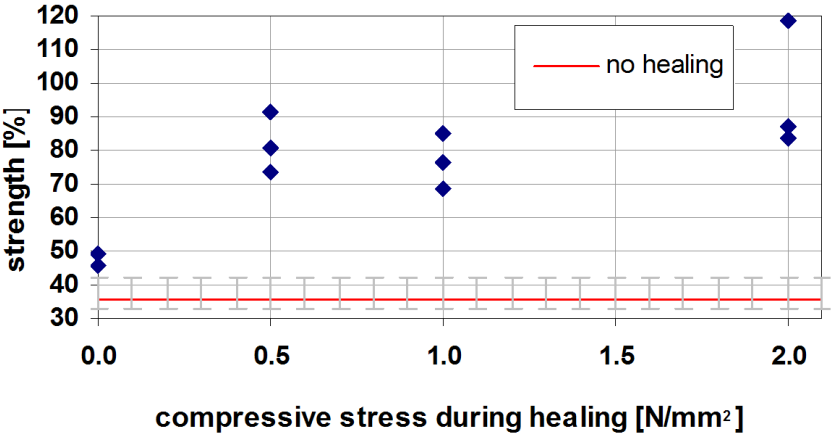


**Fig. 4.19** Relative strength of specimens after healing

(a)

(b)

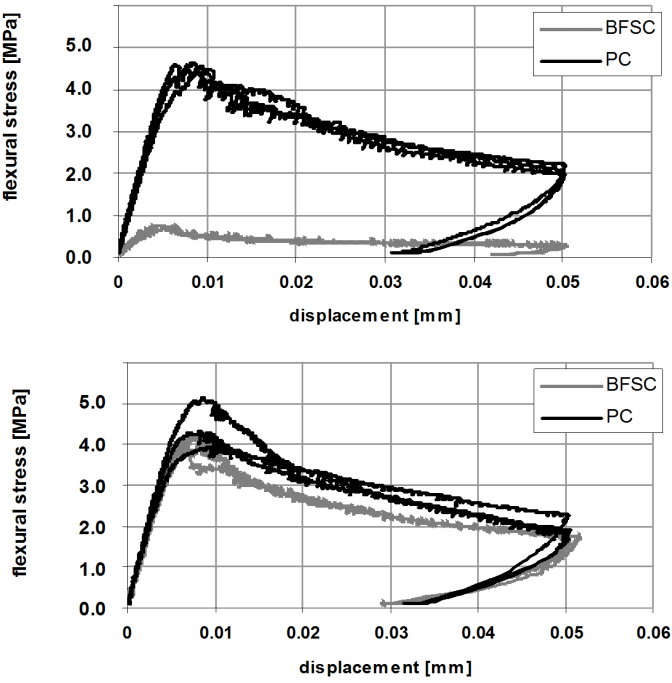


**Fig. 4.20** Flexural stress versus crack opening for tests (a) after 1 day and (b) after healing with compression for BFSC and PC concrete

The influence of the cement type in the concrete mix is presented in Fig. 4.20 and Fig. 4.21. In Fig. 4.20a the flexural stress is plotted versus the crack opening displacement for the test performed on a 1 day old specimen. It can be seen that the specimens containing the faster reacting PC have a much higher strength. The

concrete with PC is further matured. In Fig. 4.20b the result is plotted for the tests after healing on both materials. Now the strength for both materials is almost equal. Also, for the specimen tested for the first time after 15 days (Fig. 4.21a) it can be seen that the strength of both materials is almost equal. Fig. 4.21b gives the plots for the reloading test, which represents the strength of the unhealed specimens. From these tests it is clear that in the BFSC-concrete the strength gain after 1 day is minimal. Healing of the crack can then take place more readily because there is still a large amount of hydration of the cement which has not yet taken place. However, in the PC-concrete the result that is obtained is remarkable, since here also the strength is almost fully recovered. Probably this concrete has after hydration a large amount of unhydrated cement left. Thus, the potential for early-age crack healing is much higher in PC-concrete.

(a)

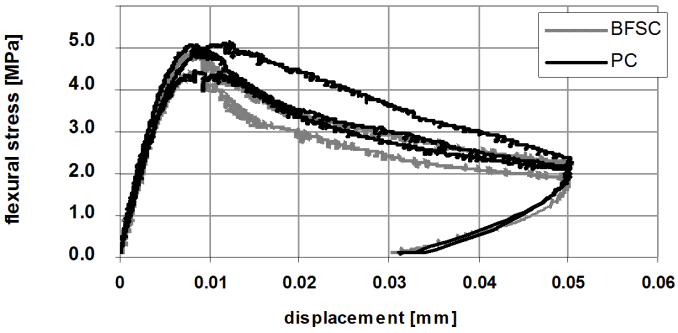


(b)

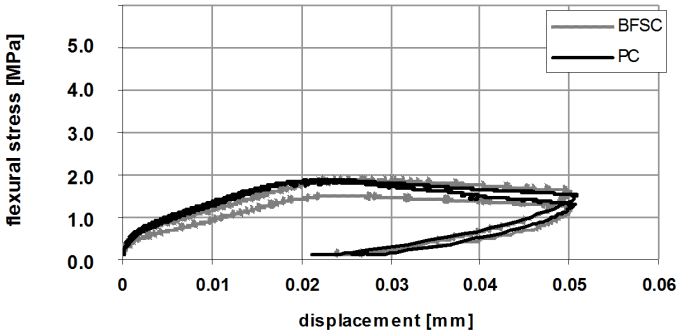


**Fig. 4.21** Flexural stress versus crack opening for reference during first test (a) and reloading after 15 days (b) for BFSC and PC concrete

The third parameter that is investigated is the moment of cracking or the age of the specimen when the first crack is produced. In Fig. 4.22 the stress-displacement curves are shown for specimens at different ages when the first crack was introduced. In these tests the crack is opened up to a crack mouth opening of 50 μm. Subsequently, the specimens are loaded in compression with a compressive

stress of 1 MPa and stored under water for 2 weeks. The strength after healing (relative to the strength of the virgin specimen) is plotted in Fig. 4.22 for the various ages at which the first crack is made. The reference test for each series is always performed at the same age. So this means that for instance the strength of the specimen tested for the first time at 72 hours and subsequently healed for 2 weeks is compared with the strength of a specimen loaded for the first time at an age of 17 days. The difference in strength of the virgin material between the ages of 14 and 17 days is, however, very small. A clear decrease in strength recovery is observed with increasing age of the specimen when the first crack is made.

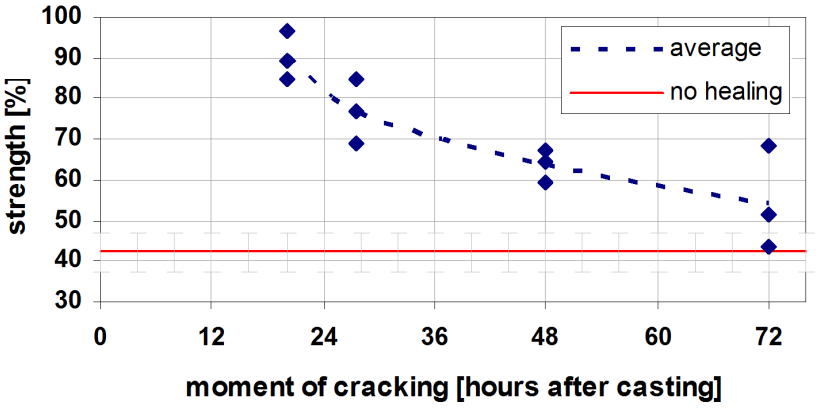


**Fig. 4.22** Influence of age at pre-cracking on recovered bending strength [4.31]. Compressive stress 1 MPa, storage 2 weeks.

The fourth parameter discussed in this section is the influence of the width of the crack that is made in the specimen on the strength recovery. In these tests the specimens are loaded at an age of 1 day and the compressive stress during healing is equal to 1.0 MPa. A larger crack mouth opening will result in a longer crack which has propagated further into the specimen. The load that can be carried at a larger crack opening will be smaller. The results show a significant amount of scatter, but there seems to be no influence of crack opening on the strength recovery after healing.

The last parameter studied is the influence of the relative humidity on crack healing. It turned out that only for the case when the specimens were stored under water during the healing period, recovery of strength was possible. For the cases when the specimens were stored in an environment of 95% or 60% RH almost no increase in strength was observed. For the case of 95% RH the specimens were even stored for a period of 3 months, however, even under these conditions no crack healing was observed.

From the experimental results it can be concluded that:

- Cracks do heal when the conditions are such that the cracks are made at an early age and the cracks are closed again (a compressive stress is applied) and the specimens are stored under water.
- The amount of compressive stress does not seem to influence the strength recovery. The results indicate that a compressive stress is needed to close the crack, but once the two crack faces touch each other again, or the distance between the crack faces is small enough, crack healing can occur.
- Both for concrete made with BFSC and OPC crack healing takes place. Most probably in the case of OPC there is a lot of unhydrated cement left in the crack. Storing the specimens in water probably opens the way to further hydrate this cement in the crack. In the bulk material water cannot reach these unhydrated particles. This means that concrete with OPC probably has additional capacity for crack healing at a later stage when compared to BFSC-concrete.
- With increasing age of the specimen at the moment the first crack is made, a decrease in strength recovery is found. The age of the specimen when the first crack is made indicates the degree of hydration that has already occurred. The amount of hydration that can still take place is therefore fixed. The amount of potential strength recovery is therefore limited when the concrete has already reached a high degree of hydration when the crack is made.
- The width of the crack does not seem to influence the strength recovery due to healing. The tests with different crack mouth openings all show similar amounts of strength recovery.
- Crack healing is only observed when the cracked specimens are stored under water.

Ter Heide and Schlangen believe that ongoing hydration is the mechanism for crack healing that leads to the strength recovery in this investigation. This mechanism only works when the crack is closed again. It has been shown that crack healing does take place when enough humidity is present. The simulations that have been performed strengthen this hypothesis. It has been shown through simulation that the increase in strength in the crack due to further hydration could be sufficient to explain the observed recovery in flexural strength found in the experiments. The simulations also showed that higher strengths can be obtained in the crack compared to the bulk material when it is assumed that due to the water in the crack the final degree of hydration is reached faster in this zone.

For the practical situation of early age surface cracks in (massive) concrete structures, which are a concern from a durability point of view, this investigation shows some promising results. It indicates that these surface cracks can disappear again, at least under the right conditions as discussed above.

### 4.1.5 Self-Healing in Self-Compacting Concrete

Self-compacting concrete (SCC) has almost the same composition as conventional compacted concrete, however, due to adjustment of the aggregate content, especially the fine part, and the addition of chemicals and mineral admixtures, a concrete type is obtained which doesn't need to be compacted. One of the main advantages of using SCC is the reduction in construction time, however, this may result in situations where the concrete is subjected to early overloading. Therefore, Abdel-Jawad and Dehn [4.32] decided to investigate the ability of self-healing in self-compacting concrete.

Concrete specimens (100 mm x 100 mm x 100 mm) from three self-compacting concrete mixes with different water to cement ratios (0.45, 0.5 and 0.55) were prepared and loaded to different stress levels, namely; 40%, 60% and 80% of its maximum strength at the ages of 1 day and 3 days. These specimens were wet-cured in companion with control specimens up to the age of 28 days. At 28 days, the previously loaded specimens, along with the control specimens, were tested by measuring the compressive strength and the ultrasonic pulse velocity through the specimens in the direction perpendicular to the loading direction.

Fig. 4.23 a and b present the compressive strength obtained at 28 days for previously loaded specimens at stress levels of 40%, 60% and 80% of their obtained strength at the age of 1 day and 3 days, respectively. The compressive strength of the control specimens (not subjected to previous loading) is shown along. It is obvious that the previously loaded specimens achieved almost the same strength as that of the control specimens, especially for the 0.45 w/c ratio concrete. The same conclusion can be stated for the specimens preloaded at the age of one day, or at the age of three days.

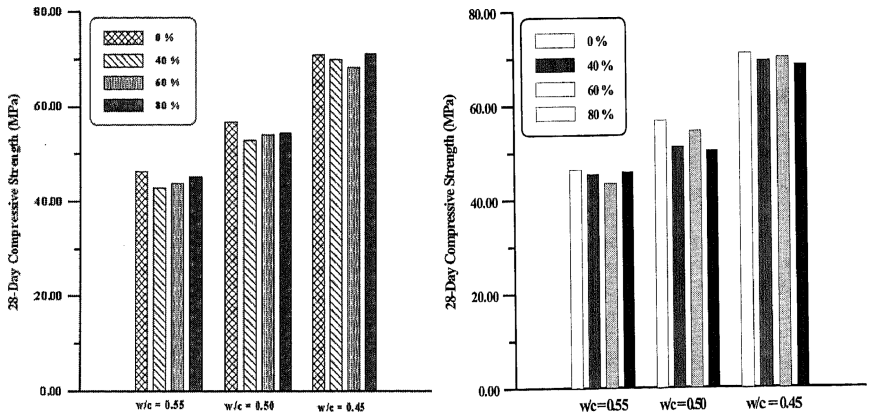


**Fig. 4.23** Compressive strength at 28 days for previously loaded specimens at the age of one day (a) and three days (b) [4.32]

It is well known that the velocity of ultrasonic pulses through any solid material is affected by the existence of cracks in the material. Abdel-Jawad and Dehn [4.32] employed this technique to evaluate the potential of crack healing. From Fig. 4.24 it is seen that the ultrasonic pulse velocity of the previously loaded specimens is the same or even sometimes higher than that obtained for the control specimens. This means that all the cracks produced due to the earlier loading have been healed as a result of the subsequent hydration of the cement, as the concrete was cured in water up to 28 days. The same behaviour was obtained when analyzing the date for the concretes exposed to the different loading levels at the age of three days (data not shown).

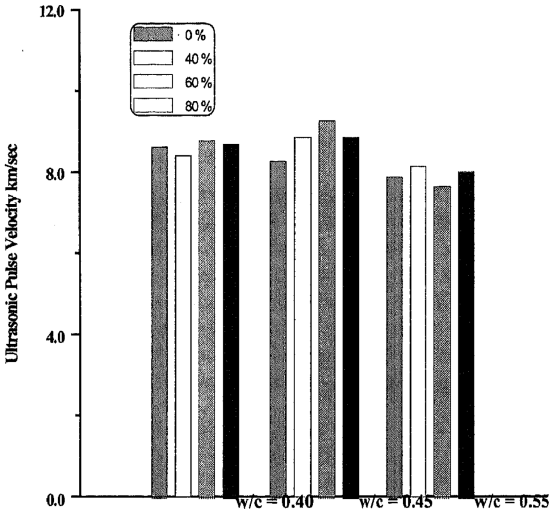


**Fig. 4.24** Ultrasonic pulse velocity at 28-days for previously loaded specimens at the age of one day [4.32]

## 4.2 Autonomic Self-Healing

Autonomic self-healing has been defined in chapter 1 as a self-healing process where the the recovery process uses materials components that would otherwise not be found in the material (engineered additions).

### *4.2.1 Autonomic Crack Closure*

Studies on crack healing of cementitious materials have shown that the degree of healing is a function of crack opening, with little likelihood of healing in cracks wider than 0.1 mm. [4.5]. Furthermore, it has been demonstrated that autogenic crack healing is significantly enhanced if a crack is subjected to compression. [4.30].

In the approach suggested by Sakai *et al.* [4.33] and Kuang and Ou [4.34, 4.35], cracks develop until normal width but at the time of unloading, cracks are closed due to the super elastic behaviour of embedded shape memory alloys (SMA). In addition, SMA exhibit a shape memory effect, where upon the system of the research group of Cardiff University is relying [4.36-4.40]. This research group tries to develop a cementitious material system in which shrinkable polymer tendons are activated by heating so as to generate a low level of pre-stress capable of autonomic crack closure and thus enhancing autogenic self-healing. Details of this system (Fig. 4.25), have been discussed by Lark *et al.* [4.41] and Jefferson *et al.* [4.42] and a recent experimental study has sought to identify what the combined activation method and curing regime should be to maximize the degree of autogenic self-healing [4.43].

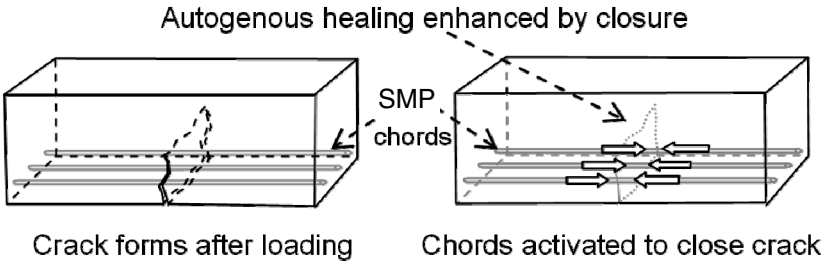


**Fig. 4.25** Schematic illustration of autogenic crack healing enhanced by autonomic crack closure [4.36].

In this study small scale hollow prismatic mortar beams that were tested in a series of 3-point bending experiments were used. Fig. 4.26 illustrates the specimen configuration.

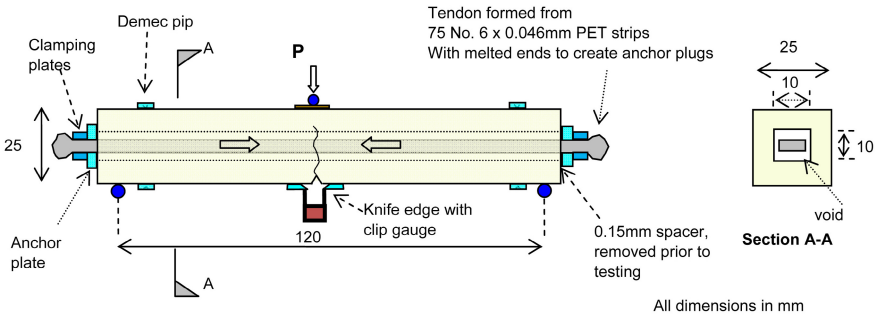


**Fig. 4.26** Specimen configuration [4.36]

All mortar specimens were cast using a water:cement:sand mix ratio of 0.6 : 1 : 3 by weight. The cement used was ordinary Portland-fly ash cement, designation CEM II/V-V32.5 R, and the sand was 0/4 mm, EN12610 compliant sea dredged

sand. Prior to mixing, the sand particles were passed through a 1 mm sieve to give a maximum aggregate size of 1 mm.

To ensure that the polymer tendons did not bond with the cementitious matrix, the specimens were manufactured as hollow beams. The hollow void through the specimens was produced by inserting polystyrene rectangular formers prior to casting. The polystyrene rectangular formers were removed on day 3 and a central 3mm notch was cut, as shown in Fig. 4.26, to predetermine the location of the crack.

The shrinkable polymer tendons comprised 75 individual Polyethylene terephthalate (PET) strips, each measuring 6 mm x 0.046 mm. The tendons had a cross-sectional area of approximately 4% of the un-notched specimen. The ends of the tendons were bonded together using a soldering iron and were inserted into the hollow voids of the specimens. An end plate and clamp system were securely attached to one end of the tendon to act as an anchorage. The specimens were then held vertically with the tightened clamp end at the top so that a 1 kg weight could be hung from the clamp to be attached at the bottom end of the tendon and a 0.15 mm spacer inserted between the beam and the end plate. With the spacer in place, the lower clamping system was securely tightened. The spacers were removed prior to testing, their thickness having been calculated so that the tendons would not provide any pre-stress to the specimens prior to heat activation. This ensured that the tendons remained completely loose within the specimens during stage 1 testing.

**Table 4.7** Stages of experimental procedure

| Stage | Description |
|---|---|
| 1 | Casting (day 1) |
| | Curing under sealed conditions (days 1 to 4) |
| | Initial cracking at day 4 |
| 2 | (a) heat activation (Starting on day 4 for 18 hours) |
| | (b) 'healing' (for 48 hours) |
| 3 | Loading to failure at day 8 |

N.B. The curing regime during the 'healing' phase is referred to as the healing regime.

The experimental procedure was divided into three stages as shown in Table 4.7.

In stage 1, specimens were loaded under 3-point bending at a rate of 0.001 mm/s to a crack mouth opening displacement (CMOD) of 0.30 mm and then unloaded. This CMOD was measured by a light crack mouth opening displacement gauge ($CMOD_{CG}$), which was inserted between two knife edges that

were glued either side of the notch on the underside of the specimens. Load was controlled via feedback from a linear variable displacement transducer (LVDT) which measured the displacement of the loading platen, as illustrated in Fig. 4.27.

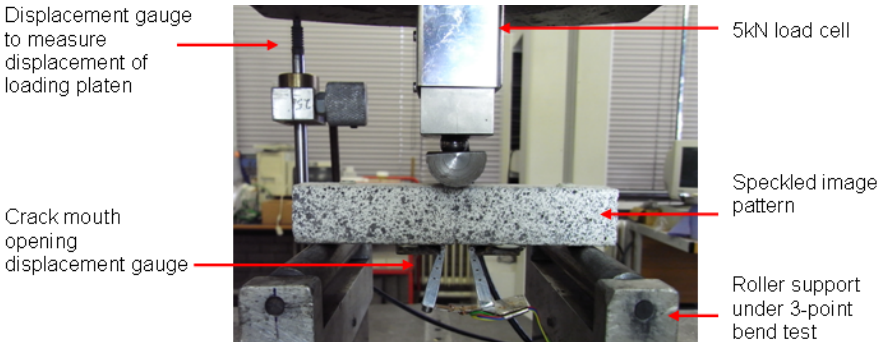


**Fig. 4.27** Three-point bend test setup [4.43]

In stage 2a, the specimens were subjected to heat treatment at 90°C for 18 hours in order to activate the polymer tendons. This generated a pre-stress in the specimens of which was anticipated that it would close the crack formed in stage 1. Then, in stage 2b, the specimens were self-healed for a further 48 hours. At the end of this 'healing' stage (2b), the specimens were tested to failure in stage 3 in order to identify the success of the tendons in closing the pre-formed crack and to examine whether any autogenic self-healing had taken place. Three activation-healing (AH) regimes were investigated for stages 2a and 2b as shown in Table 4.8.

Twelve 145 mm x 25 mm x 25 mm specimens were cast for each of the procedures. For each procedure, the twelve specimens were divided into four groups of three beams. Three of the beams had the polymer tendon left inside the beam for all stages (PET specimens); three of the beams had the tendon left in place for stages 1 and 2, but removed before stage 3, (PETr specimens) and six control beams were tested to failure with no tendons, three of which were tested at stage 1 (Ctrl1 specimens) and three tested at stage 3 (Ctrl2 specimens). Material tests were also carried out using six small scale 25 mm x 25 mm x 25 mm cubes to determine the compressive strength and six 160 mm x 40 mm x 40 mm prismatic mortar beams, three of which were used for fracture energy tests and three for elastic modulus tests.

**Table 4.8** Heat activation methods and healing regimes

| AH regime | Heat activation method | | | Healing regime | |
|---|---|---|---|---|---|
| | Description | Temp. (°C) | Time (Hrs) | Description | Time (Hrs) |
| 1 | Dry heat activation | 90 | 18 | Cured in water at ambient temperature | 48 |
| 2 | Steam heat activation | 90* | 18 | Specimens left in the steam chamber with the steam production turned off and the chamber allowed to return to ambient conditions | 48 |
| 3 | Water heat activation | 90 | 18 | Specimens left in the water tank with the temperature allowed to return to ambient conditions | 48 |

N.B. *the atmospheric temperature was measured at 90 °C and the water in the tank was heated to 100 °C in order to produce steam conditions

One side face of each specimen was sprayed with a black and white speckled pattern to enable Digital Image Correlation (DIC) [4.44] to be used to monitor the displacements of the specimen. Two cameras were set up that tracked the speckled pattern every 5 seconds throughout the test enabling displacements and strains to be measured in 2D. The selection of two points either side of the notch allowed a second measurement of the CMOD which is denoted $CMOD_{DIC}$ and applies to a level 1.75mm above the lower surface of the specimens.

The results of this work are to be published in a paper by Isaacs *et al.* [4.43, 4.44] and from this work it was concluded that crack closure and autogenic self-healing can be achieved on small scale hollow prismatic mortar beams post tensioned with shrinkable polymer tendons. It was demonstrated that autonomic self-closure was achieved as a result of the shrinkage stress developed by the activated tendons and in two of the regimes adopted for activating and healing the specimens it was clear that effective autogenic self-healing had been achieved, i.e.:

- Dry heat activation and water based healing (AH1)
- Steam activation and healing (AH2)

In the former, the initial mechanical stiffness was recovered and strength recoveries of approximately 80 % (PETr) and 125 % (PET) were achieved. In the latter, the initial mechanical stiffness was again recovered and load recoveries of approximately 80 % (PETr) and 200 % (PET) were achieved. It was concluded that both dry heat activation followed by water curing, and steam activation and curing are both effective heating/healing regimes, with the latter providing the highest prestress force.

Only 16% of the initial strength was recovered in specimens activated and healed in water at 90 °C although the regime did activate the tendons and produced sufficient prestress to achieve autonomic self-closure. It is possible that the reduced level of autogenic self-healing in this case was related to the formation of bubbles in the crack which may have impeded the healing process but this requires further investigation.

## *4.2.2 Tubular Encapsulation of Liquid Healing Agents*

### 4.2.2.1 Mechanical Activation

*4.2.2.1.1 Internal Supply of Healing Agent*

Carolyn Dry [4.45-4.47] already proposed the use of encapsulated liquid healing agents to repair cracks in concrete autonomously, in the early 1990's. In her experiments she used hollow brittle glass fibers which contained air-curing cyanoacrylate as healing agent. Cement prisms contained 2 metal reinforcing fibers and 16 adhesive filled 150 ml glass pipettes which were embedded inside the matrix. A second set of samples had the same composition lacking the adhesive. A schematic representation of the sample setup is shown in Fig. 4.28.

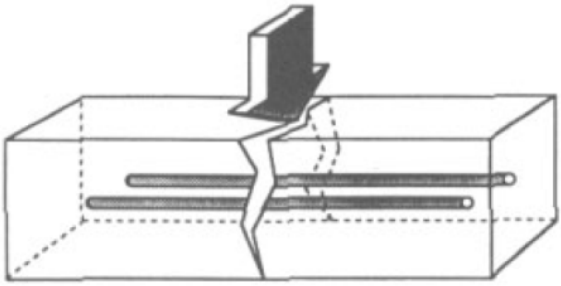

**Fig. 4.28** Timed release of chemicals occurs when the brittle fiber breaks under load [4.46]

Each sample was loaded in three-point-bending, causing the repair fibers to break and release their chemicals into the cement matrix. Auditory confirmation of glass pipette breakage was accomplished. After two weeks of drying of the repair agent, the samples were reloaded in three-point bending. Fig. 4.29 represents a record of the load displacement for those two loading events on the samples.

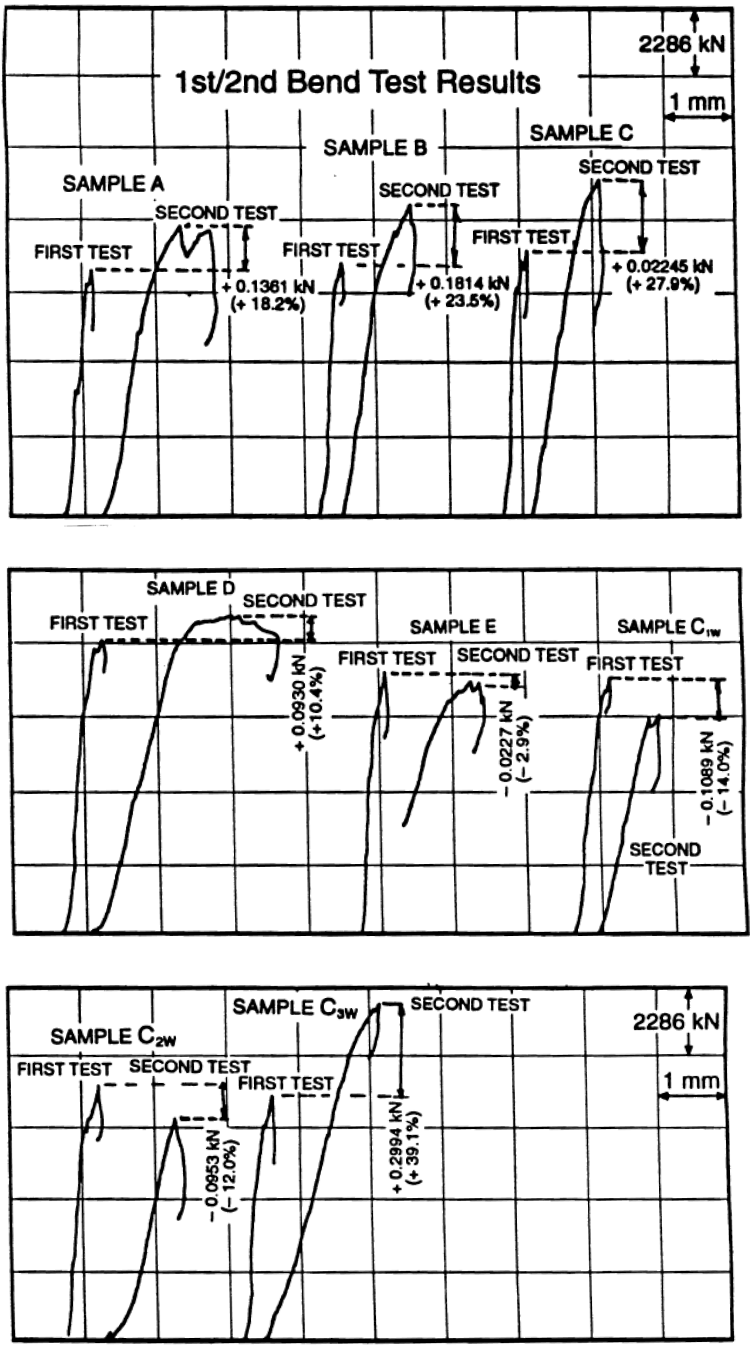


**Fig. 4.29** Load displacement diagram obtained for different test series during first and the second 3-point bending test [4.47, 4.48]

A comparison of the records obtained during the first loading in flexure (before release of the chemical) and the second bend test loading (after release of the adhesive into the matrix) revealed several important facts. Most of the adhesive-loaded samples carried more of the load on the second bend than on the first bend, while in general, that was not the case for the controls. The inference made from this is that the crack opening displacement curve for the controls follows the normal reduction in load resistance, while the adhesive filled samples reverse it, in that crack opening displacement is reduced with the next loading and the fitted samples carry more load in the second test than controls. Also ductility as measured by deflection was improved for the samples containing released adhesive.

In a second series of experiments, Carolyn Dry [4.45] investigated the possible rebonding of fibers after debonding of the fibers occurred. In order to test this, mortar samples were made, containing adhesive filled glass pipettes proximate to a metal fiber and a second set of samples containing pipettes with no adhesive. In each of these samples, the metal fiber was pulled in tension until debonding occurred. The load displacement curve revealed a debond release typical of a bond with a brittle material in all cases (Fig. 4.30). The samples were then loaded under three-point bending in order to break the adhesive filled glass pipettes. After two weeks of curing, the metal wire was pulled again. The load displacement curve for the samples with adhesive revealed a bond release that was typical of an elastic-bonded material, while the samples without adhesives exhibited no rebonding to release. The authors concluded that these results were positive and suggested that fibers could be rebonded with adhesive released upon loading.

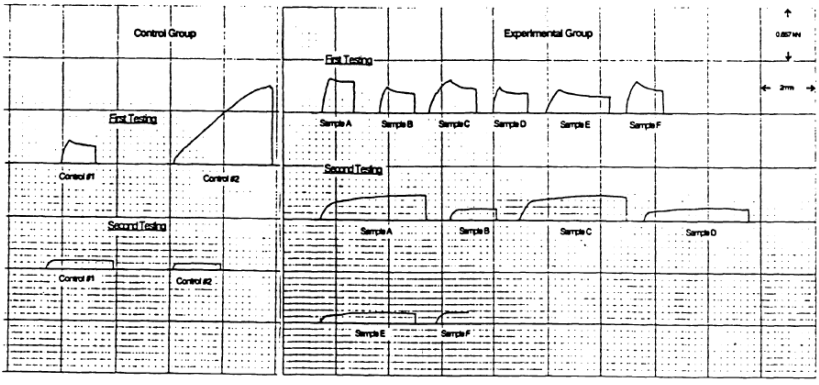


**Fig. 4.30** Comparison of load displacement diagrams for control versus experimental group during first and second pull of metal fibers [4.45]

Tran Diep Phuoc Thao *et al.* [4.49, 4.50] proposed the use of an air-curing epoxy resin as healing agent. Perspex tubes and glass tubes were tested as possible encapsulation materials. It was found that Perspex tubes showed visible cracks on

the surface due to a chemical reaction between the healing agent and the tubes. As Perspex tubes are stronger and more ductile in comparison with glass tubes, the rupture of the tubes would be delayed and therefore glass tubes were chosen as encapsulation material. Tubes with an inner diameter of 4 mm and a length of 250 mm were used in the experiments as this size seemed most suitable according to the preliminary tests.

Concrete specimens 300 mm x 80 mm x 50 mm were cast using a mortar mix of 0.8:1:1 (water, cement, sand). In each beam two glass tubes were embedded. The tubes were filled with epoxy (POR-15) and aquastick was used to seal both ends. The tubes were placed at 10 mm from the bottom of the specimen whereas the steel wire mesh (ø1.3 mm) was placed at 20 mm from the bottom of the specimens. A similar set of specimens but without glass tubes was cast to serve as control specimens. All specimens were compacted using a vibrating table, demoulded after 24 hours and air-cured for 3 days before test were carried out (Fig. 4.31).

Specimens were subjected to a 3-point bending test. The control specimens were loaded till failure, in order to determine the load displacement curve. Each specimen with self-healing properties was tested beyond the point where an audible 'pop' sound was heard, which indicated fracturing of the glass tubes. The load was held until leakage of epoxy was observed on the bottom surface of the specimen. The specimen was then unloaded and left unloaded for 4 days before being loaded again. The second test was terminated soon after more leakage of epoxy was observed. The load was then removed and the specimen was left to heal again for 3 days before being loaded again and tested to failure in the third loading test.

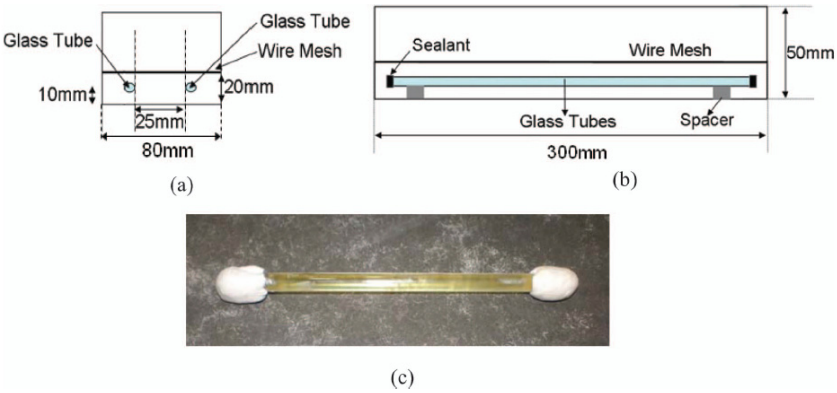


**Fig. 4.31** Self-healing system, (a) front elevation, (b) side view, (c) epoxy filled glass tube with aquastick as sealant [4.49]

The presence of the self-healing system decreased the overall elastic modulus of the beam as the epoxy filled glass tubes were less stiff than the concrete that was replaced. During the first loading cycle, the strength of the beam with

self-healing properties, represented by the first peak at a load of 2.23 kN, was similar to the strength of the control beam (see Fig. 4.32). A second peak was observed which was caused by breakage of the glass tubes, typically occurring within 10 seconds after the crack in the mortar beam was initiated. Once the tubes were broken, gravity and capillary forces acted as the driving force for the epoxy to flow towards the gaps formed by the crack.

During the second loading cycle, an initial peak of 1.44 kN was noticed, which corresponded to the initiation of a second crack. However, the specimens could be further loaded up to a higher load of 2.31 kN. The newly formed crack initiated from a point at the bottom surface of the beam that was very close to the first crack and they bridged together when the second crack propagated further into the specimen. From these findings the authors suggested that the first crack had been partially healed. The epoxy in the vicinity of the crack mouth cured fully having been in contact with air for four days. However, in regions close to the crack tip, which is depleted of air for curing, curing may not have completed with some epoxy still in its liquid state. This weak zone attracted nearby propagating cracks. Next, the smaller damage initiation load of 1.44 kN may be due to softening of the beam caused by the formation of micro cracks in the vicinity of the first crack zone during the first loading, Although, the specimens were partially healed after three days, the recovered strength equaled the strength of the control specimen.

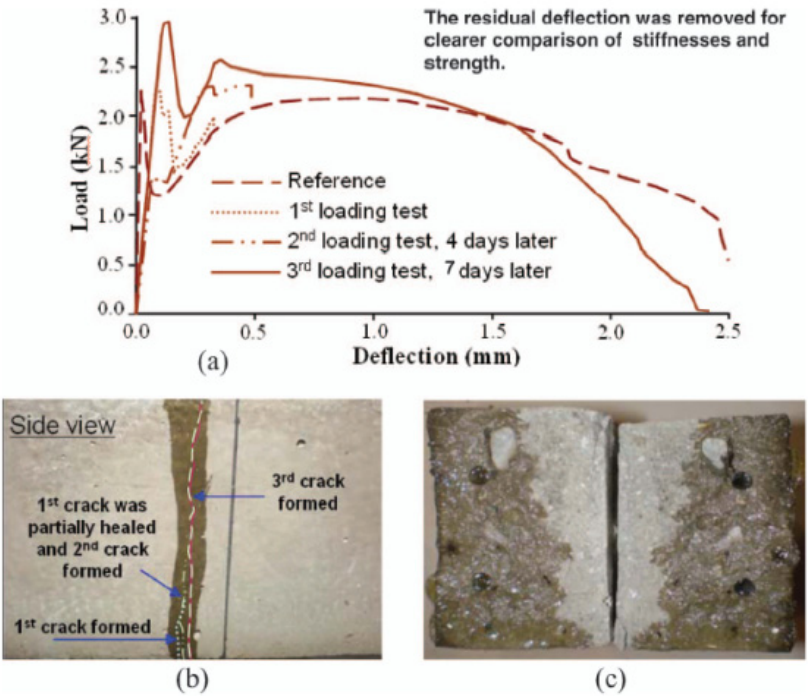


**Fig. 4.32** Experimental results of self-healed specimen, (a) load-deflection curve, (b) order of crack formation, and (c) dissected specimen after healing thrice [4.49]

During the third loading cycle, a new crack was formed but this time it did not merge with the previous crack suggesting that the damage has been fully healed. As cracking only starts from the weakest point in a specimen, complete healing strengthened this zone and it is not surprising that a new crack initiated at a location corresponding to the next weakest zone in the specimen. This is confirmed by the result of the experiment showing the strength of the specimen has increased to 2.95 kN, which is 32% higher than that of the reference specimen.

In their later research, Pang *et al.* [4.51] embedded their encapsulated healing agent inside bigger sized structural concrete members namely a beam (125 mm x 200 mm x 2000 mm, Fig. 4.33a), a column (Ø 200 mm x 800 mm, Fig. 4.33b) and a slab (100 mm x 1000 mm x 1000 mm, Fig. 4.33c). Here, the glass tubes were coiled with spiral wire followed by a 3.5 mm thick mortar layer to protect them from premature damage during casting. The self-healing efficiency was qualified as the stiffness recovery of the members after repeated loading and unloading cycles.

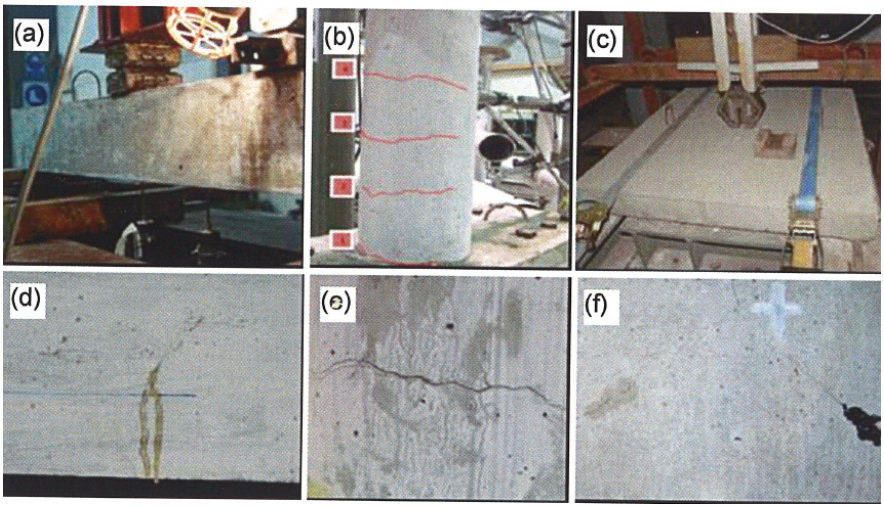


**Fig. 4.33** Evaluation of the self-healing efficiency of a beam (a), a column (b) and a slab (c). Self-healing of a crack inside a beam (d), a column (e) and a slab (f)

The beam element exhibited multiple crack healing capabilities with 84% of the initial flexural stiffness being recovered. The column element showed a stiffness recovery of up to 70%. This high healing efficiency was not expected as in this case, the crack planes developed in a direction normal to the direction of the gravity flow (Fig. 4.33b). The slab was assessed for its healing capability when subjected to multiple drop weight impacts. Again, multiple crack healing was observed, with the maximum healing efficiency, in terms of stiffness recovery, found to be 99%.

In both studies mentioned before one-component, air curing healing agents were used. Mostly, single-component agents are preferred above multi-component healing agents because incomplete mixing of the different compounds is feared. However, air-curing may be limited as limited air is available inside the crack. In the study of Tran Diep Phuoc Thao *et al.* [4.49, 4.50] it was already mentioned that incomplete curing of the agent inside the crack was noticed. Therefore, Carolyn Dry [4.52], proposed in her later research to make use of a multi-component healing agent. Multi-components agents have more stability than a single component adhesive because they are activated at a later date i.e. in situ. She proposed the use of methyl methacrylate (MMA) as healing agent. This agent consisted of three compounds: the MMA monomer, cumene hydroperoxide and cobalt neodecanoate, the latter two components being the initiator and activator, respectively. The cobalt neodecanoate solution and MMA solution were mixed together, being the first compound while the second compound was cumene hydroperoxide.

In previous experiments of Dry, glass tubes were used as delivery system [4.45, 4.46]. However, in this study she proposed the use of hollow tunnels which were coated with a brittle sealer [4.52]. In order to obtain these hollow tunnels, rounded steel rods were cast in concrete beam samples and pulled out after 24 hours of curing. They left small tunnels through the length of the samples. The inside of the tunnels was coated with a thin layer of Thompson's water seal and capped using brass pipe fittings set in the concrete at the ends of the beam. The larger tunnels were loaded with the cobalt/MMA solution while a single small tunnel was made and loaded with the cumene hydroperoxide initiator. The beam samples had a 1.8" triangular notch, set in the middle underside of the beam. The concrete beam samples were $15^{1/4}$" long, 3" deep and $2^{3/4}$" wide. The concrete was reinforced by three pair of 0.2 gauge piano wires (see Fig. 4.34).

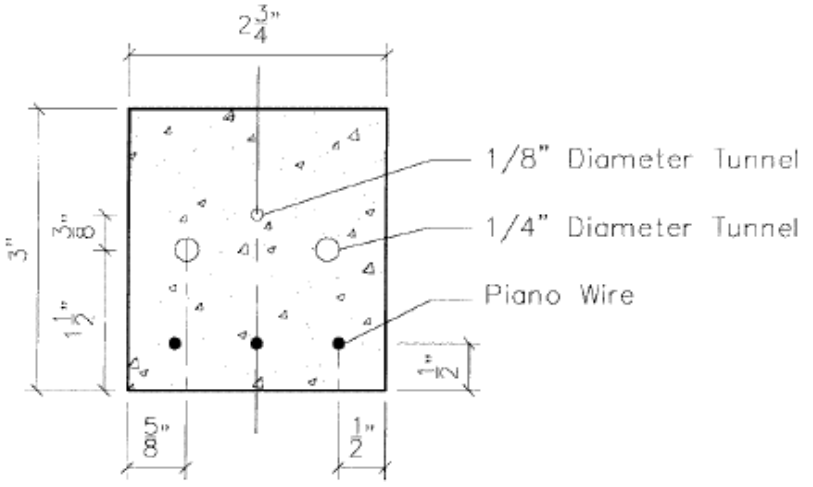


**Fig. 4.34** Beam sample section [4.52]

Cracks were created by performance of three-point bending tests. During the bending test, the two liquids leaked out into the cracks and entirely filled them with a solid plexiglass like matrix within 24 hours. When standardized for 0.5 mm of deflection, the adhesive repaired beams (1, 2 and 3 in Table 4.9) carried more load in the second test (+130%), while the two controls (C1 and C2 in Table 4.9) carried 117% and 65%. When standardized to 1 mm of deflection, the results show even more strength gain from the adhesive repaired specimens. This means that at specific points of deflection (0.5 mm and 1 mm) after failure, the beams proved to be more ductile and continued to resist more load in the second test. As shown in Table 4.10, the adhesive repaired samples had also greater deflection at failure (100%-800%), while the controls did not (-77% - 135%). The authors concluded that the MMA adhesive bond restored strength and made the beam more flexible.

**Table 4.9** Three-point bending strength test results when standardized to specific points of deflections [4.52]. Resistance (kN) given at points of deflection beyond failure.

| | 0.5 mm deflection | | | 1.0 mm deflection | | |
|---|---|---|---|---|---|---|
| Sample no. | Test 1 (kN) | Test 2 (kN) | Test 2 (%) | Test 1 (kN) | Test 2 (kN) | Test 2 (%) |
| 1 | 0.8 | 1.1 | 137.5 | 0.5 | 1.2 | 240 |
| 2 | 0.9 | 1.2 | 133.3 | 0.6 | 1.1 | 183.3 |
| 3 | 0.4 | 1.25 | 312.5 | 0.3 | 1.1 | 366.6 |
| C1 | 1.5 | 1.75 | 117 | 2.375 | 2 | 84 |
| C2 | 1.375 | 0.9 | 65 | 1.75 | 1.8 | 103 |

**Table 4.10** Three-point bending test deflection results [4.52]

| Sample no. | | First test (max. mm at failure) | Second test (max. mm at failure) |
|---|---|---|---|
| 1 | Test sample | 0.2 | 1.6 (+ 800% of first test) |
| 2 | Test sample | 0.25 | 0.025 (+ 100% of first test) |
| 3 | Test sample | 0.175 | 0.35 (+ 200% of first test) |
| C1 | Control sample | 0.35 | 0.27 (-77% of first test) |
| C2 | Control sample | 0.24 | 0.325 (+ 135% of first test) |

In their research, Van Tittelboom and De Belie [4.53, 4.54] compared the efficiency of different types of healing agents. Both, single-component and multi-component healing agents were tested on their suitability. Selection of the healing agents was based upon several requirements, such as: viscosity, reaction time, shelf life. In Table 4.11 an overview of the healing agents used and their most important properties is given.

Glass tubes with an internal diameter between 1 mm and 2 mm and a length ranging from 100 mm – 150 mm were used as encapsulation material. In case 2-component healing agents were used, 2 glass tubes were glued next to each other, so tubes with two compartments were obtained. One compartment was filled with the first component while the other compartment was filled with the second component. When a crack appears, both tubes break and both components flow into the crack. Upon contact of both components, the healing agent reacts inside the crack which is then healed. For 1-component, air-curing healing agents, singular tubes were used. Breakage of these tubes brings the healing agent into contact with the air inside the crack which causes hardening of the glue and crack repair.

**Table 4.11** Overview of the different types of healing agents used and of their most important properties [4.53]

| Healing agent | Type | Code | Number of compounds | Viscosity of most viscous compound at 20°C | Reaction time |
|---|---|---|---|---|---|
| | | | [-] | [cPs] | [sec] |
| Rite Lok EC5 | Cyanoacrylate | CA | 1 | 5 | 5 - 15 |
| Prime Rez 1100 HM | Epoxy | EP1 | 2 | 150 | 1.740 |
| Prime Rez 1200 LM | Epoxy | EP2 | 2 | 80 | 1.800 |
| Concresive EP 2055 | Epoxy | EP3 | 2 | 360 | 2.400 |
| Meyco MP 355 1K | Polyurethane | PUR1 | 2 (or 1) | 600 | 50 - 300(*) |
| Icema R 145/31 | Polyurethane | PUR2 | 1 | 7.200 | 2.400 - 10.800 |

(*) when 10% accelerator is added

Specimens with internal glass tubes were prepared as shown in Fig. 4.35. When the mortar matrix had hardened, the prisms were cracked, and thus the healing mechanism was triggered, by means of a crack width controlled three-point-bending test.

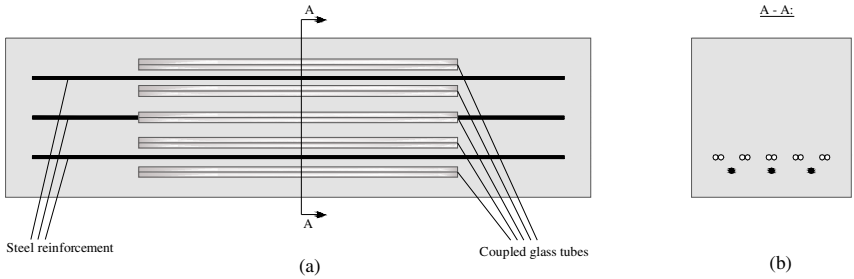


**Fig. 4.35** Top view (a) and cross section (b) of the mortar prisms in the case coupled tubes are used [4.53]

The self-healing efficiency of the different types of healing agents was evaluated by comparing the regain in mechanical strength. One day after performance of the bending test, when the healing agent inside the cracks of the autonomic self-healed specimens was thought to be hardened, samples were loaded again in three-point-bending. From the obtained loading curves, the peak load was determined and this value was used as an indication of the strength. The strength of the beams after self-healing was compared with the original strength for each type of healing agent used. After performance of both loading cycles samples were completely broken and cross sections were examined to evaluate the amount of glue that came out of the tubes and to verify if the glue had hardened inside the crack.

In Fig. 4.36, regain in strength is shown for all test series in terms of percentage. For the reference sample (REF), containing empty glass tubes, no strength regain was observed upon reloading.

Samples containing encapsulated cyanoacrylate (CA) showed some regain in strength, however, during crack formation, no glue migration was seen at the crack faces. Even when specimens were completely broken and cross sections were examined, no leakage of the glue was seen. It is thought that the glue already hardened inside the glass tubes, before crack formation, and that due to this fact the glue did not come out of the tubes. Presence of small air bubbles inside the tubes is sufficient to cure the glue before tube breakage. The regain in strength, which was observed during reloading, may then be attributed to the fact that the 'hardened glue bars' acted as a kind of reinforcement, bridging the two crack faces. This is similar to the mechanism, examined by Sakai *et al.* [4.33] and Isaacs *et al.* [4.36], to obtain self-healing properties in concrete.

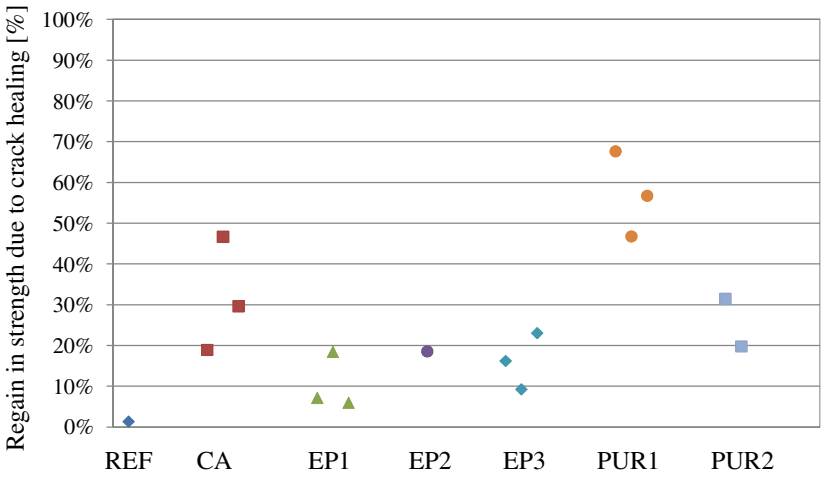


**Fig. 4.36** Regain in strength in terms of percentage for the different types of healing agent used [4.53]

When epoxy (EP1, EP2 and EP3) was used as healing agent, regain in strength was rather low. Again, during crack formation no glue migration was seen at the crack faces. When the beams were completely broken, it was seen that the glue partly came out of the tubes. However, the migration front was limited and moreover it was seen that the glue was still liquid at the moment the beams were broken. Minor mixing of both components, leading to imprecise stoichiometry may be the reason. These results prove the dependence of epoxy resins to the precise mix ratio which makes this type of glue unsuitable as healing agent in self-healing concrete.

When polyurethane was used to heal the cracks, good results were obtained. Two types of polyurethane were used here. PUR2 is a quite viscous, 1-component healing agent, consequently cracks were only partly filled with this type of glue. During examination of the cross sections, it was also seen that part of the glue was still liquid. Therefore, only 20-30% of regain in strength was obtained with this agent. The other type of polyurethane, PUR1, gave better results. PUR1 is a low viscous, 1-component polyurethane that starts foaming upon contact with water or air. However as the reaction time of this product may be shortened by addition of an accelerator, double glass tubes were used, like in the case of 2-component healing agents. One compartment was filled with polyurethane while the other compartment was filled with a mixture of accelerator and water. When PUR1 was used, 45-70% of strength regain was observed. It was already seen during the first loading cycle, when cracks were created, that the glue leaked out of the tubes, into the cracks. In Fig. 4.37, one of the specimens is shown during the bending test and migration of the glue at the crack faces is visible. When examining the cross sections it was seen that almost half of the surface was covered with healing agent when PUR1 was used.

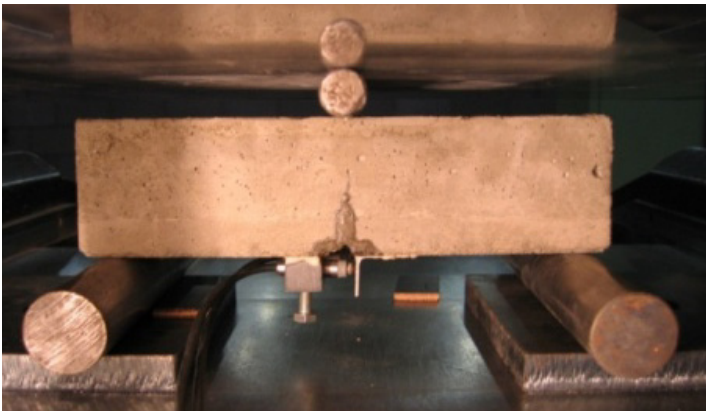

**Fig. 4.37** Migration of polyurethane (PUR1) to the crack faces observed during the bending test [4.53]

From the experiments described above it may be concluded that the type of healing agent used is very important when striving for self-healing properties in concrete. 1-component, air curing healing agents have the drawback that the glue may already start hardening inside the tubes when air bubbles are enclosed; 2-component epoxy resins are very sensitive to the mix ratio and no polymerization reaction will occur when the compounds are mixed randomly.

As best results were obtained when the polyurethane *Meyco MP 355 1K* was used, more experiments were performed with this type of healing agent [4.55, 4.56]. Glass tubes with an internal diameter of 2 mm and 3 mm with a varying length (so the internal volume was the same for both types of tubes) were filled with the polyurethane. Mortar beams and mortar cylinders with internal tubes were prepared and regain in mechanical properties and decrease in water permeability due to self-healing were tested.

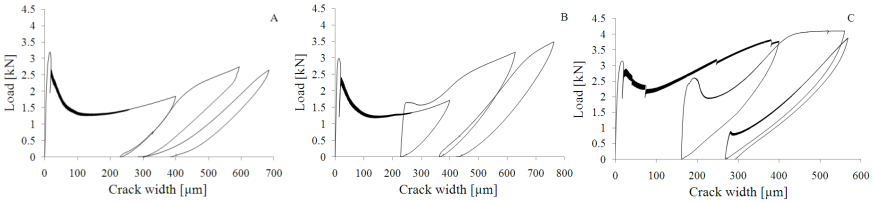


**Fig. 4.38** Load [kN] versus crack width [μm] during crack formation (first curve) and first (second curve) and second (third curve) reloading cycle for a reference sample (A), a sample with a manually healed (B) and autonomic self-healed (C) crack [4.55]

Regain in mechanical strength was compared against reference samples, from which cracks were not healed. Samples were compared with manually healed cracks and samples with autonomic self-healing properties. First, cracks were

created in all samples during a first loading cycle. After this loading cycle, cracks of the specimens for manual healing were treated. Specimens with glass tubes inside were autonomously healed during loading due to release of glue out of the tubes. One day later all beams were reloaded and regain in mechanical properties was tested. Again one day later a second reloading cycle was performed. In Fig. 4.38 the loading curves are drawn for three specimens, one of each group.

When cracks are not healed, no regain in mechanical strength is observed during reloading. For the manually healed specimens only during the first reloading cycle regain in strength is observed while for the specimens with autonomic self-healing properties strength regain is obtained during the first and the second reloading cycle. From these loading curves, the strength and the stiffness of the beams was calculated and the mechanical properties after (self-)healing were compared with the original values. The peak load $F_c$ was used as an indication of the strength while the slope of the curve, joining the points 0 $F_c$ and 0.4 $F_c$, was used to indicate the stiffness.

In Fig. 4.39A regain in strength is shown for all test series in terms of percentage. It is seen that for the reference samples no regain in strength was obtained nor during the first, nor during the second reloading cycle. In the case cracks were manually healed 56 till 71 % of the original strength was regained, during the first reloading cycle. However, when the samples were reloaded again no regain in strength was obtained. If encapsulated healing agents were present inside the mortar matrix, it is shown that during the first reloading cycle 33 till 83 % of strength regain is obtained due to leakage of the glue out of the tubes. When those specimens were loaded again, some additional glue leaked out of the tubes and during the second reloading cycle again 11 till 28 % of regain in strength is observed.

In Fig. 4.39B regain in stiffness is shown. It is seen that for the reference samples no regain in stiffness was obtained. In the case cracks were manually healed 21 till 59 % of the original stiffness was regained. However when these samples were reloaded again no additional regain in stiffness was observed. If encapsulated healing agents were present inside the mortar matrix, it is shown that during the first reloading cycle 29 till 62 % stiffness regain is obtained. When those specimens are loaded again, 20 till 38 % regain in stiffness is observed.

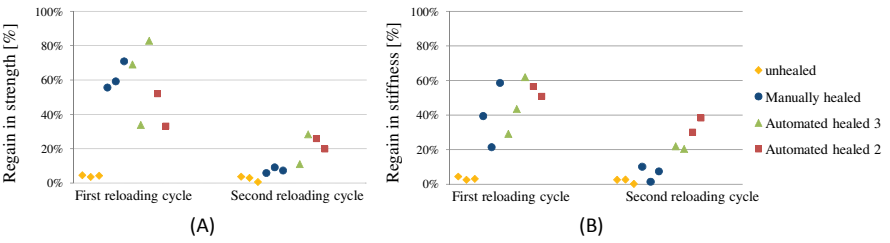


**Fig. 4.39** Regain in strength (A) and regain in stiffness (B) in terms of percentage during the first and the second reloading cycle for unhealed samples, samples of which the cracks are manually healed and samples with self-healing properties obtained by means of embedded glass tubes with an internal diameter of 2 mm and 3 mm which are filled with glue [4.55]

Normally, the efficiency of emptying of the tubes is dependent on the capillary forces inside the tubes, which are reduced when the tube diameter increases. However, an alteration in the diameter of the glass tubes from 2 mm to 3 mm does not seem to give significant differences in outcome, as it can be seen in Fig. 4.39A and B. Release of the glue seems to be more influenced by coincidental effects.

Besides regain in mechanical properties, it is also aimed that the autonomic self-healing leads to crack closing, so aggressive liquids and gasses cannot longer enter the concrete matrix through cracks. Therefore, water permeability measurements were performed (with the test setup shown in Fig. 2.19) onto unhealed, manually healed and autonomously healed specimens. The permeability coefficient of those specimens was compared with the one obtained for uncracked specimens.

In Fig. 4.40 it is seen that even in the case of uncracked specimens, some water leakage appears, however, the amount is very low. When created cracks were manually treated with polyurethane, the water permeability still remains low and the results are comparable with those obtained for uncracked specimens. When samples with self-healing properties were cracked and subjected to a water permeability test, it is seen that the water permeability coefficient $k$ is higher than in the case cracks were manually healed, however, the water leakage is 100 times till 10000 times less than in the case cracks are left untreated. In this graph it is also seen that there is no difference between the efficiency of tubes with an internal diameter of 2 mm or 3 mm.

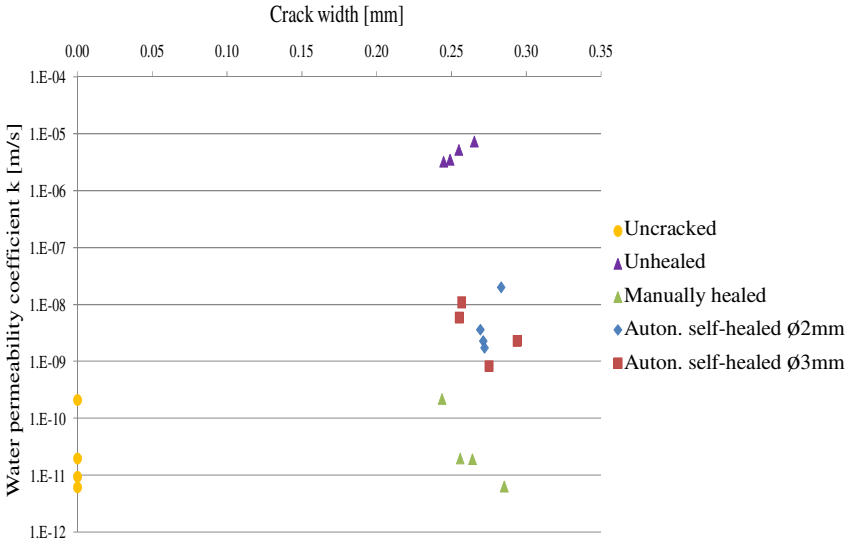


**Fig. 4.40** Water permeability coefficient k [m/s] obtained for uncracked and unhealed samples, samples of which the cracks are manually healed and samples with self-healing properties obtained by means of embedded tubes with an inner diameter of 2 and 3 mm [4.55]

The experiments described before were laboratory experiments, proving the concept of self-healing concrete. However, Carolyn Dry [4.57, 4.58] already incorporated the proposed self-healing mechanism into real scale structures. In 1997, the research group of Dry casted continuous bridge deck slabs containing encapsulated healing agent. Part of the capsules were used as delivery system to heal shrinkage cracks while other capsules were used to repair internal shear cracks.

In order to heal shrinkage cracks, scored hollow glass fibers were embedded in the top surface of the bridge decks (Fig. 4.41 A). Due to drying shrinkage, stresses occur which causes cracking near the surface and so fibers are pulled apart at the scored line. Subsequently the adhesive flows out from the broken tubes and fills the control joint crack, as seen in Fig. 4.41 B. The used repair adhesives had a low modulus of elasticity and allowed future movement to resist stresses and strains in the deck without additional cracks extending from the shrinkage micro cracks.

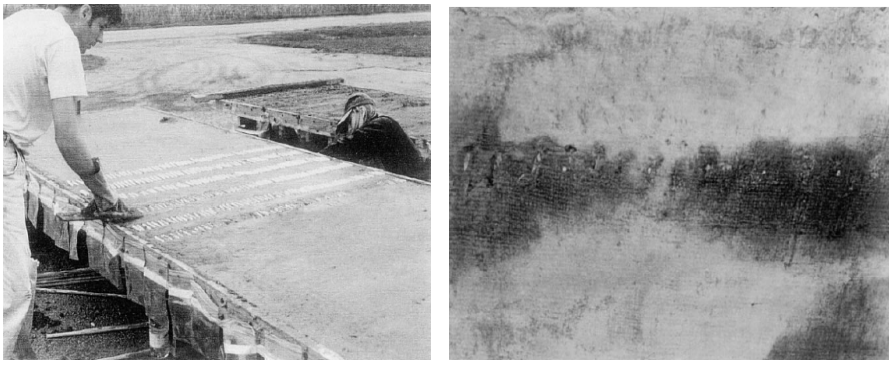

(a) (b)

**Fig. 4.41** (a) Photo of the tubes embedded in the top surface of the deck; (b) Photo of the control joint line created by the release of sealant from embedded tubes or fibers [4.58].

Visual assessment was the primary means used for assessing behaviour of the sealant-filled tubes. The sealant, VOC, changed color, first to light blue and then orange, when released into contact with concrete. It was noticed that tubes which were partly or fully embedded, broke and released their content, as shown in Fig. 4.41 B. Repair tubes which were not covered did not break, although these were more exposed to the environment and freezing and thawing weather cycles than the fully embedded tubes (Fig. 4.42). From this it was concluded that the environmental forces did not cause breakage of the tubes, but tubes were broken due to shrinkage stresses. During these experiments the authors also attempted corrosion monitoring, but no conclusive data were obtained. Therefore, the authors concluded to pond salt water onto the surface and due to leakage through the cracks change on voltage potential can be measured. Later, they also want to measure the reduction in water permeability due to shrinkage crack repair.

In order to repair internal shear cracks, tubular capsules containing stronger, high modulus adhesives were placed below the surface in areas of tension caused by bending. All four decks were tested three times each, in bending. Deck 1 had VOC embedded at its surface and cyanoacrylate repair capsules through its section. Deck 2 was the control deck, and contained no repair adhesives. Deck 3 had several hundred Tripp-adhesive-filled capsules embedded randomly through the section at mid-span of the deck length. It also had a transverse row of longitudinally aligned capsules with VOC just beneath the top surface of the decks. These are within the tensile zone during load-induced bending. Deck 4 had Trip on its surface and nothing through its section. The structural cracks, which were induced by loading (Fig. 4.43), were successfully repaired as evidenced by higher strength than a tested control deck without adhesives and by the creation of new cracks in some places where the old repaired cracks had not re-opened (Table 4.12).

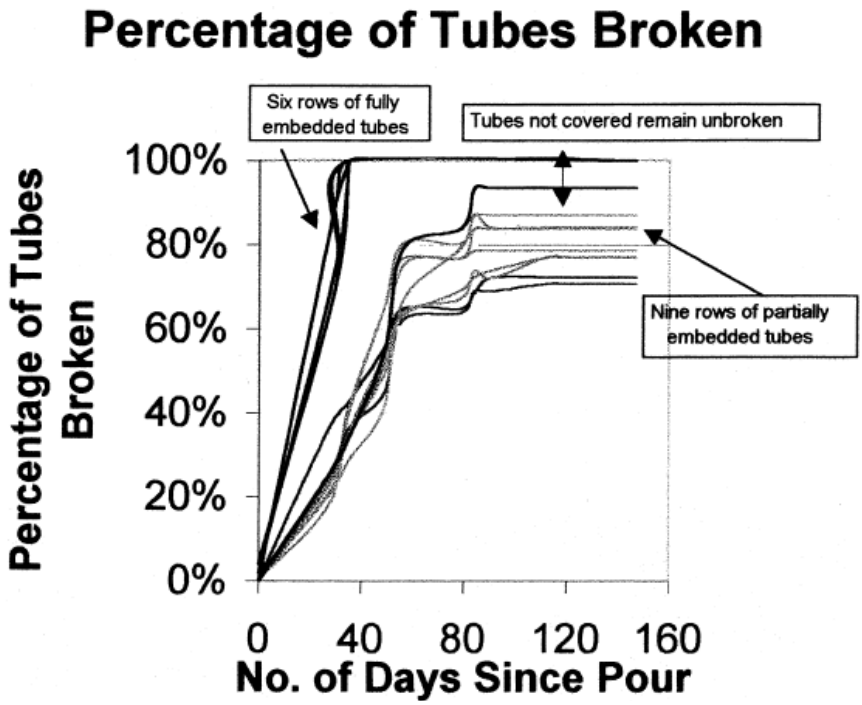


**Fig. 4.42** Chart of the percentage of tubes, which released sealant over time [4.58]

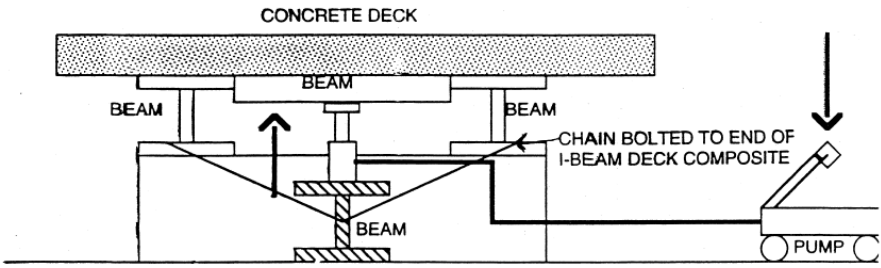


**Fig. 4.43** A diagram of the testing method setup used to induce structural shear cracking [4.58].

**Table 4.12** A listing of loads carried at failure point by the four bridges in three bending tests [4.58]

| | Strength increase | | | | |
|---|---|---|---|---|---|
| Deck no. | 1st Load (kips) | 2nd Load (kips) | % change | 3rd Load (kips) | % change |
| 1 | 1250 | 1250 | 0% | 1100 | -12% |
| 2 | 1200 | 800 | -33% | 800 | -33% |
| 3 | 1500 | 1500 | 0% | 1200 | -20% |
| 4 | 1500 | 1800 | 20% | 1700 | 13% |

To reduce the suction effect exerted by the sealed ends of cylindrical capsules, de Rooij and coworkers [4.59, 4.60] proposed to encapsulate the healing agent inside coated hollow plant fibers. When cracks propagate in the concrete matrix, the fiber bundles tend to delaminate and subsequently the healing agent is released from the splintered fiber bundles into the damaged areas where it subsequently reacts.

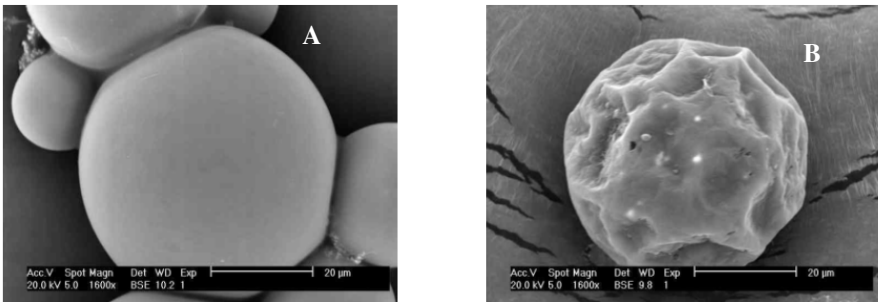


**Fig. 4.44** Microcapsule filled with tung oil (A) and microcapsule filled with $Ca(OH)_2$ (B) [4.61]

In all studies listed before, capsules had a tubular shape. Although, it is less commonly investigated, in some studies capsules with a spherical shape are incorporated in the matrix to provide cementitious materials with self-healing properties. For example in the study of Cailleux and Pollet [61], where it was aimed to provide repair mortars with self-healing properties, tung oil, $Ca(OH)_2$ or bisphenol-F epoxy were encapsulated by spherical gelatin microcapsules (Fig. 4.44).

When the encapsulated healing agent was mixed into the repair mortar, it was shown that some capsules were destroyed during mixing, resulting in release of the encapsulated agent (Fig. 4.45A). Capsules which survived the mixing process (Fig. 4.45B) only ruptured upon crack appearance. At that time, tung oil hardened upon contact with air. The other proposed healing agent, being $Ca(OH)_2$, formed $CaCO_3$ crystals upon reaction with carbon dioxide ($CO_2$). For the epoxy, a hardener was dispersed through the mortar and hardening of the epoxy resin was obtained when the resin came into contact with the hardener.

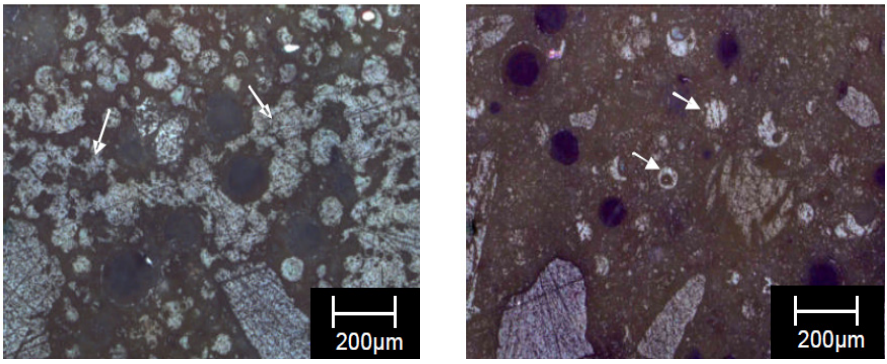


**Fig. 4.45** Polished cross-section of mortar matrix containing damaged microcapsules filled with tung oil (A) and mortar matrix containing intact microcapsules filled with epoxy (B) [4.61]

To evaluate the self-healing efficiency, specimens with dimensions of 150 mm x 150 mm x 30 mm were cast and subjected to a three-point bending test in order to create cracks with a width of 40 µm. For samples containing encapsulated epoxy resin, the two fractured surfaces adhered again after some time, proving that self-healing of the introduced damage had occurred.

Huang and Ye [4.62] and Pelletier *et al.* [4.63] encapsulated a sodium silicate ($Na_2SiO_3$) solution by spherical capsules. Huang and Ye encapsulated the solution through storage in sponge pieces with a diameter of 5 mm which were afterwards sealed with wax (Fig. 4.46A). In the study of Pelletier *et al.*, the solution was encapsulated by polyurethane microcapsules with sizes ranging from 40 – 800 µm (Fig. 4.46B). While in the study of Huang and Ye, mixing in of the capsules by

hand was necessary to survive the process, the capsules used by Pelletier *et al.* seemed to survive the mixing process. Moreover, the latter capsules did not seem to affect the compressive strength while those used by Huang and Ye did have a negative effect on the mechanical properties.

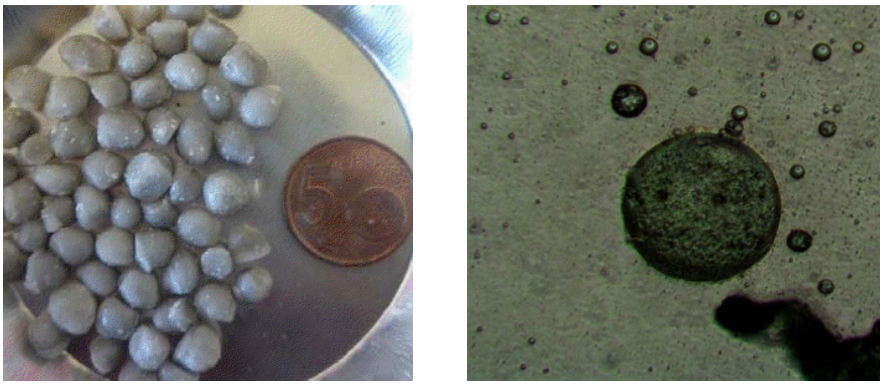

**(A)** **(B)**

**Fig. 4.46** Image of the encapsulated sodium silicate solution as it was done by Huang and Ye (A) [4.62] and light microscopy image of a polyurethane microcapsule used by Pelletier (B) [4.63]

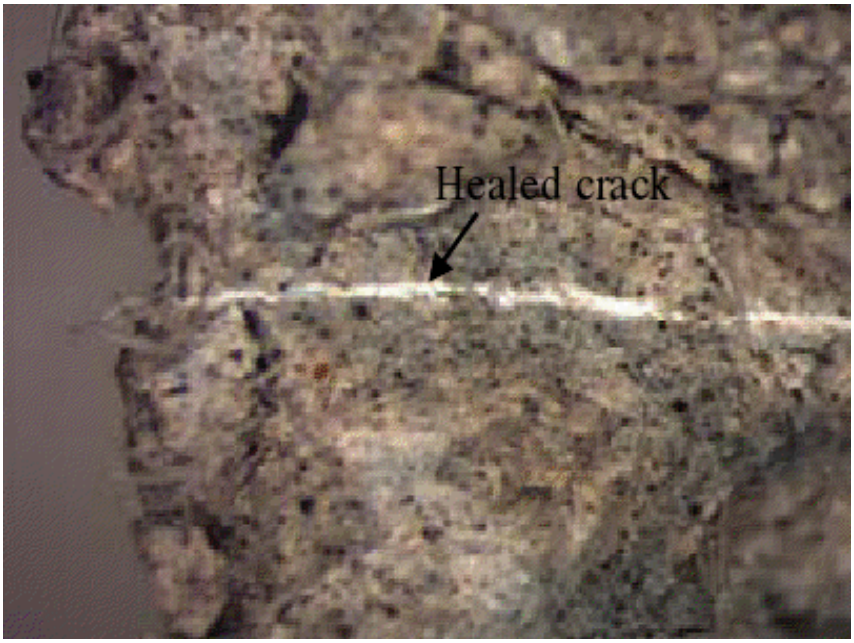


**Fig. 4.47** Cracked sample after healing occurred [4.62]

Both authors [4.62, 4.63] mentioned that at the moment of crack appearance, the capsules broke and the $Na_2SiO_3$ solution was released. The latter will reacted with the $Ca(OH)_2$, naturally present in concrete, to form a calcium silicate hydrate (CSH) product that healed the crack (Fig. 4.47). By means of EDS analysis, the formation of CSH inside the cracks was proven by Huang and Ye [4.62].

In their study, Pelletier *et al.* [4.63] evaluated the healing efficiency as the possibility to recover some of its strength after acquiring some minor micro scale damage. Therefore, samples were loaded to incipient failure, indicated by a sharp decrease in the load displacement curve. After the samples were left to heal for one week, they were reloaded. Pelletier noticed that the load at failure of the capsule-containing samples was 26 % (Fig. 4.48A) of the original value while the samples without capsules displayed only a recovery of 10% (Fig. 4.48B).

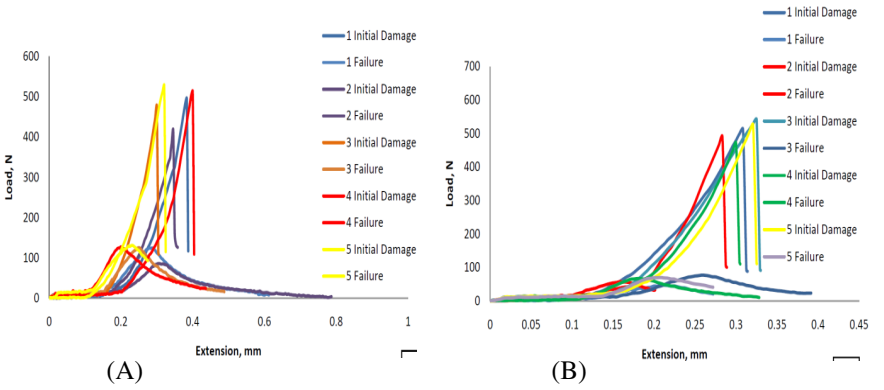


**Fig. 4.48** Load versus displacement (extension) for flexural strength characterization of capsule-containing (A) and control samples (B) [4.63]

In the studies mentioned before, all embedded capsules had the same content and the healing agent was able to cure upon contact with the air, the cementitious matrix or a hardener which was dispersed through the matrix. In addition to the single-capsule approach, multi-capsule systems exist. This means that two or more different types of capsules which sequester separate components of the healing agent are embedded in the matrix. In the latter case, healing occurs upon rupture of both types of capsules and release of both components which then contact each other.

An example of this approach, is the system proposed by Mihashi *et al.* [4.64]. They used spherical capsules with a urea formaldehyde formalin (UFF) shell containing a two-component epoxy resin. The researchers, however, noticed that it was difficult for the two-component epoxy to harden, due to insufficient mixing of both components in the crack. Feng *et al.* [4.65] also used spherical microcapsules with a urea formaldehyde (UF) shell filled with a two-component epoxy resin. However, these researchers modified the epoxy resin with a diluant chemical to adjust the viscosity, with the aim of obtaining superior mixing of both

components. Although reaction of this epoxy resin may occur at room temperature upon contact with the curing agent, crosslinking of the structure and beneficial properties are obtained when a thermal curing process at 120°C is provided during 1 h. This additional heat treatment makes this technique less convenient. Kaltzakorta and Erkizia [4.66] encapsulated a two-component epoxy resin by silica microcapsules, instead of their polymeric counterparts. This research is still in its initial phase and up to now researchers have only proven the possibility to mix in this type of capsules in cement paste, so no statements can be made about the healing efficiency.

Yang *et al.* [4.67, 4.68] used silica gel shell microcapsules with a diameter of around 4.15 µm which were prepared through an interfacial self-assembly process and sol-gel reaction. In Fig. 4.49 a schematic overview of the capsule preparation is depicted. While part of the microcapsules were filled with MMA oil, the rest was filled with triethylborane (TEB) oil which was used as initiator.

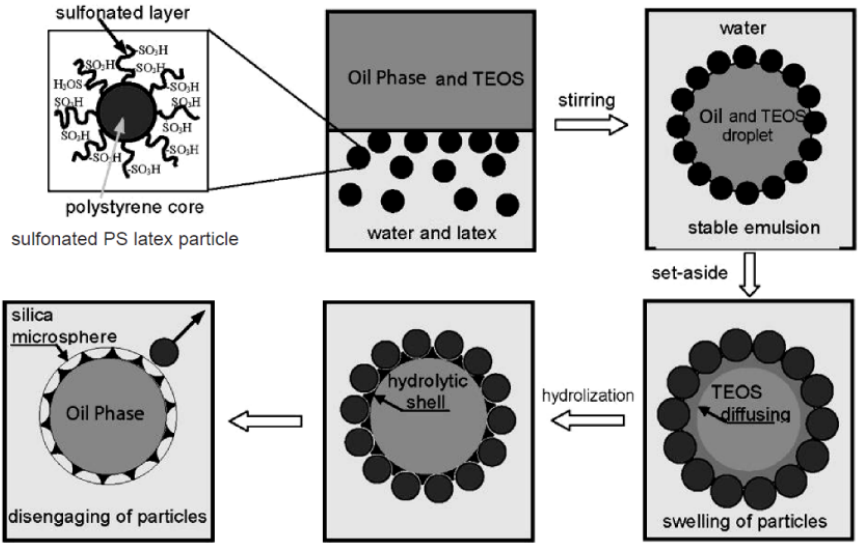


**Fig. 4.49** Schematic illustration of the capsule formation [4.67, 4.68]

It was possible to mix both types of microcapsules into a mortar matrix containing carbon microfibers which were added to mitigate cracking at the micro scale. As both MMA and TEB have a viscosity similar to that of water, they can easily migrate into micro cracks through capillary action after rupture of the capsules. Polymerization of the healing agent is then initiated by contact of both components, bonding the crack faces together.

In order to evaluate the healing efficiency, electrochemical impedance measurements were performed at 28 days, just after being loaded under 80% of the compressive strength and 24 hours and 7 days after being loaded. From these

measurements it was shown that at least part of the artificially induced micro cracks could be healed. In addition, the gas permeability was measured for samples after being loaded till 80% of the ultimate compressive strength and set aside for 24 hours to allow the released healing agent to polymerize. Relative to the control, the highest decrease in permeability coefficient, measured for the samples with encapsulated healing agent was 66.8% (Fig. 4.50A). Also the fatigue behaviour of these samples was tested and it was shown that the samples with encapsulated healing agent showed a significant prolonged second stage and their strain increment curves were less steep (Fig. 4.50B). This clearly demonstrates the beneficial role of the embedment of encapsulated healing agent to inhibit the initiation and propagation of cracks.

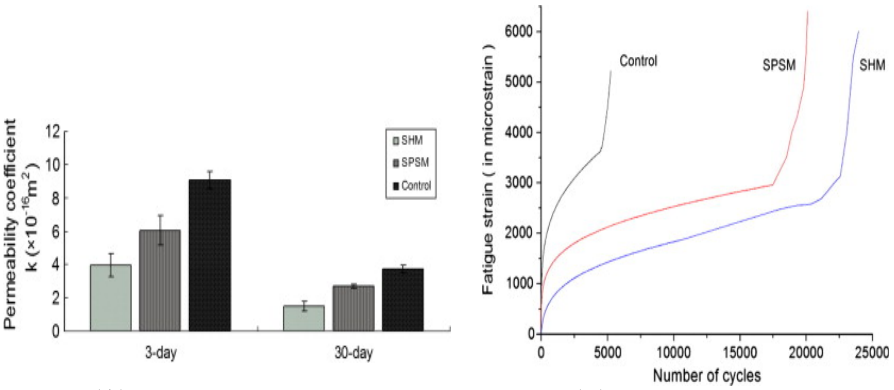


**Fig. 4.50** Permeability coefficient of cement mortar composite at 3-day and 30-day curing ages, after being loaded under 80% of ultimate compressive strength and set aside for 24 hours (A) and relationship between the fatigue strain and the number of cycles under uniaxial compression cyclic loading for SHM (with microcapsules filled with MMA and TEB admixed), SPSM (with sulfonated polystyrene particles admixed), and control mortar specimens respectively (B) [4.68]

#### *4.2.2.1.2 External Supply of Healing Agent*

Preliminary investigations by Joseph *et al.* [4.39, 4.69] revealed difficulties in achieving the release of a cyanoacrylate healing agent from glass tubes embedded completely within the mortar beams. It was believed that the negative pressure forces created by the wax plugs at the ends of the borosilicate glass capillary tubes were the cause of this. Future experiments revised the encapsulation system to longer capillary tubes which extended outside of the mortar specimens and thereby removed the issue created by the wax plugs [4.39, 4.69].

Joseph *et al.* [4.39, 4.69, 4.70] subsequently undertook a substantial parametric study on adhesive based self-healing of mortar beams. The parameters examined by the authors were the effect of loading rate, reinforcement level and specimen age on self-healing. A summary of the specimen configuration can be seen in Table 4.13.

**Table 4.13** Specimen configuration

| | Set 1. Notched, lightly reinforced | Set 2. Notched, lightly reinforced | Set 3. Notched, moderately reinforced | Set 4. Notched, heavily reinforced | Set 5. Notched, lightly reinforced, varied loading rate |
|---|---|---|---|---|---|
| No. of Beams | 2 Ctrl | 2 Ctrl | 2 Ctrl | 2 Ctrl | 1 Ctrl |
| Ctrl=Control | 4 SH | 4 SH | 4 SH | 4 SH | 3 SH at each loading rate |
| SH = Self-Healing | | | | | |
| Age at first test | 28 days | 28 days | 28 days | 70 days | 70 days |
| Mix ratio by weight | 0.55:1:3.5 | 0.6:1:3.5 | 0.6:1:3.5 | 0.6:1:3.5 | 0.6:1:3.5 |
| (water : OPC : sand) | | | | | |
| Reinforcement | 1No. 3.15mm | 1No. 3.15mm | 2No. 3.15mm | 1 No. 6.7mm | 1No. 3.15mm |
| | ϕ high yield steel bar | ϕ high yield steel bar | ϕ high yield steel bar | ϕ high yield steel bar | ϕ high yield steel bar |
| 5mm deep notch | Yes | Yes | Yes | Yes | Yes |
| Stroke loading rate (mm/s) | 0.003 | 0.003 | 0.003 | 0.003 | 0.00075, 0.003 and 0.012 |

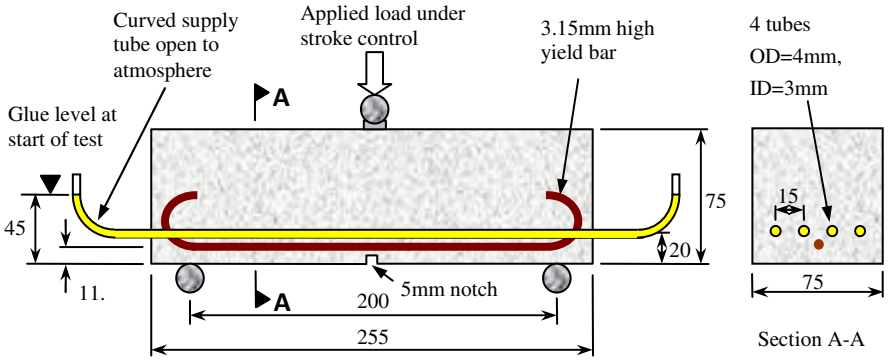


**Fig. 4.51** Testing arrangement for self-healing experiments on notched beams [4.71]

The experimental setup in each of the tests comprised 4 hollow capillary tubes of inner diameter 3 mm, open to the atmosphere, filled with a low viscosity cyanoacrylate, encased within mortar beams, as illustrated in Fig. 4.51.

The capillary tubes in the SH beams were filled with cyanoacrylate and the control beams were filled with ink, or left empty, prior to 3-point bend testing. All tests were conducted in two stages, whereby a predefined amount of damage (crack mouth opening displacement (CMOD)) was produced during the first 3-point bend test, followed by unloading and then reloading to failure after a curing period of 24 hours. The experimental set up is shown in Fig. 4.52.

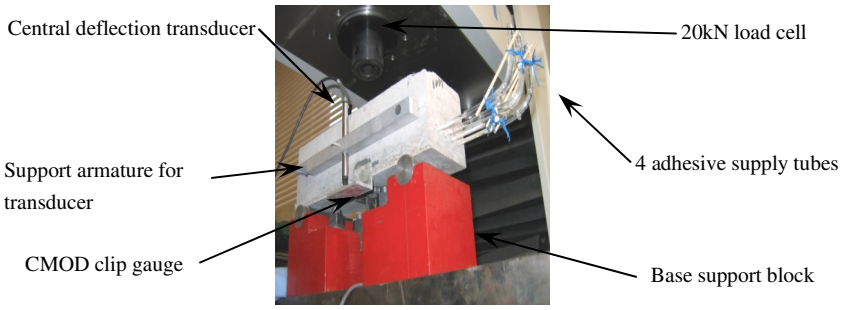


**Fig. 4.52** Experimental set up for first and second stage loading [4.71]

Fig. 4.53 shows a typical load-CMOD response for a notched autonomic self-healed beam during the first and second (denoted SH beam (healed)) 3-point bend tests, compared to that of a control beam. The glass capillary tubes, once broken, released cyanoacrylate into the crack plane which flowed rapidly under the influence of attractive capillary forces across the two crack faces. The cyanoacrylate experienced extremely rapid curing due to the moist alkaline environment of the mortar. This resulted in what can be considered as an instantaneous 'primary' autonomic self-healing effect and is characterised by the change in gradient of the autonomic self-healed beam compared to the control beam after the fracture of the glass tubes.

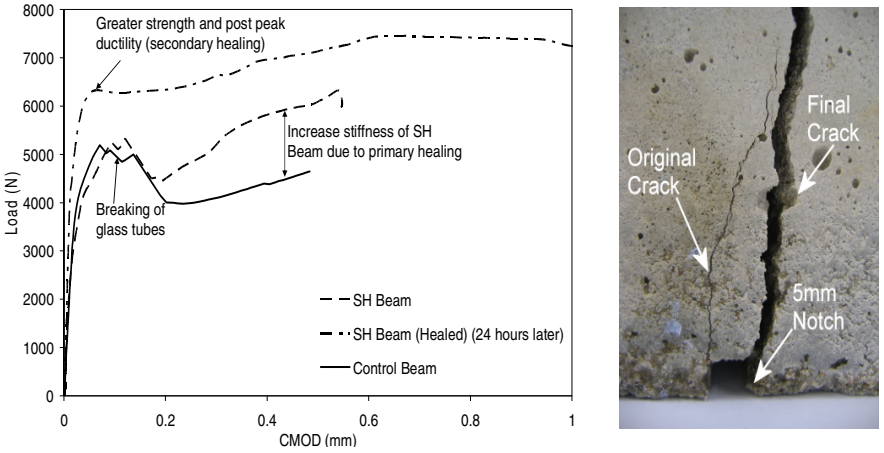


**Fig. 4.53** Typical Load-CMOD response for a notched self-healed (with cyanoacrylate) and control beam

Secondary autonomic self-healing was also apparent in all experimental sets, whereby in the second loading stage the specimens exhibited increased stiffness, higher peak load and a more ductile post peak response. The authors concluded that this could be attributed to the ability of the low viscosity cyanoacrylate to permeate into an extended zone around the crack face. This created a modified

"polymer-cementitious composite" zone around the crack face which better resisted the final crack that was forced to propagate through this zone as a result of the loading arrangement.

The authors noted that when the reinforcement level was increased the stiffness of the primary autonomic self-healing response also increased. This was attributed to the slower growth of macro cracks with the higher levels of reinforcement, which resulted in the cyanoacrylate being loaded at a slower rate, thereby allowing more bonds to form to heal the specimen. Moreover similar results were observed when considering the effect of loading rate on the primary autonomic self-healing response, with slower loading rates affording the cyanoacrylate greater time to form bonds, resulting in increased primary autonomic self-healing stiffness [4.39].

With regards to the effect of specimen age on autonomic self-healing Joseph *et al.* [4.39] reported that there was no apparent effect on healing ability with increasing specimen age. Unlike autogenic self-healing, which is highly dependent on specimen age as shown by Schlangen *et al.* [4.29], autonomic self-healing is primarily dependent on the efficacy of the healing agent, in terms of its viscosity and curing abilities within the mortar, and the delivery system and therefore it is not unexpected that specimen age is not an important parameter in autonomic self-healing experiments.

Qualitative evidence was also provided by Joseph *et al.* [4.39, 4.70, 4.71] to support their quantitative results. They noted the distinct sound of the glass tubes breaking in the first loading stage together with evidence of ink staining on the surface and the presence of glue on the underside of the crack. They reported that the cyanoacrylate in the supply tubes was still in liquid form during the second loading stage and thereby could contribute to a tertiary autonomic self-healing response as it is released over the duration of the second loading stage, however, this particular effect was not measured. The authors also reported proof of glue flow into the crack plane demonstrated by staining patterns above and below the glass tubes, as shown in Fig. 4.54. Moreover, Joseph *et al.* [4.39] reported evidence of new crack formation between the first and second loading stages as seen previously in Fig. 4.53. This work is being developed further to enhance the delivery system, making it more robust for its application in reinforced concrete structures.

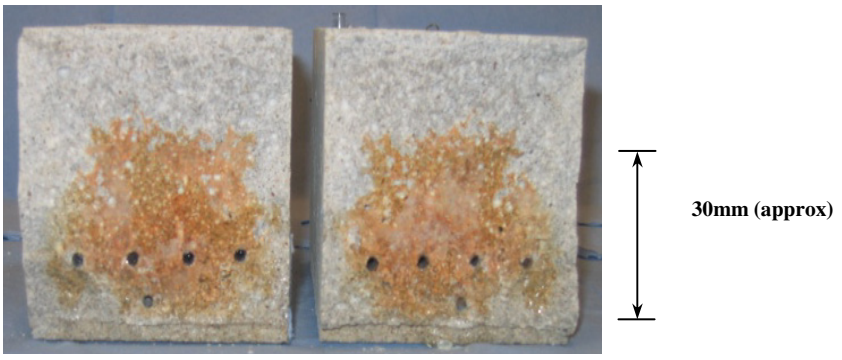


**Fig.4.54** Typical glue migration and effective zone of healing for self-healed beams

Mihashi *et al.* [4.72] carried out three-point bending tests onto single notched (20 mm) specimens with dimensions of 40 mm x 40 mm x 130 mm (Fig. 4.55). Into the specimens glass pipes were embedded which were connected with the outer side of the specimen. In addition two more test series were prepared; specimens without glass pipes from which cracks were not repaired and specimens without glass pipes from which cracks were repaired manually. Each test series consisted of three specimens.

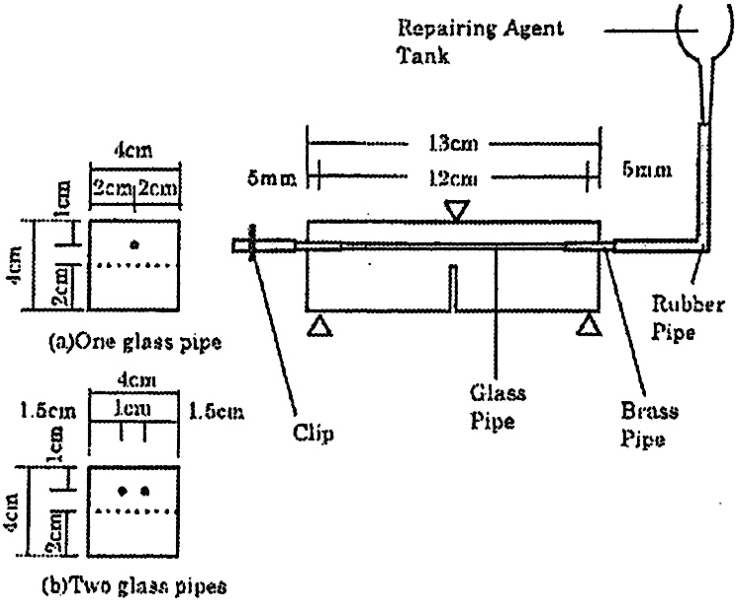


**Fig. 4.55** Test setup and specimen [4.72]

Three different healing agents were used; stereochromy with alkali-silica as major element (27% diluted solution, indicated with B in Table 4.14), stereochromy with alkali-silica as major element (main solution, indicated with B' in Table 4.14) and epoxy resin (two fluid blend, indicated with C in Table 4.14). For the test series in which epoxy was used as healing agent, two glass pipes were embedded (Fig. 4.55b), one for the principal agent and one for the hardener; for the other test series, only one glass pipe was used (Fig. 4.55a).

**Table 4.14** Overview of the performed experiments [4.72].

| Sample | W/B (%) | SF/BI (%) | $V_a$:$V_m$ | $V_f$ (%) | Repairing agent | Second curing duration (days) | Use of repairing agent |
|---|---|---|---|---|---|---|---|
| P1 | *All:* | *All:* | *All:* | *All:* | - | 7 | None |
| P4 | 40 | 10 | 1:1 | 0.5 | | 28 | |
| B1 | (38+2) | | | | Agent B | 7 | Injection by hand |
| B4 | | | | | | 28 | |
| B'1 | | | | | Agent B' | 7 | |
| B'4 | | | | | | 28 | |
| C1 | | | | | Agent C | 7 | |
| C4 | | | | | | 28 | |
| g-B1 | | | | | Agent B | 7 | Glass pipe |
| g-B4 | | | | | | 28 | |
| g-B'1 | | | | | Agent B' | 7 | |
| g-B'4 | | | | | | 28 | |
| g-C1 | | | | | Agent C | 7 | |
| g-C4 | | | | | | 28 | |

Cracks were created in the specimens by means of a three point bending test. The specimens were unloaded when penetration of the repair agent was observed at the surface of the concrete after the maximum load has been reached. These specimens were then cured for 7 or 28 days (see Table 4.14) before they were loaded again in a similar bending test.

Fig. 4.56. shows schematically the relation between the load and the CMOD in the bending test. The specimens were unloaded at the load level P1 after the maximum load, and the maximum load after reloading is defined Pr. Pr/P1 is defined as strength recovery ratio. In Fig. 4.57. the strength recovery ratio is shown for the different crack treatment techniques. From the relation between the residual CMOD and the strength recovery ratio for every 'P' and 'g' test series, it is clearly observed that the repaired specimens in the zone indicated by '*1' in Fig. 4.57 show an extremely high strength recovery ratio for the repairing agent of both B and B'. Thus, the restraint of crack propagation may be effective for repair. On the other hand the repaired specimens with larger residual CMOD than this zone give a relatively constant strength recovery ratio with asymptotic convergence. From these finding the authors concluded that the strength recovery may not be achieved by the repairing agent used in this paper beyond a certain level of crack width.

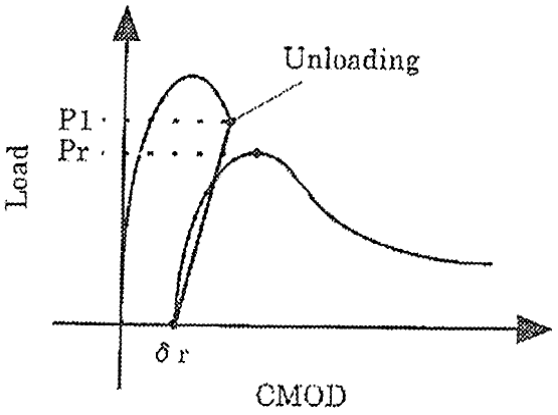


**Fig. 4.56** Load versus CMOD relation [4.72]

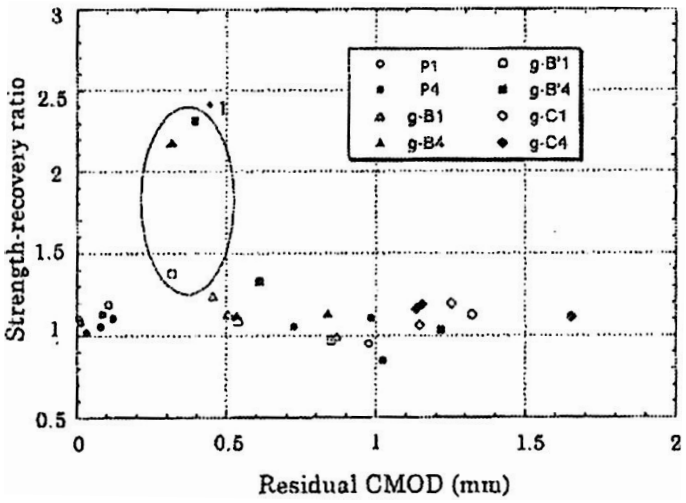


**Fig. 4.57** Residual CMOD versus strength recovery ratio [4.72]

The method by which healing agents are embedded in a cementitious material is of utmost importance, as the ability to release the healing agent from the system will govern the degree of autonomic self-healing that is achieved. The volume of required healing agent depends upon the aggressiveness of the environment and the ability of the chemical to move into the matrix. In instances in which a very large volume of chemical is required or where fibers have been depleted of their chemical over many years, vehicles for outside replenishment would be useful.

Dry [4.73] tested the efficiency of filling the glass tubes before or after crack appearance. She concluded that it is better to provide an external reservoir with healing agent which is released after cracks appear. Thus, enough quantity of agent to fill the generated crack can be supplied. Therefore, in her later

experiments glass capillaries were connected with the outside of the concrete structure (Fig. 4.58) [4.73]. A large volume of chemical was delivered by vacuum pressure, drawing it through hollow fibers into the matrix interior. When the vacuum is released, the chemicals flow through the fibers porous walls into the matrix.

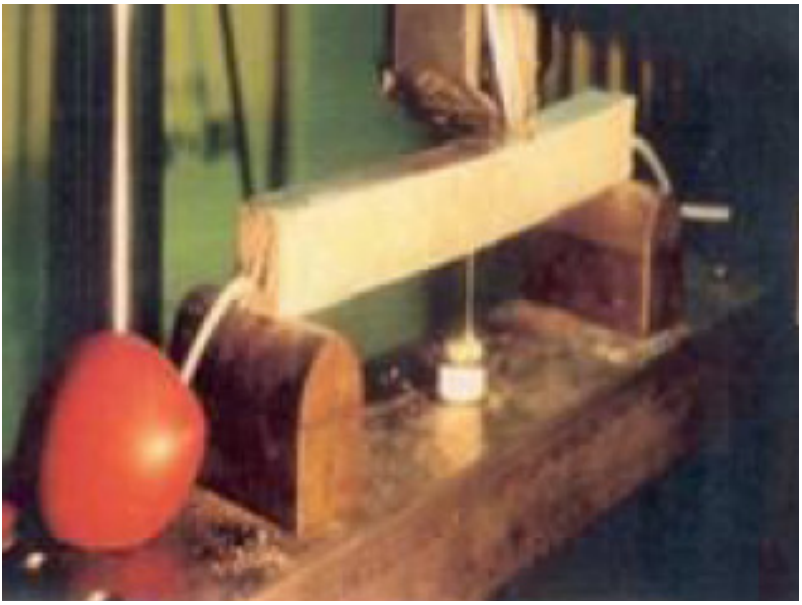

**Fig. 4.58** Demonstration of the pressure release concept. Adhesive in the fiber and a balloon is under pressure. When the specimen cracks, the pressure differential causes the adhesive to flow rapidly into the crack site.

Carolyn Dry [4.47, 4.48, 4.74-4.76] also made use of frame structures as test specimen (see Fig. 4.59a). These frames represent in a general form, buildings and bridges or components thereof. Glass pipettes were situated throughout the beam and into the moment connections at the columns (Fig. 4.59b). Glass pipettes can be seen extending from the frame for filling (Fig. 4.59a).

In these experiments, the authors tried to control the locations of structural damage by the strategic release of appropriate internal repair adhesives. High modulus, stiff adhesives released at the structural joints allow damaged joints to regain stiffness, thus preventing future damage at joints and insuring the translation of forces elsewhere. Low modulus adhesives released within the structural members close or seal cracks, but do not increase member stiffness. Thus, these sealed cracks are allowed some movement before additional cracking occurs. The combination of these adhesives into a single system allows forces in members to be safely transferred through connections to the more flexible members where failure should occur at ultimate loading. Furthermore dynamic

load energy is dissipated within these structural members while maintaining the critical structural integrity of the connections. Such systems, intelligently react in the event of excessive damaging forces – by driving forces through the structure to adequate members during the process of structural self-repair.

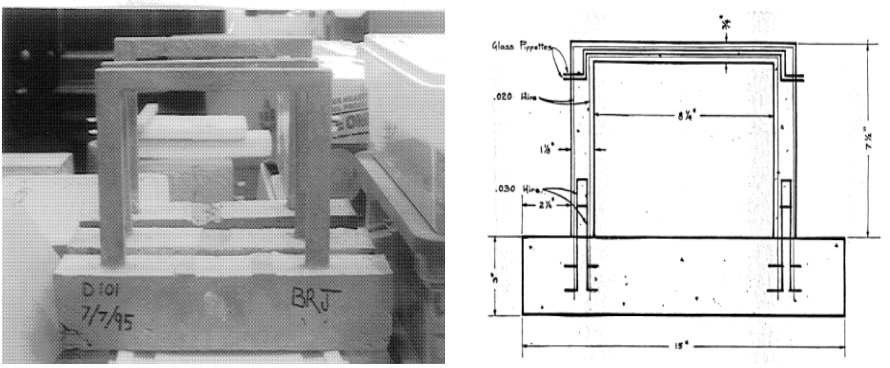


(a) (b)

**Fig. 4.59** (a) Photo of test frame, glass pipettes can be seen extending to the exterior for filling with adhesive; (b) Drawing of a concrete test frame [4.48].

During this experiment, three different adhesives were tested, each of them separately, within a generic concrete structural model. One stiff adhesive, cyanoacrylate, and two non-stiff adhesives, epoxy and silicon, were encapsulated. The crack healing efficiency was compared to control specimens which contained empty glass tubes.

The samples were poured, allowed to cure for 24 hours inside the forms, then removed and placed inside a water bath and allowed to continue curing for an additional 28 days. When the samples were removed from the bath, water was forced out of the pipettes with compressed air. The samples were then allowed to dry for 2 weeks before any tests were run.

The tests were performed through the use of a universal testing machine subjecting the frames to a constant in plane compressive force applied at the beam column joint and in a direction parallel to the base. During the first of two tests, each sample was loaded to a deflection of 5 mm in order to induce minor cracking in the frame. The corresponding resistant force in the frame was recorded and cracks were clearly marked. Load was applied in the same manner during the second test, two weeks later, this time until the sample reached failure. Load and deflection were recorded and the number of cracks located within the area of the adhesive's coverage were observed and identified as either "re-opened" or "new" (see Table 4.15).

**Table 4.15** Re-opened versus new cracks

| Sample | Avg. Old | Avg. Reopen | Avg. New | Ratio (new/reopen) |
|---|---|---|---|---|
| Control | 3.33 | 3.67 | 2.0 | 0.55 |
| Cyanoacrylate – | 2 | 1.67 | 3.0 | 1.80 |
| stiff adhesive | 3 | 0.67 | 1.67 | 2.50 |
| | 3 | 1.67 | 1.33 | 0.80 |
| | 4 | 1.67 | 1.33 | 0.80 |
| | 2 | 1.67 | 1.33 | 0.80 |
| Epoxy – | 2 | 2.33 | 0.33 | 0.14 |
| Non-stiff adhesive | 4 | 2.33 | 0.33 | 0.14 |
| | 4 | 2.33 | 0.33 | 0.14 |
| | 4 | 3.0 | 0.67 | 0.22 |
| | 4 | 3.0 | 0.67 | 0.22 |
| | 3 | 3.0 | 0.67 | 0.22 |
| Silicon – | 3 | 3.0 | 0.67 | 0.22 |
| Non-stiff adhesive | 3 | 3.0 | 0.67 | 0.22 |
| | 4 | 3.0 | 0.67 | 0.22 |

The cyanoacrylate, stiff adhesive, samples had the highest ratio of new cracks to re-opened cracks. This indicated that old cracks sealed by the cyanoacrylate in the first test provided increased strength in the second test, causing redistribution of stress to the uncracked section, where new cracks were formed. All of the other samples had an average new/reopened crack ratio of less than 1.0, indicating that the cracks sealed by the epoxy and silicon, non-stiff adhesives, experienced reopening without transferring stress to the uncracked region.

Instead of providing the healing agent by long glass tubes, which are very prone to cracking during casting of the beam, Pareek and Oohira [4.77] provided holes inside the concrete (Fig. 4.60). These were filled with epoxy, before or after crack formation, by means of a syringe which was connected to the open end.

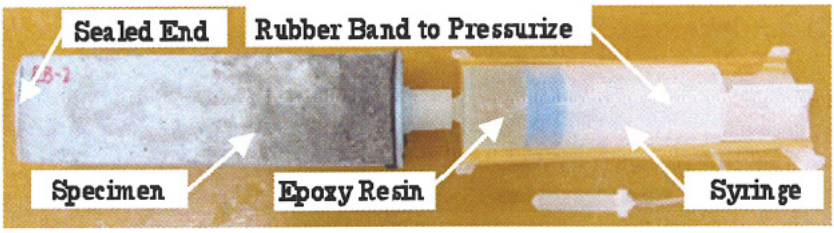


**Fig. 4.60** View of crack injection system [4.77]

As the hollow core will result in strength reduction, Sangadji and Schlangen [4.78, 4.79] proposed to use a hollow network which consisted of porous concrete. Their approach was inspired by the structure of human bones, consisting of an outer compact part and an inner spongy part. Sangadji and Schlangen casted porous concrete cylinders surrounded by a PVA film inside concrete beams. When the dense concrete matrix is casted around the porous part, the PVA film will dissolve and thus exchange becomes possible between the inner and the outer layer. They plan damage to be detected by sensors, which switch on a pump that injects the epoxy healing agent available in a reservoir through the porous network concrete layer to make it dense and seal the cracks (Fig. 4.61).

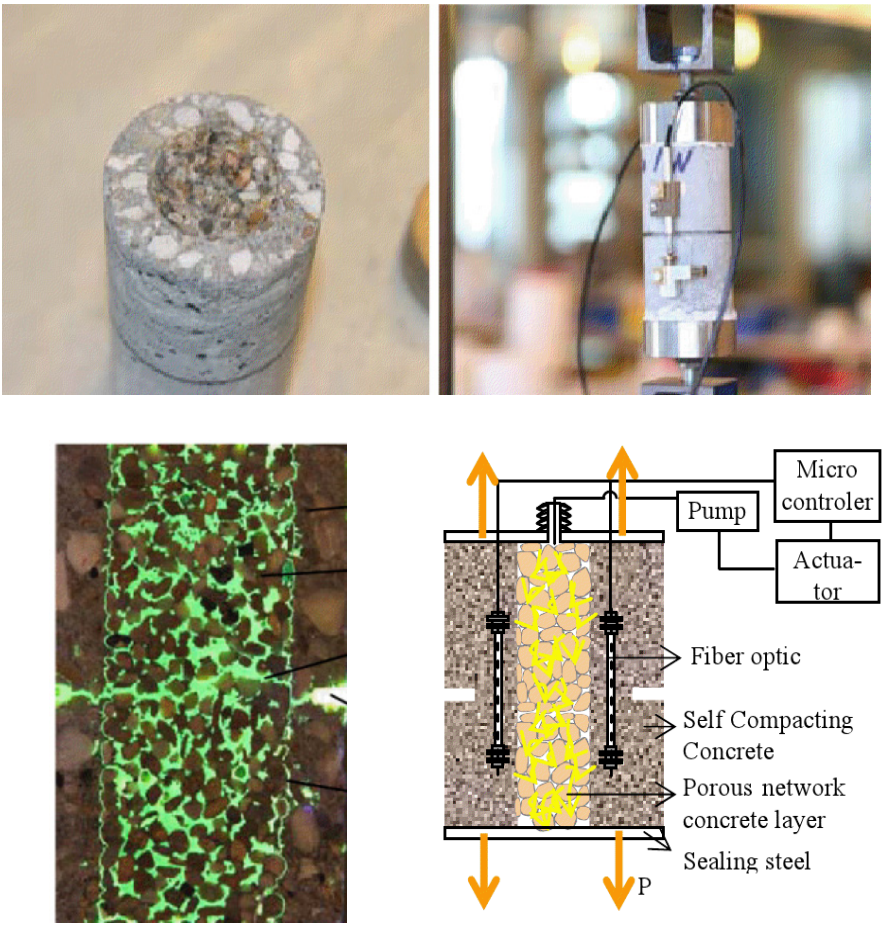


**Fig. 4.61** Porous concrete as reservoir for healing agent

### 4.2.2.2 Physical Activation

*4.2.2.2.1 Internal Supply of Healing Agent*

The healing mechanisms described in the previous section were activated through mechanical impact. Crack appearance caused breakage of the brittle encapsulation materials. However, the trigger mechanism may also be a physical action such as release of heat. This way of activation has been used by several researchers in order to release the healing agent.

In one of her studies, Carolyn Dry [4.46, 4.58] used hollow, porous-walled, polypropylene fibers, filled with liquid methyl methacrylate and coated with wax. These fibers were positioned inside concrete beams, as shown in Fig. 4.62 a. At the moment cracks are noticed, the concrete matrix needs to be heated. Due to this heating, the wax coating on the porous fibers will melt and the methyl methacrylate will move out into the cracked matrix (Fig. 4.62 b). Afterwards the heat is raised and the methylmethacrylate will polymerize inside the crack (Fig. 4.62 c).

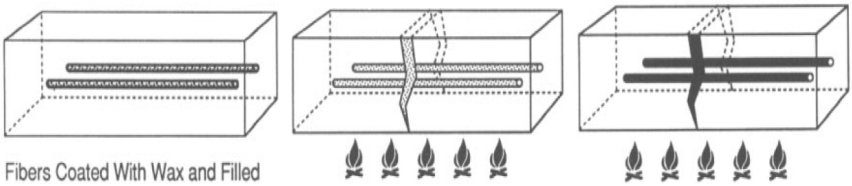


a) Fibers coated with wax and filled with methylmethacrylate

b) Wax coating melted with initial heating, methylmethacrylate released from fibers into cracks

c) Methylmethacrylate polymerized during second heating, closing previous cracks

**Fig. 4.62** Schematic diagram of the active repair system proposed by Dry [4.46]

As shown in Fig. 4.63, research results showed that after the methyl methacrylate polymerizes in the pores and cracks of the concrete, permeability is reduced. Permeability tests were done in accordance with the method described in [4.80].

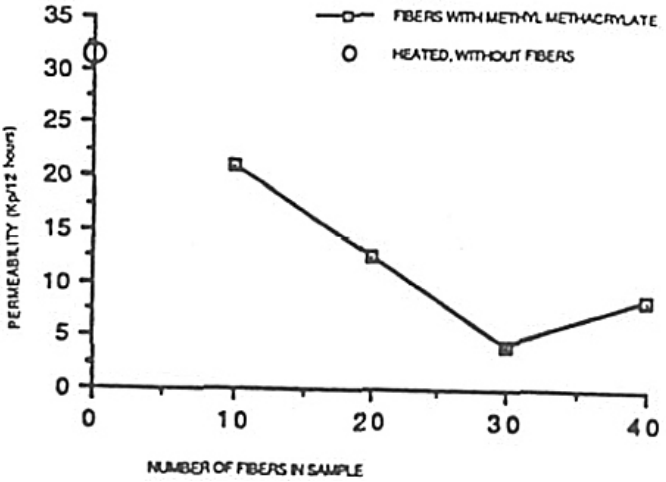


**Fig. 4.63** Permeability of Portland cement containing methyl methacrylate and wax released from polypropylene fibers (samples cured for 7 days, heated to 212 °F for 30 min [4.46]

A comparison of internal release versus exterior application with gravity feed was made (Fig. 4.64). The results showed samples with internally released chemicals had better compressive strength and less permeability than those using conventional surface application of methyl methacrylate and heating. Research has shown that this interior chemical delivery system works in the sense of delivering chemicals inside the matrix.

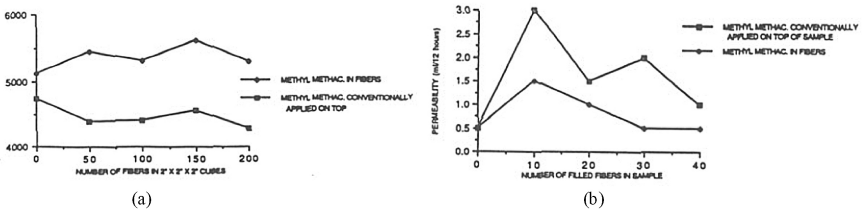


**Fig. 4.64** Effect of internal release of methyl methacrylate and wax from porous polypropylene fibers and internal polymerization against conventional application from the exterior top surface on compressive strength (a) and permeability (b) (samples heated to 212°F for 30 min.) [4.46]

*4.2.2.2.2 External Supply of Healing Agent*

Nishiwaki *et al.* [4.81-4.83] suggested a smart autonomic self-healing system for concrete which is composed of a self-diagnosis composite and a heat-plasticity

organic film pipe. The self-diagnosis composite is functionalized as heating device that can selectively heat around a generated crack by electrification. The heat-plasticity organic film pipe containing repair agent is embedded in concrete beside the heating device and is melted only in the heated zone. Next, repair agent is released from the melted surface of the pipe and fills the crack.

A concept of the proposed smart autonomic self-healing system is schematically shown in Fig. 4.65. A strain monitoring sensor fabricated using a specific fiber type and conductive matrix functions as the heating device. This sensor is not only a strain gauge but also both structural material and functional material for measuring the damaged area, recording damage history and so on. In this study, a smart autonomic self-healing composite fabricated using fiber-reinforced composites and conductive particles was employed as a heating device. Fig. 4.66 shows a schematic diagram of the structure of this sensor.

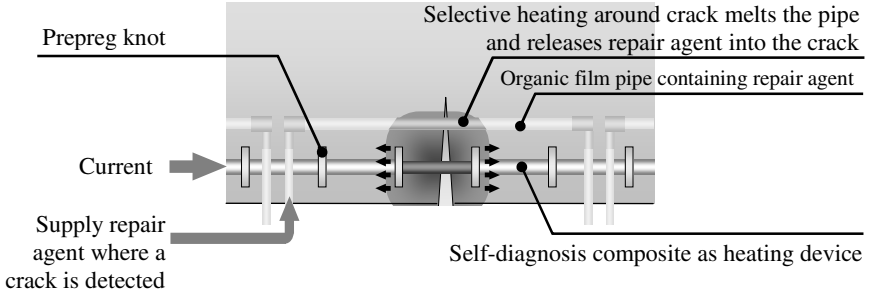


**Fig. 4.65** Schematic diagram of proposed self-healing concrete system [4.82]

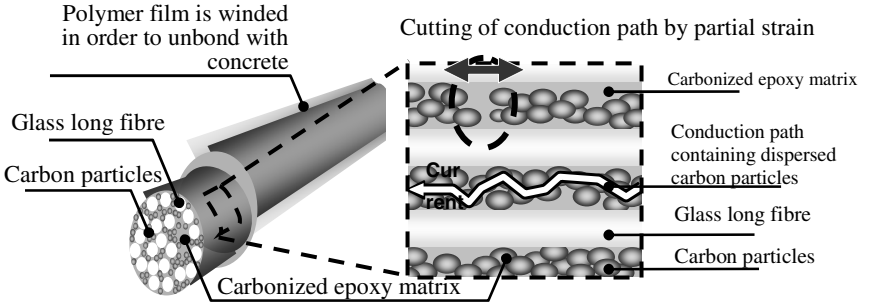


**Fig. 4.66** Schematic diagram of dispersed conductive particles in strain monitoring sensor [4.82]

The proposed self-healing system is implemented with a suitable arrangement of heating devices and thermal-plastic pipes containing repair agent in concrete. To decide on a proper arrangement, a three-dimensional thermal analysis was

carried out to simulate the temperature distribution in concrete with embedded heating devices. After this analysis, experimental studies were carried out to prove the effectiveness of the proposed self-healing system. Fig. 4.67 shows the geometry of the employed specimen.

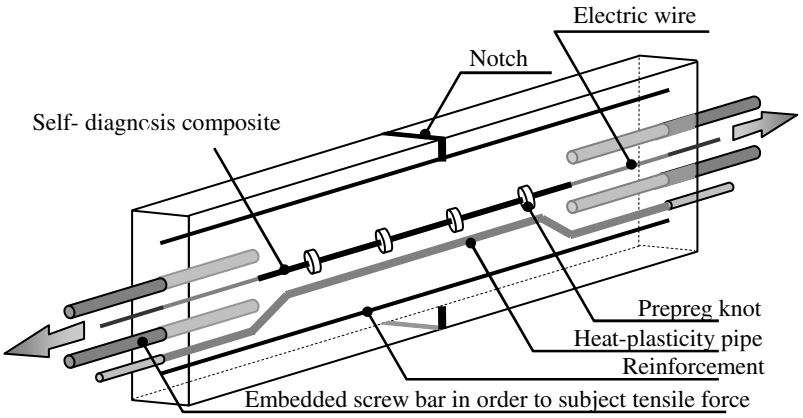


**Fig. 4.67** Geometry of employed specimen [4.82]

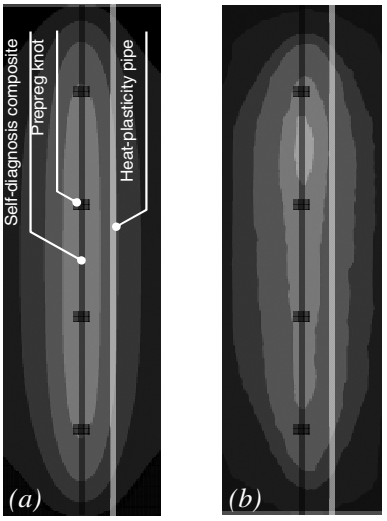


**Fig. 4.68** Temperature distribution before cracking: (a) analyzed, (b) experiment [4.82].

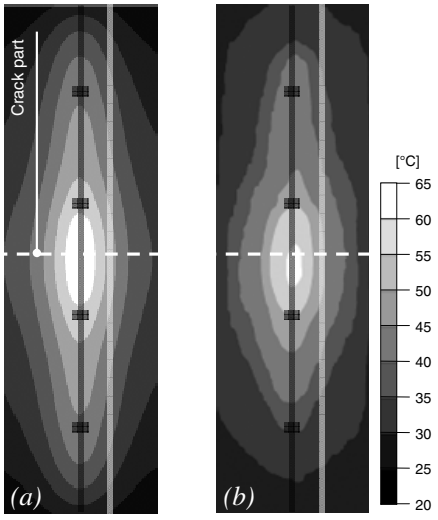


**Fig. 4.69** Temperature distribution before cracking: (a) analyzed, (b) experiment [4.82].

Fig. 4.68 (a) shows the temperature distribution at the surface of the model without any cracking as obtained through thermal analysis after 30 min from the start. Fig. 4.68 (b) is an experimental result corresponding to Fig. 4.68 (a).

Fig. 4.69 (a) shows the result of the analysis on the specimen with cracking that leads to a partial increase in electric resistance. Fig. 4.69 (b) is an experimental result corresponding to Fig. 4.69 (a). These figures clearly show that the high temperature part is concentrated between two prepreg knots including the generated crack part where the electrical resistance partially increases. Thus, the selective heating around generated crack is expected to be able to melt the embedded pipe selectively and to perform the proposed self-healing system effectively.

To confirm the effect of self-closing a permeability test was carried out [4.33]. Fig. 4.70 shows the relationship between the generated crack width and the quantity of water leakage through the crack. This graph shows that cracks in the specimen repaired with the self-healing system let in a much smaller amount of water than cracks in specimens without repair.

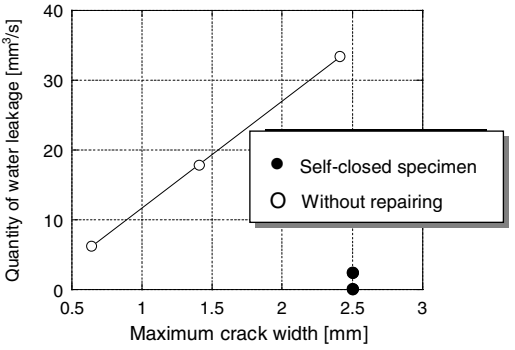


**Fig. 4.70** Relationship between generated maximum crack width versus quantity of water leakage [81].

In their latest work, Nishiwaki *et al.* [4.84] embedded their self-repairing device (SRD), composed of a self-diagnosis composite (SDC), a heat-sensitive pipe (HSP) and a copper plate which connects both of them, inside a layer of fiber reinforced concrete which was provided at the bottom of a beam (Fig. 4.71).

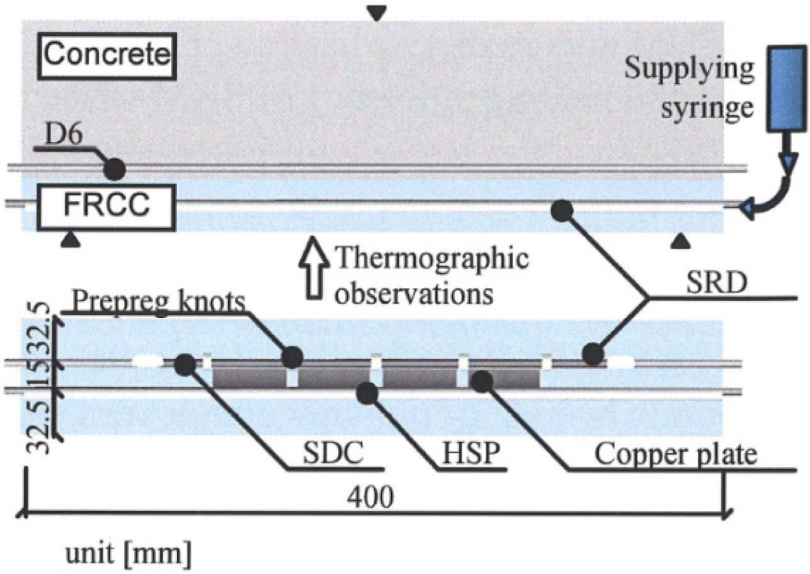


**Fig. 4.71** Geometry of the specimen [4.84]

#### 4.2.2.3 Recovery of Water Tightness and Mechanical Properties

When tubular vials with healing agents are applied to normal concrete, the amount of chemical available for crack closure and autonomic self-healing is rapidly exhausted, especially in case of wide cracks. Li *et al.* [4.7] therefore suggested an autonomic self-healing concept called: Passive Smart Self-healing Engineered Cementitious Composite (PSS-ECC) which has regaining water tightness and mechanical properties. ECC is used because it can control the width of the tensile crack to be narrow. So called SAC fibres (Self-healing Agent Carrying fibres) are embedded in ECC matrix.

Self-healing mechanism of PSS–ECC is demonstrated by regain in material stiffness after damage is imposed by a mechanical load in a 3-point bending test. Fig. 4.72 shows the arrangement of the embedded pipes in the cross section of two series (M1 and M2).

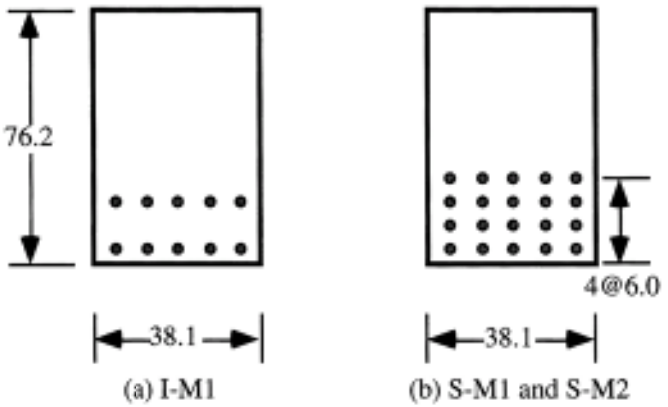


**Fig. 4.72** Cross-section of flexural specimen, showing position of glass fibers (units: mm)

The stiffness changes are reported in Fig. 4.73 a and b for materials M1 and M2, respectively. Each stiffness is normalized by the initial stiffness (uncracked) of each specimen. Solid symbols represent PSS–ECC systems. Six out of nine specimens showed higher regained stiffness on first reloading than the initial stiffness, and two specimens were close to the initial stiffness. As a result, eight out of nine PSS–ECC specimens indicated recovery of stiffness. In contrast, specimens having no SAC fibers all suffered stiffness degradation from 10% to 40%. The self-healing effect is validated by regaining of flexural stiffness in beams reloaded after an initial cycle of loading to beyond first cracking followed by unloading.

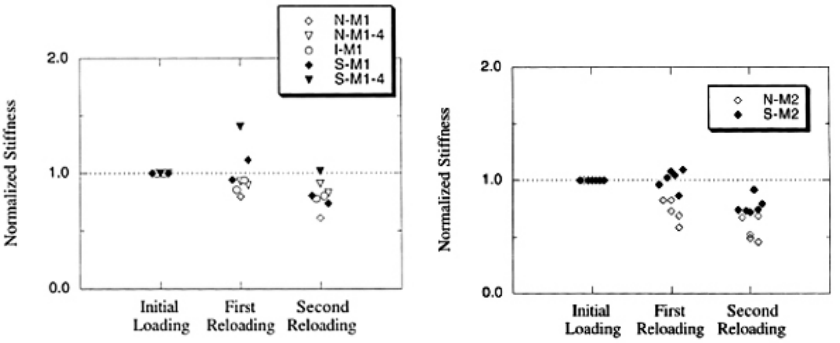


(a) Material M1 (b) Material M2

**Fig. 4.73** Normalized stiffness in flexural beam

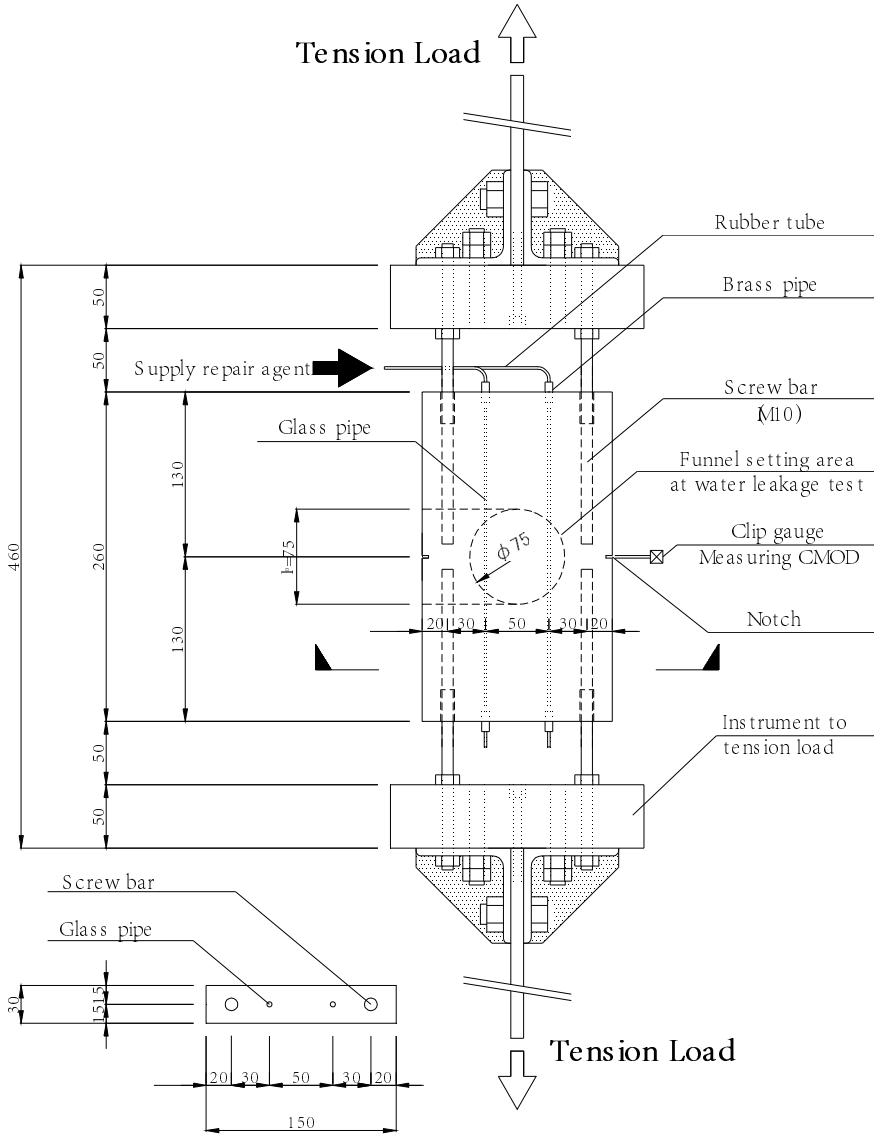


**Fig. 4.74** Specimen and test method [4.85]

Nishiwaki *et al.* [4.85] suggested an autonomic self-closing system with glass pipes embedded in HPFRCC (High-Performance Fibre Reinforced Cement Composites) which shows multiple cracking and strain hardening in tension as well as in bending, see Fig. 4.74. A fluid repair agent, which when in contact with concrete material chemically reacts forming solid crystals, is injected to the embedded glass pipes. The testing procedure was carried out in two separate steps.

In the first step the test specimen was subjected to uniaxial tensile load until desired damage (cracking) level. Thereafter, the specimens were unloaded and a permeability test was carried out using the cracked specimen.

Fig. 4.75 shows the relation between maximum crack width and the calculated coefficient of water permeability. The results show that the self-closing system was effective in HPFRCC specimens with maximum crack width above 0.2 mm, but not often effective when the maximum crack width was below this value. However, in mortar specimens the self-closing system was ineffective. For mortar specimens whose maximum crack width was from 2.5 to 4.5 mm, the permeability test could not be performed, since discharge was instantly.

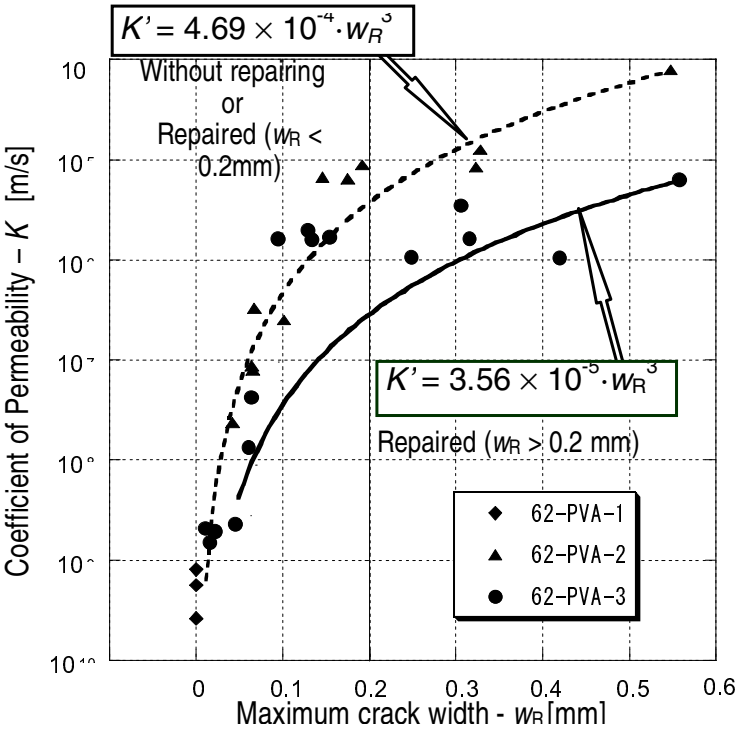


**Fig. 4.75** Relationship water permeability coefficient (K) and maximum crack width ($w_R$) [4.85]

## *4.2.3 Particles Mixed into the Mortar*

### 4.2.3.1 Self-encapsulation

The Japanese research group of Ohama and Demura proposed the use of polymer modified mortars containing epoxy resins without hardeners to repair cracks

autonomously [4.86]. When epoxy resins are added to the concrete matrix without addition of hardeners, the outer layer of epoxy will harden due to the presence of alkalis or hydroxide ions in the matrix [4.87]. Due to this, the outer epoxy layer will be solid while the inner layer is still liquid. This means that the epoxy resin phases exist as self-capsuled epoxy resins. By preloading, the mortar matrix is cracked, and the self-caspuled epoxy resins are partially broken. The unhardened epoxy resin flows out of the capsules into the micro-cracks, and the unhardened epoxy resins filling the micro cracks may be hardened by alkalis of hydroxide ions in the mortars. Due to this, autonomic self-repair of cracks is obtained (see Fig. 4.76).

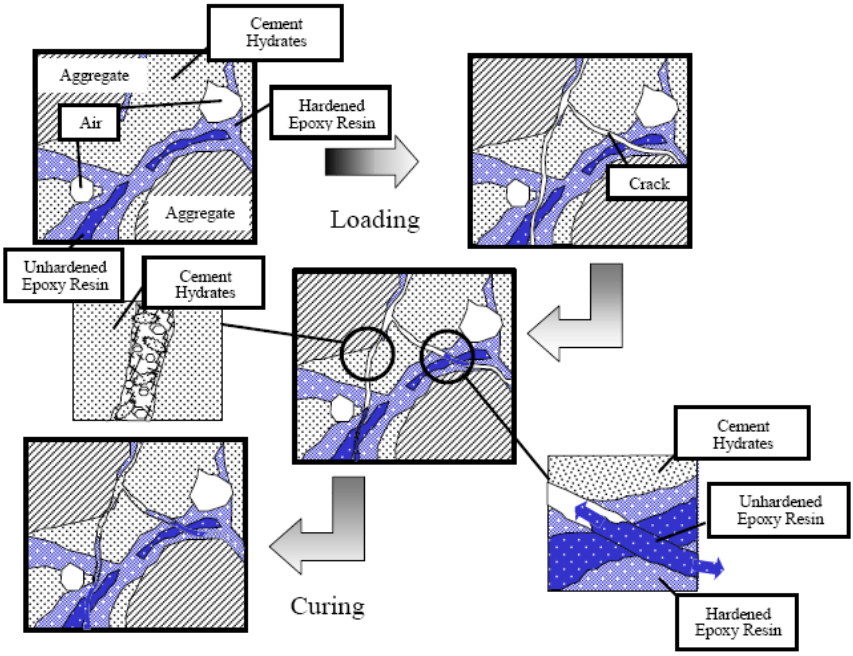


**Fig. 4.76** Simplified model for self-repair mechanism for microcracks by self-capsuled epoxy resin in epoxy modified mortar.

In their experiments, the authors [4.86] used diglycidyl ethers of bisphenols A and F as epoxy resins. The epoxy modified mortars were mixed with a mass ratio of cement to fine aggregate of 1:3. The polymer-cement ratios amounted 0%, 5%, 10%, 15% and 20% and the flow was adjusted to be constant at 170±5 in the water cement ratio range of 73 to 78%. Prismatic specimens of 40 mm x 40 mm x 160 mm were molded and subjected to combined wet/dry curing. Then, half of the specimens were cut down to make cubic specimens of 40 x 40 x 40 mm. Afterwards, compressive loads of 0% and 85% of the maximum compressive load were applied to the longitudinal direction of the specimens for preloading (Fig. 4.77). After

loading, the specimens were dry-cured again at 20°C and 50% relative humidity. After 28 days the prismatic and cubic specimens were tested for flexural and compressive strength and compressive strength, respectively.

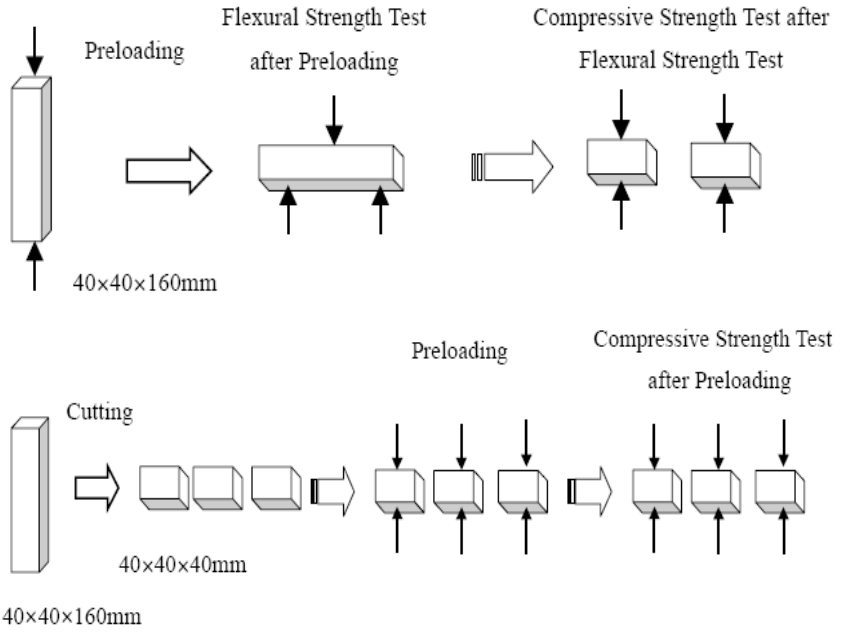


**Fig. 4.77** Methods for preloading and strength test for prismatic and cubic specimens

It was found that the 56 days flexural and compressive strengths of the preloaded epoxy-modified mortars were almost the same as those of the unpreloaded epoxy-modified mortars and were higher than the 28 days flexural and compressive strengths of the unpreloaded epoxy-modified mortars. Similar results were found for the cubic specimens. From these findings the authors concluded that strength developed after pre-loading. According to the authors this strength development was caused by the combined effect of acceleration of cement hydration and self-repair of microcracks with epoxy resins.

#### 4.2.3.2 Expansive Chemical Agents

Ahn *et al.* [4.88-4.90] propose to obtain self-healing properties in concrete by using a combination of expansive agent, geo-materials and chemical agent. Self-healing concrete cylinders (10 cm x 20 cm) were prepared by mixing in the three mentioned compounds. Specimens were cured for 1 month and then artificially cracked. Crack width was controlled between 0.1 mm and 0.3 mm according to the maximum allowable crack widths dictated by the construction codes. Subsequently the specimens were water cured for 1 month.

In Fig. 4.78 the healing process of one of the cracked specimens is shown. In this case, the crack with an initial width of 0.2 mm was almost completely healed after 28 days. Rehydration products were clearly observed after 14 days, and the crack self-healed perfectly even though there were small cracks between the rehydration products after 200 days as shown in Fig. 4.78f.

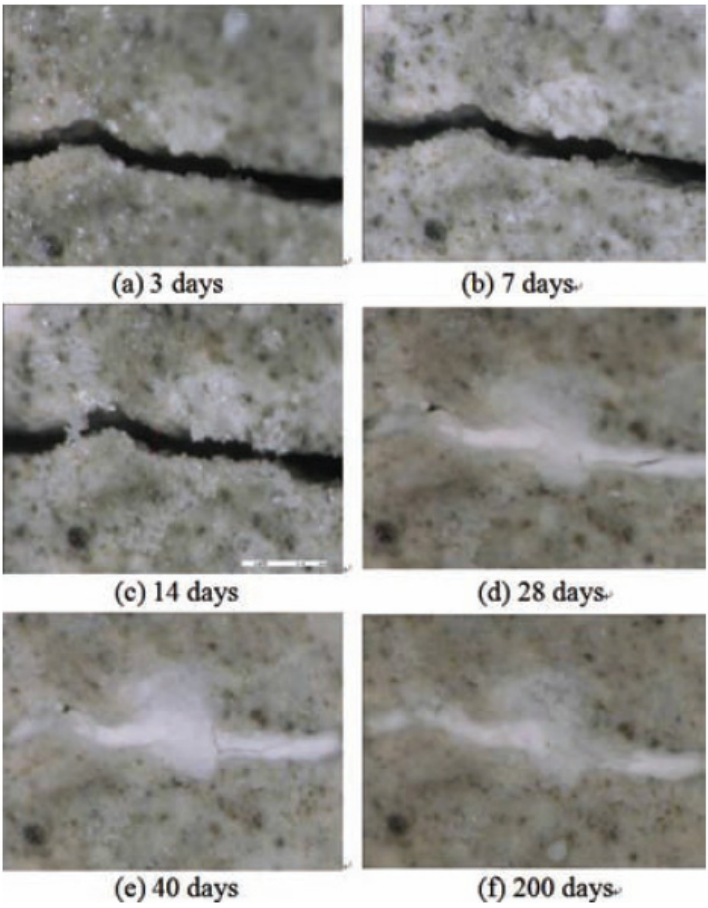


**Fig. 4.78** Process of self-healing on [OPC90%+CSA5%+Geo-materials5%] pastes at normal water/binder ratio of 0.45 [4.88]

Fig. 4.79a shows the entire self-healed shape of one of the cracked specimens by top, side, bottom and cross-section. It was noticed that there was a difference between the phases of the original matrix and the self-healing zone. Therefore, microscopy and SEM analysis with EDS detector were carried out to investigate the morphology, shape and size of rehydration products and to clarify re-hydration.

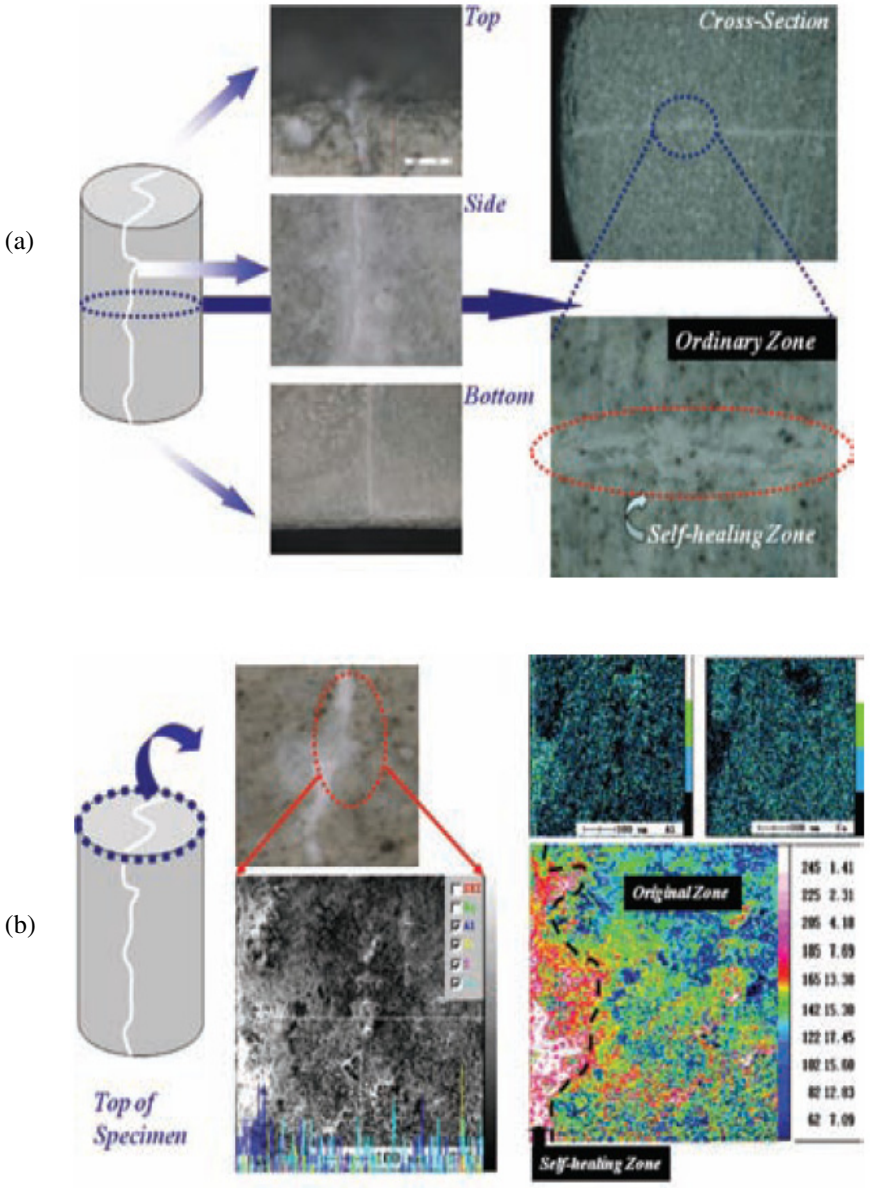


**Fig. 4.79** (a) Self-healed shape of cracked pastes according to regions such as top, side, bottom and cross-section; (b) Self-healing phenomenon of crack by crystallization of aluminosilicate phases on the cementitious pastes incorporating CSA and geo-materials (surface analysis of specimen) [4.88].

Fig. 4.79a shows the rehydration products on the surface of the specimen between the original and self-healing zone. Fig. 4.79b shows the X-ray map and spectra taken from rehydration products. It was found that re-hydration products were mainly composed of high alumina silicate materials as shown in the X-ray mapping results. This self-healing phenomenon seems to be related to the crystallization of aluminosilicate with calcium ion.

When tests were done onto concrete with the same mix composition, self-healing was noticed after 33 days of curing in water. This healing mechanism was also caused by the swelling effect, expansion effect and re-crystallization of the cementitious matrix. However, it was also noticed that cracks along aggregates were not completely sealed. Some recrystallization products were deposited from the cementitious paste onto the aggregate surface as shown in Fig. 4.80. The authors concluded that self-healing of these cracks would take more time.

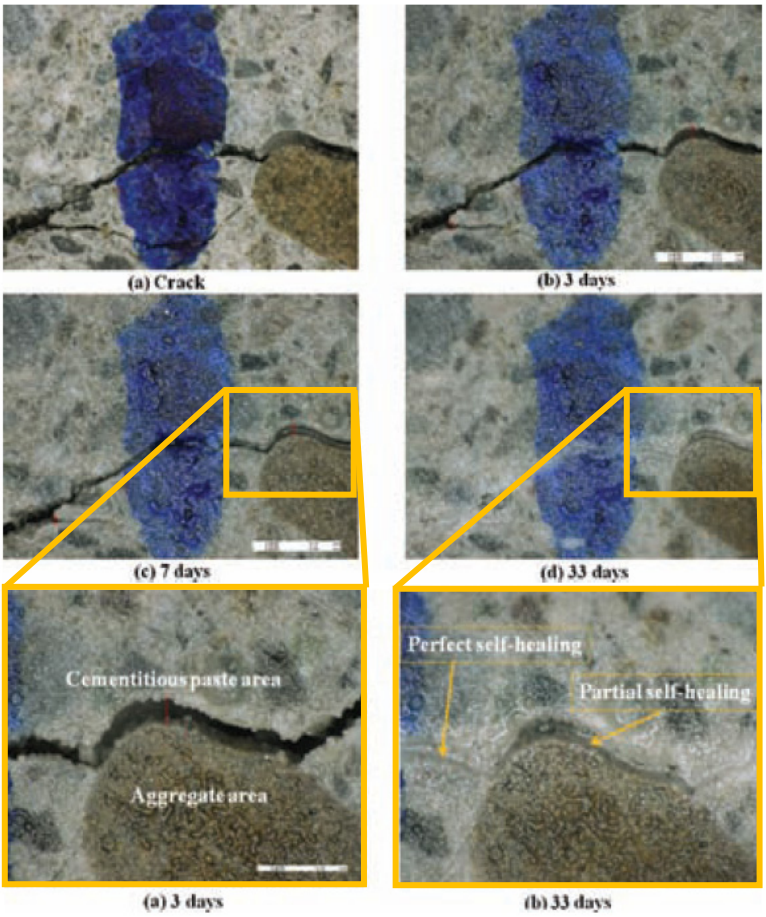


**Fig. 4.80** Process of self-healing on self-healing concrete at water to binder ratio of 0.47 [4.88]

Sisomphon and Copuroglu [4.91] mixed in calcium sulfo aluminate (CSA) based agents and crystalline admixtures (CA) in order to obtain autonomous crack healing. It was meant that, upon the ingress of water into a crack, ettringite crystals would form, which would fill the crack. Investigation of the crack width reduction with respect to the wetting period of the samples led to the conclusion that mortar containing CSA and CA showed superior self-healing ability. It was noticed that small cracks (< 200 µ) could heal completely even without the addition of CSA or CA, however, it takes some more time (Fig. 4.81A). For larger cracks (> 300 µm), the addition of CSA or CA and certainly the addition of both components significantly improves the reduction in crack width (Fig. 4.81B).

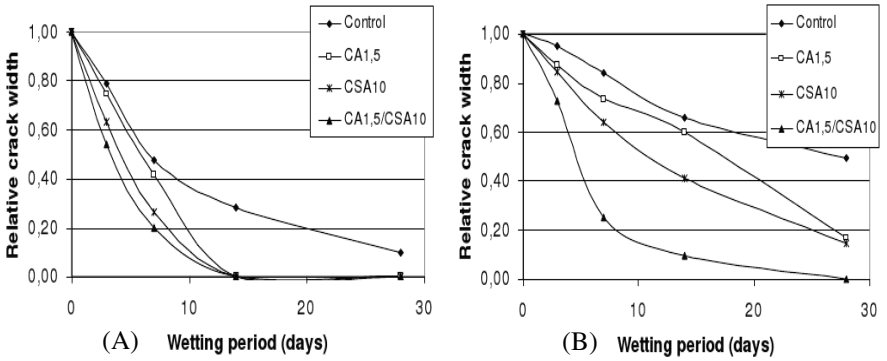


**Fig. 4.81** Crack width reduction in function of the wetting period for samples with small cracks (< 200 µm) (A) and larger cracks (> 300 µm) (B) [4.91]

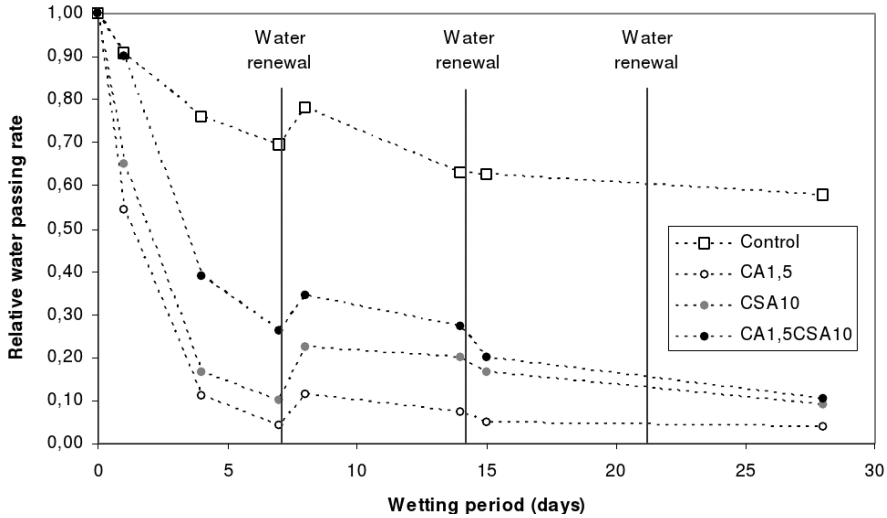


**Fig. 4.82** Relative water passing rate of pre-cracked mortars [4.91]

Observation of the amount of water passing through a cracked sample led to similar conclusions (Fig. 4.82). While for the control mortar a slight reduction in water passing rate was observed in the early period, mortars with CA or CSA showed rapid reduction of water passing ability at the first 5 days. Currently, Sisomphon *et al.* [4.92] incorporate CSA's with different chemical compositions in an effort to further enhance the self-healing potential.

In another study, Copuroglu *et al.* [4.93] mentioned that using ettringite formation as mechanism to cause autogenous crack healing might pose certain risk regarding uncontrolled expansion and cracking. Therefore, they proposed to encapsulate the ettringite producing agents to find out whether or not it could provide technical advantages. In Fig. 4.83. the encapsulation process is schematically depicted.

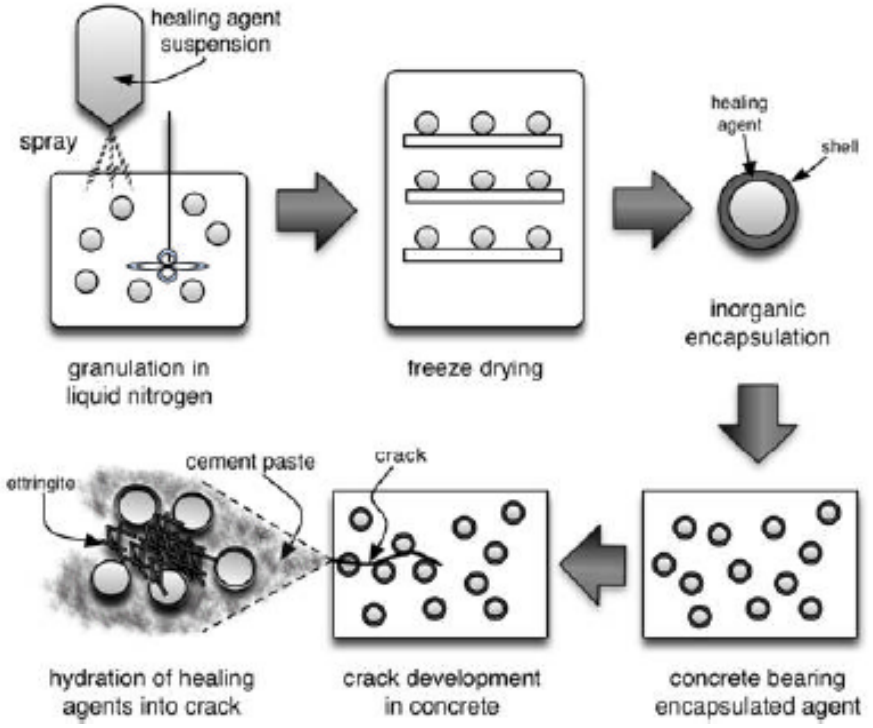


**Fig. 4.83** Concept for stages of calcium aluminate based agent encapsulation and its use in concrete [4.93]

Yuan *et al.* [4.94-4.96] proposed the use of ethylene vinyl acetate (EVA) heat-melt adhesive (Fig. 4.84) to heal cracks in concrete. Optical fibers and shape memory alloys (SMA) will be embedded in the concrete matrix together with the solid EVA particles. Once a crack is generated and detected by the optical fibers, the SMA particles will be heated by means of electrifying. When the temperature is raising higher than the martensite start temperature ($M_S$) [4.33], SMA starts to

impose compressive force onto the concrete matrix and forces the crack to close. In addition, with the increase of temperature, EVA particles will soften and melt, and then penetrate into the cracks through gravity and capillary action.

**Fig. 4.84** Ethylene vinyl acetate (EVA) particles [4.96]

Up to now the researchers tested the effect of adding EVA particles onto the properties of mortar and they determined the potential of EVA to be used as healing agent. In their experiments [4.94, 4.95] 1%, 3% and 5% of EVA particles with a particle size of ø=3 mm x 2.5 mm were added to the mortar mixture. Specimens were pre-cracked by loading them in three-point bending until 30%, 50% or 70% of their peak load. Afterwards the pre-damaged mortars were placed into a furnace for 2 days at 150°C. In order to evaluate the self-healing efficiency, the strength of EVA specimens before and after repair was compared. The damage repair rate was defined according to Eq. (4.6).

$$R = \frac{P_{strengthafterrepair}}{P_{strengthbeforepre-damage}} \text{ x100\%} \tag{4.6}$$

The strength of the pre-damaged mortar beams before and after repair is shown in Fig. 4.85a. The amount of strength regain in shown in Fig. 4.85b.

The authors concluded from Fig. 4.85 that all pre-damaged specimens were successfully repaired by using EVA particles as the flexural performance exceeded that of control intact specimens. They also concluded that the repair rate in the same pre-damage level increases with the increase in EVA content. It was noticed that due to heating of the samples containing EVA particles, the gaps between EVA particles and concrete matrix are filled improving the properties of the matrix (Fig. 4.86). Besides it was observed visually that the melted particles covered the damaged surface after heating, satisfying the need for repairing.

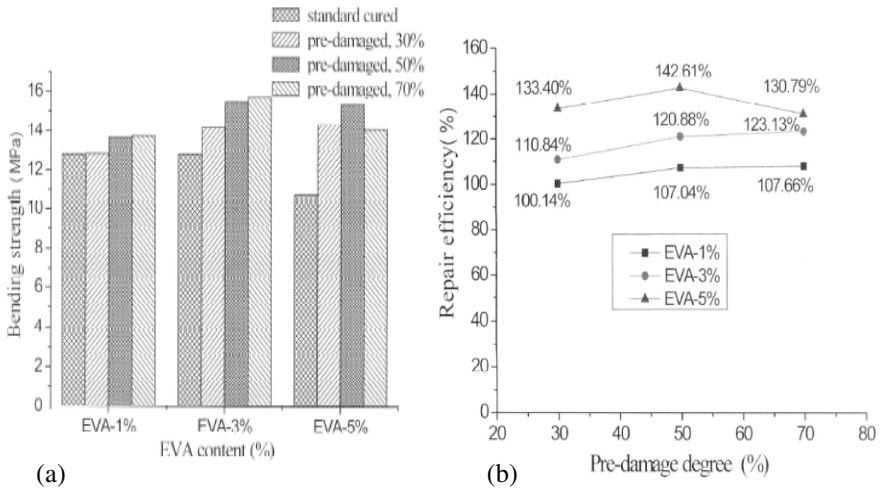


**Fig. 4.85** (a) Strength of pre-damaged samples after repair; (b) Repair efficiency of pre-damage in various degrees [4.94]

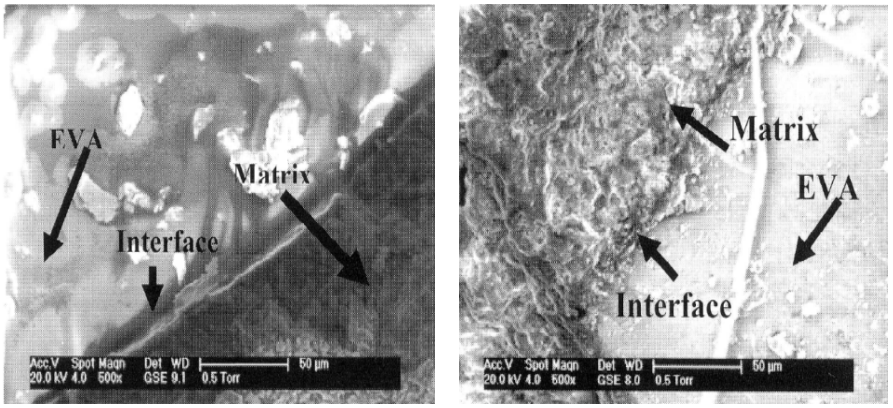


**Fig. 4.86** SEM photograph of interface between EVA and matrix of specimen before (A) and after (B) being heated for 2 days [4.94]

#### 4.2.3.3 Super Absorbent Polymers (SAP)

Kim and Schlangen [4.97, 4.98] proposed to combine engineered cementitious composites (ECC) with super absorbent polymers (SAP), which are polymeric materials which can absorb and retain extremely large amounts of liquids relative to their own mass (see Fig. 4.87). As already mentioned before, ECC cracks in narrow hairlines and therefore makes self-healing possible. However, self-healing

of cracks in ECC is only possible when the cracked specimens are stored under water. As this is not realistic for practical application, Kim and Schlangen [4.97, 4.98] proposed to mix in SAP. The water which is stored in SAP will be released during or shortly after the first hydration. When the material cracks at a later stage, no water will be left anymore. But after some rain on the structure, the SAP's located in the cracked zone are again filled and then slowly release the water for the self-healing mechanism. While Dennis Lee *et al.* [4.99, 4.100] used SAP in order to seal cracks in concrete, this research goes one step further and tries to obtain regain in mechanical properties.

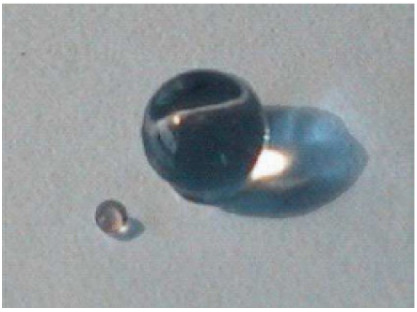

**Fig. 4.87** A dry and a swollen SAP [4.101]

Three different mix proportions were made as shown in Table 4.16. Specimens belonging to group 1 were composed according to the standard ECC mix, while specimens belonging to group 2 and 3 contained 0.5% and 1% SAP in proportion to the cement weight. ECC was cast into moulds with dimensions of 240 mm x 60 mm x 10 mm. These coupon specimens were moisture cured for 24 hours and then demoulded. After demoulding, the coupon specimens were evenly sawn into four pieces with dimensions of 120 mm x 30 mm x 10 mm.

**Table 4.16** Proportion of fibers and SAP's [4.97]

| Group | Proportion |
|---|---|
| 1 | PVA 2% |
| 2 | PVA 2% and 0.5% of SAP's |
| 3 | PVA 2% and 1% of SAP's |

Part of the specimens were loaded in four-point bending at the age of 7 days, the other part at 28 days. Half of the specimens were stored in the laboratory (approx. 5% RH and 20°C), the other half of the specimens were subjected to nine cycles of wetting and drying. Each cycle consisted of submersion in water of 20°C for 1 hour and subsequently drying in laboratory air for 3 days. This regime was used to simulate cyclic outdoor environments such as rainy days and unclouded days. Finally, specimens were loaded till failure in four-point bending. Each time

the results were compared with those of virgin specimens which were loaded till failure at the age of 7 days or 28 days. The overall testing program is depicted in Fig. 4.88.

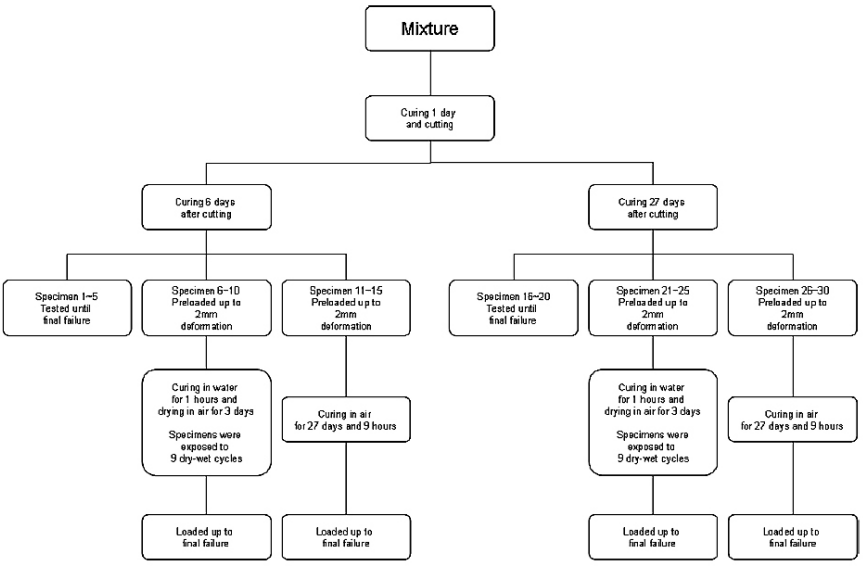


**Fig. 4.88** Loading and curing scheme [4.97]

It is seen from Fig. 4.89 that all specimens that were air cured, have a flexural stress-strain curve which has a smooth and even shape. The authors explained this by the fact that when the preloaded specimens are reloaded, there were no new cracks formed but the pre-existing cracks re-opened and extended, proving that no crack healing occurred. In contrast, the stress-strain curves obtained from the specimens that went through the wet-dry cycles of group 2 and 3 had a significant roughness and unevenness. The principle of multiple cracking in ECC-like materials lies on the assumption that, after the first crack has formed, the energy needed to let this crack grow is larger than the energy needed to form a new crack. So, the experimental results obtained in these tests could be explained by the fact that new cracks occurred because of the strength of the self-healed part was higher than the strength of the existing matrix. The specimens of group 1 (without SAP) that followed also the wet-dry cycles have again a smooth and even shape. In that case the material could not hold enough water during the wetting cycle to create any significant self-healing in the sample.

As it is shown in Table 4.17, the strength of cyclic wet-dry cured specimens exceeds the strength of the virgins in all mixtures for both cases of 35 and 56 days old. Particularly, strength recovery ratio of group 2 and 3 is higher than for the specimens of group 1. Apparently, this is also an evidence that SAP's kept the water in the cracked zone and helped the self-healing. It can be seen that the

influence of SAP is limited for air cured specimens. In case of 35 days curing the SAP still contributed because they probably helped to store a small amount of water that can be used for self-healing. However at 56 days air curing, the contribution of SAP has a negative effect.

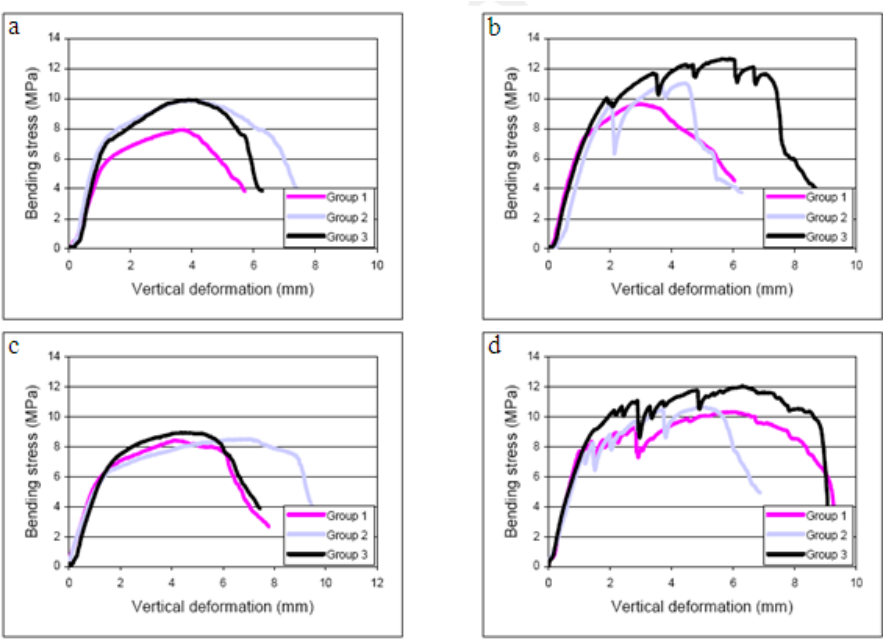


**Fig. 4.89** Reloading after 28 days in laboratory air (a and c) or 9 wet-dry cycles (b and d) of 7 days (a and b) or 28 days (c and d) cured ECC specimens [4.97]

**Table 4.17** Ultimate flexural stress and strength recovery ratio for cyclic wet-dry cured specimens and air cured specimens

| | Group 1 | | Group 2 | | Group 3 | |
|---|---|---|---|---|---|---|
| | Stress [MPa] | Recovery [%] | Stress [MPa] | Recovery [%] | Stress [MPa] | Recovery [%] |
| 7 days | 8.25 | - | 7.14 | - | 8.84 | - |
| 35 days_water cured | 9.96 | 17.17 | 9.84 | 27.44 | 11.33 | 21.98 |
| 35 days_air cured | 8.51 | 12.72 | 7.55 | 15.72 | 9.63 | 13.44 |
| 28 days | 8.37 | - | 8.63 | - | 10.24 | - |
| 56 days_water cured | 9.59 | 3.06 | 10.24 | 5.43 | 11.83 | 8.2 |
| 56 days_air cured | 8.4 | 0.36 | 8.55 | -0.94 | 8.96 | -14.29 |

Snoeck *et al.* [4.102, 4.103] performed four-point-bending tests to investigate the regain in mechanical properties upon crack healing. Table 4.18 shows the studied mortar specimens, which contained 2 vol.% of PVA fibres. Table 4.19 gives the main properties of the two types of superabsorbent polymers (SAPs) used.

**Table 4.18** Studied mortar samples with their code (n=3), m% of SAP and curing conditions [4.102]

| Specimen-Code | m% SAP | Curing |
|---|---|---|
| REF | 0 | Wet/dry cycles |
| P90 | 0 | RH > 90% |
| P60 | 0 | RH = 60% |
| A1 | 1 (SAP A) | Wet/dry cycles |
| B1 | 1 (SAP B) | Wet/dry cycles |
| B90 | 1 (SAP B) | RH > 90% |
| B60 | 1 (SAP B) | RH = 60% |
| B2 | 2 (SAP B) | Wet/dry cycles |
| B4 | 4 (SAP B) | Wet/dry cycles |

**Table 4.19** Mean diameter of SAP A and SAP B particles [µm] (n=50), absorption capacity of SAP [g fluid/g SAP] (n=3) in de-ionised water; tap water and cement slurry with standard deviations, and absorption determined in a dynamic vapour sorption test (DVS) in air of 100% RH [g moisture/g SAP]. [4.102-4.104]

| Method | SAP A | SAP B |
|---|---|---|
| Diameter | 100±22 | 477 ± 53 |
| de-ionised water (pH=6.5) | 305.0 ± 3.7 | 283.2 ± 2.4 |
| tap water (pH= 6.8) | 163.9 ± 1.2 | 148.9 ± 0.9 |
| cement slurry (pH=12.8) | 61.0 ± 1.0 | 58.4 ± 1.7 |
| Water vapour | 1.68 | 1.50 |

By performing four-point-bending tests at an age of 28 days, eight to nine small healable cracks were formed instead of a single large unhealable crack. The crack width ranged between 6-36 µm. After cracking, the specimens were stored in different curing conditions (Table 4.18). After curing, the specimens were loaded under four-point-bending to compare the mechanical properties.

Fig. 4.90 shows the first-cracking strength and the regain in first-cracking strength of the studied specimens [4.102]. The macro pores left behind by the formerly saturated SAP particles reduce the tensile strength due to a reduced

active cross section of the matrix. Samples with SAP A show a lower first-cracking strength compared to SAP B samples due to a reduced workability and the smaller particle size. A SAP B content of 1 m% relative to the cement weight gives analogous properties of the first-cracking strength compared to the REF samples without SAPs. Curing by means of SAPs has a positive influence on the amount of regain in mechanical properties. SAPs can sustain hydration by yielding their absorbed water and provide water for the precipitation of $CaCO_3$ and for the formation of new C-S-H crystals. As water is steadily provided to the matrix for healing, samples containing SAPs show more regain in mechanical properties. Furthermore, in a relative humidity of more than 90% and 60%, only samples with SAPs show partial healing. The moisture uptake by SAPs (Table 4.19) seems to be enough to promote autogenic healing in a small extent.

Fig. 4.91 shows the visual closure of all cracks after the curing period [4.103]. Results show that cracks up to 30 µm heal completely and up to 150 µm heal partly when specimens without SAP are subjected to wet/dry cycles. Storage in an environment with a relative humidity of more than 90% only showed visual closure of cracks for samples containing SAPs. SAP particles manage to take moisture out of a humid environment and provide it to the cementitious matrix for crack healing. Due to possible suction of the mortar matrix, the water is provided to the cementitious matrix. This causes autogenic healing to occur as further hydration of the unhydrated cement grains. In wet/dry cycles, cracks up to 130 µm are able to close in specimens containing SAP (Fig. 4.92). Deposition of crystals is not only due to further hydration, but mainly due to precipitation of $CaCO_3$ crystals.

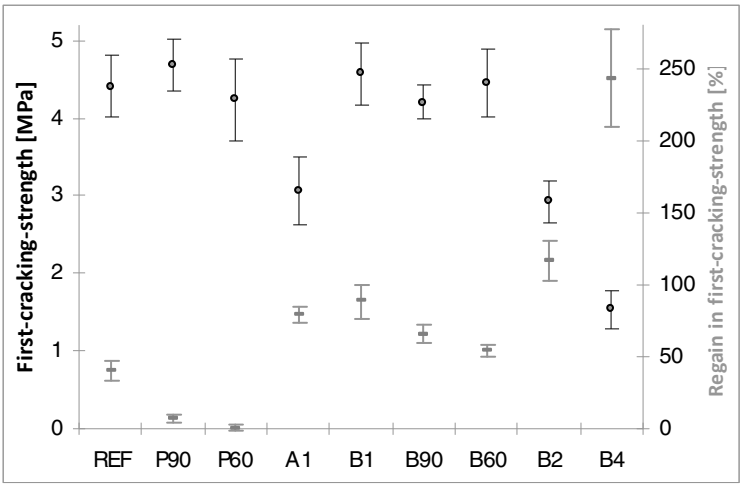


**Fig. 4.90** Mean values and standard deviations for first-cracking-strength for virgin (black, left axis) and healed specimens (grey, right axis). REF, A1, B1, B2, B4 = wet/dry cycles; P90, B90 = RH>90%; P60, B60 = RH=60%. REF, P90, P60 containing no SAP; A1 containing 1 m% of cement weight SAP A; B1, B90, B60 containing 1 m% SAP B and B2, B4 containing 2 m%, 4 m% SAP B [4.102]

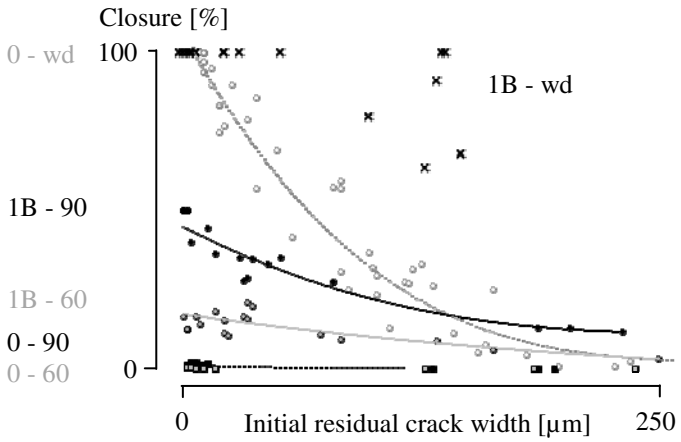


**Fig. 4.91** Closure of the cracks [%] after curing as a function of initial crack width [µm] by performing microscopic analysis [4.103]

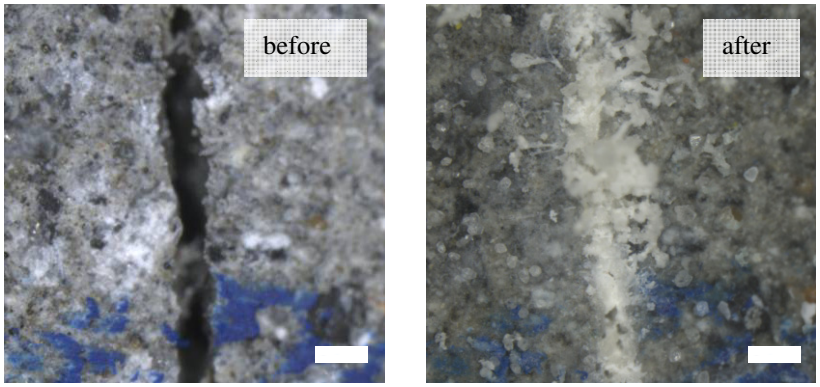


**Fig. 4.92** Total healing of a 138 µm crack of a specimen containing 1 m% SAP B after wet/dry cycles. The scale bars have a height of 200 µm [4.102].

The white product formed in the cracks was subjected to thermogravimetric analysis (TGA) [4.102]. TGA showed that the crystals consisted of $CaCO_3$ and washed out hydration products. SAP particles were not found in the TGA analysis, supporting the conclusion that SAPs effectively seal the crack without dissolving or degrading.

The autogenic healing also occurred when flax fibres were used [4.105].

To prevent leaching of the water absorbed by the SAP particles during cement hydration, and hence, to prevent loss of the autogenous healing capacity, Xia [4.102] coated swollen SAP particles with paraffin wax. Before the paraffin could be applied on the SAP core, an extra shell of cement powder was needed.

As the initial swelling of SAP particles during concrete mixing causes the formation of pores and thus a reduction in strength, Lopez-tendero *et al.* [4.107]

tried to modify the polymers so they only swell at reduced pH level (Fig. 4.93). During concrete mixing the pH is around 13, preventing swelling of the SAP.

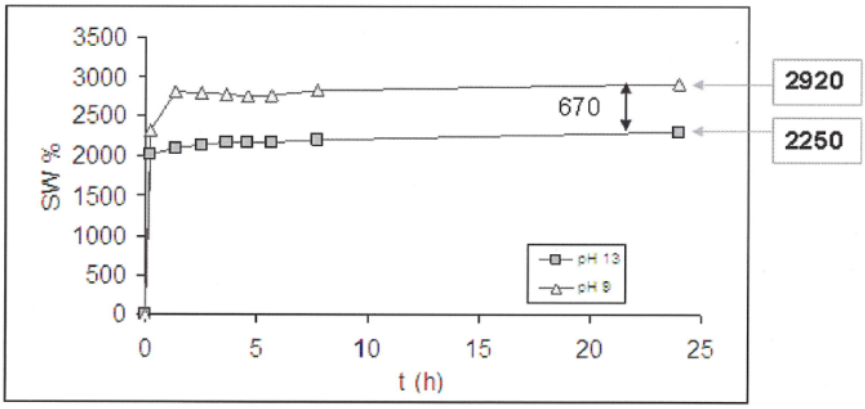


**Fig. 4.93** Swelling kinetics for the hydrogel in pH 13 and 9 buffered solutions [4.107]

In their research, Reddy and Liang [4.108] searched for a mechanism to make oil well cements watertight. They mentioned that the sealing efficiency of SAP particles depends on contacting the right type of fluid. Therefore, they preferred to use elastomers with low glass transition temperature, low melting point or low solid to liquid phase transition temperature or those which show cold flow, allowing fractured samples to self-heal without requiring contact with any type of fluid. In their research, elastomeric materials were chemically modified to contain functional groups, particularly carboxylate groups, that are capable of bonding not only to cement surfaces but also to the metal casing used in oil wells. The flow rate through separated cement pieces reduced upon heating showing the efficiency of this technique.

## References

4.1. Taylor, H.F.W.: Cement chemistry, p. 475. Academic Press, San Diego (1990)
4.2. Abd-Elmoaty, A.-E.: Self-healing of polymer modified concrete. Alexandria Engineering Journal 50(2), 171–178 (2011)
4.3. Edvardsen, C.: Water permeability and autogenous healing of cracks in concrete. ACI Materials Journal 96(4), 448–454 (1999)
4.4. Jacobsen, S., Marchand, J., Hornain, H.: SEM observations of the microstructure of frost deteriorated and self-healed concretes. Cement and Concrete Research 25(8), 1781–1790 (1995)
4.5. Reinhardt, H.-W., Jooss, M.: Permeability and self-healing of cracked concrete as a function of temperature and crack width. Cement and Concrete Research 33(7), 981–985 (2003)

4.6. Li, V.C., Yang, E.H.: Self-healing in concrete materials. In: van der Zwaag, S. (ed.) Self-healing Materials: An Alternative Approach to 20 Centuries of Materials Science, pp. 161–193. Springer, Dordrecht (2007)
4.7. Li, V.C., Lim, Y.M., Chan, Y.-W.: Feasibility study of a passive smart self-healing cementitious composite. Composites Part B: Engineering 29(6), 819–827 (1998)
4.8. Ying-zi, Y., Lepech, M.D., Li, V.C.: Self-healing of engineered cementitious composites under cyclic wetting and drying. In: International Workshop on Durability of Reinforced Concrete under Combined Mechanical and Climatic Loads (CMCL), Qindao, China, pp. 231–242 (2005)
4.9. Ahmaran, M., Li, V.C.: Durability properties of micro-cracked ECC containing high volumes fly ash. Cement and Concrete Research 39(11), 1033–1043 (2009)
4.10. Yang, Y., Yang, E.-H., Li, V.C.: Autogenous healing of engineered cementitious composites at early age. Cement and Concrete Research 41(2), 176–183 (2011)
4.11. Li, M., Li, V.C.: Cracking and healing of engineered cementitious composites under chloride environment. ACI Materials Journal 108(3), 333–340 (2011)
4.12. Li, M., Sahmaran, M., Li, V.C.: Effect of cracking and healing on durability of engineered cementitious composites under marine environment. In: Reinhardt, H.W., Naaman, A.E. (eds.) Conference on High Performance Fiber Reinforced Cement Composites (HPFRCC 5), Mainz, Germany, pp. 313–322 (2007)
4.13. Li, V.C.: On engineered cementitious composites (ECC): A review of the material and its applications. Journal of Advanced Concrete Technology 1(3), 215–230 (2003)
4.14. Homma, D., Mihashi, H., Nishiwaki, T.: Self-healing capability of fibre reinforced cementitious composites. Journal of Advanced Concrete Technology 7(2), 217–228 (2009)
4.15. Koda, M., et al.: Self-healing capability of fibre reinforced cementitious composites. In: International Conference on Advances in Construction Materials through Science and Engineering, Hong Kong, China (2011)
4.16. Lepech, M.D., Li, V.C.: Water permeability of engineered cementitious composites. Cement and Concrete Composites 31(10), 744–753 (2009)
4.17. Homma, D., et al.: Experimental study on the self-healing capability of fiber reinforced cementitious composites. In: 7th RILEM International Symposium on Fibre Reinforced Concrete: Design and Applications, pp. 769–774. RILEM, Chennai (2008)
4.18. Yang, Y., et al.: Autogenous healing of engineered cementitious composites under wet-dry cycles. Cement and Concrete Research 39(5), 382–390 (2009)
4.19. Yamamoto, A., Kan, L.-L., Li, V.C.: Self-healing behaviour of engineered cementitious composites under different number of wet-dry cycle. In: 11th International Summer Symposium of the Japan Society of Civil Engineers, Tokyo, Japan, pp. 1–4 (2009)
4.20. Kan, L.-L., et al.: Self-healing characterization of engineered cementitious composites (ECC) materials. ACI Materials Journal 107(6), 619–626 (2010)
4.21. Qian, S., et al.: Self-healing behavior of strain hardening cementitious composites incorporating local waste materials. Cement and Concrete Composites 31(9), 613–621 (2009)

4.22. Sahmaran, M., Li, V.C.: Deicing salt scaling resistance of mechanically loaded engineered cementitious composites. Cement and Concrete Research 37(7), 1035–1046 (2007)
4.23. Sahmaran, M., Lachemi, M., Li, V.C.: Assessing the durability of engineered cementitious composites under freezing and thawing cycles. Journal of ASTM International 6(7), 1–13 (2009)
4.24. Bensted, J.: Uses of raman spectroscopy in cement chemistry. Journal of the American Ceramic Society 59(3-4), 140–143 (1976)
4.25. Termkhajornkit, P., et al.: Self-healing ability of fly ash-cement systems. Cement and Concrete Composites 31(3), 195–203 (2009)
4.26. Granger, S., et al.: Mechanical characterization of the self-healing effect of cracks in Ultra High Performance Concrete (UHPC). In: 3rd International Conference of Construction Materials, Performance, Innovations and Structural Implications, Vancouver, Canada (2005)
4.27. Granger, S., et al.: Self-healing of cracks in concrete: from a model material to usual concretes. In: Marchand, J., et al. (eds.) 2nd International RILEM Symposium on Advances in Concrete through Science and Engineering. RILEM Publications SARL, Quebec (2006)
4.28. Morimoto, T., et al.: Self-healing properties of Ultra High Performance Strain Hardening Cementitious Composites (UHP-SHCC). In: 4th International Conference on Construction Materials, Nagoya, Japan, pp. 319–326 (2009)
4.29. Schlangen, E., ter Heide, N., van Breugel, K.: Crack healing of early age cracks in concrete. In: ECF 16, Alexandroupolis, Greece, pp. 1–8 (2006)
4.30. ter Heide, N., Schlangen, E., van Breugel, K.: Experimental study of crack healing of early age cracks. In: Knud Hojgaard Conference on Advanced Cement-based Materials, Denmark, pp. 1–11 (2005)
4.31. ter Heide, N., Schlangen, E.: Self-healing of early age cracks in concrete. In: van der Zwaag, S. (ed.) 1st International Conference on Self-healing Materials, p. 81. Springer, Noordwijk aan Zee (2007)
4.32. Abdel-Jawad, Y., Dehn, F.: Self-healing of self-compacting concrete. In: SCC 2005 Conference, Orlando, Florida, USA, pp. 1023–1029 (2005)
4.33. Sakai, Y., et al.: Experimental study on enhancement of self-restoration of concrete beams using SMA wire. In: Liu, S.-C. (ed.) Conference on Smart Structures and Materials, San Diego, California, pp. 178–186 (2003)
4.34. Kuang, Y., Ou, J.: Self-repairing performance of concrete beams strengthened using superlastic SMA wires in combination with adhesives released from hollow fibers. Smart Materials and Structures 17, 1–7 (2008)
4.35. Kuang, Y., Ou, J.: Passive smart self-repairing concrete beams by using shape memory alloy wires and fibers containing adhesives. Journal of Central South University Technology 15, 411–417 (2008)
4.36. Isaacs, B., et al.: Enhancement of self-healing in cementitious materials, post-tensioned with shrinkable polymers. In: White, S., Bond, I. (eds.) 2nd International Conference on Self-healing Materials, Chicago, USA, p. 102 (2009)

4.37. Isaacs, B., et al.: Enhancement of self-healing in cementitious materials. In: Bond, I., Varley, R. (eds.) 3rd International Conference on Self-healing Materials, Bath, UK, pp. 119–120 (2011)
4.38. Lark, R.J., et al.: Active confinement of cementitious composites with shape memory plastics. In: 2nd International Conference on Self-healing Materials, Chicago, USA, p. 138 (2009)
4.39. Joseph, C., et al.: Experimental investigation of adhesive-based self-healing of cementitious materials. Magazine of Concrete Research 62(11), 831–843 (2010)
4.40. Jefferson, A., et al.: A new system for crack closure of cementitious materials using shrinkable polymers. Cement and Concrete Research 40(5), 795–801 (2010)
4.41. Lark, R.J., Jefferson, A.D., Joseph, C., Dunn, S., Isaacs, B.: Active Confinement of Cementitious Composites with Shape Memory Plastics. In: Proceedings of Seond International Conference on Self- Healing Materials, Chicago (2009)
4.42. Jefferson, A., et al.: A new system for crack closure of cementitious materials using shrinkable polymers. Cement and Concrete Research 40(5), 795–801 (2010)
4.43. Isaacs, B., Lark, R.J., Jefferson, A.D., Joseph, C., Dunn, S.: Autogenous healing in SMP cementitious material system. Magazine of Concrete Research (Sumitted for publication)
4.44. Bornert, M., et al.: Assessment of digital image correlation measurement errors: methodology and results. Experimental Mechanics 49(3), 353–370 (2009)
4.45. Dry, C.: Smart multiphase composite materials that repair themselves by a release of liquids that become solids. In: Symposium on Smart Structures and Materials, Orlando, Florida, pp. 62–70 (1994)
4.46. Dry, C.: Matrix cracking repair and filling using active and passive modes for smart timed release of chemicals from fibers into cement matrices. Smart Materials and Structures 3(2), 118–123 (1994)
4.47. Dry, C.: Smart earthquake resistant materials (using time released adhesives for damping, stiffening, and deflection control). In: 3rd ICIM/ECSSM, Lyon, France, pp. 958–967 (1996)
4.48. Dry, C.: Improvement in reinforcing bond strength in reinforced concrete with self-repairing chemical adhesives. In: SPIE, pp. 44–50 (1997)
4.49. Thao, T.D.P., Johnson, T.J.S., Tong, Q.S., Dai, P.S.: Implementation of selfhealing in concrete - Proof of concept. The IES Journal Part A: Civil & Structural Engineering 2(2), 116–125 (2009)
4.50. Pang, S.D., Tran Diep, P.T., Quek, S.T.: On implementation of self-healing function in concrete - Proof of concept and practical issues. In: White, S., Bond, I. (eds.) 2nd International Conference on Self-healing Materials, Chicago, USA, p. 119 (2009)
4.51. Pang, S.D., Tran Diep, P.T., Quek, S.T.: Self-healing concrete structural elements. In: Bond, I., Varley, R. (eds.) 3rd International Conference on Self-healing Materials, Bath, UK, pp. 322–323 (2011)
4.52. Dry, C., McMillan, W.: Three-part methylmethacrylate adhesive system as an internal delivery system for smart responsive concrete. Smart Materials and Structures 5(3), 297–300 (1996)

4.53. Van Tittelboom, K., De Belie, N.: Self-healing concrete: suitability of different healing agents. International Journal of 3R's 1(1), 12–21 (2010)
4.54. Van Tittelboom, K., De Belie, N.: Self-healing concrete by the internal release of adhesive from hollow glass tubes embedded in the matrix. In: 2nd International Conference on Self-healing Materials, Chicago, USA, p. 101 (2009)
4.55. Van Tittelboom, K., De Belie, N.: Self-healing concrete by means of encapsulated polymers. In: 13th International Conference on Polymers in Concrete, Madeira, pp. 681–688 (2010)
4.56. Van Tittelboom, K., Van Loo, D., De Belie, N., Jacobs, P.: Evaluation of the efficiency of selfhealing in concrete by means of micro-CT. In: 3rd International Workshop on X-ray CT for Geomaterials, New Orleans, pp. 132–139 (2010)
4.57. Dry, C.: Repair and prevention of damage due to transverse shrinkage cracks in bridge decks. In: Liu, S.-C. (ed.) Symposium on Smart Structures and Materials, pp. 253–256 (1999)
4.58. Dry, C.: Three designs for the internal release of sealants, adhesives, and waterproofing chemicals into concrete to reduce permeability. Cement and Concrete Research 30(12), 1969–1977 (2000)
4.59. de Rooij, M.R., et al.: Using natural wood fibers to self heal concrete. In: Alexander, M.G., et al. (eds.) 2nd International Conference on Concrete Repair, Rehabilitation and Retrofitting, Cape Town, South Africa, pp. 229–233 (2008)
4.60. Liu, H., et al.: Self-healing of concrete cracks using hollow plant fibres. In: 2nd International Conference on Self-healing Materials, Chicago, USA, p. 189 (2009)
4.61. Cailleux, E., Pollet, V.: Investigations on the development of self-healing properties in protective coatings for concrete and repair mortars. In: 2nd International Conference on Self-healing Materials, Chicago, USA, p. 120 (2009)
4.62. Huang, H., Ye, G.: Application of sodium silicate solution as self-healing agent in cementitious materials. In: International Conference on Advances in Construction Materials through Science and Engineering, Hong Kong, China (2011)
4.63. Pelletier, M., et al.: Self-healing concrete with a microencapsulated healing agent (2010)
4.64. Mihashi, H., et al.: Fundamental study on development of intelligent concrete characterized by selfhealing capability for strength. Transactions of the Japan Concrete Institute 22, 441–450 (2000)
4.65. Feng, X., et al.: Self-healing mechanism of a novel cementitious composite using microcapsules. In: International Conference on Durability of Concrete Structures, Hangzhou, China, pp. 195–204 (2008)
4.66. Kaltzakorta, I., Erkizia, E.: Silica microcapsules encapsulating epoxy compounds for self-healing cementitious materials. In: 3rd International Conference on Self-healing Materials, Bath, UK, pp. 271–272 (2011)
4.67. Yang, Z., et al.: Laboratory assessment of a self-healing cementitious composite. Journal of the Transportation Research Board (2142), 9–17 (2010)
4.68. Yang, Z., et al.: A self-healing cementitious composite using oil core/silica gel shell microcapsules. Cement and Concrete Composites 33(4), 506–512 (2011)

4.69. Joseph, C., Jefferson, A.D., Canoni, M.B.: Issues relating to the autonomic healing of cementitious materials. In: Van der Zwaag, S. (ed.) 1st International Conference on Self-healing Materials, Noordwijk aan Zee, The Netherlands, p. 53 (2007)
4.70. Joseph, C., Jefferson, A.D., Isaacs, B., Lark, R.J., Gardner, D.R.: Adhesive based self-healing of cementitious materials. In: Proceedings of 2nd International Conference on Self-healing Materials, Chicago (2009)
4.71. Joseph, C., Gardner, D.R., Jefferson, A.D., Lark, R.J., Isaacs, B.: Self-healing Cementitious Materials: A review of recent work. In: Proceedings of the ICE: Construction Materials (2009)
4.72. Mihasi, H., Kaneko, Y., Nishiwaki, T., Otsuka, K.: Fundamental study on development of intelligent concrete characterized by self-healing capability for strength. Transactions of the Japan Concrete Institute 22, 441–450 (2000)
4.73. Dry, C., Corsaw, M.: A comparison of bending strength between adhesive and steel reinforced concrete with steel only reinforced concrete. Cement and Concrete Research 33(11), 1723–1727 (2003)
4.74. Dry, C.: Use of embedded self-repair adhesives in certain areas of concrete bridge members to prevent failure from severe dynamic loading. In: Conference on Smart Materials Technologies, Newport Beach, California, pp. 126–130 (1999)
4.75. Dry, C.: Release of smart chemicals for the in-service repair of bridges and roadways. In: Aatre, V.K., Varadan, V.K., Varadan, V.V. (eds.) Symposium on Smart Materials, Structures, and MEMS, San Diego, California, pp. 140–144 (1998)
4.76. Dry, C.: Design of self-growing, self-sensing, and self-repairing materials for engineering applications. In: Wilson, A.R., Asanuma, H. (eds.) Smart Materials Conference, pp. 23–29 (2001)
4.77. Pareek, S., Oohira, A.: A fundamental study on regain of flexural strength of mortars by using a self-repair network system. In: 3rd International Conference on Self-healing Materials, Bath, UK, pp. 46–47 (2011)
4.78. Sangadji, S., Schlangen, E.: Feasibility and potential of prefabricated porous concrete as a component to make concrete structures self-healing. In: International Conference on Advances in Construction Materials through Science and Engineering, Hong Kong, China (2011)
4.79. Sangadji, S., Schlangen, E.: Porous network concrete: a new approach to make concrete structures self-healing using prefabricated porous layer. In: Bond, I., Varley, R. (eds.) 3rd International Conference on Self-healing Materials, Bath, UK, pp. 291–292 (2011)
4.80. Ludirdja, D., Berger, R.L., Young, J.F.: Simple method for measuring water permeability of concrete. ACI Materials Journal 86(5), 433–439 (1989)
4.81. Nishiwaki, T., et al.: Development of self-healing system for concrete with selective heating around crack. Journal of Advanced Concrete Technology 4(2), 267–275 (2006)
4.82. Nishiwaki, T., et al.: Development of smart concrete with self-healing system using selective heating device. In: 5th International Conference on Concrete under Severe Conditions Environment and Loading, Tours, France, pp. 665–672 (2007)

4.83. Nishiwaki, T., et al.: Smart concrete system with strain monitoring sensors including conductive particles. In: Marchand, J., et al. (eds.) 2nd International RILEM Symposium on Advances in Concrete through Science and Engineering, Quebec, Canada (2006)
4.84. Nishiwaki, T., Oohira, A., Pareek, S.: An experimental study on the application of self-repairing system to RC structures using selective heating. In: Bond, I., Varley, R. (eds.) 3rd International Conference on Self-healing Materials, Bath, UK, pp. 320–321 (2011)
4.85. Nishiwaki, T., de B. Leite, J.P., Mihashi, H.: Enhancement in durability of concrete structures with use of high-performance fibre reinforced cementitious composites. In: 4th International Conference on Concrete under Severe Conditions: Environment & Loading, pp. 1524–1531 (2004)
4.86. Katsuhata, T., Ohama, Y., Demura, K.: Investigation of microcracks self-repair function of polymermodified mortars using epoxy resins without hardeners
4.87. Ohama, Y., Demura, K., Endo, T.: Strength properties of epoxy-modified mortars without hardener. In: 9th International Congress on the Chemistry of Cement, New Delhi, India, pp. 512–516 (1992)
4.88. Ahn, T.H., Kishi, T.: The effect of geo-materials on the autogneous healing behaviour of cracked concrete. In: Alexander, M.G., Beushausen, H.-D., Dehn, F., Moyo, P. (eds.) Concrete Repair, Rehabilitation and Retrofitting II, London, pp. 235–240 (2009)
4.89. Ahn, T.H., Kishi, T.: Crack healing behaviour of cementitious composite materials incorporating geo-materials. In: White, S., Bond, I. (eds.) 2nd International Conference on Self-healing Materials, Chicago, USA, p. 100 (2009)
4.90. Ahn, T.H., Kishi, T.: Crack self-healing behaviour of cementitious composites incorporating various mineral admixtures. Journal of Advanced Concrete Technology 8(2), 171–186 (2010)
4.91. Sisomphon, K., Copuroglu, O.: Self-healing mortars by using different cementitious materials. In: International Conference on Advances in Construction Materials through Science and Engineering, Hong Kong, China (2011)
4.92. Sisomphon, K., Copuroglu, O., Koenders, E.A.B.: Surface crack self-healing behaviour of mortars with expansive additives. In: Bond, I., Varley, R. (eds.) 3rd International Conference on Self-healing Materials, Bath, UK, pp. 44–45 (2011)
4.93. Copuroglu, O., Sisomphon, K., Komatsu, S.: Self-healing of cement paste by calcium aluminate based agents. In: White, S., Bond, I. (eds.) 2nd International Conference on Self-healing Materials, Chicago, USA (2009)
4.94. Yuan, X.Z., et al.: Experimental research on the crack self-healing properties of cement mortar with EVA heat-melt adhesive. In: International RILEM Conference on Material Science, Aachen, Germany, pp. 433–442 (2010)
4.95. Yuan, X.-Z., et al.: The crack self-healing properties of cement-based material with EVA heat-melt adhesive. Journal of Wuhan University of Technology - Materials Science Edition 26(4), 774–779 (2011)
4.96. Yuan, X.-Z., Sun, W., Zuo, X.-B.: Study of feasibility of heat melt adhesive being used in crack self-healing of cement-based materials. Applied Mechanics and Materials 99-100, 1087–1091 (2011)

4.97. Kim, J.S., Schlangen, E.: Super absorbent polymers to stimulate self-healing in ECC. In: 2nd International Symposium on Service Life Design for Infrastructure, Delft, The Netherlands (2010)
4.98. Kim, J.S., Schlangen, E.: Self-healing in ECC stimulated by SAP under flexural cyclic load. In: Bond, I., Varley, R. (eds.) 3rd International Conference on Self-healing Materials, Bath, UK, pp. 324–325 (2011)
4.99. Dennis Lee, H.X., Wong, H.S., Buenfeld, N.: Self-sealing cement-based materials using superabsorbent polymers. In: Jensen, O.M., Hasholt, M.T., Laustsen, S. (eds.) International RILEM Conference on Use of Superabsorbent Polymers and Other New Additives in Concrete, pp. 171–178. RILEM Publications s.a.r.l, Lyngby (2010)
4.100. Lee, H.X.D., Wong, H.S., Buenfeld, N.R.: Potential of superabsorbent polymer for selfsealing cracks in concrete. Advances in Applied Ceramics 109(5), 296–302 (2010)
4.101. Jensen, O.M., Hansen, P.F.: Water-entrained cement-based materials: I. Principles and Theoretical Background. Cement and Concrete Research 31(4), 647–654 (2001)
4.102. Snoeck, D., et al.: Self-healing cementitious materials by the combination of microfibres and superabsorbent polymers. Journal of Intelligent Material Systems and Structures (2012)
4.103. Snoeck, et al.: The use of superabsorbent polymers as a crack sealing and crack healing mechanism in cementitious materials. In: 3rd International Conference on Concrete Repair, Rehabilitation and Retrofitting, Cape Town, pp. 152–157 (2012)
4.104. Snoeck, D., et al.: Visualization of water penetration in cementitious materials with superabsorbent polymers by means of neutron radiography. Cement and Concrete Research 42, 1113–1121 (2012)
4.105. Snoeck, D., De Belie, N.: Mechanical and self-healing properties of cementitious composites reinforced with flax and cottonised flax, and compared with polyvinyl alcohol fibres. Biosystems Engineering 111, 325–335 (2010)
4.106. Xia, H.: Self-healing of engineered cementitious composites (ECC) in concrete repair system. Delft Univeristy of Technology, Delft (2010)
4.107. Lopez-tendero, M.J., et al.: Optimized hydrogel for application as repairing agents in cement based products. In: Bond, I., Varley, R. (eds.) 3rd International Conference on Self-healing Materials, Bath, UK, p. 160 (2011)
4.108. Reddy, B.R., Liang, F.: Self-healing cement compositions for use in oil field applications. In: White, S., Bond, I. (eds.) 2nd International Conference on Self-healing Materials, Chicago, USA, p. 163 (2009)

# 5 Modelling of Self-Healing Cementitious Materials

E. Schlangen[1] and C. Joseph[2]

[1] Microlab, Delft University of Technology, The Netherlands
H.E.J.G.Schlangen@tudelft.nl
[2] Cardiff School of Engineering, Cardiff University, United Kingdom

## 5.1 Introduction

Self-healing, especially the autonomic one with engineered additions to promote self-healing, is still a young research topic. During the past decade the amount of research performed progressed very rapidly. However, the publications that can be found mainly focus on experimental work and modelling is still limited. In this chapter the state of the art on modelling is given. Most work is related to experimental work described in the previous chapters. The models described in section 5.2 deal with self-healing mechanisms that make use of embedded tubes containing healing agents and is based on the work of Joseph [5.1]. Section 5.3 describes modelling techniques to study autogenic self-healing of concrete on the macro-level, mainly due to on-going hydration and focusing on cracks in the early age of hydration. This work is based on the work of Schlangen *et al.* [5.2]. Section 5.4 describes models that can be used to study self-healing of fibre reinforced materials. Some analytical models to study the self-healing probability of cementitious materials containing encapsulated materials are presented. Here it is focused on the amount and size of capsules needed to obtain complete crack filling. Finally, section 5.6 deals with self-healing due to on-going hydration of cement paste and models to study this phenomenon on the micro-scale.

## 5.2 Lattice Modelling for Concrete with Tubular Encapsulation

For the modelling of cracks, a lattice type model is used by Joseph which is described in detail in [5.1]. Cracks are modelled discretely in the lattice approach, crack openings are therefore determined automatically. For a notched beam tested under three-point loading the CMOD may therefore be obtained directly from the model. The value of the CMOD can therefore be used as the criterion for governing the breakage of the glass capillary tubes, and hence the onset of healing. Once the capillary tubes have broken, it is assumed that the flow of the adhesive is controlled by the varying aperture of the crack at that location.

Glue setting may then be modelled in a staged manner whereby broken beams are replaced with ‘healed’ beams at predefined CMOD limits. The height of glue rise, and therefore, determination of which broken beams are to be healed, is

M. de Rooij et al. (Eds.): *Self-Healing Phenomena in Cement-Based Materials*, RILEM 11, pp. 217–240.
DOI: 10.1007/978-94-007-6624-2_5 

obtained from the non-uniform capillary flow theory described in the next sections. The healed beams are considered to be composite beams comprising part mortar and part glue. The axial stiffness of these composite beams is therefore determined from the axial stiffness of the mortar part and the glue part combined in series. The length of the glue part is determined by the width of the crack opening at the beam location just prior to healing. The same principle of modelling could also be adopted in other self-healing concepts using embedded long or short tubes described in the previous chapters.

### 5.2.1 Healing Algorithm in 1D

The numerical algorithm, as outlined above, is illustrated schematically in Fig. 5.1 for the simple case of a 1D parallel bar model comprising two elements supported between two rigid bar supports. The support bar on the left is fully fixed and the one on the right is only allowed to translate in the x-direction. The elements have identical stiffness ($k_1=k_2$), but the tensile strength of element 1 is less than that of element 2 ($ft_1<ft_2$).

The system is initially subjected to a prescribed displacement ($u_p$), and resists this displacement with a stiffness, $k$ ($k=k_1+k_2$), as illustrated by line (i) in Fig. 5.1(b). When the stress in element 1 reaches its tensile strength ($ft_1$), element 1 breaks and its stiffness is removed from the system. The difference in the distance between the supports and the unstrained length of element 1 is defined as the crack mouth opening displacement (CMOD) for this simple 1D model.

As the prescribed displacement ($u_p$) increases further, the CMOD increases by the same amount. The stiffness of the system at this point is $k=k_2$ as represented by the gradient of line (ii) in Fig. 5.1(b). When the value of the CMOD reaches the predefined level of healing (CMOD 1 in Fig. 5.1(b)), element 1 is considered healed. This involves replacement of the element with a new composite mortar/glue element. The new composite element is therefore considered as comprising two springs in series. The axial stiffness of this element ($k'_1$) is given by Eq. (5.1).

$$k'_1 = \left(k_m^{-1} + k_g^{-1}\right)^{-1} \tag{5.1}$$

where $k_m$ is the axial stiffness of the mortar part, and $k_g$ is the axial stiffness of the glue part, as given by:

$$k_m = \frac{E_m A_m}{L_m} \tag{5.2}$$

and

$$k_g = \frac{E_g A_g}{L_g} \tag{5.3}$$

where $E_m$, $E_g$, $A_m$, $A_g$, $L_m$ and $L_g$ are the Young's modulus, cross-sectional area and length of the mortar and glue parts respectively.

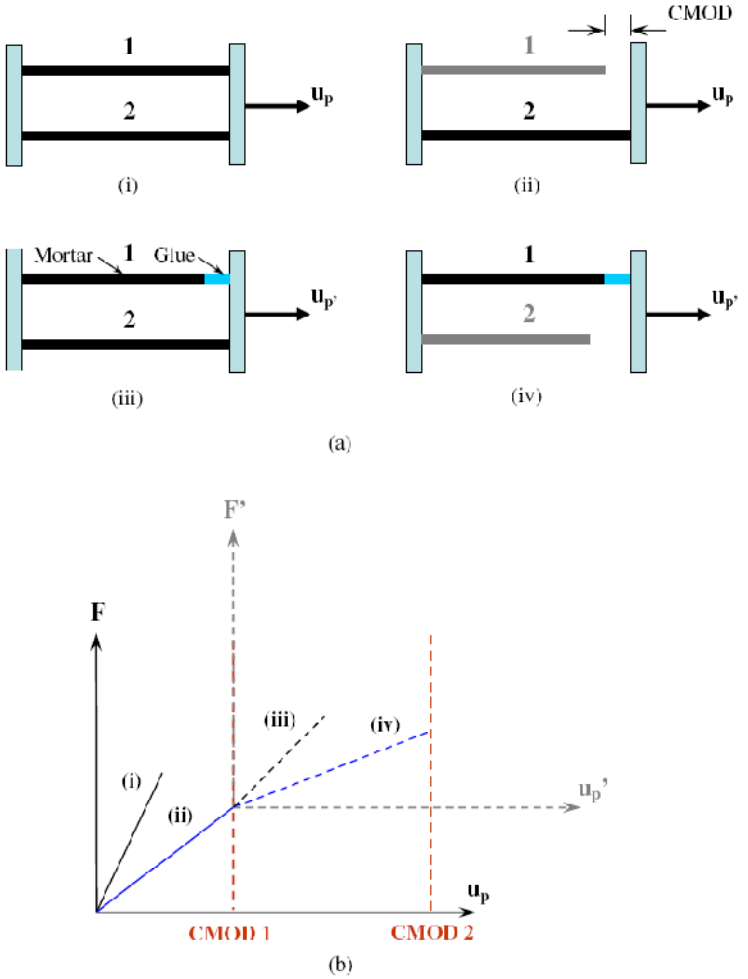


**Fig. 5.1** Schematic illustration of (a) healing process in a 1D parallel bar model, and (b) mechanical response of model pre- and post-healing

$L_m$ is taken to be the original unstrained length of element 1 and $L_g$ is taken to be the CMOD value at the point of healing. Therefore, the adhesive is assumed to completely fill the crack at the time of healing. The stiffness of the system now becomes $k=k'_1+k_2$, as given by (iii) in Fig. 5.1(b). It should be noted that the gradient of line (iii) is less than line (i) since $E_g < E_m$, and therefore $k'_1 < k_1$. It should also be noted that the origin of the force-displacement response has been reset to the value of these variables ($CMOD_1$, $F_{CMOD1}$) at the point of healing. This is necessary in order to achieve an unstrained state in the new composite element prior to subsequent loading of the system.

Finally, the prescribed displacement is increased further until the axial stress in element 2 equals the failure strength ($f_{t2}$), and the element breaks. The stiffness of the system from this point onwards is then given by $k= k'_1$, as depicted by line (iv) in Fig. 5.1(b). Due to resetting of the origin at the point of healing the total displacement of, and force within, the system during stage (iv) is given by:

$$u_p = CMOD_1 + u_p^* \tag{5.4}$$

and

$$F = F_{CMOD_1} + F^* \tag{5.5}$$

### 5.2.2 Extension of Healing Algorithm to 2D

The 1D healing theory, as explained above, may be extended for use in a 2D lattice simulation. In this respect, element 1 can be considered to represent the group of beams that initially break and are subsequently healed when the CMOD reaches the predefined healing point. Element 2 can then be considered to represent the group of elements that break after healing, when the specimen is tested to failure.

The point at which healing occurs (CMOD 1) takes on a physical meaning in the two dimensional case. In the 2D model CMOD 1 is the value of the CMOD when the capillary tubes are said to have broken and healing is considered to have begun. It should be noted that CMOD 1 is a predefined value and is based on the average CMOD value at which the capillary tubes are heard to break during the experiments. At the point at which healing is considered to occur and the selected broken beams are healed, the value of the crack opening at the location of the broken beams varies depending on the location of the beam. The width of the opening, which is also the length of the glue segment in the composite healed element, is therefore defined as the difference between the extended length of the original stressed beam (assuming that it never broke) and the length of the original unstressed beam element. The length of the glue part ($L_g$) in the composite elements is therefore far less for elements healed at the crack tip during stage (iv) (Fig. 5.1(b)) than at the bottom of the crack just above the notch. The healed

composite elements at the bottom of the crack are therefore less stiff than those at the crack tip. This is because a greater $L_g$ results in lower stiffness for the glue segment $k_g$ and for the beam as a whole $k_I'$, as shown by Eq (5.1) and (5.3).

It should be noted that the 1D methodology described above when applied to a 2D lattice simulation can be extended to allow for multiple healing events at a range of predefined CMOD values. The nodal displacements would have to be zeroed at every healing point in order to ensure that the newly healed elements are unstrained at each point of healing. The nodal displacement values and system forces recorded prior to each healing point could then be summed, as shown for the 1D case in Eq. (5.4) and (5.5), to obtain the overall mechanical response of the system. In essence this procedure means that the overall nonlinear mechanical response of the system can be modelled as a series of linear simulations.

### 5.2.3 Glue Flow Theory

When the borosilicate glass tubes break the adhesive is free to flow into the crack. This occurs in a downward and upward direction. In both the downward and upward directions, the capillary attractive force of the narrow crack draws the adhesive out of the tubes. In the downward direction this is assisted by gravity, and conversely in the upward direction gravity resists the flow of adhesive. The main forces acting on the adhesive following the cracking of the tubes are illustrated in Fig. 5.2. For the purpose of this model the adhesive is assumed to migrate fully in the downward direction, and therefore all fractured lattice elements situated below the level of the tubes are automatically healed. This assumption is consistent with experimental evidence of free glue flow out of the bottom of the beam shortly following the cracking of the tubes.

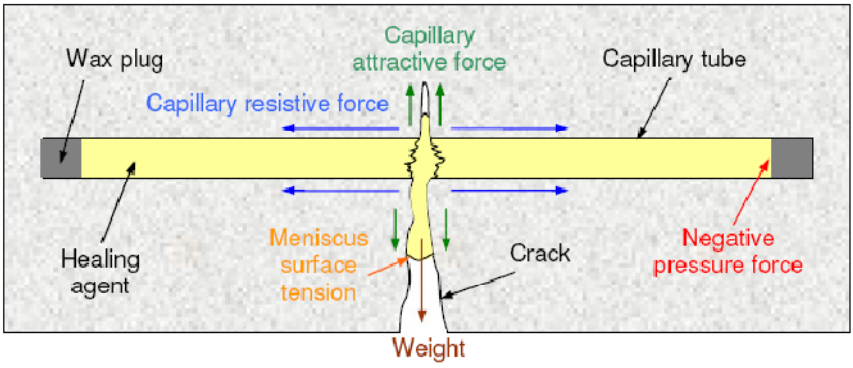


**Fig. 5.2** Schematic illustration of the main forces acting on an internally encapsulated healing agent

In order to model the flow of adhesive in the upward direction, however, the balance of capillary and gravitational effects must be considered. The approach utilised within this model is therefore based on capillary flow theory through non-uniform sections [5.3] and is similar to that employed by [5.4] for modelling moisture flow in discrete cracks in building materials. This involves using a 1D moving front model in which both capillary and gravity forces are considered. The governing equations are Darcy's equation of flow and mass continuity.

The two main crack faces (Fig. 5.3) which are opening up about a hinge at the top of the mortar beam, when under three-point loading, are simply considered in this model as plates with a linearly varying spacing.

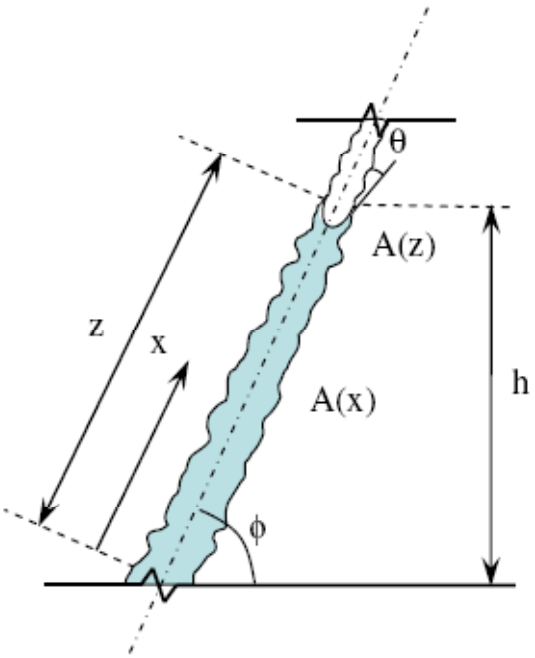


**Fig. 5.3** Illustration of the flow of adhesive in a crack, above the reservoir position

The velocity of the viscous flow $v(x)$ inside a capillary tube or between two plates can be given by the basic 'Darcy like' flow equation:

$$v(x) = -\frac{k}{\mu}\left(\frac{dP}{dx} - \rho g \sin\phi\right) \tag{5.6}$$

where $\mu$ is the viscosity, $P$ the pressure, $g$ the gravity, $\phi$ the inclination angle of the capillary/crack (Fig. 5.3) and $\rho$ and $k$ are the density and permeability of the adhesive respectively.

Rearranging equation (5.6) and integrating from the reservoir to the meniscus interface gives:

$$\mu \int_0^z \frac{v}{k} dx - p_c - \rho g z \sin \phi \tag{5.7}$$

where $z$ is the distance of the fluid front from the reservoir and $p_c$ is the capillary potential. The capillary potential for a plane opening of width $b$ is given by:

$$p_c = \frac{2\gamma \cos \theta}{b} \tag{5.8}$$

where $\theta$ is the angle that the meniscus forms with the wall of the opening (or face of the crack), as shown in Fig. 5.3, and $\gamma$ is the surface tension of the fluid. For a non-uniform cross-section ($b=b(x)$) the capillary potential depends on the position of the interface.

The velocity can also be related to the speed of the fluid front based on the conservation of mass:

$$v(x) = \frac{dz}{dt} \frac{A(z)}{A(x)} \tag{5.9}$$

where $A(x)$ is the cross-sectional area of the capillary and $A(z)$ is the cross-sectional area at the meniscus interface.

Substituting Eq. (5.9) into equation (5.7), and rearranging gives an expression for the flow velocity at the front ($dz/dt$):

$$\frac{dz}{dt} = \frac{1}{\eta} \left( p_c - \rho g z \sin \phi \right) \tag{5.10}$$

where:

$$\eta = \mu A(z) \int_0^z \frac{dx}{kA(x)} \tag{5.11}$$

From Eq. (5.10) is can be seen that the flow velocity at the front is zero when the capillary potential drawing the fluid up the crack is matched by the weight of the fluid acting downwards. Therefore, by placing $dz/dt=0$ in Eq. (5.10) and substituting the expression given in Eq. (5.8) for $p_c$, the rise height $h$ may be defined as:

$$h = z\sin\phi = \frac{2\gamma\cos\theta}{b\rho g} \tag{5.12}$$

The theory given above has been implemented within a relatively simple time-stepping algorithm for tapering cracks, as shown in Fig. 5.4.

- Choose $\Delta t$
- Start with very small $z = z_0$
- Evaluate $\eta$
- $t = t + \Delta t$
- $\Delta z = \frac{\Delta t}{\eta}\left(p_c - \rho g z \sin\phi\right)$
- $z = z + \Delta z$
- If $\Delta z < tol$ exit, otherwise continue
- Repeat process with smaller $\Delta t$ to ensure that the solution is time-step converged

**Fig. 5.4** Time-stepping algorithm to calculate z versus t

The algorithm has been evaluated in MathCAD, and rise height versus time graphs for two different crack openings have been calculated, as given in Fig. 5.5.

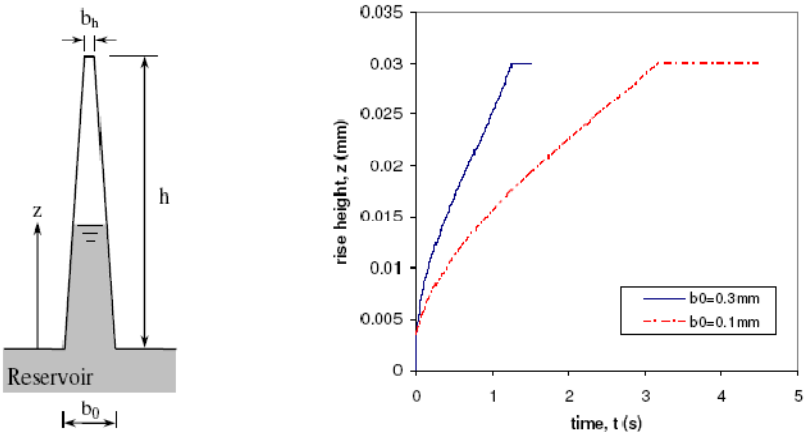


**Fig. 5.5** (a) Idealised vertical tapering crack, and (b) rise height versus time for two different crack openings, $b_0$

The parameters used for the glue in the above calculation are viscosity, $\mu=5\ mPa.s$, density, $\rho=1060\ kg/m^3$, meniscus angle, $\theta=0$ and surface tension, $\gamma=0.033\ N/m$. The viscosity was obtained from the adhesive data sheet, and the surface tension was determined experimentally from measured glue rises in capillary tubes of known diameter. The maximum experimentally observed crack height was 30mm above the level of the supply tubes. This was therefore taken to be the height of the cavity, $h$, in the above simulations. The crack opening at the top of the cavity, $b_f$, was assumed to be a nominal 0.01mm.

It can be seen from Fig. 5.5(b) that for both sizes of crack opening ($b_0=0.1\ mm$ and $0.3\ mm$) the glue rises to the maximum rise height, $h$. More significantly, for both examples, this occurs within a period a few seconds. As a result of these findings, all of the broken beams in the lattice model, up to the total rise height, $h$, have been healed in an instantaneous manner, as described in the following section.

Finally, it should be noted that 'sink' terms, associated with glue going into the surrounding area (fracture process zone), have been ignored in the current theory.

### 5.2.4 Example with 2-D Modelling

In this section a 2-D lattice simulation is used to model the self-healing response of a typical adhesive healed mortar beam. The specific experimental beam that has been considered is SH beam 1 from the second experimental set on notched, lightly reinforced prismatic beams. This has been chosen since the mechanical response of this beam is considered to be representative of the general form of healing response obtained for a typical notched beam.

For the purpose of examining whether or not the lattice model is capable of capturing the main mechanical behaviour observed during the self-healing experiments, a relatively coarse mesh has been used for the analysis. The regular triangular mesh discretisation used has an element length of 4mm and boundary conditions as shown in Fig. 5.6(a). The notch is modelled via the removal of 5 elements prior to the application of any load, and the CMOD is measured as the increase in distance between the nodes at either side of the notch at the bottom of the beam. The crack mouth opening under the three-point bending arrangement is controlled within the model by a line of stronger and stiffer steel reinforcement elements, as illustrated in Fig. 5.6(a). The strength and stiffness values for the mortar, steel and glue phases used in the model are given in Table 5.1.

**Table 5.1** Material properties used in the numerical simulation

| | Strength, $f_t$ (MPa) | E-value (MPa) |
|---|---|---|
| Mortar | 1 - 6.5 | 15800 |
| Steel | 597 | 205200 |
| Glue | 20 | 3500 |

The strength of the ethyl cyanoacrylate healing agent, used in the model is taken from the RiteLok EC5 data sheet. The Young's modulus of the adhesive is taken to be 3500 MPa. The strength and stiffness values used for the steel have been obtained from tensile testing of the 3.15 mm reinforcing bar used in the experiments. The lattice beam analysis is a 2D plane stress simulation with a beam width of 1 mm. Therefore, in order to account for the single 3.15 mm diameter steel reinforcing bar used in the 75 mm wide experimental beam, the steel lattice element crosssectional area ($A_s$) has been reduced to 0.104 mm$^2$ ($A_s=\pi.(3.15/2)^2/75$). It should be noted that in reality this element is a composite element comprising part steel and part mortar (either side of the steel). Once the beam becomes cracked up to the level of the steel, the stiffness of the mortar part is lost and the stiffness of the element is based on the stiffness of the steel alone. Since consideration of the mortar part makes only a small difference to the initial stiffness of the beam, and also to maintain simplicity of the algorithm, the horizontal elements at the level of the steel have been considered to be steel only elements.

The E-value for the mortar phase has been estimated from three point bending fracture energy tests that were conducted on plain mortar beams cast from the same mortar mix used in the self-healing experiments. Based on the average central deflection of the fracture energy beams in the elastic region, the E-value of the mortar has been back calculated to be approximately 15,800 MPa as given in Table 5.1.

In order to capture the shape and tortuosity of the crack that propagates upwards from the notch, the central band of mortar elements are assigned randomly distributed strengths selected from a predefined strength range. The strength range used for the simulation presented in Fig. 5.6 and Fig. 5.7 is 1 to 6.5 MPa. The width of this central band of mortar elements, whose strength is drawn from this range, has been set to 16mm, as illustrated in Fig. 5.6(a). The remainder of the mortar elements are then set to elastic (i.e. very high failure strengths). The choice of the width of the central band is based on the estimated width of the fracture process zone (fpz) obtained from the experimental investigation. This simplified method of introducing heterogeneity into the current model also allows for subsequent post-healed cracking to deviate away from the original crack.

Fig. 5.6(b) illustrates the development of initial cracking, healing, and final crack formation of the three-point bend beam under the prescribed displacement ($u_p$), and the boundary conditions shown in Fig. 5.6(a). The displacements shown in the meshes of Fig. 5.6(b) have been scaled by a factor of 50 for the purpose of clarity.

Meshes (i) to (vii) illustrate the development of the macro crack which propagates from the notch upwards, to a distance of approximately 50 mm above the base of the beam. At this point the value of the CMOD reaches 0.05 mm and all of the previously broken mortar beams are healed and replaced with composite

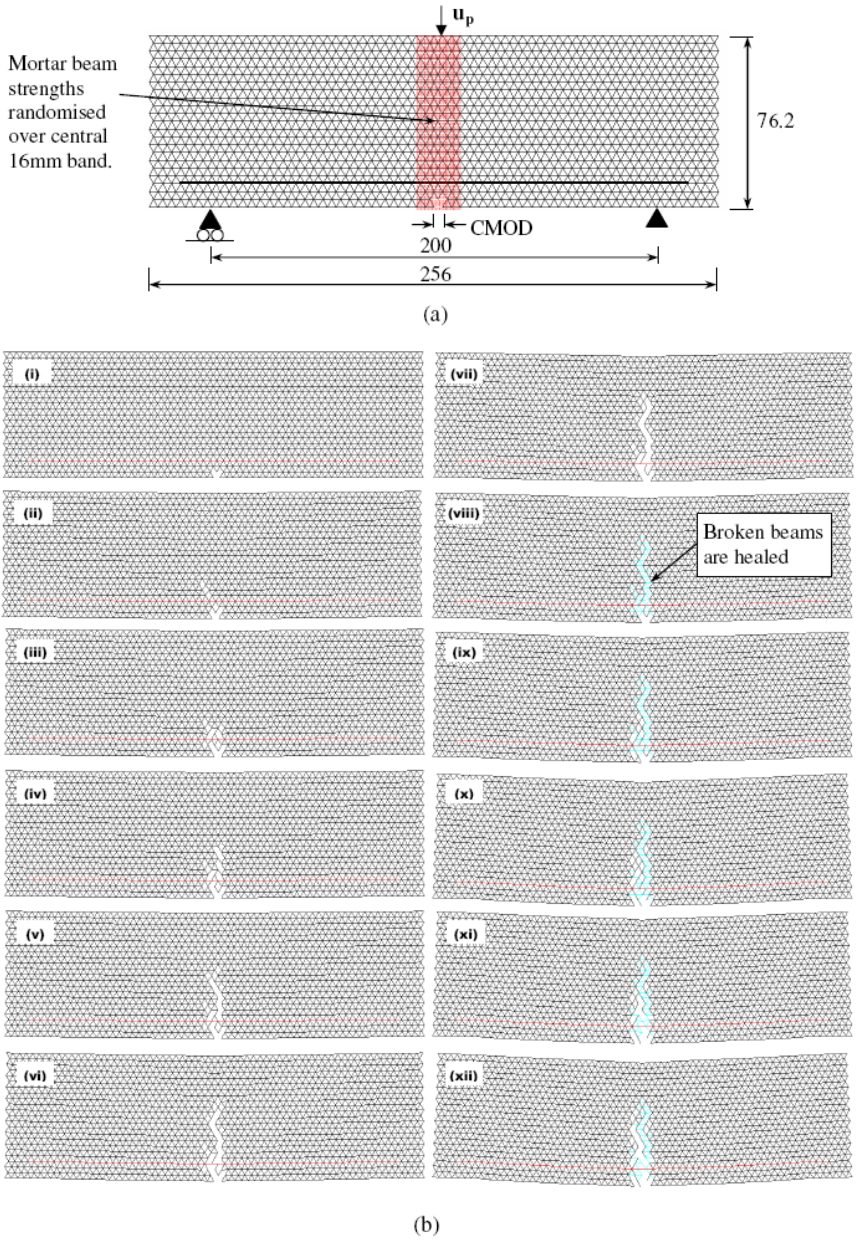


**Fig. 5.6** Coarse mesh discretisation of SH beam: (a) boundary conditions, and; (b) development of initial cracking, healing, and final crack formation

mortar/glue elements, as outlined previously in the description of the model algorithm. It should be noted that from Fig. 5.7(a) the first capillary tube fractures in the experimental test at a CMOD of approximately 0.1 mm. The healing in the model has, however, been initiated at a CMOD value of 0.05 mm. This is due to the inability of the model to capture some of the non-linear processes which increase the ductility of the experimental response. These are discussed in more detail later in this section.

The healing in this simulation occurs instantaneously, in one stage, and is applied to all previously broken beams. The reason for the decision to heal instantaneously is based on the idealised glue rise calculations (section 5.2.3), and experimental evidence; in particular, the occurrence of ink staining very shortly (several seconds) after tube fracture and the rapid rate dependent primary healing effect observed in the SH experiments. This evidence indicates that the adhesive is not only drawn up the crack very quickly but also cures rapidly. The fixture time according to the RiteLok EC5 data sheet is 5-15 seconds, however, this is likely to be further accelerated by the alkaline environment of the mortar and the presence of moisture. The decision to heal in one stage is justified by the large reservoir of adhesive that is provided by each and every one of the individual capillary tubes, and also the relatively short time period over which all four capillary tubes are heard to crack. Therefore, it is felt that there is a readily available and plentiful source of adhesive available at the crack faces within a few seconds of the first tube breaking. Finally, the justification for healing all of the broken beams shown in mesh (vii) (Fig. 5.6(b)) is based upon the observed glue rise of approximately 30 mm above the capillary tube level (50 mm above the base of the beam).

The strength of the healed composite mortar/glue phase in the current model is set instantaneously to 20 MPa following healing. Whilst this element is considered to comprise two distinct separate parts for the purpose of modelling, in reality, the glue, due to its very low viscosity, is likely to permeate into the fracture process zone surrounding the main crack face. Indirect experimental evidence of this is found in the observed differences between the initial and final post-healing crack patterns on the side faces of the beams. The effect, therefore, of setting the strength of the healed beam elements to 20 MPa is to cause the final crack pattern to deviate from the initial crack pattern. This can be seen in meshes (viii) to (xii) in Fig. 5.6(b). In mesh (xii) the specimen is effectively broken through. Its residual strength is due to the triangulation caused by the mortar hinge at the top of the beam, the steel reinforcement bridging the crack, and the elastic mortar elements at either side of the central band.

The force-displacement response from the simulation shown in Fig. 5.6 is given in Fig. 5.7(b). Since the lattice beam analysis is a 2D plane stress simulation of unit depth, the forces obtained from the simulation have been multiplied by 75 so that they may be compared directly with the experimental results of SH beam 1, as shown in Fig. 5.7(a).

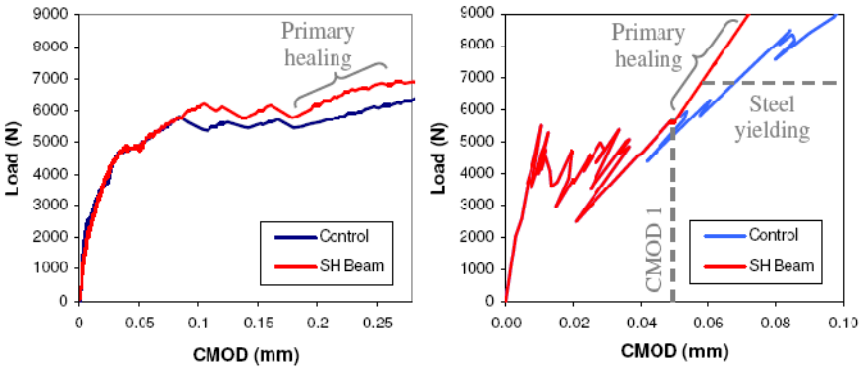


**Fig. 5.7** (a) Experimental and (b) numerical load – CMOD response for a notched mortar beam subject to adhesive based autonomic healing

The initial stiffness of the lattice response agrees well with the experimental response. This confirms that the stiffness values used for the mortar and steel in the model are correct. Between 0mm and 0.05 mm CMOD the response of the experimental beam shows a gradually increasing drop-off in stiffness as a result of initial micro-cracks which then coalesce to form a larger macrocrack. During the same period the numerical response is significantly stiffer and oscillates considerably. The increased stiffness is largely due to the limits of the current model, in that the mortar elements outside of the central fracture process zone band are considered to be perfectly elastic. The model is therefore not able to adequately capture initial microcracking which serves to reduce the stiffness of the beam. The oscillatory response is mainly due to the very coarse mesh used in this analysis, and also the omittence of any form of smoothing. The value of the load towards the end of this initial stage is nevertheless predicted correctly by the model at about 5 kN.

The response of the experimental beam between 0.05 mm and 0.18 mm CMOD is largely due to the combined effect of the four borosilicate tubes and the steel reinforcement. The stiffness increase between 0.05 mm and 0.1 mm CMOD is due to the action of the steel and glass, and the discontinuities, signified by the drops in the force-displacement response, are a result of the individual tubes breaking. There is also possibly a degree of steel/mortar slip occurring during this period as a result of the smooth steel bars that were used as reinforcement in the experiment. Since, neither the non-linear effects of the glass tubes breaking nor the steel/mortar slip are included in the model it is not able to capture the additional ductility in the force-displacement response that these processes provide. For this reason the value chosen for initiating healing in the model (CMOD 1) has been set to 0.05 mm rather than a value corresponding to actual tube breakages in the experimental beam.

After the breakages of the tubes in the experimental beam, the primary healing effect is observed. This is identified in Fig. 5.7(a) by the increased stiffness of the

force-displacement response from 0.18 mm CMOD onwards for the SH beam, when compared to the control beam. Likewise, for the numerical response, the simulation whereby healing is undertaken shows a stiffer response than the one where no healing occurs (control) and the crack shown in mesh (vii) (Fig. 5.6(b)) simply continues to open up.

In the present model the axial and bending stiffness of the mortar part of the composite mortar/glue element has been reduced to account for the loss of stiffness that will occur in this area due to microcracking of the mortar in the fracture process zone around the macro crack. The axial and bending stiffness of the mortar part have therefore been pre-multiplied by a microcracking factor, *m*. The axial stiffness of the mortar part for example, as given in Eq. (5.2), then becomes:

$$k_m' = mk_m = m\frac{E_m A_m}{L_m} \tag{5.13}$$

The value of *m* used in the simulation shown in Fig. 5.7(b) is 0.1. It can be seen from this figure that the stiffness of the beam post-healing is significantly less than the initial stiffness of the beam pre-damage. However, this post-healing stiffness is also substantially greater than the primary healing response obtained in the experiments (even after allowing for the different x-axis scales in Fig. 5.7). It is possible to further reduce the gradient of the primary healing response with an even lower value of *m*. However, it is felt that the main reasons for the overly high stiffness of the model at this point are the absence of the non-linear effects of steel yielding and slip, and the overestimation of the degree of healing.

Both the healing and control responses of Fig. 5.7(a) begin to plateaux out at approximately 7 kN due to the yielding of the steel reinforcement. The numerical results shown in Fig. 5.7(b), however, show a continuation in the load carrying capacity of the beam since the Young's modulus of the steel remains constant in the current model. In respect to the second point, since the model is a 2D plane stress model, healing all of the beams up to a level of 30 mm above the capillary tubes is equivalent to full healing across the entire width of the beam in the experiment. However, as indicated by the glue migration pattern on the face of the experimental beam, the adhesive flow is mainly confined to the middle two thirds of the crack face.

## 5.3 Simulation of Autogenic Self-Healing for Concrete at Early Age

For the simulation of crack healing of in early age cracks, as discussed in chapter 4, the module MLS of FEMMASSE [see 5.2] was used. MLS is a finite element model based on the state parameter concept. This means that the material properties are a function of the state of the material. The state can be maturity, degree of hydration, temperature or moisture potential. The simulations with the

model are performed in order to check the hypothesis that the healing observed in the experiments is due to ongoing hydration of the cement. The ageing of the concrete and the development of the properties in time is taken into account in the analysis. In the analysis a concrete with BFSC is used. The purpose of the analysis was not to exactly match the behaviour as found in the experiment, but more to be able to simulate the mechanism. The properties of the material used in the simulation correspond with an average concrete with BFSC, a w/c of 0.5 and a compressive strength of about 45 MPa. The development of the E-modulus and the tensile strength is shown in Fig. 5.8.

(a)

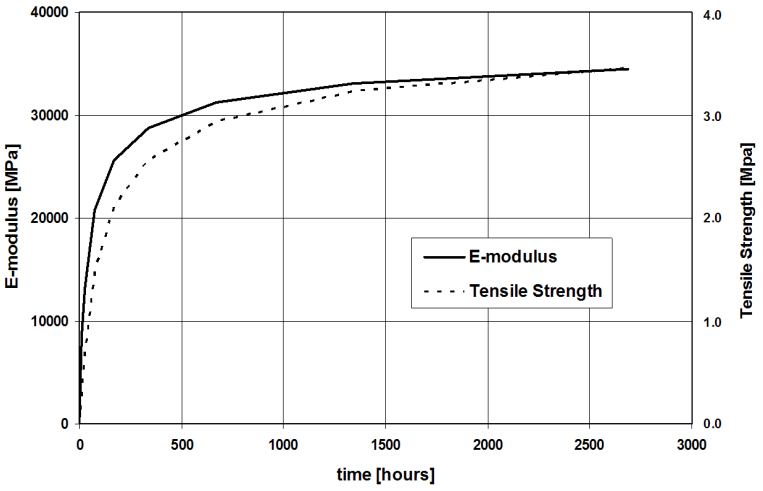


(b)

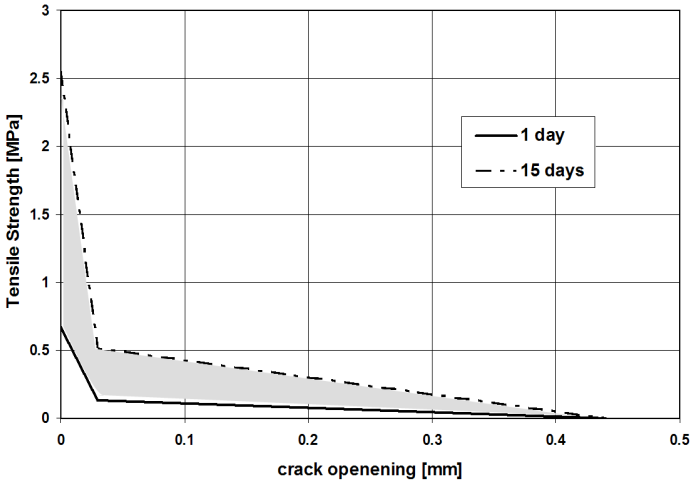


**Fig. 5.8** (a) Development of E-modulus and tensile strength in time, (b) softening behaviour in interface element

In the analysis the 3-point bending test is simulated in 2D using plane stress conditions. In the middle, under the loading point, a discrete crack is created in the mesh using an interface element with a stress-crack opening relation. The strength of the interface element is taken to be equal to the strength of the neighbouring concrete at the specific age when the 3-point-bending test is performed. The values used for the different simulations are shown in Table 5.2.

The softening relation is taken to be bi-linear in all cases, with the bending point in the descending branch set at 20% of the strength and at a crack opening of 0.03 mm. The final crack opening (at zero load) is set to 0.44 mm. In Fig. 5.8b the bi-linear softening curve for a concrete at 1 and 15 days old is shown. Also, a simulation is performed of a specimen which is cracked at an age of 1 day and then healed for a period of 14 days. It is assumed that the bottom half of the specimen is cracked and that the strength gain of the material in the crack is equal to the strength gain of the concrete itself in these 14 days. This means that the strength of the interface is equal to the strength at 15 days minus the strength at 1 day. The softening relation is then equal to the grey area on the graph in Fig. 5.8b. In the experiments the cracked specimens are stored under water during healing. This means there is sufficient water available for the crack to heal. The unhydrated cement particles present in the crack are therefore possibly able to fully hydrate and are thus able to generate a higher strength than similar particles situated in the bulk of the specimen. To check the maximum load that could be reached in such a case a simulation is performed in which the strength of the interface is taken equal to the final strength of the specimen after full hydration minus the strength at one day.

**Table 5.2** Values used for different simulations

| simulation | Tensile strength [MPa] |
|---|---|
| 1 day | 0.67 |
| 15 days | 2.56 |
| 1-15 days | 1.89 |
| 1-final | 2.79 |
| (final strength) | (3.46) |

The results of the simulations are shown in Fig. 5.9-Fig. 5.11. Fig. 5.9 gives a typical deformed mesh in which the open discrete crack is visible. Fig. 5.10 shows a stress-contour plot when the crack-tip is at half height of the specimen. It can also be seen from this figure that the crack is not completely stress free, but stress can be transferred by the interface when it is in the descending branch.

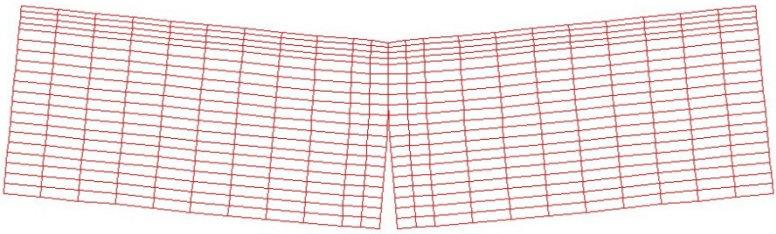

**Fig. 5.9** Typical deformed mesh

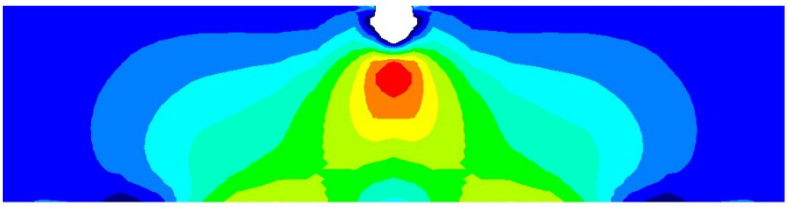

**Fig. 5.10** Stress contour plot

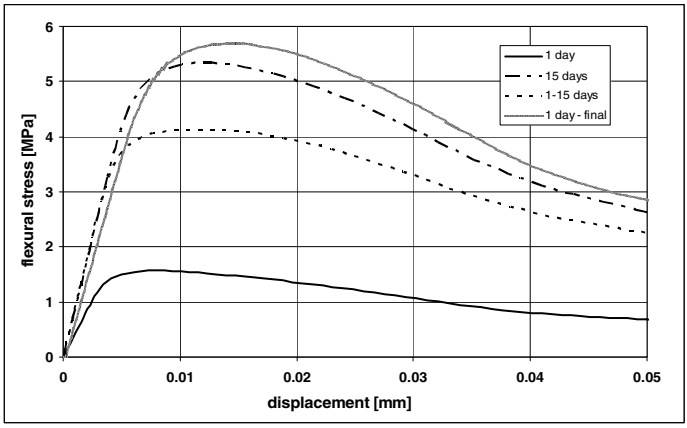


**Fig. 5.11** Flexural stress versus displacement for different simulations

In Fig. 5.11 the flexural stress is plotted versus the displacement (same measuring length as in the experiments (55 mm)) for the different simulations. From this graph the following observations can be made:

- The flexural stress as well as the stiffness in the specimen tested at 1 day is lower than the specimen tested at 15 days.

- The specimen which is pre-cracked after 1 day and tested after 14 days of healing (1-15 days) has the same stiffness as the un-cracked specimen tested at 15 days. The strength of this specimen is about 77% of the un-cracked specimen.
- If the strength gain in the 14 days of healing is equal to the final strength minus the strength at 1 day then the obtained flexural stress is higher (about 106%) than the strength of the un-cracked specimen tested at 15 days.

## 5.4 Simulation of Self-Healing Capacity of Hybrid Fibre Material

Fibre cement based materials have been developed during the past decades for many applications and with many different properties. Fibres of different dimensions and of different materials have been used, e.g. steel, PVA, PE, glass or several kind of natural fibres. The fibres are added to the cement composites to enhance material toughness, strength, fatigue life, impact resistance and/or cracking resistance. A special type of fibre reinforced cement based composites is the group of materials that have a very high strain capacity of sometimes more than 6%. An example of these materials is ECC (Engineered Cementitious Composites) as described in [5.5] and chapter 4. These materials show upon loading a distributed crack pattern with fine cracks and a high strain capacity which make them especially suitable for application where imposed deformation is the loading mechanism. The design of these composites is based on an analytical micromechanical approach [5.5].

The parameters that determine the strain capacity in fibre cement based composite can be summarized as follows:

- Fibre parameters: fibre length, fibre diameter, fibre stiffness, fibre strength, fibre volume fraction and fibre shape.
- Matrix parameters: matrix stiffness, matrix strength and matrix fracture energy.
- Fibre-matrix interaction parameters: interfacial frictional bond strength, stiffness and fracture energy.

All these parameters can be derived from measured data obtained in experiments, see [5.6]. Experiments, however, are time-consuming, especially while certain time has to be allowed for the hydration of the cement and development of the mechanical properties. Therefore it was decided to adapt the 3D numerical lattice model to be used to predict the strain capacity of fibre reinforced materials. Inputs in the model are all the different parameters for fibres, matrix and interface as discussed above.

Two self-healing processes are being studied, i.e. filling cracks to block the path to the steel reinforcement and repair the crack to regain mechanical properties.

Ductile fibre cement based materials are an excellent candidate to serve as a self-healing material. The material itself is such that it spreads strain out over

many cracks and as such only relatively small cracks develop in the material, which are easier to heal. Furthermore, when the material is functioning in a structure, there are still unhydrated cement particles in the material, which hydrate further when water penetrates into the crack [5.7-5.10]. However, by this mechanism only the smaller cracks (<20 μm) will be closed [5.9]. Therefore it was decided to start developing a hybrid fibre material and prepare a model to simulate the behaviour.

This hybrid fibre material consists of a fibre cement based material, similar to ECC, with PVA or PE fibres and with some additional hollow (natural) fibres containing healing agent. The principle is that the additional hollow fibres are relatively weak and break upon stretching, i.e. when the cement matrix breaks. At that moment the healing agent will be released and can either fill or repair the crack. The healing agent can just be water. In that case it could be used to heal micro-cracks in an early stage by ongoing hydration of the unhydrated cement with the water from the hollow fibres. Alternatively the healing agent could be glue or an (expansive) gel, in which case it could be used to heal bigger cracks. With the model described in the next section the hybrid material can be designed. It can be studied what the optimum amount of fibres and mix of fibres should be to obtain a ductile behaviour, with a desired strain capacity and crack width. The amount, size and distribution of hollow fibres and the amount of healing agent in the fibres needed to obtain proper healing can be determined with the model.

Simulation of fibre concrete with lattice models is applied by Bolander [5.11]. The application of their models is mainly reduction of shrinkage cracks. The model presented in this paper is based on the principle of embedding discrete fibres in a random lattice representing the matrix.

In the model presented here, the (cement) matrix is represented by a random lattice [see also 5.12]. The fibres are discrete beam elements connected to the lattice elements by interface beams. The procedure to generate the network is as follows:

- A cubical grid is chosen. In Fig. 5.12 a schematic representation is shown in 2D. The real mesh is 3D, but more difficult to clearly visualize.

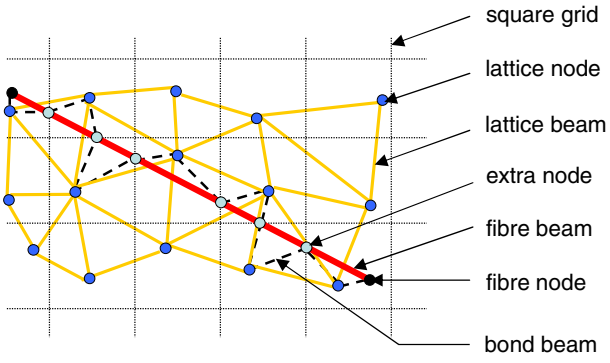


**Fig. 5.12** Schematic 2D representation of generation of fiber-lattice

- In each cell of the square (cubical for 3D) lattice, a random location for a lattice node is generated.
- Then always the 3 nodes (4 nodes for 3D) which are closest to each other are connected by beam elements.
- Next step is to generate fibre elements. First the number of fibres is calculated that have to be placed in a certain volume based on the length, diameter and volume percentage of fibres. These fibres are then a mix of fibres to obtain the proper ductile behaviour of the material and hollow fibres for the healing. Then the location of the first node of the fibre is randomly chosen in the volume. Next the x, y and z direction of the fibre is chosen randomly which determines the location of the second node. If the second node falls outside the volume the fibre is cut off at the boundary. The fibre-volume of the cut off part of the fibre is subtracted from the already placed fibre-volume in order to ensure enough fibres at the end of the procedure.
- Extra nodes inside the fibres are generated at each location where the fibre crosses the square (cubical for 3D) grid.
- Then interface elements (bond beams) are generated between fibre nodes and the lattice node in the neighbouring cell. Also the end nodes of the fibres are connected with an interface element to the cell-node in which the end node is located.
- All the elements in the network are beam elements (with normal forces, shear forces, bending moments and torsion moments), which have a local brittle behaviour. The beam elements fail only in tension (except for the interface elements, which can also fail in compression) when the stress of the element exceeds its strength. For the fracture criteria only the normal force is taken into account to determine the stress in the beams. The fracture modelling in the lattice model is only a sequence of linear elastic steps, which makes it fast and without numerical difficulties. For the set of equations and model properties the reader is referred to [5.12].

With the model tensile tests and four point bending tests are simulated with different amount of fibres. In Fig. 5.13 the final crack pattern for tensile tests with a low (1%) and high (4%) amount of mechanical fibres are shown as well as for a bending test with 4 % fibres. In case of 1% fibres a single crack develops and a brittle response is noticed. In case of 4% fibres a ductile response is obtained with multiple cracking. In the mixes also healing fibres are placed, with an amount equal to the 1% mechanical fibres. In Fig. 5.13 also the healing fibres that are broken in each of the specimens are shown. It can be seen that in the case of the ductile material much more fibres are broken, however the cracks that should be healed are also much smaller. If it is assumed that the specimen in both cases is stretched to the same strain, then in the present simulations, (with the present specimen length) it means that the crack width in the 1% fibre material is about 10 times larger. Also the amount of healing fibres that is broken is 10 times less. From this it can be concluded that 10 times more healing agent would be needed in the 1% fibre material and that most of the healing agent will not be used.

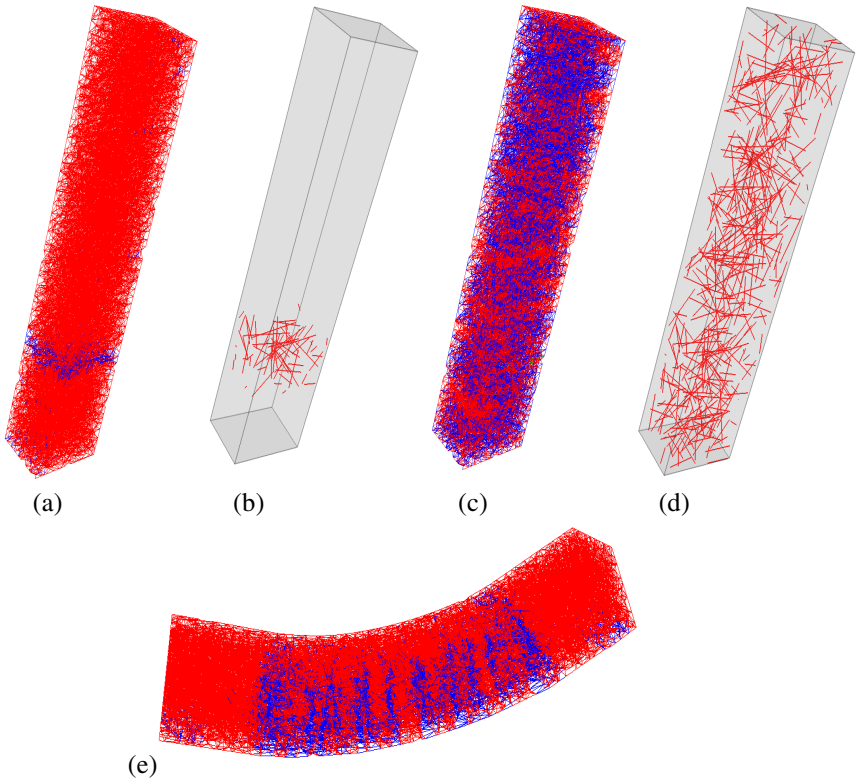


**Fig. 5.13** Cracked specimens with 1% (a) and 4% (c) mechanical fibres loaded in tension and 4% fibres in bending (e) and healing fibres broken in simulation with 1% (b) and 4% (d) mechanical fibres

In case of a ductile hybrid material (in this case with the 4% mechanical fibres) the healing agent is used everywhere and the healing agent is not placed at locations where it is not used. It is optimized for perfect healing ability and use of material. As explained above the healing mechanism can be ongoing hydration (water in the healing fibres) or crack filling with glue or even an expanding epoxy.

In principle this way of modelling could also be adopted to simulate the self-healing mechanisms in which embedded tubes with encapsulated healing agent are used.

## 5.5 Analytical Models for Cracks Hitting Encapsulated Materials

Zemskov *et al.* [5.13] developed two-dimensional analytical models for the computation of the probability that a crack hits an encapsulated particle. Most computations are performed in closed algebraic form which allows to perform the

last calculation steps numerically with a higher accuracy. The functions built in this study allow to estimate combinations of crack lengths, capsule size, and mean intercapsule distance in order to analyse the efficiency of a self-healing material. The study is performed in the framework of the investigation of the potential of bacteria to act as a catalyst of the self-healing process in concrete, i.e. their ability to repair occurring cracks autonomously. The self-healing technology that is dealt with in this study is based on the use of spherical clay capsules, containing the healing agent (calcium lactate) and nutrients for bacteria, embedded in the concrete structure. The concepts developed are generic and can be applied to other cases in which encapsulated particles are possibly hit by cracks.

## 5.6 Self-Healing by On-Going Hydration

He *et al.* [5.14] used an hydration model with expanding cement particles to investigate the possibility of crack closure by on-going hydration. Fig. 5.14 shows a graphical interpretation of a single crack intersecting with cement paste. The degree of hydration, the fineness of the cement and the crack width are parameters in the model that are varied in this study. A similar approach is used in Lv and Chen [5.15], but the difference in this study that the shape of the crack, when propagating around particles is taken into account.

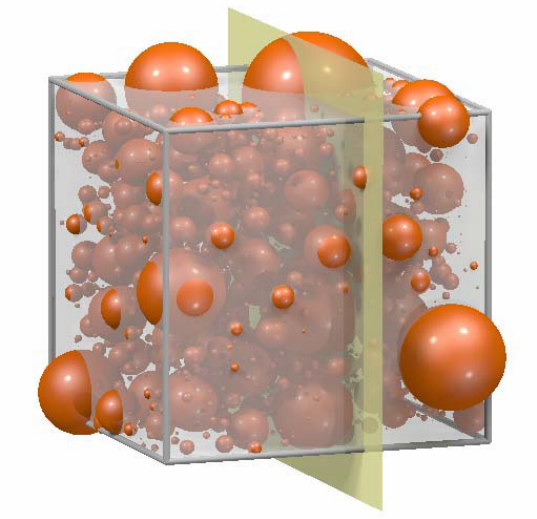

**Fig. 5.14** Single crack intersected with cement paste

Huang and Ye [5.16] developed a model for self-healing of cracks to be realized by providing extra water for further hydration of unhydrated cement particles, see Fig. 5.15. In order to provide theoretical guidance for the practice, self-healing by providing extra water to promote further hydration was simulated.

The simulation was based on water transport theory, ion diffusion theory and thermodynamics theory. In the simulation, self-healing efficiency under different conditions as a function of time was calculated. The relationship between self-healing efficiency and the amount of extra water from the broken capsules was determined. According to the results of the simulation, the amount of extra water can be optimized by considering self-healing efficiency and other performances.

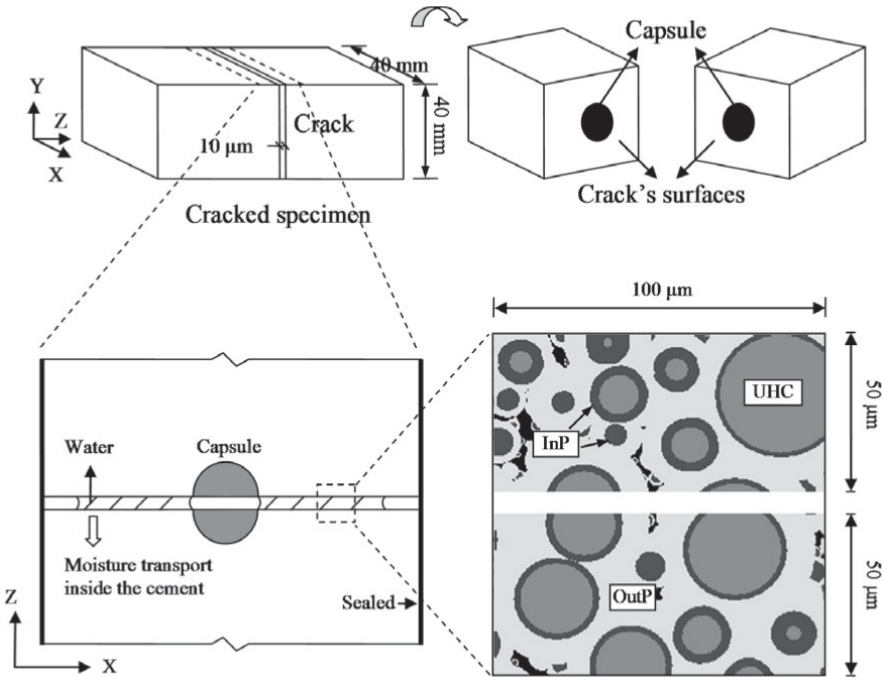


**Fig. 5.15** Schematic diagram of modelling system (InP represents inner products, OutP represents out products, UHC represents unhydrated cement particles)

## References

5.1. Joseph, C.: Experimental and numerical study of the fracture and self-healing of cementitious materials. PhD-thesis Cardiff University, UK (2008)
5.2. Schlangen, E., ter Heide, N., van Breugel, K.: Crack healing of early age cracks in concrete. In: Proc. ECF16, Alexandroupolis (2006)
5.3. Young, W.-B.: Analysis of capillary flows in non-uniform cross-sectional capillaries. Colloids and Surfaces A: Physicochemical and Engineering Aspects 234(1-3), 123–128 (2004)
5.4. Roels, S., Vandersteen, K., Carmeliet, J.: Measuring and simulating moisture uptake in a fractured porous medium. Advances in Water Resources 26, 237–246 (2003)

5.5. Li, V.C.: On Engineered Cementitious Composites (ECC) – A Review of the Material and its Applications. J. Advanced Concrete Technology 1(3), 215–230 (2003)
5.6. Schlangen, E., Qian, Z., Sierra-Beltran, M.G., Zhou, J.: Simulation of fracture in fibre cement based materials with a micro-mechanical lattice model. In: Proceedings ICF12, 12th International Conference on Fracture, Ottawa, Canada, July 12-17 (2009)
5.7. Li, V.C., Yang, E.: Self-healing in Concrete Materials. In: van der Zwaag, S. (ed.) Self-healing Materials – an Alternative Approach to 20 Centuries of Materials Science. Springer Series in Materials Science, vol. 100, pp. 161–193 (2007)
5.8. Schlangen, E., Joseph, C.: Self-healing Processes in Concrete. In: Ghosh, S.K. (ed.) Self-healing Materials: Fundamentals, Design Strategies, and Applications, pp. 141–182. Wiley-VCH (2008)
5.9. Qian, S., Zhou, J., Rooij, M.R., de Schlangen, E., Ye, G., van Breugel, K.: Self-Healing Behavior of Strain Hardening Cementitious Composites (SHCC). Accepted for publication in Cement and Concrete Composites (2009)
5.10. Qian, S., Zhou, J., Liu, H., de Rooij, M.R., Schlangen, E., Gard, W., van de Kuilen, J.W.: Self-Healing Cementitious Composites under Bending Loads (2009)
5.11. Bolander, J.E.: Numerical modeling of fiber reinforced cement composites: linking material scales. In: Proc. Rilem Symposium BEFIB 2004, Varenna, Italy, pp. 45–60 (September 2004)
5.12. Schlangen, E., Qian, Z.: 3D Modelling of Fracture in Cement Based Materials. Journal of Multiscale Modelling 1(2) (2009)
5.13. Zemskov, S.V., Jonkers, H.J., Vermolen, F.J.: Two analytical models for the probability characteristics of a crack hitting encapsulated particles: Application to self-healing materials. Computational Materials Science 50, 3323–3333 (2011)
5.14. He, H., Guo, Z., Stroeven, P., Stroeven, M.: Numerical assessment of concrete's self-healing potentials for promoting durability. Int. J. Modelling, Identification and Control 7(2), 142–147 (2009)
5.15. Lv, Z., Chen, H.: Modeling of self-healing efficiency for cracks duet o unhydrated cement nuclei in hardened cement paste. Procedia Engineering 27, 281–290 (2012)
5.16. Huang, H., Ye, G.: Simulation of self-healing by further hydration in cementitious materials. Cement & Concrete Composites 34, 460–467 (2012)

# 6 Other Materials, Applications and Future Developments

E. Schlangen

Microlab, Delft University of Technology, The Netherlands
H.E.J.G.Schlangen@tudelft.nl

## 6.1 Introduction

This state of the art report discusses self-healing concepts in cement based materials. Cement based materials have a self-healing property by nature. This autogenic self-healing ability of these materials is known for years and also investigated and proven my many authors, as described in the previous chapters. The autonomic self-healing ability, in which the material is designed to be self-healing, is rather new. This area of research received a strong boost after the paper on 'autonomic self-healing of polymer composites' by White *et al.* [6.1] in Nature in 2001. This paper was the motivation for a lot of research teams to start investigating and developing self-healing concepts for various engineering materials. Several of these concepts are discussed in the next section.

It also initiated an international conference series on self-healing materials, which was organized already three times: in Noordwijk, The Netherlands in 2007, in Chicago, USA in 2009 and in Bath, UK in 2011. The fourth conference will be held in Ghent, Belgium in 2013. Conference proceedings of these events are available with many different ideas and suggestions how to approach the self-healing phenomenon and improve the solutions [6.2-6.4]. Also various smaller workshops and special sessions at general material conferences were organised in the last decade.

Furthermore a number of text-books are published dedicated to the theme of self-healing materials in general [6.5, 6.6], with also special attention for self-healing of cementitious materials. Last but not least, already a number of PhD-theses have come out on the topic. Several of them are referred to throughout this report. Real applications of self-healing materials already exist, also for cementitious materials, but are still limited. Some of them are discussed in section 6.3. In the final section some on-going projects are mentioned and an outlook to the future is given

## 6.2 Self-Healing in Other Materials

In a publication [6.7] of AgentschapNL in the Netherlands a short overview is given of self-healing techniques applied in different material fields. For further

M. de Rooij et al. (Eds.): *Self-Healing Phenomena in Cement-Based Materials*, RILEM 11, pp. 241–256.
DOI: 10.1007/978-94-007-6624-2_6 

references it is better to have a look at the conference proceedings [6.2-6.4]. In the sections below the various material classes are discussed.

### *6.2.1 Self-Healing in Polymers*

The first widely appreciated demonstration of an intentional self-healing engineering material is the epoxy–encapsulated liquid adhesive system developed by a multidisciplinary research team at the University of Illinois, USA [6.1]. A thermosetting epoxy was used as the matrix material for two reasons: epoxies are versatile engineering polymers with excellent mechanical and chemical properties and secondly they are synthesised via a low temperature crosslinking reaction starting with two precursors having a low viscosity. The low processing temperature and the low viscosity in the starting phase made it easy to introduce discrete healing agents. Realising that liquids are intrinsically mobile and therefore meet the key requirement for the healing concept, the Illinois team has chosen for a reactive liquid resin stored within brittle thin-walled inert poly(urea-formaldehyde) capsules. Upon fracture the capsules in the crack plane are ruptured and liquid resin flows over the fracture surface due to the surface tension. There it comes into contact with crushed catalyst particles also mixed into the epoxy. The catalyst triggers a crosslinking reaction of the liquid resin and, provided enough liquid is available to bridge the gap between the two crack surfaces, a mechanical bond is restored. The cracked material can now be considered to be healed.

A new approach for autonomous healing of polymer networks is based on cross-linking induced by local stresses. These stresses activate a latent polymerization catalyst – completely unreactive until activated – by removing a polymer-bound ligand, revealing a ruthenium-based or other metal-based catalyst that is ready for polymerization. In the most ideal case, when the local stresses have been removed, the polymer-bound ligand would reconnect to the metal, to form again the latent, ‘sleeping’ catalyst that is ready for a new stress-induced activation.

As a new self-healing concept, plasticity can be introduced in a thermosetting polymer material by a radical-induced redistribution of cross-links. In this way, stresses in the polymer structure can be relieved, and the induced plasticity has the ability to repair the material. A photo-induced initiator decomposition can act as a radical source.

Self-healing is not only of interest for thermosetting polymers to repair the three-dimensional network of cross-links, but also for thermoplastic materials: plastics which are processed by melting them, for example, in extruders. As about 80 per cent of the world’s plastic consumption consists of thermoplastic materials, the importance of healing these materials is self-evident. Self-healing in thermoplastic polymers (like polystyrene or polymethyl methacrylate) with a one-component healing system can be established by embedding microcapsules containing well-selected polymer solvents (such as dichlorobenzene). When a crack proceeds in the thermoplastic, the crack eventually opens embedded

microcapsules. Solvent is released into the crack, where it wets the surfaces of the crack. Swelling of the thermoplastic allows a decrease in glass transition temperature, and the increased polymer mobility causes re-entanglement of the polymer chains. The material is healed when the solvent diffuses out or evaporates. Healing of thermoplastics is a physical process, in contrast to chemical healing in thermosetting materials. An improved self-healing mechanism is based on latent solvent storage and in situ release upon damage. To this end, a microporous filler filled with a high boiling solvent encapsulated by a polymer can be used. Advantages of microporous fillers, such as microporous silica, pumice, expanded clay or zeolites, are that they are melt processable – which is crucial for thermoplastic resins – and that better mechanical properties are likely. Although the basic self-healing principle has proven to work for specific thermoplastic materials, applying it to industrially manufactured engineering plastics is another challenge.

### *6.2.2 Damage-Healing in Fibre-Reinforced Composites*

Applications in aerospace and automotive use light, strong and stiff structures made of continuous fibre-reinforced composites. The lifetime of these composites – usually glass or carbon fibres embedded in an epoxy resin matrix - is strongly influenced by delamination of layers that make up the composite material, or by matrix cracks in these layers after impact. Delamination in these composite materials is normally not visible on the outside. Conventional ways to repair thermoplastic matrices in composites are mainly applicable to external and accessible damages, instead of internal and invisible microcracks.

Internal delamination and matrix cracks need an unconventional solution, and one approach is the autonomous healing of composite materials using supramolecular polymers where fourfold reversible hydrogen bonds are present between ureidopyrimidinone (UPy) dimers. By breaking and restoring the relatively weak hydrogen bonds between the dimers, healing can be established. In a practical way, this is done by developing supramolecular thermoplastic polymer as matrix material, and attaching this matrix to the (glass) fibres of the composite. Somewhat above room temperature the supramolecular polymers are present as long chains. At higher temperatures, but below 100 °C, these chains break at the hydrogen bonds, rendering shorter-chained supramolecular polymers. When a crack is present in the matrix part of the composite, it will be healed by increasing the temperature, as this results in breaking of the hydrogen bonds, leading to shorter polymers, which behave liquid-like and flow to the void of the crack. The crack becomes smaller and vanishes eventually. When the healing is completed, the temperature can be lowered to ‘normal’ conditions. The possibilities and limitations of supramolecular polymers in composite materials will be explored further.

Somewhat related are self-healing supramolecular polymer nanocomposites. They consist of a dynamic physically cross-linked polymer network that is

reinforced by inorganic nanoparticles. The polymeric part takes care of self-healing as a result of the high mobility level at a molecular scale, whereas the nanoparticles give the system mechanical strength and stiffness. As the self-healing concept – purely based on polymer dynamics and physical interactions - is built into the material itself, such materials can repair themselves an unlimited number of times. Envisaged applications are the use as the matrix of fibre-reinforced composite panels. In a different approach for self-healing in composite materials, moulded-in shape memory alloy wires are used. The shape memory effect, caused by a thermo-elastic phase transformation, results in contraction of pre-strained wires upon heating. This contraction is used to put a compressive force onto both sides of the delaminated area, while - due to the heating - the thermoplastic matrix material is soft and ductile and, hence, easy to reshape. In this way a pure physical healing occurs. Healing of fibre-reinforced composites can also be performed if a part of the reinforcing fibres is replaced by continuous hollow glass capillaries containing a healing agent. After failure of the matrix and capillaries, the healing agent will be released to do its repairing task. However, as these capillaries are continuous and long reservoirs, they will be drained completely into the damaged region. In case of a future damage, the previously drained healing agent can no longer be used. This issue can be overcome by dividing the continuous hollow capillary in compartments, allowing controlled release of healing agent on a local scale. In this way it would be possible to repair small damages several times. Liquid containing fibres are spun from ortho-dichlorobenzene - $H_2O$ $Na^+$ alginate emulsions. The alginate forms the solid matrix of the capillary, whereas the compartments are filled with 'oily' ortho-dichlorobenzene. Testing of compartmented alginate fibre (diameter ~350 μm) containing 45 weight per cent of ortho-dichlorobenzene embedded in epoxy resin with 30 per cent fibre content shows that the theoretical concept is proven. In future steps, to develop a more practical system, two-component epoxy glues can be used instead of the ortho-dichlorobenzene.

### *6.2.3 Unravelling of Porous Asphalt Pavements*

Due to good water drainage and noise reduction properties, over 60 per cent of the surface of the Dutch highways is covered with porous asphalt concrete: coarse mineral aggregates held together by a bituminous binder, in a porous structure. However, porous asphalt concrete is less durable than its dense counterpart. During its lifetime, the material is exposed to many factors which have a deteriorating influence. Traffic loads, rain, snow, de-icing salts, temperature differences due to day/night cycles, UV radiation. They all age the binder, making it more rigid - more prone to crack - and less acting as a glue between the mineral aggregates.

A phenomenon called 'ravelling' causes the main durability problem with porous asphalt concrete. Ravelling comprises the loss of aggregates from the surface layer of an asphalt road, and occurs after a few years of using the porous

asphalt concrete. It can increase very fast due to the friction of the tires of passing vehicles. Hence, there is a need for a self-healing mechanism – unravelling the asphalt – with the intention to increase the lifetime of the material. From 12 to at least 15 years for the conventionally used single-layer porous asphalt concrete, and from 8 to at least 12 years for more recently introduced two-layer porous asphalt concrete. Two ways are being explored to make aged asphalt 'softer' and to prevent or close as many (micro)cracks as possible. In the first approach (Fig. 6.1), oil- containing capsules are made. When a microcrack in the bitumen further develops and enters a capsule, the oil flows into the crack and partly fills the crack. The asphalt is rejuvenated by the diffusion of bitumen and oil, decreasing the stiffness of the bituminous binder.

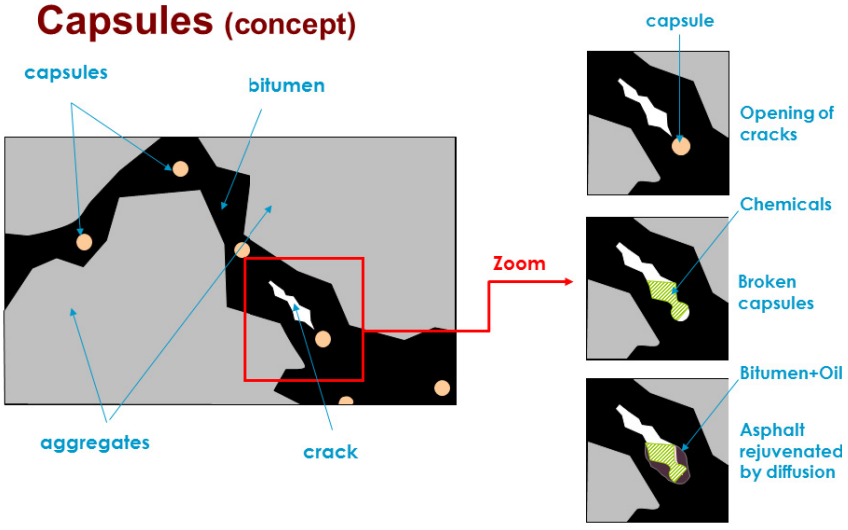


**Fig. 6.1** Self-healing asphalt with encapsulated rejuvenator

In the second approach (Fig. 6.2), conductive fibres like steel wool are incorporated into the bitumen. Bitumen melts by the heat generated by electric currents in these fibres, induced by an alternating magnetic field by a coil placed above the asphalt, resulting in crack closure and restoring the material properties. The principle of the induction heating approach has already been proven. To increase the conductivity, electrically conducting fibres appear to be much more efficient than non-fibrous fillers. A practical test has been conducted successfully on a highway in the Netherlands [6.8]. This method is ready to be applied commercially (see also section 6.3).

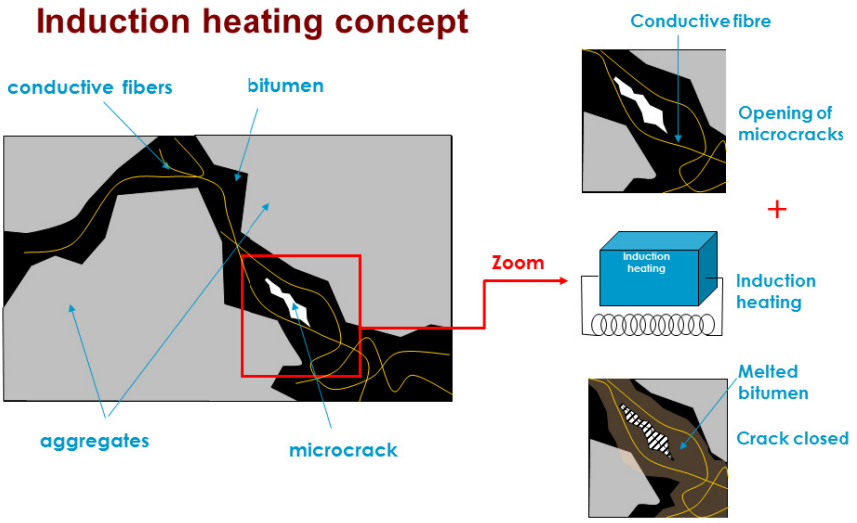


**Fig. 6.2** Self-healing asphalt with induction heating approach

### *6.2.4 Metals and Ceramics*

$Ti_2AlC$: is it a metal or a ceramic? Its lattice structure and resistance to high temperatures are ceramic characteristics, whereas its machinability and toughness are typical for metals. Another remarkable feature of this metal-ceramic is its self-healing ability when used at high temperature, as can be demonstrated by the bending strength recovery after heat treatment. The initial flexural strength of more than 200 MPa drops to about 150 MPa after damage has been introduced. However, heat treatment at 1200 °C in air for only two hours reveals a strength of more than 200 MPa. This remarkable recovery is attributed to the formation of α-$Al_2O_3$ and $TiO_2$ by thermal oxidation, which heals cracks, pores or other damaged micro-areas. Cracks of typically 4-10 micron width have been healed. However, the maximum dimensions of crack widths to be filled have not been determined yet. The quantification of the processing window for thermal healing of these materials in relation to the dimensions of the damage is on-going.

As an alternative for this high-temperature oxidative healing, electrochemical healing is a new approach. Here, the desired crack-filling product is obtained by controlled electrochemical reactions at room temperature. Furthermore, this concept would open up interesting opportunities for surface crack healing in tribological applications - as these metalceramics are very sensitive to surface defects - and healing of anti-corrosive coatings.

#### 6.2.4.1 High-Temperature Lubricants

Other self-healing developments in the field of ceramics occur by introducing soft surfaces on the originally hard ceramics. Softening of hard ceramics is especially important when two ceramic surfaces come into contact with each other - and possibly damage each other - as is the case in the contact between ceramic valves and valve seats in car engines. Ceramic materials in car engines allow for higher combustion temperatures, resulting in a better efficiency. Introducing a soft phase on one surface can reduce friction between two ceramic surfaces. By doping yttria-stabilized tetragonal zirconia with 5 weight per cent of the solid lubricant copper oxide and sliding it along alumina, the 'soft phase' copper oxide is squeezed out mechanically, forming a thin surface layer and restoring the damaged surface. At high temperatures, above 500 °C, first there is an increase in friction followed by a reduction. At room temperature, the friction is reduced somewhat more due to the fact that a 'soft' aluminum hydroxide surface layer forms between the two ceramics.

#### 6.2.4.2 Self-Healing of Nanocracks in Alloys by Nanosized Precipitation

Aluminium is the second most commonly used industrial metal – only to iron. Precipitation hardened aluminium alloys are of great interest in applications where a combination of low weight and high mechanical strength is necessary, such as in airplanes, cars and buildings. Plastic deformation of this type of alloys, due to forces applied to the material, ultimately leads to its failure. Plastic deformation first leads to the displacement of dislocations – linear lattice defects in a crystal structure – through the material, which in turn leads to the formation of defects. When the level of deformation increases, the defects get connected to each other to form voids. These voids initiate cracks on a nanoscale, which subsequently grow and ultimately lead to the material's failure. How to prevent such a degradation process of metals? As substantial mobility of atoms in metals is only limited to high temperatures, self-healing at room temperature seems to be difficult. However, recent investigations have shown that treatments at temperatures lower than usual or interrupted treatments lead to improved resistance to creep – deformation due to long term exposure to levels of stress below the yield strength – and extend the fatigue lifetime of aluminium alloys. These heat treatments appear to leave a substantial amount of alloying atoms as copper and magnesium in a super-saturated solid solution. During static loading (creep) or varying loading (fatigue), these atoms may become available to precipitate at dislocations and nanoscale voids. Here, they decrease the dislocation mobility and void growth rate, a process which can be considered as self-healing.

A similar approach is used for self-healing of deformation damage in steel. Since its mechanical properties can be tailored to get the desired combination of strength and formability, steel is a popular construction material. However, in demanding applications varying loads and temperatures cause the formation of nanoscale cracks, which grow and ultimately lead to failure of the steel components. In the same way as with aluminium alloys, self-healing of

nanocracks in steel can be achieved by the formation of nanosized precipitates to fill these cracks. Again, the presence of super-saturated mobile solute atoms in the steel is required here. In boron steels, boron and nitrogen atoms migrate to the nanocrack to form boron nitride. The same holds for copper added steels, where copper atoms migrate to the nanodefect to form a precipitate, either as spherical copper particles or as a network of copper along dislocations or interfaces. In addition to the aluminium alloys and iron-based model alloys mentioned above, steels of higher technological importance for industrial applications are investigated – such as alloyed austenitic and martensitic steels. In both systems, mobile elements should form precipitates at the initial creep damage, and immobilise further crack growth.

### *6.2.5 Organic Coatings*

Polymeric coatings can add functionalities like protection against corrosion or UV radiation to a product. The highly crosslinked network structure of these coatings gives them high resistance to mechanical stress and solvents. Coatings with low surface energy groups at the surface – such as fluorinated groups - have an additional feature: they display weak interactions with anything that is in contact with the surface. Hence, it is difficult for dirt and other substances to stick to these coatings, and these coatings are easy to clean. When such coatings get damaged during use, it is desirable to retain the coating functionalities. Preferably in a self-healing way using self-replenishing materials, where the underlying cross-linked polymeric network should act as a reservoir of low surface energy groups. After the damage has occurred in the upper 5 to 10 nm of the coating, there is a driving force for groups with lower surface energy to move towards newly created interfaces of the damaged surface, while still connected to the network. The level of the low surface energy groups in the bulk of the coating, as well as their homogeneous distribution throughout the coating depth, should be adequate to have a sufficient amount of these groups available at the newly created interface during replenishment.

In an investigated model system, a polycaprolactone based precursor combined with a tri-isocyanate cross-linker forms a polyurethane cross-linked network. This network is expected to have adequate flexibility so that movement of the low surface energy groups to the surface is possible within an acceptable timeframe. The low surface energy groups are based on perfluoro-alkyl groups connected to the tri-isocyanate cross-linker of the coating network via dangling chains.

A next step is to introduce inorganic nanoparticles into the polymer matrix that contains self-replenishing functional groups with low surface energy. Using this hybrid organic/inorganic material it will be possible to achieve self-healing and retain the surface structure at the same time. Both experimental and modelling investigations have to be performed to understand the competing factors that affect the segregation of the functional groups to the air/coating interface.

Existing paint coatings for inhibiting corrosion of metals (especially aluminium alloys used in aerospace) are made of three layers: conversion coating, primer layer and topcoat. The primer layer acts as a reservoir for the corrosion inhibitor, which is released whenever the coating system gets damaged. The inhibitor reacts with the surface and forms a passivating layer, thereby inhibiting corrosion. So the coating is really a self-healing paint system. However, these coatings are toxic as both the primer and the conversion coating contain the toxic and carcinogenic compound chromate Cr(VI). So there is a need for alternatives – in particular new and safe inhibitors - to be incorporated in the organic coating. Ideally, for self-healing of defects in coating systems, it is desirable to have a component to inhibit corrosion of the underlying metal and also to repair the polymer coating. Since rare earth metal ions are known to be effective corrosion reducers for metals, they form the basis for a new coating system. In this respect cerium dibutylphosphate is a multifunctional inhibitor. It displays both cathodic inhibition via the cerium ion, as well as anionic inhibition via the dibutylphosphate anion.

Alternatively, pH changes can trigger self-healing. Currently available coatings to protect metals from corrosion are fully hydrolysed and polymerised into networks of, for example, siloxane bonds. Damage to these layers will allow the corrosion process to proceed. Furthermore, a damage site triggers pH changes and accelerates deterioration of the metal surface. To solve this problem, new multilayer sol-gel coatings are being developed which - thanks to pH changes inherent to the corrosion process - can initiate a self-healing process. Internal stresses in polymer coatings have a negative influence on mechanical performance of the coating and adhesion to the metal substrate. Early cracking of the material when deformed or bent, and self-propagating cracks are the result of these stresses. Normally, the cross-linked polymer chains are hindered to relax these stresses due to the highly cross-linked thermoset nature of the coating. To avoid these detrimental phenomena, internal stresses may be released by replacing a part of the covalent cross-links in the coating with reversible cross-links, for example dimers of quadruple hydrogen-bonding ureidopyrimidinone (UPy) moieties. The reversible character of these supramolecular cross-links stems from the non-covalent hydrogen bond between the dimers. These reversible cross-links cause superior relaxation of stresses and good creep relaxation behaviour, even below the glass transition temperature where the coating normally becomes rigid and brittle.

This type of preventive healing is completely autonomous, as no external stimuli are required for the material to recover from internal stresses. This approach can not only be used inside the polymer coating, but also at the interface between the polymer coating and the metal substrate to repair the adhesion in case of delamination. The use of reversible, supramolecular bonds across the coating/substrate interface offers the possibility of restoring much of the original adhesion force after delamination has occurred. Besides ‘normal’ thermoset coatings, powder coatings are also very well suited to protect metal components against corrosion. Although powder coatings are generally harder than their liquid applied counterparts, cracks in these coatings are ‘hard’ to repair, as the

functionality and looks of the coatings are often worse after repair. Self-healing should be ideal for this type of coating. Best results are expected with a two-stage corrosion protective self-healing powder coating using a combination of active and passive corrosion protection. When the coating is damaged in such a way that the metal substrate becomes exposed to the environment, corrosion inhibitors embedded in the coating will be released. They shield the open surface from corrosives in the atmosphere - protect the metal in a passive way - and bridge the period between damage and subsequent active self-healing. From that moment on, active self-healing of the coating commences via a heating/cooling cycle to carry out a thermo-reversible (retro-) Diels-Alder reaction. By increasing the temperature - currently to about 170 °C - the polymeric network originally synthesized by a Diels-Alder reaction at low temperatures reverts into its constituents, furan and maleimide groups - the retro- Diels-Alder reaction. After cooling down, these compounds react with each other again in a Diels-Alder way to the polymeric network, and the self-healing procedure has come full circle. The 'self-healing' retro-Diels-Alder reaction temperature of 170 °C is rather high for a practical application, and can be decreased by introducing electron-accepting groups in the furans and electron-donating groups in the maleimide.

Rubber is a special type of organic material. Rubber coatings and liners are widely used in chemical industry – flue gas desulphurization units, as an example – to protect steel structures from corrosion. Due to extreme operating conditions, such as high temperatures and extremely low pH values, they have a tendency to degrade in time. As removing and replacing the rubber liners is a time-consuming and expensive procedure, another solution has to be found. To develop a more sustainable polymer barrier liner for this purpose, the protective coating should be able to repair the barrier function autonomously when it is lost by damage. Hence, an appropriate polymer blend has to be found which exhibits a phase separation when the originally present dense top layer has been damaged. This phase separation should subsequently initiate migration of the most mobile component of the blend to the outer surface of the coating. When this component crystallizes or hardens – possibly by using the reactive environment of the flue gas treatment unit – the damaged part of the barrier liner will be restored.

### *6.2.6 Self-Healing Thermal Barrier Coatings*

To improve engine efficiency and to protect them against high temperatures, vanes and blades in turbine engines of airplanes and power plants need to be coated. These so-called thermal barrier coatings allow a temperature of combustion gases of 1200 to 1300 °C, a much higher temperature than even superalloys normally can withstand. However, due to thermal cycling, delamination of the coating occurs. During heating and cooling, high mechanical and thermal stresses develop due to a mismatch between the thermal expansion coefficients of the metal blades and the different layers in the mainly ceramic coating system. Small cracks and pores, which have been present in the coating since its manufacturing, coalesce

into delamination cracks due to the release of these stresses. As the small pores and cracks themselves play a positive role with respect to heat conductivity and creep resistance of the yttria-stabilized zirconia topcoat of the coating system, only the coalescence into delamination cracks should be prevented or healed.

Application of a self-healing thermal barrier coating will extend the coating lifetime and increase the time towards expensive revision of these turbine engines. A self-healing approach of which the principle has been demonstrated is by co-depositing $MoSi_2$-based healing particles to the thermal barrier coating. In case of delamination crack formation in the coating, oxygen from the surroundings flows in these cracks and oxidizes molybdenum disilicide to form $SiO_2$, which heals the crack, and volatile $MoO_3$ to compensate for volume increase. Remarkably, damage which has been generated in thermal barrier coatings of airplane turbines upon cooling can be repaired during take-off, when the engine temperature is more than 1200 °C. This implies self-healing 'in the flight'. During cruise flight (800 to 900 °C) the healing particles are inactive. Over the past few years, the proof of principle of this healing mechanism has been demonstrated. However, for a successful application this mechanism has to be developed further. To this end, healing particles will be encapsulated in a shell of alumina to prevent premature oxidation of the healing agent, so that the healing mechanism will become active only when required.

### *6.2.7 Self-Healing Functional Materials*

The possibilities for self-healing materials in functional devices are virtually inexhaustible. An example is the repair of conductivity in (transparent) electrodes or conducting leads because the conducting pathway has interrupted. Or repair of cracks in membranes in fuel cells and batteries. Or healing of surface areas which have to separate two phases and are vulnerable due to differences in thermal expansion coefficients, or sensitive to creep. Other examples are damage caused by fatigue due to alternating loads in microelectromechanical systems (MEMS). Or healing of layers that are 'buried' in a composite device, such as a multilayer that cannot be disassembled, like in OLEDs, solar cells, foil displays, etc.

By measuring the conductivity through a material, it is possible to detect and possibly quantify microcracks in an electrically conducting material, as these cracks (locally) interrupt the conductivity. By incorporating conducting structures in a material that originally is not conducting, it will be possible to determine the structural integrity of this material in real-time. In line with this argument, it will be possible to apply an electrical field (potential difference over the material) or an electrical current to heal the material. This is advantageous on locations which are hard to access, but also in consumer electronics. As an illustration, conducting polymers can make use of such an electrically driven self-healing process. Suitable multifunctional monomers can form a conducting polymer network after polymerization. Suppose a microcrack is formed in the material, for example, by a mechanical load, which interrupts the polymerization-formed bonds. Consequently,

the total number of electrically conducting pathways in the material decreases, resulting in an increase in electrical resistance in the material. This increase in resistance – or decrease in conductivity – can be used as a trigger to increase an applied electrical field over the material. As the microcrack is the cause of the increased resistance, this larger electrical field generates heat at the site of the microcrack. When this thermal energy is large enough to make polymerization possible, the cracked material can be healed again to the originally conducting polymer network. American research reveals that complexes between N-heterocyclic carbenes and transition metals are very promising as electrically conducting self-healing materials.

## 6.3 Applications

### *6.3.1 Applications in Various Fields*

As mentioned before, the applications of self-healing materials are still limited, but will grow in the coming years. A few applications are available, mainly in the coating industry. Several products can be found for car-paints [6.9, 6.10]. (Small) Scratches on cars disappear when the car is placed in the sun if this coating is applied. The coatings are also available for applications in many other areas [6.11].

### *6.3.2 Applications in Civil Engineering; Asphalt*

As presented in section 6.2 the development of self-healing asphalt has led to real applications of the material in the field. A first test section has been made of 400 meter long on a Dutch Highway and after that it has been applied already at three other locations in the Netherlands. Details of the application are described in [6.8]. To make a quantitative prediction of the financial benefits that can be obtained when using self-healing materials the balance between increased material costs and reduced maintenance and user costs are key. Operating costs, disposal costs and environmental costs also contribute to the equation. It is expected that periods between road maintenance will extend when self-healing asphalt is used, resulting in a decrease in user costs. Rijkswaterstaat in the Netherlands made a study of the financial benefits of using self-healing asphalt in the surface layers on highways. This calculation will be used as an example. According to this study, the average annual costs for major repairs of 74 $km^2$ of standard PAC in the Netherlands are amounted to 180 million euros. By extending the life span of standard Porous Asphalt Concrete (PAC) by 25 percent - so from 12 years on average to 15 years – the annual costs for major repairs can be reduced by 35-50 million euros. At an extension of the life span from 12 years on average to 18 years - so by 50 percent - the annual savings on major repairs could be as much as 60-80 million euro. In

this simplified analysis, the additional cost pertaining to the use of enhanced self-healing asphalt are not taken into account.

Besides these 'direct' maintenance savings, self-healing asphalt yields indirect advantages, for instance less traffic jams due to road maintenance and hence less social traffic jam costs. Traffic jam costs, expressed as capitalised hours of time loss of waiting people and their alternative routes, amounted in 2008 in the Netherlands to 2.8 billion euros, of which 'only' 4 percent or about 110 million euros were caused by road maintenance. It would be reasonable to assume that the number of traffic jams decreases proportionally with the length of the maintenance period. Therefore, a life span extension for self-healing asphalt with 25 percent from 12 years on average to 15 years would render 22 million euros less traffic jam costs. At a life span extension of 50 percent - from 12 years on average to 18 years - the social traffic jam costs would be 37 million euros less. Again, here the additional cost for applying self-healing asphalt is not taken into account.

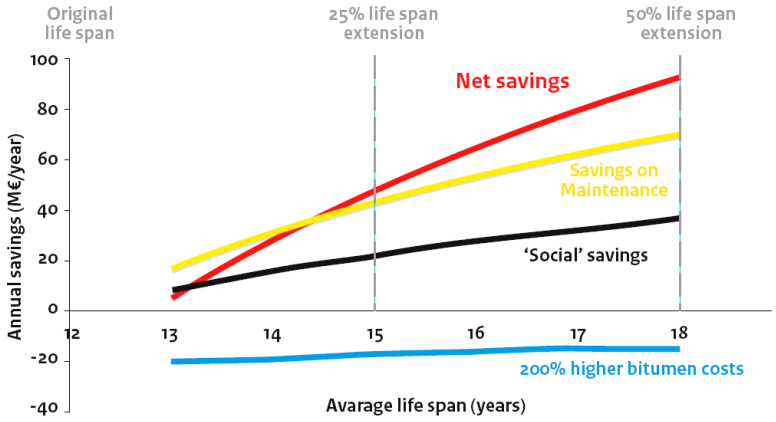


**Fig. 6.3** Annual savings that can be achieved using asphalt with extended life span. The net savings are the sum of savings related to maintenance and social costs and higher bitumen costs.

The combined annual savings related to major repairs and social traffic jam costs are approximately 65 million euros at a life span extension of 25 percent and over 100 million euros at a life span extension of 50 percent, for the entire PAC area in The Netherlands. To determine the net savings, the additional costs for self-healing asphalt have to be subtracted. A 100 percent (or 200 percent) higher bitumen price results in approximately 8 million (or 16 million) euros additional annual costs. So even if the price of self-healing bitumen will be twice as high as for standard bitumen, The Netherlands can save approximately 90 million euros annually by investing in self-healing asphalt with a 50 percent extended life span compared to traditional PAC (see Fig. 6.3).

The Netherlands is fairly small. It has only 3% of the European asphalt production and only 1/3 of this (so only 1%) is used in surface layers. If we extend the analyses of savings by using self-healing asphalt from the Netherlands to Europe, the number of 90 million euros has to be multiplied at least by a factor 100. (actually it should be a larger factor since only the highways in the Netherlands have PAC surface layers and not the secondary roads).

According to this analysis the total annual savings for Europe would be 9000 million euros.

Benefits accrue for both 'society', as road users, and the road maintenance authorities with the use of self-healing asphalt. Planning of maintenance agreements will be facilitated for road contractors using this new material.

Investments for the development of self-healing asphalt in road construction will need to be made now, with long-term performance investigation required to prove a successful investment. Return of this investment will materialise in the form of an extended life span of the asphalt and consequently less maintenance costs. In practice, the financial risk can only be taken by the road manager or by road contractors with a combined construction and maintenance contract. To evaluate this risk it is important to understand the capacity of self-healing asphalt at an early stage, for example through pilot projects with a sufficiently long evaluation time.

### *6.3.3 Applications in Cement Based Materials*

Several applications have been realized in cement based materials. The fibre reinforced materials, which are self-healing by nature, but can also be 'upgraded' to become more self-healing, are applied in several projects. An overview of the applications can be found in [6.12].

The self-healing concept in which cementitious composites are produced that incorporate various mineral admixtures is applied in projects in Japan [6.13].

The bacterial concrete is tried out to repair a leaking concrete structure in the Netherlands. Details can be found in [6.14].

## 6.4 Future Developments and Outlook

In [6.7] it is stated that future applications of self-healing materials are most likely to be applied in places where reliability and/or durability play a key role:

- In places that are difficult to access to perform (expensive) repairs, such as at high altitude (high buildings, wind turbines at sea), underground (piping) or under the water surface (cables and piping).
- Applications where reliability and safety are key issues, even during overload or unforeseen circumstances: storm surge barriers or nuclear reactors or long-term storage of nuclear waste.

- Structures which have to last very long (several decades), such as in large infrastructural applications as dikes, dams and tunnels.
- Applications where large repairs result in a lot of inconvenience in society, such as repairs of roads and in energy supply.
- High-tech equipment for the production of high-quality products; machines which have to be in operation 24/7, where downtime should be minimized.

For cement-based materials various concepts and methods are developed in the laboratory. To apply them on a larger scale, some up-scaling should be done. In real structures large amounts of healing agents should be produced on an industrial scale. This is not always an easy task. Industrial production involves usually a different approach and some more research to obtain equivalent material to the one that is produced in the laboratory. However, projects are under development to realize this. If enough healing agent is available real applications can be made. First this will be done, still, on a relatively small scale, in which monitoring of the self-healing process is performed. If enough experience is gained larger applications will follow.

Another aspect of bridging the gap to real applications is creating more confidence among contractors and owners of structures in the use of self-healing materials. In order to do this it is important to be able to show the long term behaviour of structures build with self-healing materials. This is of course not an easy task. Accelerated tests can help for this, to show that self-healing materials will perform also on the long term. Furthermore, it is necessary to perform Life-Cycle-Analyses to show that in the end structures with self-healing materials will last longer, perform better and are more durable and sustainable in the end. Investing some more when the structure is built, can definitely pay off.

## References

6.1. White, S.R., Sottos, N.R., Geubelle, P.H., Moore, J.S., Kessler, M.R., Sriram, S.R., Brown, E.N., Viswanathan, S.: Autonomic healing of polymer composites. Nature 409, 794 (2001)
6.2. Schmets, A.J.M., van der Zwaag, S. (eds.): Proceedings 1st International Conference on Self-healing Materials. Springer, Noordwijk aan Zee (2007)
6.3. White, S.R. (ed.): Proceedings 2nd International Conference on Self-Healing Materials 2009, Chicago (2009)
6.4. Bond, I. (ed.): Proceedings 3rd International Conference on Self-Healing Materials, Bath, UK, June 27-29 (2011)
6.5. van der Zwaag, S.: Self-healing materials, an alternative approach to 20 ceturies of materials science. Springer Series in Materials Science, vol. (100). Springer, Dordrecht (2007)
6.6. Ghosh, S.K. (ed.): Self-healing Materials: Fundamentals, Design Strategies, and Applications. WILEY-VCH Verlag GmbH & Co., Weinheim (2009)

6.7. NL-Agency, Self-healing materials, concept and application, Ministry of Economic affairs, The Netherlands (2011)
6.8. http://www.selfhealingasphalt.blogspot.com
6.9. AkzoNobel, http://www.akzonobel.com/aac/news/pressreleases/2009/new_self_healing_clearcoat_from_akzonobel.aspx
6.10. Bayer MaterialScience Self-healing Coatings, http://www.youtube.com/watch?v=FYfhk9ZBxa0
6.11. Beckman Institute, University Illinois, Autonomic Materials, http://www.autonomicmaterials.com/applications/
6.12. http://ace-mrl.engin.umich.edu/
6.13. Ahn, T.-H., Kishi, T.: Crack self-healing behaviour of cementitious composites incorporating various mineral admixtures. J-ACT 8(2), 171–186 (2010)
6.14. http://www.selfhealingconcrete.blogspot.com

# Author Index

# Keyword Index